


UNIVERSITÀ
DEGLI STUDI
DI TORINO

Research Programme
Doctoral Program in Urban and Regional Development (XXXVIIth Cycle)

Experimental, Numerical, and Full-Scale Assessment of Hemp-Lime and Confined Recycled Aggregates for Load-Bearing Feasibility in Architecture.

Multiscale Structural Characterisation of Sustainable Materials.

Arthur Bohn

* * * * * *

Supervisor
Prof. Andrea Bocco

Doctoral Examination Committee
Prof. Sofiane Amziane, Université Clermont Auvergne, France
Prof. Patrick Borer, Centre for Alternative Technology, United Kingdom
Prof. Naima Boumediene, Referee, Université de Picardie Jules Verne, France
Prof. Alessia Monaco, Politecnico di Torino, Italy
Prof. Paulien Strandberg-De Bruijn, Referee, Lund University, Sweden

Politecnico di Torino
September, 10th 2025

La tesi di dottorato è stata redatta a conclusione del percorso di dottorato finanziato a valere sul PON REACT-EU 2014-2020 - azione IV.4 "Dottorati e contratti di ricerca su tematiche dell'innovazione" e azione IV.5 "Dottorati su tematiche green" a valere sul Decreto Ministeriale del 10 agosto 2021, n. 1061.

This PhD was carried out with the support of the Italian Ministry of University and Research, under Ministerial Decree No. 1061 dated August 10, 2021, within the framework of the National Operational Programme (PON) "Research and Innovation" 2014–2020, and with the support of the companies "Calce Piasco Srl." and "MTM Costruzioni Srl.".

I hereby declare that the contents and organisation of this dissertation constitute my own original work and does not compromise in any way the rights of third parties, including those relating to the security of personal data.

Arthur Bohn Turin, September 10th, 2025

Abstract

In the context of rapid construction and increasing environmental constraints, this research focuses on low-impact technologies as innovations rooted in traditional building culture, due to their reliance on bio-sourced or reused materials and the use of slow, craft-based techniques, offering potential structural substitutes for conventional construction systems. However, assessing their performance remains a challenge; particularly in bridging experimental and numerical approaches.

The study focuses on two materials: a bio-sourced composite (hemp-lime) compatible with wet construction methods and confined recycled aggregates (CRA) used in dry, reuse-based applications. Two main objectives are pursued: first, to examine the mechanical properties of various hemp-lime mixtures for structural applications; second, to evaluate the feasibility of using CRA in foundation systems by measuring resulting settlements.

For hemp-lime, a cross-disciplinary approach integrating laboratory experiments and a scale model was employed to investigate the relationship between the internal thermo-hygrometric conditions, its carbonation process, and its mechanical strength. For CRA, results from a full-scale prototype subjected to loading were compared with digital simulations using two open-source tools: OpenFOAM (FEM) and LIGGGHTS (DEM).

The primary findings on the hemp-lime demonstrate congruence with scientific literature. The hydraulic base sample demonstrates enhanced resistance in comparison to the samples composed of putty lime, excepted the pozzolana and quicklime mixture, likely due to increased hydraulicity induced by the quicklime. These results point to the relevance of further chemical analysis to optimise self-supporting, low-impact construction materials.

CRA proved to be a viable foundation material despite the absence of Italian standards. FEM simulations did not yield satisfactory results in terms of the overall mechanical behaviour of the CRA. Conversely, the DEM allowed granular-level representation, thereby significantly reducing the computational demands. This finding yielded settlements values close to real measurements (5 mm in simulation vs 7-17 mm in reality). These findings are encouraging, as they suggest that the DEM numerical simulation could serve as a viable approach for the design and validation of CRA. These findings suggest enhancement of the DEM Model code by opensource collaboration, as CRA presents a viable alternative to the prevalent use of reinforced concrete as the standard solution in Italy.

Acknowledgements

I would like to thank my partner Antonella, without whom this research would not have received the energy it needed, and also my children Euplio and Sélène, who aroused in me the virtuous and ingenuous curiosity that children have by nature. I dedicate this research to them.

I would also like to thank all the students who took part in this project, as well as the experts who provided guidance and support. Special thanks to Filippo Caggiano and the entire Green Think team, ANAB, Lorenzo Torre, Federico Giacone, Angelo Iurlaro, Andi Dani and Louis Geiswiller.

Contents

Preface

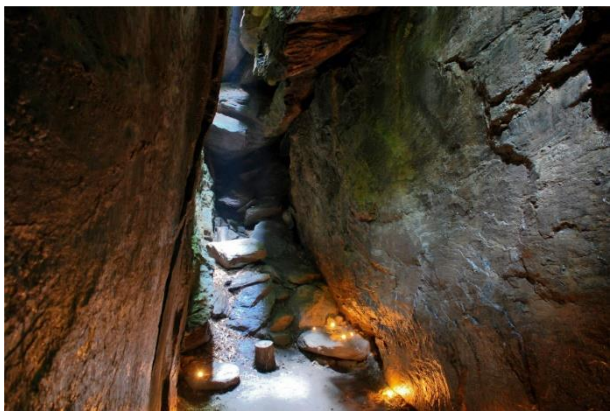

Figure 1 : Gheisa d'la Tana _ Angrogna, Italy [1]

Figure 1 represents a religious human sanctuary, yet within this space, no construction has been undertaken. The concept under discussion involves the appropriation of natural elements by humankind, thereby giving them a human essence. The humanisation process transpired through belief and divine protection during the repression of the Waldensian faith. The management of natural resources by human beings represents an extraordinary accomplishment, entailing both technical and animal expertise, primarily driven by a mental and even spiritual projection. It is imperative to get this intricate substance in order to grasp the profound connection between humanity and our quest for knowledge of natural building materials.

1 Introduction

1.1 Research topic

This research explores the structural potential of low-impact construction materials and some of their relative technics through full-scale architectural experimentation, combining physical testing, numerical modelling, and in-situ measurement. By examining a hemp-lime prototype and a dry gabion system made from recycled aggregates, the study develops reliable, non-destructive evaluation methods and assess the validity of simulation tools in real-world conditions.

Today the conventional materials for construction field are represented by concrete, fired masonry and steel. However, their global warming potentials are very high and problematic. Finding alternatives in bio-based materials could decrease the emissions of GHG[1] during the process of production by sinking into buildings the atmospheric carbon dioxide.

Vernacular housing of a local territory is one of the main losses as a heritage. In Italy, and more particularly in Piedmont, modern building construction techniques are mostly made of concrete produced by multinational companies. However, many technical issues were already solved by traditional habits. Nevertheless nowadays, beware of global heating, and energy saving in the building sector, this heritage is being abandoned. The research focuses on low-impact technologies that can be considered innovations rooted in traditional building culture, due to their reliance on bio-sourced or recycled materials and the use of slow, craft-based techniques. By low-impact technologies, I refer to those whose ecological footprint is minimised, meaning that the manufacturing processes—whether industrial or artisanal—are not damaging to the environment in the short, medium, or long term through various means (such as the use of minimally processed raw materials, integrated recycling within the life cycle, and reuse even in sectors outside of construction). This approach is articulated in the theoretical framework of Vegetarian Architecture [2]. This term highlights how attention to materials and the traditional practices of certain cultures in vernacular architecture has contributed to the development of practical wisdom. This wisdom has not only safeguarded communities but also preserved our planet, a vital "container" for humanity. Consequently, in a context of ecological transition where the

[1] The main Greenhouse Gas are H_2O, CO_2, CH_4, N_2O and 0_3 .

building sector is expected to undergo significant transformation, architectural research faces the imperative to conceive in a novel manner, characterised by reduced resource consumption, reduced energy usage, increased reuse, and the incorporation of bio-based materials. Despite the clarity of these objectives, the implementation of these concepts is often confronted by the complexity of existing construction realities, and the integration of unconventional materials as structural elements remains a challenge.

1.1.1 The global climate situation

In order to provide a large overview of the global context concerning the challenges posed by natural resources, it appeared to be a worthwhile endeavour to revisit the basic principles of ecological analysis on a global scale. One of the preliminary scientific studies initially disseminated through global media is documented here. This study was among the first to raise societal awareness of the ecological and sociological dimensions of the issue.

The great oil shocks of the 1970s imposed the consideration that the world has limited resources. The team of researchers led by the Meadows published their report "The Limits to Growth" in 1972 [3]. By simulating a number of key factors using a computer model, The team concluded that if world population growth and consumption continued unchecked, the Earth's resources would be exhausted within a few decades, leading to economic and ecological collapse. The factors used are essentially demographic, food and industrial production, limited natural resources and the pollution emitted by our human activities. These simulations show that if capitalist yield policies continue, the risk of ecological collapse would lead to a collapse in industrial production, then food production, and consequently a global demographic catastrophe. These results, have been confirmed by contemporary research [4]. Figure 2 is the original plot showing the post-peak decreasing, and Figure 3 represents the recent study built with recent computational engines.

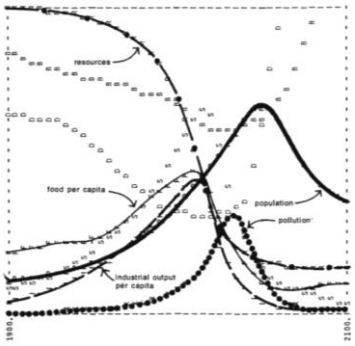

Figure 2 : Original plot _ "The Limits to growth" (1972)

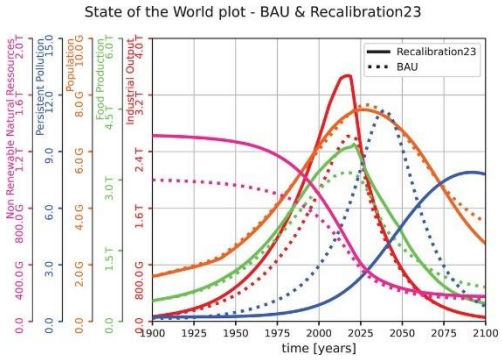

Figure 3 : Recalibration plot _ source : Nebel et al. (2024)

From a technological point of view, Humanity has grown exponentially in a century. The psychological stress caused by current circumstances has triggered a physiological response in the natural environment, a phenomenon that is supported by the findings outlined in the climate report. Natural resources and cycles are not able to keep up with the unbridled speed of human technological development on a large scale. Humans must question their activities to avoid cutting themselves off. The reaction is very simple and instinctive on the scale of an individual. But would it remain so for a global population of nearly 10 billion thinking individuals, organised into complex societies, governed by global structures, and embedded within a hierarchical world order? On this subject, research has attempted to demonstrate through computer simulation that the concept of self-regulation exists in nature. Gaya's theory explains that the planet is in synergy with the populations that inhabit it. Lovelock and Watson developed the "Daisy World" simulation in 1983, demonstrating that the temperature of a planet stabilises in accordance with the mix of populations that inhabit it, balancing out (in terms of concentration) in the same way according to the climate context [5].

The IPCC, co-founded by the UNEP and the WMO in 1988, plays a crucial role in providing scientific assessments on climate change, which UNEP helps to translate into policy frameworks globally. The IPCC report outlines the consequences of different scenarios based on temperature increases. Specifically, it illustrates the potential impacts of global warming ranging from 1.5°C to 4°C. When comparing this report with Figure 4, it becomes evident that a 4°C rise above the mid 20th-century baseline would represent a level of warming not experienced on Earth for over 3 million years. The potential effects on today's society could be catastrophic. If global average temperatures exceed 3°C, significant disruptions could occur in the very short term. Conversely, limiting temperature rise to 1.5°C or even 2°C would require an immediate and substantial decline in CO_2 emissions. The issue has been analysed from every angle, yet temperature itself is not a variable that can be directly controlled. The rise in global temperature can only be limited

through coordinated global actions that reduce greenhouse gas emissions [6]. However, urgent action is required, as the window of opportunity to act is confined to this decade [6].

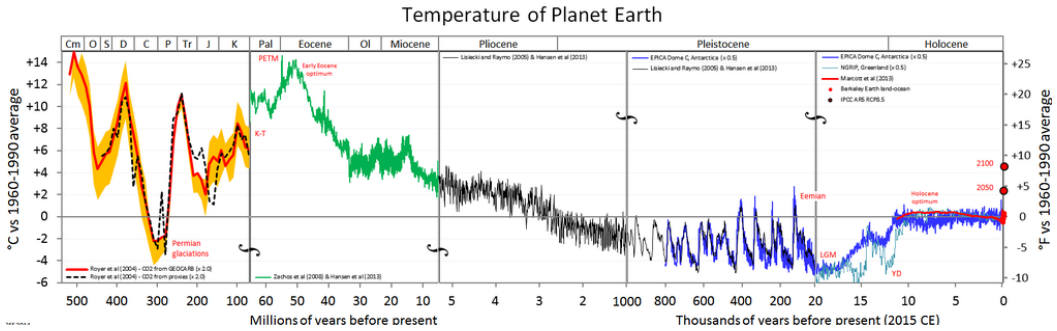

Figure 4 : Combination of 7 scenarios of the past from different authors gathered by Rob Rohde

By extension, humans could be their own cure. Unfortunately, many critics dismantle the principle of homeostasis caused by the living organisms that inhabit the Earth [7]. However, it would be important to understand that if humanity fails to respect this self-regulation, the planet will enforce it regardless. And natural regulation may be failed to be perceived.

1.1.2 The construction sector in figures

The construction sector consists of all the stages in the realisation of the world's building stock. From the extraction of raw materials to the use of the buildings, each process has its own pollution factors [8], but it is interesting to note that the ecological impact of each stage is fertile ground for technological improvement.

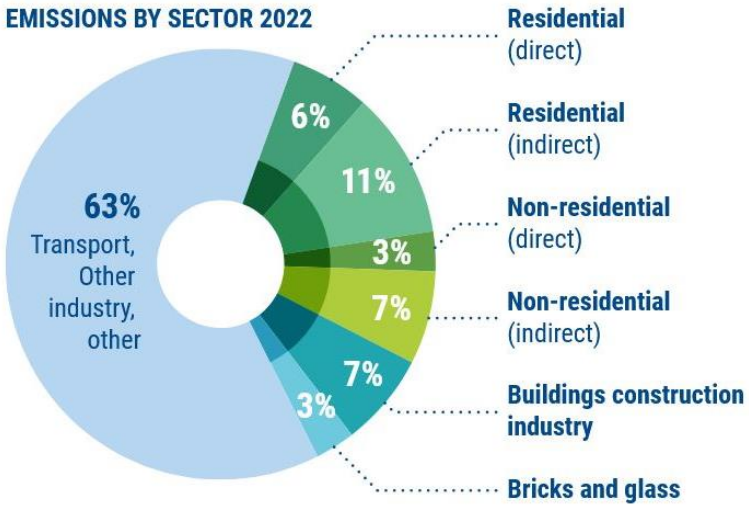

Figure 5 : Share of buildings in emission in 2022
(Source: IEA 2023a. Adapted from 'Tracking Clean Energy Progress')

According to Figure 5, the construction sector emitted 37% of greenhouse gas emissions in 2022, the majority of which are grouped under the term direct emissions, i.e. emissions linked to the extraction and production of materials, and their installation. The remaining third corresponds to the use and maintenance of the building stock.

A similar observation can be made regarding the global demand for energy on Figure 6. It is noteworthy that 34% of the demand is attributable to the construction sector. In contrast to common assumptions, the residential sector constitutes the most significant segment of the energy demand, with the non-residential sector ranking second. The production and construction sectors of the building sector account for 4% of the total energy consumption.

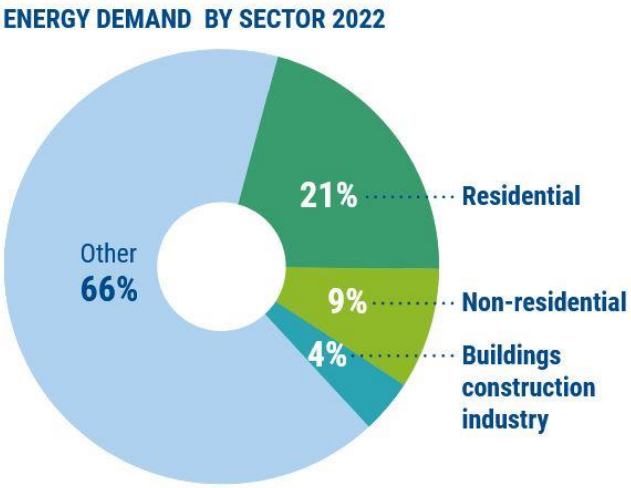

Figure 6 : Share of buildings in total final energy consumption in 2022
(Source: IEA 2023a. Adapted from 'Tracking Clean Energy Progress')

Figure 7 shows the distribution of energy consumed by each construction sector, and it quickly becomes apparent that industrial mechanical installations account for the largest share of energy consumption. However, if the share of the residential and tertiary sectors is added up, the share ends up by 30%, which is the same as for the installations mentioned above. It is therefore clear that there is a huge role to be played in bucking this trend for designers, engineers and architects.

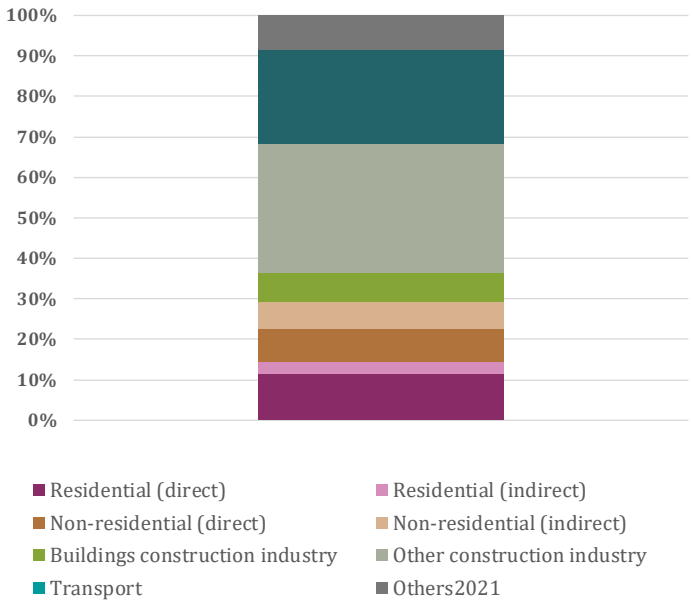

Figure 7 : Global energy, and process emissions from buildings, including embodied emissions from new construction, 2021, IEA, Paris

In addition to the chart presented in Figure 7, the 2024/2025 UNEP report also states that the cement and steel industries together account for 18% of global emissions [6].

It is evident that the construction sector is undergoing a substantial transition towards a decarbonised framework. A matter of contention is the manner in which the states were expected to comply with the stipulations set forth in the 2015 Paris Accords. Despite the endeavours to enhance energy efficiency through research and development, local institutions have not yet allocated sufficient resources to the establishment of construction codes that are designed to manage natural resources.

Indeed, the process of decarbonisation is experiencing robust growth, particularly in developed countries, as these nations increasingly utilise renewable energy sources for the operation and maintenance of their respective building sectors. Governments are procuring information technology systems designed to enhance energy efficiency in key sectors, particularly electricity generation. Western societies are witnessing a proliferation of labels in the design of buildings, such as LEED and BREEAM, which are driving investors, architects, and engineers to develop new construction and technological strategies. Additionally, Building Information Modelling (BIM) plays a pivotal role in this research endeavour focused on optimisation, as it constitutes a fundamental component of the

evaluation criteria employed by the aforementioned labels. In fact, the field of computer-aided design (CAD) has come to rely on the sophistication made possible by this technological advancement to achieve optimal results It has now been incorporated into the criteria for managing public competitions in Italy, France, and numerous other countries. However, assessing its actual contribution to internal project management, communication between engineering disciplines, and the transmission of data for integrated design can be challenging.

Nonetheless, certain issues are becoming evident, despite the indications of an upward trend in decarbonisation. The revision of construction codes has undergone a significant decline in the global context. In 2023, there were 20 substantial updates to these codes, whereas in 2024, this number decreased to 20. This phenomenon could be indicative of a potential stagnation among governments in terms of making technical decisions. This inquiry pertains to the global economic context, wherein the enhancement of coding protocols necessitates the implementation of structural security measures, manifesting in increased material usage and enhanced performance outcomes. In such circumstances, numerous countries lacking efficient industrial infrastructure may elect to maintain their autonomy from the global market and the economic volatility characteristic of major producers. It is imperative to emphasise that the utilisation of advanced materials in construction represents a pivotal element in the pursuit of a low-carbon growth strategy. Indeed, the recycling, reuse, alternative selection, and plurality of materials for construction are inadequate. The utilisation of recycled materials is inadequate due to the prevalence of concrete and steel as the predominant construction materials. In 2018, these two materials accounted for 45 out of 48 billion tonnes utilised in the building sector [9]. On the global scale, there has been no significant, lasting improvement, nor are there any low-carbon competitors in terms of demand. As illustrated in Figure 8, the global distribution of materials in 2018 was characterised by specific patterns.

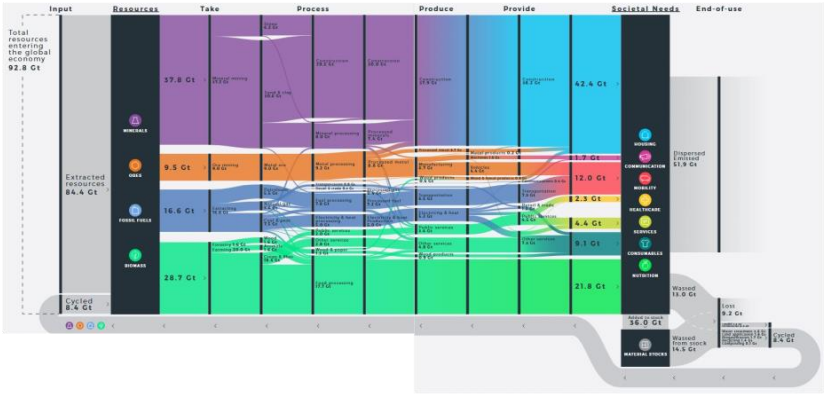

Figure 8 : The global resource footprint behind satisfying key societal needs.

1.2 Research problem

The world of construction took a global turn in the last century with the invention of concrete mixes design. Once humans were able to extract the needed resources to produce an improved, fast-setting hydraulic binder, the reproducible formula knew no bounds and seeped even into building practices of the most remote societies. As a result, structures based on the concepts of Modern Architecture (Le Corbusier's "Domino" House with the Column-and-beam system) are found in contexts where the first local thinking would not support this kind of reasoning at all. It is sufficient to consider a territory with few clay quarries and no appropriate sand to realise that high energy consuming transport is the only solution to build in concrete in such territory.

The term “Glocalization” helped to raise global awareness of ecological issues. This is a concept created in the 1980's as a reaction to globalisation thinking that focuses the world on a single mode of evolution [10]. In practice, it implies the adaptation of products, services or ideas from a global level to the cultural, economic and social specificities of a local area. This process recognises that while living in an increasingly interconnected world, people's needs, tastes and expectations may vary significantly from one region to another. A certain awareness that globalisation cannot strive to become the evolution of humanity can be recognised here, because it would totally affect the context and environment in which Humanity is evolving. The speed of climate change due to man's technological evolution would become excessive in terms of biology condition in general, able to collapse the fragile equilibrium of the planet, such a fundamental principle of life.

Ten years before, in the 1970s, the notion of "appropriate technology" has developed due to the first effects of the global ecological crisis [11]. The idea was to transfer self-sufficient technologies to regions of the world in need, with the aim of fostering a know-how that could enhance resilience. The concept appeared in the 60's but was theorised with the help of Schumacher in his work “Small is beautiful” [12]. However, this conception of international aid has been somewhat criticised due to the imposition of education “from the top”, without taking into account local specificities and cultures [13].

Moreover, beyond the limitations of the approaches previously discussed, it is important to note that non-conventional construction techniques still lack a solid and universally recognised position within building codes globally. Despite efforts in some countries—such as the United States, where structural straw-bale, hempcrete, and compressed earth blocks have been standardised through the inclusion of specific appendices in the International Residential Code (IRC) [14], these materials remain marginal. Similarly, countries like Germany, France, and New Zealand have taken steps

toward integrating natural materials into nationally recognised codes, yet such examples remain exceptions rather than the norm.

The main limitation of the standardisation of modern industrial construction techniques lies in the increasing flow of materials and the reliance on high-impact production processes. A more sustainable approach would be to preserve local specificities by taking into account the availability of natural resources, in order to meet the growing demand for buildings without further increasing their ecological footprint.

1.3 Research aim

The research collects the study of two materials with minimal environmental impact: hemp-lime and confined recycled aggregates, with the aim of assessing their applicability to structural applications in support of more sustainable construction.

In the context of the necessary ecological transition in the building sector, the use of environmentally friendly materials in load-bearing elements remains a key issue. So, this research investigates how the aforementioned construction technologies derived from the combination of traditional materials, such as lime and hemp, or from the circular management of construction waste, such as recycled gabions, can be integrated into modern architectural practices to reduce the carbon footprint of buildings while meeting contemporary regulatory requirements. Indeed, understanding the mechanics of these techniques is essential.

1.4 Research questions

It is important to acknowledge that the mechanical behaviour study of a material cannot be limited to small-scale tests. This is because the geometry, dimensions, and the relationship between applied loads and the volume of material in place can lead to unexpected results that deviate significantly from those observed in sample testing. It is therefore essential to carry out experiments at multiple scales, both numerical and physical, in order to establish a coherent physical correlation between these different levels of analysis.

Furthermore, is it possible to establish reliable, non-destructive methods for assessing the mechanical performance of ecological materials within real architectural contexts? Developing such techniques would enable real-time evaluation of a structure’s load-bearing

capacity, opening the door to new forms of in situ testing adapted to sustainable construction.

Firstly, it is hypothesised that the strength properties of a hemp-lime full-scale prototype can be evaluated non-destructively by establishing physical correlations between measurements within the prototype, such as its moisture content and temperature, using data collected by integrating sensors during its construction, and the carbonation measured after destructive testing. This approach should allow evaluation of the mechanical properties of the material without compromising its integrity. Secondly, it is suggested that the mechanical properties of the hemp-lime mixture can be improved by the incorporation of specific additives. However, it is imperative to recognise that these improvements must be evaluated in direct interaction with the building application and hydration conditions, which have a significant influence on the behaviour of the material in a real-world context. Consequently, the present study will focus on an empirical observation of compressive strength and carbonation phenomena in a large population of hemp-lime mixtures incorporated with various additives and already scientifically documented.

The other hypothesis is based on the validity of numerical models, such as the discrete element method (DEM) and the finite element method (FEM), applied to structures of the gabion type manufactured from recycled aggregates. These models should enable the simulation of behaviour under load with a reasonable degree of accuracy. However, the validation of these models necessitates experimental validation through physical experimentation. This validation is imperative for the consideration of complex phenomena such as chain forces, settlements, and internal friction that can be visualised by numerical modelling. In order to establish a dialogue between the modelling process and empirical observation, it is hypothesised that the full-scale experiment is regarded as a critical research instrument. Thus, the latter would serve not only as valid documentation for testing the CRA (Confined recycled aggregates) as a shallow foundation, but also to connect scientific theories with measurement tools and construction constraints. This experimental method would render possible to confront theoretical assumptions with field reality, thereby ensuring a concrete and pragmatic validation of design concepts under real implementation conditions.

1.5 Objectives

These materials, that are bio-sourced or coming from re-use process, suffer from a lack of structural recognition, mainly because of the difficulty of assessing their mechanical performance in a reliable, reproducible way that is adapted to the actual conditions of use. However, the lack of protocols for measuring their performance on a real scale without destroying them stands as an obstacle.

The research attempts to observe physical and mechanical phenomena on the materials under consideration, whose characteristics are difficult to predict by virtue of their dependence on natural factors, such as temperature and air humidity, but also on their installation and the feasibility of their operability.

Accordingly, the present work proposes the hypothesis that two materials with low environmental impacts have the potential to be used in the construction of load bearing structures and investigates this hypothesis through an experimental approach that integrates scientific analysis, numerical modelling, and empirical testing on full scale.

Throughout the evolution of the species, one technique has greatly amplified, namely that of a paste that hardens. In Italy, building with natural materials is not an exception, and scientific interest is primarily focused on the binders that have shaped history [15].

In accordance with this rationale, the initial case examined is that of hemp-lime, a bio-sourced material that has received significant acclaim for its environmental benefits. However, it has not been determined to be structurally stable yet. A critical review of the existing scientific literature was conducted to identify additives that could improve the mechanical strength of the material, and promising additives were selected for testing on samples and a commercial binder has been used for full-scale prototype. However, the collapse of the structure occurred shortly after its completion, highlighting the limitations not only of the material itself but also of the processes involved in its implementation and hydration. This incident underscored the disparities between the predicted performance and the actual results in construction, leading to further investigation of the relationship between theoretical predictions and practical applications in this field.

The second case refers to a construction system using gabions filled with recycled demolition aggregates, based on the principle of dry reuse. Worldwide, the construction industry produces around two billion tons of construction and demolition waste (CDW) each year, making up nearly one-third of the total global waste stream. Despite this significant volume, only a limited portion is recycled or repurposed, while the vast majority ends up in landfills or is incinerated [16]. This composite material has been the subject of numerical modelling (particularly through DEM and FEM softwares), and in a real scale experiment. The present study proposes the construction of a digital model using open-source software, with the intention of comparing it to the results of an experimental study in which the effects of a known load on the stability of the structure are measured. The objective is to demonstrate the existence of a simple digital model that can estimate the actual deflection.

Despite their marked differences in terms of nature, implementation, and scientific framework, these two cases are unified by a shared objective: to assess the structural feasibility of materials with low environmental impact under conditions realised within real

experiments. By integrating theoretical models, laboratory experiments, and field tests, this research seeks to inform a critical evaluation of the validity and limitations of contemporary architectural design tools within the context of low impact technology in sustainable construction.

1.6 Methodological approach

This entire research is based on a cross-experimental methodology that integrates different complementary approaches to investigate the mechanical behaviour of hemp-lime composites and modelling confined recycled aggregates structures.

As the doctoral research presented here concerns the behaviour of two construction products, two complementary approaches will be used. The first, which will be highlighted here (3 : Hemp-lime : a wet construction technique), is a more experimental approach in the sense that the results are obtained from data collected on the material. The purpose is then to understand whether there are correlations between the different analysed parameters. On the other hand, the second approach requires the opposite effort, in the sense that the object of study is the encounter between a real construction built by a team of students, and the attempt to build a numerical model that can respond to the same inputs as the existing structure, and that achieves similar mechanical behaviour results in terms of settlements (4 : Confined Recycled Aggregates: a dry construction technique).

The theoretical approach is to consider that empirical observation enables to create mathematical models that can represent with a certain fidelity a known set of events. Furthermore, the presumed reciprocity between empirical analysis and numerical modelling, may render possible to use computational models to measure settlement on confined recycled aggregate. However, the question remains: how can digital tools, experimental data and construction reality be combined to reinforce the structural validity of these materials in a project-based approach?

The first method involves a critical bibliographic review aimed at identifying additives that may improve the mechanical performance of hemp-lime materials. The second phase consists of laboratory-scale experimentation on samples. These tests are designed to evaluate mechanical responses and explore correlations between carbonation and strength. The outcomes of these tests serve as a basis for subsequent non-destructive analysis of a full-scale prototype.

Concerning confined recycled aggregates, the methodological framework presents two stages simultaneously, involving the use of open-source numerical modelling tools to

simulate the behaviour of gabion structures filled with reused materials, and testing of a full-scale prototype. These simulations include analyses of load-bearing behaviour, force chains, settlements, and deformation patterns, and are later compared with data collected during full-scale testing.

In both cases, the final phase which is the full-scale prototype testing hemp-lime and recycled gabions respectively equipped with embedded sensors, and settlement markers. Tests and monitoring are performed on these prototypes, enabling a detailed comparison between the modelled predictions, laboratory data, and the actual structural response observed under realistic conditions. This comprehensive, multi-scalar approach allows for a robust evaluation of the material's performance and the reliability of the predictive models. The different projects required many hours of anticipation, management, design and construction, which is why it took almost two years to obtain the stage that enabled the themes researched in these case studies to be explored.

For the sake of clarity in writing, the paratactic structure of the thesis first strived to present in detail the method and the data identified through the literature review for each of the two materials [Part I / Framework], and in the next two parts, to present the experiments conducted [Part II / Methodology], their results, and the conclusions drawn [Part III/ Case studies].

The first theme of the research (3 Hemp-lime : a wet construction technique) was based on the design, production and monitoring of full-scale prototypes, but also of samples allowing the replication of mechanical tests. Two experiments were done, the first based on the human-scale prototype, and the second based on the creation of samples and the observation of mechanical characteristics by destructive compression tests. The latter activity involved presenting the results in terms of mechanical strength, depth of carbonation and density, in order to find a connection with the prototype. In fact, the prototype was observed from the inside using a set of temperature and moisture content probes capable of providing real-time data on these two parameters at 10-minute intervals over a period of one year. Once it has been destroyed, the arch, built entirely from a mixture of hemp-lime, was observed from the point of view of carbonation in order to measure the depth of carbonation. Using this parameter as the “keystone”, it was attempted to establish a link between parameters that can be simply measured by direct non-destructive measurement (temperature and moisture content), and mechanical strength parameters that could provide the information needed to assess the strength of the construction.

The second case study (4 Confined Recycled Aggregates: a dry construction technique) involved documenting the construction steps and identifying critical aspects in order to enhance the acquired construction knowledge. Secondly, deformations of the gabions subjected to a specific concentrated load were observed. By measuring the local

settlement, a result can be obtained which can be compared, studied, and correlated with a numerical result. This is why an attempt was made to produce a computer code that can represent and simulate the behaviour of a model composed of averaged virtual material. If, after performing the numerical calculation, it is observed that the deformation and settlement values are deemed satisfactory, one may also hypothesise that the results of load transfer between aggregates are similarly close to reality to pretend to use them for designing.

1.7 Contributions

As far as possible, this research therefore plans to demonstrate the technical, reproducible attributes that can be recognised in such non-conventional materials.

The choice of this research stands that the alignment of different alternative and ecological construction techniques is hardly ever carried out [2]. There is a lot of research based on a single composition or technique, but it does not communicate directly with each other. Here, the choice was made to offer the same attention to all stages of research on both of these two non-conventional low impact technologies.

This research contributed to several key areas in the field of sustainable construction and architectural experimentation. In the development of non-destructive full-scale evaluation methods, it expanded the range of analytical tools available for alternative materials. In the articulation between physical experimentation and numerical modelling, the study enhanced our understanding of the limitations and application conditions of digital tools when used in non-standardised frameworks. Regarding the full-scale validation of alternative construction systems, this research connected theoretical studies and real-world construction conditions. This type of empirical contribution still remains quite rare in the academic context.

1.7.1 Hemp-lime research contribution

As the first element studied here, hemp-lime is a combination that offers multiple advantages for sustainable development, human health, and indoor comfort. According to several researches [17,18],taking into account both the carbon sequestration during hemp growth and lime carbonation, the embodied carbon value of hemp-lime is around from -0.44 to -0.34 $kgCO_2/kg$, with an embodied energy (EE) between 3.3 to 3.72 MJ/kg (approximately 1 kWh/kg) [18,19]. Its thermal properties and ability to regulate moisture

make it an effective solution for reducing energy consumption for heating. The thermal conductivity of hemp-lime ranges from 0.06 to 0.23 W/m.K [19,20], depending on factors such as drying time and density, and its water vapor resistance factor is no more than 5, in contrast to 60 for EPS (Expanded Polystyrene) that renders hemp-lime a moister buffering system suitable for living constructions. Consequently, hemp-lime is gaining popularity in construction, primarily due to its capacity to behave as an insulation and hygroscopic material with some promising mechanical properties.

A key challenge remains in determining whether certain hemp-lime mixtures can support external loads. The contribution of this research, in particular on the theme of the load-bearing behaviour of hemp-lime, concerns the possibility that certain hemp-lime mixes can exhibit stable mechanical behaviour that is sufficiently resistant not only to withstand their own weight, but also to bear external loads. With this in mind, and with the idea of proposing a structural alternative, the idea to build an entirely compression vault seemed coming naturally. Moreover, the late architect David Lea had already built a low-pointed arch [8] that wonderfully showcased the mechanical prowess that a mixture of lime and Roman cement could offer. Here, the challenge was to increase the size of the pointed arch, but also to modify its geometric generation so as to integrate all the compression forces within the inner third of the material and thus avoid any traction or bending moment compromising the mechanical performance of the mixture. The technical prowess of the arch enabled us to design the project for monitoring temperature and internal humidity conditions throughout the construction period. The findings of this experimental analysis have been published in the journal Sustainability [21].

At the same time, in order to be able to correlate the internal conditions of the low-pointed arch and the mechanical strength values, new air lime-based mixes have been produced on what has already been done in the past in an attempt to achieve more encouraging results (it is expressed later on this thesis that the results obtained did not live up to the objective set at the outset). One of the points of the research was therefore to observe an experimental campaign through a critical assessment of the influence, in terms of mechanical behaviour, of several additives incorporated into air lime. The results were also compared to another type of hemp-lime mixture, made with hydraulic lime (NHL5). Unlike concrete, lime hardens over a much longer period and follows a different progression from conventional concrete, which typically reaches its mechanical strength after approximately 28 days. Given this, the tests were conducted over a period extending up to 19 months for the oldest samples. The initial research plan envisaged an equal timeline for all samples; however, results could not be obtained from all samples, as the curing of some was not completed for time management and resources. Only the samples that provided satisfying results are presented here. Nevertheless, the overall campaign demonstrated a high level of robustness in the obtained values, as three samples were tested at each curing time. Consequently, the campaign was based on a total of 99 valid samples.

By utilising the carbonation data from the pointed arch prototype and integrating it into the established correlations between carbonation and compressive strength, the mechanical strength properties of the arch could be effectively extrapolated. This approach also allowed to gain insights into how internal parameters such as temperature and water content, influenced by external conditions, evolved throughout the hardening process. In this context, it is valuable to compare this study with the technics conducted by the company Cure [22], which specialises in determining the hardening phases of concrete through embedded probes in the mix during casting.

1.7.2 Confined recycled aggregates research contribution

The decision to pursue this field of study was motivated by its alignment with the principles of the circular economy. It is imperative to address this issue, as it is critical to the future of construction industry. It is therefore essential to identify constructive solutions that can adequately address the structural requirements of new constructions. Furthermore, the utilisation of CRA has the potential to play a significant role in the foundation systems employed in the context of seismic resistance in construction, particularly in residential structures. Indeed, the "bag-like" structure enables the dissipation of energy from the accelerations of the ground without the transmission of forces to the building's structure that could potentially compromise its integrity.

The intention of simulating an enclosed system of aggregates in this research was to propose a synthetic and simplified simulation method, while ensuring that the results align with the experimental data measured on the other full-scale pavilion. In order to develop such a model, it is crucial, first, to understand how a CRA can be mathematically defined. This question was addressed by the research of Professors K. Bagi and M. Brocato. The challenge lies in understanding the relationship between forces and deformations or settlements.

The challenge was to understand how stresses and strains are related by comparing them with actual results obtained by direct measurement on the full-scale pavilion.

The connection between the loads and the stress field is explained by the equilibrium equations, like the Cauchy equations in the simplest case. Deformations are represented by another state variable, strain, with geometric equations linking displacements and the strain field. Stress and strain are connected through the material's constitutive equations, which provided all the necessary details about the material's mechanical properties. The first research by Professor K. Bagi, published in 1996 [23], provided a microstructural analytical definition of the stress and strain tensors for a granular assembly, aiming to construct a constitutive equation linking forces and deformations. Then, in 2009 [24], the

research incorporated particle rotation during contact interactions, and the study relied on a numerical method using finite elements, computed on a computer. Ten years later, Professor Brocato's research focused on a bonded masonry model. This concept arose from the fact that the metal cage allowed very little movement between the elements, and each load was counteracted by a distributed stress across the entire matrix [25]. Moreover, the system upon which the results are based does not consist of spherical particles, but rather polyhedrons. This choice stemmed from the need to determine in a unique system axis, tensors for each particle over time. In contrast, the polyhedron contains three known and constant tensor axes over time, as they are intrinsically linked.

The modest scientific contribution of this research lied in the practicality of numerical calculation. The goal was not to challenge the constitutive laws or the physical assumptions from the field of physics, but rather to translate into a source code a first built physical model, attempting to replicate its deformation results. This research evaluated the accuracy of the results from two open-source software packages developed by different scientific communities. The method of finite element volumes has been explored using OpenFOAM, which primarily governs the field of fluid dynamics, and the discrete element method have been examined through the use of LIGGGHTS. These two computational engines could provide an efficient means to calculate deformation and load transfer that occur in a granular system, such as confined recycled aggregates.

PART I / FRAMEWORK

2 Technology, Techniques and Materials

Firstly, therefore, certain terms that are necessary for clarity of discussion will be defined. It is imperative to subsequently discern the manner in which the two construction techniques examined in this study signify divergent proportions of bio-sourced materials. The sequence of presentation in this context does not denote a value judgment; rather, it is an arbitrary sequence.

2.1 The technology of ecological architecture

Technology can be defined as the optimal use of techniques in a particular field based on scientific knowledge [26,27]. It is the development of systems and theories that frame the practices of a discipline. The concept of natural building technology is predicated on the premise that it preserves the integrity of the natural environment, while generating forms of habitat for humans. Humankind has learned to optimise, it is a conceptual tool to avoid tiring nature, but optimisation is a human concept that tries to reproduce a perfect and systematic approach. As Karl Marx famously said :" *What distinguishes the worst architect from the most expert bee is that he has built the cell in his head before he builds it in the hive*" [28]. The mental representation therefore generates a choice: Would it be better to build it like this, or like that? Instinct is overtaken the moment the first choice is made. And technology is born at the same moment.

On the other hand, the values between technology and techniques should not be confused. Technology is founded through the theorisation of the practical skills of the

techniques that constitute it. In the case of architecture, constructive techniques are also the essence of architectural languages. Thus, one would be hard pressed to see a tree house made of reinforced concrete, or an adobe skyscraper. For example, Hassan Fathy designed and built the Egyptian domes (otherwise known as a revival of the Nubian vaults) in bricks because the material module is consistent, as is the technique of implementation by a single craftsman. Finally, the technology of this technique using this material exists and is repeated because all the other arguments around it are reasonable. It is worth thinking about the economic aspect, the duration of the construction, the thermal performance of the form expressed in this way, and other arguments [29].

In the field of construction and housing, natural materials are associated with local and ancestral traditions. It only took a recent moment in the history of mankind to cause a break in habits. The time had come for mankind to generate its own building materials, by combining skills acquired from physics, mineralogy, and chemistry. The concept of concrete is in part the conscious observation that nature can be reorganised to suit human needs. Steel represents the same phenomenon as the fusion of two atoms in artificial proportions, but which increases tenfold the mechanical faculties of the metal already tamed in the past [13].

This research was undertaken with the understanding that it is not only possible but essential to preserve both 'traditional' and 'contemporary' technologies, using them judiciously in accordance with the specific needs at hand. Consequently, the economic management of projects can be approached through two seemingly opposing methods, while also considering the environmental impact of the chosen technical solutions. In this context, it is crucial to understand how natural materials can be integrated into the construction market, while simultaneously meeting the normative.

2.2 From natural materials to artificial products

While it is evident that natural materials were the exclusive resource for construction until the mid-18th century, this is less clear when considering the creation of the first formula for the production of Portland cement (Louis Vicat, 1818). The distinction arises in the fact that, although concrete is a human invention, the ingredients used are of natural origin. This does not consider the technological innovations of recent decades, where highly energy-intensive cooking chemistry allows certain concretes to achieve mechanical strengths of up to 150 MPa. Rather, one should recognise the ingenuity in combining ingredients that are abundantly available in nature, resulting in a material that enabled humanity to advance in its technological emancipation. So, what differentiates natural materials from those that do not appear to be of natural origin?

Although materials such as steel and concrete are composed of natural elements, it is essential to recognise that humans have had to combine them through various chemical and physical processes to unlock efficient properties. The evolution and improvement of a material occurs empirically and over a long period of time. The focus must be on the birth of such a product, the moment when human consciousness declares that it has mastered and dominated its natural context through extraction and transformation. It is only after observation that a material can be suitable for a certain transformation.

The recognition of the experience of traditional craftsmanship was transformed into the numerical results of experiments that were known and recognised by the scientific community. For example, a lumberjack had to recognise the use and load-bearing capacity of a tree by his experience. This dynamic has gradually changed in such a way that the expert craftsman is no longer, or hardly, recognised in our industrial society. This society requires an optimisation process that is coupled with an extreme exploitation of resources, which is linked to the near-total abolition of hazards for humans. Statistical evidence demonstrates that the natural differs from the designed in its multiplicity. What arises from nature is distinctive; it is not feasible to identify the same wood, with the same ribs and internal tensions. Furthermore, it is not possible to find the same grain size distribution, despite the fact that it originates from the same sand.

In the field of mechanics of materials, a primary objective is to understand and model the deformation or fracture of materials under the influence of external forces. These processes can be intricate, particularly when the materials exhibit non-linear or unpredictable behaviour. This is exemplified by natural materials, which deviate from the paradigm of homogeneous and isotropic materials. It is imperative to collect a substantial amount of experimental data to establish reliable correlations between data from limited, geometrically defined samples and the actual performance of the technique under investigation at the experimental scale. As stated by Pluvinage and Sapunov in the following quote derived from their treatise "Prévision statistique de la résistance, du fluage et de la résistance durable des matériaux de construction.", the key is to achieve sufficient precision and breadth in these relationships to ensure their reliability in the majority of cases to which they are applicable.

“The main problem in the mechanics of deformed solids is the description of the deformation (failure) processes in view of the available experimental data and the accuracy of the established relationships in view of the large number of such data. There is therefore a great interest in developing new methods that allow predictions of the characteristics of quality structural materials for the assumed service life of installations to be made on the basis of test results.” [30]

This is why the statistical study of samples allows us to create a Boolean model considering the goodness of a phenomenon by repetition correlating actions (E) to

resistance (R) (Figure 9). The choice and safety in the design lies in the use of the steepness of the Boolean. If the slope is too gentle, the safety coefficient will be that much higher. If, on the other hand, the slope is steep, meaning that the result will be reproduced more reliably, the safety factor can be lowered.

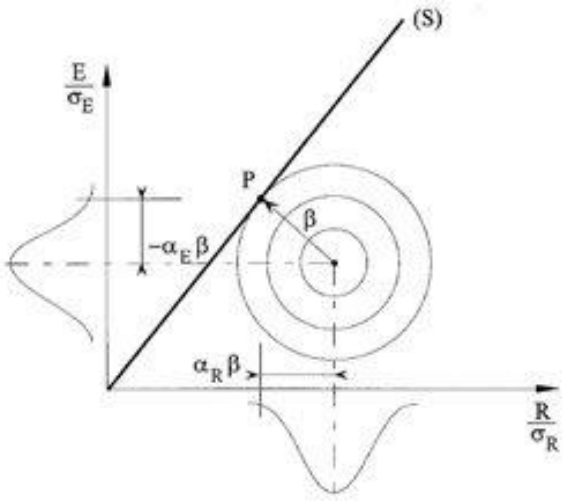

Figure 9 : Schematic design point process from Eurocode EN 1990

2.3 Overview of construction techniques

The observation starts with the distinction between techniques and materials, as it is evident that a certain implementation works for a certain material profile. It is also true that a technique can be used for two materials that do not correspond exactly in terms of composition. As an example, earth-based techniques can only be applied within a specified range of clay percentages. And this is where the characterisation of materials through statistical study is crucial.

Natural material has to be defined as opposed to artificial one. It is also necessary to recognise what is artificial but is the simple mixture of two natural materials, and therefore identical to a simple natural material from the point of view of the ecological footprint. Combining natural materials is not always an artificial product as described above. Lime is an artificial material, meanwhile cob is a natural material because it's slightly changed from nature, but both are fundamentally artificial. Only the former is more polluting than the latter in its creation. Figure 10 presents a classification developed by the author, illustrating

the degrees of naturalness versus artificiality based on the material creation process. Each creation process involves a specific degree of artificiality, which is organised into discrete steps to facilitate qualification and comparison.

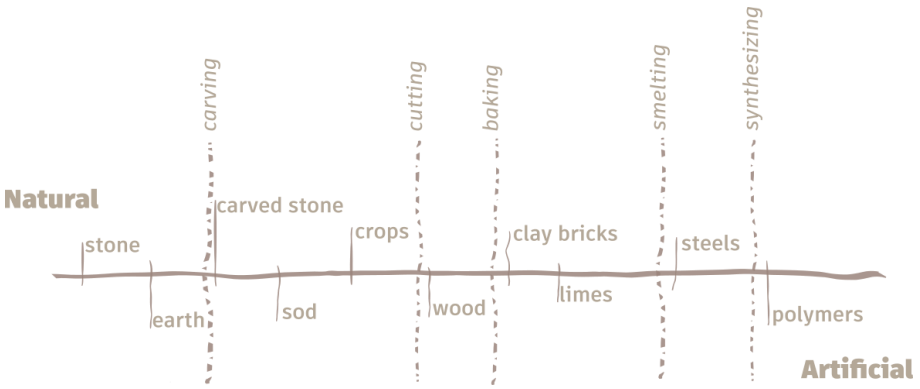

Figure 10 : Progression of building materials from natural to artificial (source: Arthur Bohn)

It is possible to distinguish between natural and artificial materials. Natural materials would therefore be those that humans can collect, cut, and shape. Artificial materials would be those that have been calcinated by humans or transformed in a more complex way (Figure 11).

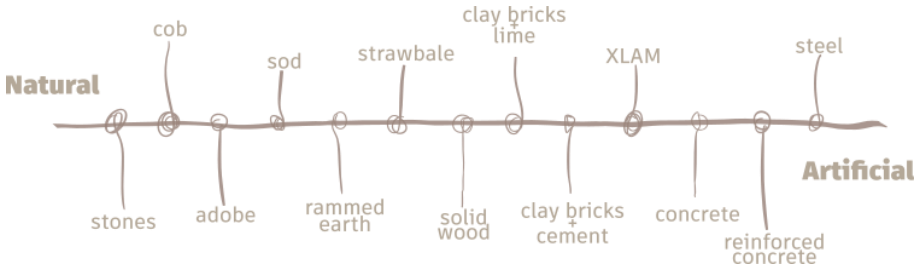

Figure 11 : Progression of building technologies from natural to artificial (source: Arthur Bohn)

The diversity of natural materials is increased tenfold by the number of techniques that humans have perfected since ancient times. A technique has its own characteristics of implementation, and a different rendering of materials, which naturally causes a degradation of habitability properties such as hygrometry, acoustics or static and dynamic thermal performances. As an example, cob can be light or very dense, thus don't have the same thermal inertia nor the same, and yet the characteristics of the materials used are very similar.

Moreover, each technique has benefits and drawbacks, which may themselves vary according to the geographical and climatic context of the implementation. But it is rather

up to the technique to adapt and create a natural product that has the advantage of solving local problems. The earth-straw mix can be formulated to be thermally resistant enough to meet the requirements of northern France or Germany, just as it can be much denser so to have the thermal inertia required in Saharan countries.

Nevertheless, techniques using natural materials are those that require more time and labour than techniques using artificial materials. While it may seem sufficient to produce a material that meets the expectations of the construction industry, it would be wise not to overlook the ecological simplicity of natural materials, whose techniques have been able to highlight their special features over time. Figure 12 is of a qualitative nature, constructed on the basis of a comprehensive understanding of the various construction techniques. This scheme enables the visualisation of two parameters: the intensity of manual labour and the duration of implementation on the construction site (time of work). As indicated, the conventional techniques located on the left side of the schema require a greater investment of time and effort during implementation. Conversely, contemporary techniques have been developed and refined to ensure reduced execution times and labour requirements, thereby accelerating construction schedules and facilitating the integration of motorised systems.

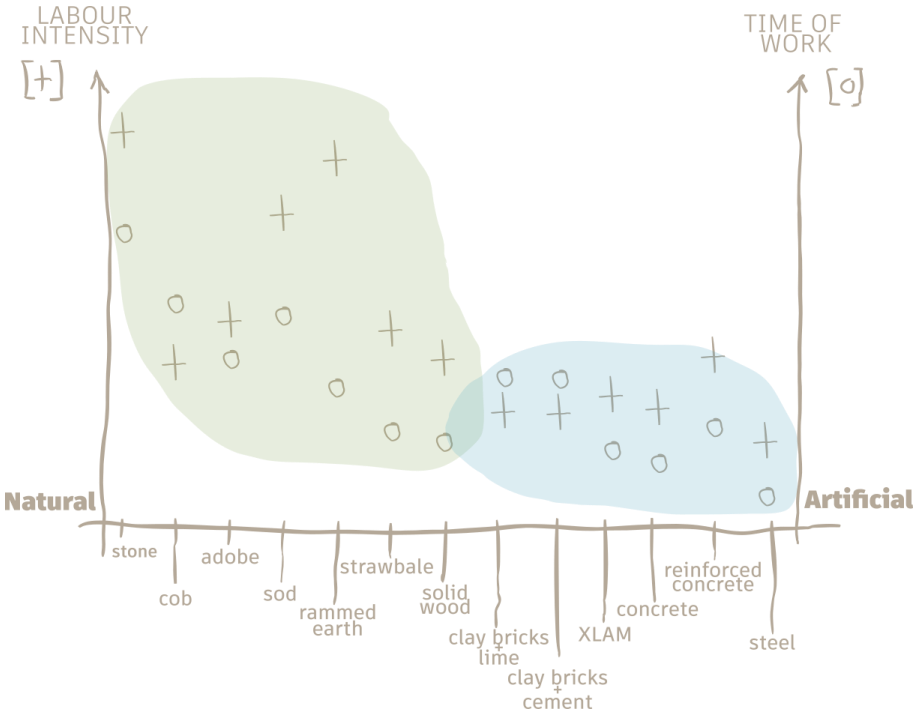

Figure 12 : Chart showing the difference between traditional and modern techniques. (source : Arthur Bohn)

The nature of this research is to observe construction products made of natural materials from the point of view of mechanical resistance. This aspect is related to many

conditions, such as the load applied to it, the number of floors, the homogeneous distribution of loads, or the climatic and topographical context of the geographical area.

The first technique is examined from two distinct perspectives. The first aspect is a full-scale study of the failure mechanisms of a low-pointed arch. The results of the test provided tangible evidence of the failure and the intrinsic resistance of the architecture, understood as an alchemy between an archetypal form and the materials that constitute it, according to a certain implementation technique. The second aspect was the appreciation of different ingredients of this material by following the research currents of the last decades on hemp-lime. The latter was done through the observation of the mechanisms of failure by compression of a set of samples.

The second technique is called “Confined recycled aggregates”, an innovation that uses the recycled crushed materials of demolition as filler of a metallic cage. The goal of this section of the research was to identify a correlation between a numerical model and a real basement built on site to load a light earth pavilion.

3 Hemp-lime : a wet construction technique

3.1 Introduction

The invention of hemp-lime comes from Charles Rasetti who conceived of mineralising hemp in the same way as wood was mineralised with sodium silicate Na2SiO3 (to make it rot-proof and non-flammable) [31]. In Italy, the production level remains inadequate, and demand remains negligible.

The first results of the Life Cycle Assessment of hemp (fibre and hurds) date back to 2006 (and was done by INRA and the French Ministry of Agriculture and Fisheries). The carbon equivalent of the hemp hurds was found to be 1.9 kg CO_2eq/kg and the carbon equivalent of the fibre was 1.7 kg CO_2eq/kg [31].

Therefore, considering these parameter values, Table 1 shows the GPW (Global Warming Potential) by presenting the equivalent carbon dioxide emissions for both a hemp-

lime construction and a brick-wall and concrete construction. For the same floor area, the result is almost opposite. This indicates that the ecological benefits of hemp lime offer opportunities for the future of construction.

	Hemp building	**Conventional building**
100m^2 housing	**- 11 t CO_2eq**	**+15 t CO_2eq**

Table 1 : Embodied carbon example [31]

The density varies according to its use. It ranges from 250 kg/m^3 for hemp concretes used as roof insulation material, to 350-450 kg/m^3 for hemp concretes used for walls and 500 kg/m^3 for hemp concretes used for floor insulation [32]. It is important to note that the density of such materials depends essentially on the binder/aggregate ratio. The density of the binder is much greater than that of the hurd.

The culmination of this research was expected to be the construction of a pavilion made of hemp-lime composite, with the intention of achieving load-bearing strength. To accomplish this objective, the research plan was to be executed on samples of various compositions. A full-scale prototype was prepared based on previous tests that had been conducted during the master's thesis of Gustavo Zapponi and Elena Tenca [33].

The primary purpose of this research was to identify and experiment with optimised formulations of hemp-lime, by enhancing the material's mechanical properties and rendering it suitable for load-bearing application. This enhancement was investigated through a cross-analysis of the effects of carbonation, moisture content, and their influence on mechanical properties. The attempt was to develop a non-destructive evaluation method for the mechanical strength of a full-scale prototype, based on established physical correlations from laboratory samples and in situ data measured using embedded sensors within the material.

3.2 Binders

The term "binder" refers to a physical effect, that is to say the property of maintaining cohesion between different elements, but in reality, it covers many functions. Binders can include additives that act as catalysts or set retarders. They can also by mixed with fillers,

mainly in cement technology, where the role can vary by enhancing the properties of the binder material such as improving workability or enhancing durability, or even improving strength (fly ash, silica, clay or slag for example).

The evolution of binders in the history of mankind is linked, as explained above (see chapter: 2.2From natural materials to artificial products), to the discovery of the firing of minerals. Professor Domenica Caputo and her team have grouped together in an essay published in 2020 the oldest archaeological discoveries demonstrating the use of different binders, which made it possible to date them. [18, p. 121]. The first artificial binder to be discovered was chalk, around 8000 B.C. Below is a timeline describing the different moments of discovery of known binders (Figure 13). This is followed by the random variability of nature, which allowed humans to create hydraulic binders, thanks to the impurities found in the raw material limestone to be fired to make lime.

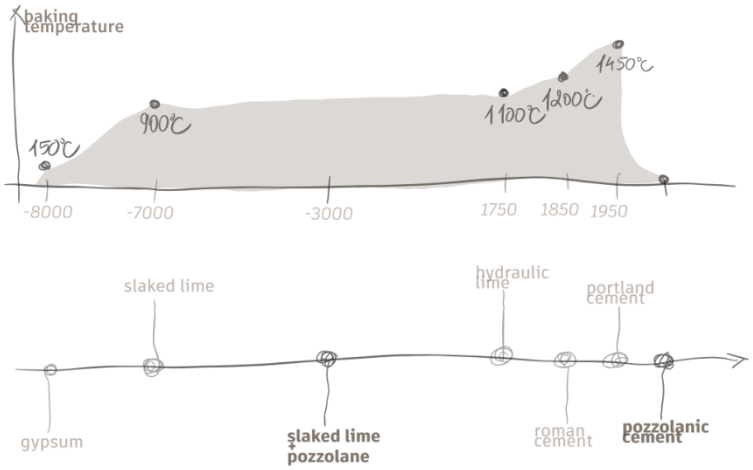

Figure 13 : Evolution of baking binders

3.2.1 Air lime

There are different types of air lime, whose chemical composition determines the sequence of crystallisation reactions. Hardening results from the carbonation of calcium hydroxide under the effect of carbon dioxide in the air, according to the reaction:

$$Ca(OH)_2 + CO_2 \rightarrow CaCO_3 + H_2O$$

Equation 1 : Carbonation of carbon hydroxyde

The main chemical elements are calcite (CaO) and magnesite (MgO), but there are also elements considered impurities, namely aluminates (Al_20_3), silicates (SiO_2) and iron oxides (Fe_2O_3).

Lime types can be defined according to three parameters: firing temperature, calcium carbonate content and clay content in the parent rock. While the first two factors can be used to classify air lime as pure, lean or fat lime, the last is essential for quantifying the hydraulic properties of the lime.

In Piedmont (Italy), the extraction of marls was started by the cement industry in the Casale Monferrato area. Over time, they have almost completely lost their economic importance, currently being replaced by limestones with a high $CaCO_3$ and low $MgCO_3$ content, which, mixed with silica-aluminous additives, become artificial Portland cement [34].

The limestone quarries in Piedmont have, in the past, quarried carbonate rocks, both sedimentary and metamorphic. This can be explained by the fact that a modest local market once made up for the difficulties of transport: in the mid-19th century, more than 400 limestone quarries were active in Piedmont, which, considering the number of employees (just over 500), were presumably very small [34].

3.2.2 Hydraulic lime

Hydraulic lime comes from the firing of a less pure limestone, containing alumina and silicates that are generally found in clays. Firing at a higher temperature (around 1400°C) gives the binder produced the ability to crystallise and harden, even when surrounded by water. Hence its use by the Romans, for example, as mortar for cisterns and aqueducts. Hydraulicity is quantified by the ratio:

$$L = \frac{\%(SiO_2) + \%(Al_2O_3) + \%(Fe_2O_3)}{\%(CaO) + \%(MgO)}$$

Equation 2 : Hydraulicity ratio formula

It is important to differentiate between the different types of hydraulic lime. The UNI EN ISO 459-1:2015 standard defines the terminology. The code NHL indicates a “natural hydraulic lime”; its hydraulic properties are due solely to the "impurity" of the stones used in the firing process, not to added artificial products.

3.3 Additives

3.3.1 Pozzolan

Pozzolan, being a volcanic material, is not an indigenous product in Piedmont. Pozzolan should be categorised according to the mineralogical order in which it is found. Natural pozzolan is a pyroclastic rock, meaning that it is of volcanic origin, where rapid contact with air has rendered the magma glassy [15]. The average density of pozzolan is around 0.85, which is particularly light, making it suitable for use as lightweight backfill or lightweight screed aggregate [35].

3.3.2 Gypsum plaster

Gypsum plaster is a product obtained by the gradual dehydration of gypsum. Gypsum is a natural rock ($CaSO_4.2H_20$) that belongs to the evaporites, the sedimentary rocks that are the most soluble in water. It is found in places where water has disappeared over millennia.

Gypsum plaster is created by eliminating the water contained in gypsum by exposure to high temperatures, according to the following equations:

$$CaSO_4.2H_2O = CaSO_4.\frac{1}{2}H_2O + \frac{3}{2}H_2O$$

Equation 3 : Dehydration I of gypsum

$$CaSO_4.\frac{1}{2}H_2O = CaSO_4III + \frac{1}{2}H_2O$$

Equation 4 : Dehydration II of gypsum

$$CaSO_4III \rightarrow CaSO_4II$$

Equation 5 : Dehydration III of gypsum

Equation 3 is obtained by exposure at 100°C. Equation 4 at 200°C. Equation 5 between 220°C and 350°C. In this study it is expected the gypsum plaster to improve the mechanical strength of the hemp-lime mix [36]

In Piedmont, there are five quarries currently in operation, all concentrated in the northern part of the province of Asti (municipalities of Castelnuovo Don Bosco, Cocconato/Montiglio, Moncalvo and Calliano) and in the westernmost part of that of Alessandria (municipality of Murisengo) [34].

3.3.3 *Cocciopesto*

Cocciopesto is a mixture of crushed terracotta fragments (such as bricks, tiles, or ceramics) combined with hydraulic lime or slaked lime. Chemically, *cocciopesto* consists of kaolinite, a mineral that, upon calcination, transforms into metakaolin. Kaolinite is contained in kaolin, a clay rock. Kaolinite includes alumina and silicate in the form $Al_2Si_2O_7$ [37].

Traditionally, it has been used as a plastering additive for walls and floors. The composition varies depending on the region and era, but all *cocciopesto* is known for its durability and resistance to moisture.

3.3.4 The quicklime

Quicklime has been used and documented in publications by Loriot [38]. Charles Frantz, the new editor of the 1774 edition of Loriot's masterpiece "Mémoire sur une découverte dans l'art de bâtir" describes:

« Le secret consiste en un simple mélange de sable fin, de brique pilée, de chaux vieille éteinte, gâchés ensemble avec une quantité suffisante d'eau, auquel mélange on ajoute un quart environ de chaux vive en poudre, au moment d'en faire l'emploi. »

("The secret consists of a simple mixture of fine sand, crushed brick and old slaked lime, mixed together with a sufficient quantity of water, to which about a quarter of quicklime powder is added when the mixture is used.")

Loriot's intuition and genius has since been put under the microscope by various research teams, among them the Seymour et al. to explain substantially the use of quicklime in the setting of air lime-based mixtures [39]. Seymour et al. consider that the high number of calcium atoms in the mortar extracted in the Naples region is due to high temperatures. These would be linked to the addition of quicklime, the exothermic nature of whose extinction by hydration is well known. The team was able to conclude that the different forms of calcium found in the samples and then reproduced in the laboratory came from several sources and several ingredients.

It might therefore be interesting to produce a series of samples in which quicklime and pozzolan come together to form a complex binder with high hydraulic properties. This

approach was followed throughout the course of the research trying to reach similar conclusions.

3.4 Aggregates

3.4.1 Hemp

Fibre and hurds (or shives) are obtained from the stem of the plant through a mechanical separation process. In the construction sector, hemp fibre is primarily used as a thermo-acoustic insulating material. Hurds, on the other hand, as a by-product, are often considered waste. Until the 1950s, Italy was the world's second largest producer of hemp, after Russia, with 100,000 hectares dedicated to its cultivation.

According to a press release of the Piedmont Regional Council dated 8 February 2022, about 200 hectares are cultivated in Piedmont today. According to Gilberto Barcella [40], in a year, one hectare produces 12 tonnes of biomass, equivalent to four years of forest cultivation. This means that each year, Piedmont produces 4,400 tonnes of biomass directly from hemp cultivation.

3.4.1.1 Hemp hurds

Aggregates of plant origin have very different characteristics to the mineral aggregates traditionally used in binding mixes, for which standardised characterisation tools and techniques exist. Due to the structure of the stem of the plant from which they are derived, they are generally elongated, highly porous and deformable, with a low bulk density.

Such aggregates (Figure 14), derived from the stalks of herbaceous plants cultivated for their fibres (hemp, flax, etc.), are deformable, elongated and highly porous due to the structure of the stalk of the plant from which they come, with a low apparent density [41].

Hemp straw is made up of very long, lightly lignified cortical fibres surrounding a woody part (short, highly lignified fibres) in the centre of the stalk, corresponding to the part that carried the sap during the plant's growth period. The woody part is the hemp hurd. The density of hemp hurd varies between 70 and 110 kg/m^3 when it is loose [41]. In fact, due to its high porosity, the apparent density of the solid phase is considerably higher, around 1500 kg/m^3. The porosity of the material poses the problem of knowing whether it is intra-granular or intergranular porosity. Indeed, if the void index is based on the quantity of solid matter in relation to the space left free, then the hemp hurd has a high intra-granular porosity, of the order of 85%, and an inter-granular porosity, located between the hemp hurd particles with accidental geometries, of around 60%.

There are no standards governing the grain size of these bio-sourced aggregates so far. They differ considerably from the mineral aggregates commonly used in hydraulic concrete, which are characterised by greater homogeneity, high rigidity, and significantly higher density, and for which standardised testing and characterisation methods have been established. There are numerous methods for classifying particle geometry. Measuring particle length and width can give different results. There are two main quantities: the Féret method considers the maximum and minimum diameters. The second method consists of applying an ellipse whose large and small diameter centres correspond to the centre of gravity, and its projected area is identical to the ellipse modelled in this way [42].

Figure 14 : Hemp hurds

3.4.1.2 Hemp fibre

Hemp is a fine bast fibre (Figure 15), characterised by a light colour. It is obtained through the retting process and has a good strength. The colour and cleanliness of the fibre can vary considerably depending on the preparation method employed. The lower grades are characterised by a dark cream colour and a high proportion of non-fibrous matter. In 2020, the main production countries were France (14,550 ha), Lithuania (6,000 ha) and Germany(3,600 ha) [43]. The fibre under consideration ranges in length from 1.0 to 2.5 metres. Hemp is now being used, amongst other natural fibres, in thermoplastic matrix composites for internal structures in similar automotive applications to those for flax fibres [44].

Hemp fibres have a very high tensile strength and were used in the past as rope materials for marine and other applications. In fact, in addition to its mechanical strength,

this fibre was known to resist chemical and physical attack from seawater and the effects of the sun. The elastic modulus of hemp is as high as that of glass fibre, but is by far the highest compared with its density [44]. On the other hand, its maximum elongation before break is lower than that of other fibres, whether vegetable or not.

Figure 15 : Hemp fibres

4 Confined Recycled Aggregates: a dry construction technique

This study investigated also the validity of numerical models applied to gabions constructed from recycled aggregates. The evaluation entailed the simulation of the internal constraints of confined recycled aggregates under a certain load, followed by a comparison of the results with those derived from a full-scale experiment. This approach facilitated the evaluation of the reliability of numerical models in real-world settings, thereby identifying potential discrepancies between simulations and experimental observations. The objective was to enhance the precision of these models for future applications in the design of sustainable structures.

4.1 Recycled aggregates in figures

Each year, the construction and demolition waste sector processes just under 80 million tons of waste, with 81% being sent for recycling. Nonetheless, only slightly more than half of the recycled material is currently reused in practice [45].

Confined Recycled Aggregates (CRA) refer to gabion-based elements. Indeed, it should be pointed out that "confined recycled aggregates" can be defined as a systemic (or circular) design innovation of the gabions, because most of the mass of the final product is derived from recycling by sorting construction debris. Sorting is important in order to fill a metal cage with as many elements as possible in order to provide excellent stability and optimum load distribution, without outflow of small particles.

In 2024, Italy ranked third among European countries in terms of C&D waste generation. The amount of C&D waste in Italy is nearly five times the average amount of waste in other European countries (10,303,676 tons in 2024). Specifically, Italy has a total of 43,045,079 tons of C&D waste [46]. It is essential to implement a comprehensive approach of the management of this significant volume of inert materials.

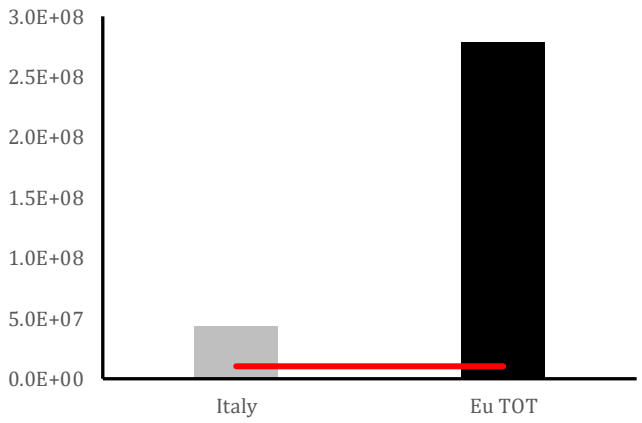

Figure 16 : Construction & Demolition Waste in Europe and in Italy [t] (source:JRC Technical Report)

Furthermore, in accordance with the findings of the study in Figure 17 [47], The distribution of C&D Waste, demonstrates the prevalence of concrete and brickwork, as well as mineral-based materials, in various European countries. The geographical distribution of the region is as follows: the western region is assigned to France, the southern region is assigned to Italy, the eastern region is assigned to Poland, and the northern region is assigned to Norway.

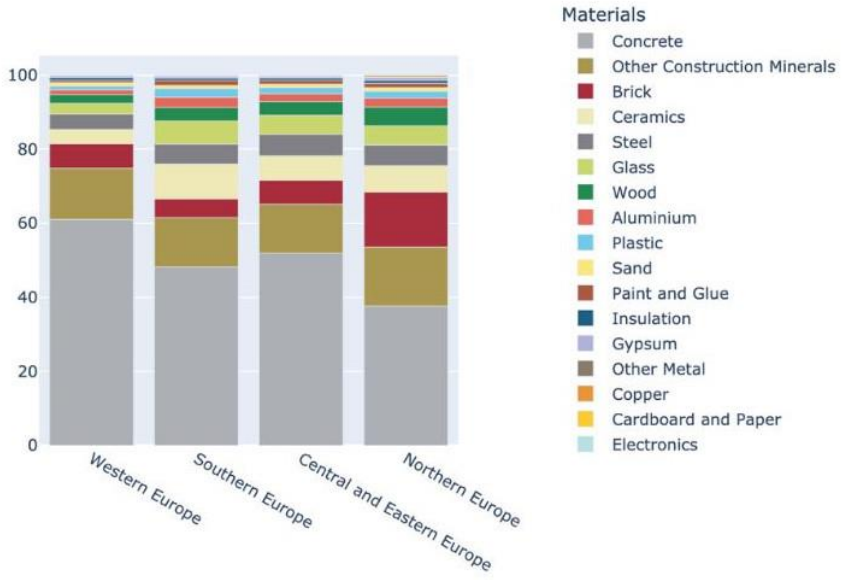

Figure 17 : Relative material mass [%] originating from Demolition and Renovation activities in 2020 [47]

However, Italy has yet to successfully transform these materials into valuable commodities. According to the Associazione Nazionale Produttori di Aggregati Riciclati (ANPAR), despite the consistent growth in the recycling of materials Figure 18, approximately 50% of these materials remain unused [48]. Therefore, it is imperative to propose an alternative method for the reuse of the demolition debris. The confined recycled aggregates gabions seem to represent a promising technology in this field.

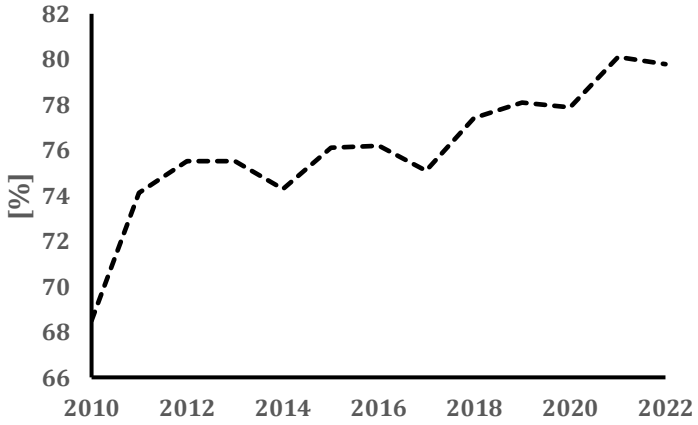

Figure 18 : Part of recycled C&D waste (source: ANPAR)

The challenge posed by gabions in confined recycled aggregate settings stems from the heterogeneity of the aggregate materials utilised. Consequently, the statistical sample size is increased to accommodate a greater degree of uncertainty. Furthermore, according to [49], there are aggravating factors present within the context, including exposure to water. Indeed, an investigation was conducted into the resistance of concrete within a cement-based mix. The results indicated that the resistance of concrete decreases in proportion to the water ratio present in the mix. The findings indicate that the resistance to compression is reduced by half when the ratio of water to cement (W/C) transitions from 0.38 to 0.58.

4.2 Steel vs Recycled Aggregates : high technology vs poor materials

Steel may be stainless or galvanised. The choice between these two materials should be made taking into account a number of factors, such as corrosion resistance, general durability, cost and aesthetic appeal.

The lifespan of a gabion is typically 20 years in natural and humid environments. This is significantly shorter than the minimum of 50 years recommended by current standards for residential structures. It was therefore necessary to consider the CRA in its entirety and in accordance with the specific context in which its implementation is desired. It is evident that within an urban or suburban context, the conditions of humidity are more favourable allowing doubling of their life span. It is conceivable that a more robust treatment for the steel could be achieved through a zinc galvanisation process. However, it is imperative to consider the environmental implications of such an approach.

It is therefore conceivable to apply a galvanising process, which would enhance its protection against corrosion and, consequently, extend its lifespan. The embodied energy of steel is estimated to be around 35 MJ/kg, while that of galvanised steel is reported to be around 39 MJ/kg [50]. This discrepancy enables the incorporation of galvanised steel in the gabions of the CRA, thereby enhancing their longevity and reducing their energy intensity.

Stainless steel is composed of a percentage of chromium. This forms a protective oxide film that makes it highly resistant to moisture, chlorides and other corrosive agents. Galvanised steel is covered with a layer of zinc that protects it from corrosion. This layer acts as a barrier, but if damaged or if exposed to very severe conditions the protection can degrade over time. Thus, the service life of galvanised steel depends on the thickness of the zinc coating, whereas stainless steel has a much longer service life. Finally, stainless steel is significantly more expensive than galvanised steel, both in terms of material cost and processing. Stainless steel is not a good solution for ecological reason, because it has a much higher embodied CO_2 value than galvanised steel, which is around 2.6 tCO2eq/ton of steel product) [51].

The grid must be made of twisted steel wires, a configuration that gives it greater resistance due to the synergy of friction and traction during service. In the case presented here, the assembly, as well as the creation of the cutting and folding pattern, was done directly on site. This can pose certain problems in terms of connections and seams, but the whole process is analysed later (8.2: Construction phases).

PART II / METHODOLOGY

5 Empirical correlation about hemp-lime

Natural materials have not yet undergone standardisation. Indeed, traditional materials had been relegated to a subordinate status, and new materials such as concrete, fired bricks, and steel were given greater prominence due to their marketability and contribution to the development of an economy based on profitable industrial processes. [52]

In a society where the efficiency is paramount, it is important to be able to translate a real phenomenon into numerical data that assesses its intensity and frequency. The challenge would be to demonstrate in quantitative terms, in the field of service, economy and life cycle assessment, that many materials with natural origin are as interesting as, or even superior to, their artificial competitors.

Are the industrial and economic effectiveness, as well as the energy efficiency, of the natural materials highlighted here, (hemp-lime), sufficiently competitive in relation to the artificial materials generated to respond solely to economic and industrial problems?

5.1 Considerations

5.1.1 Framework

This initial study, focused on the hemp-lime composite, adopts an approach in four steps. It begins with a critical review of the scientific literature sought at identifying the most relevant additives for enhancing the mechanical performance of hemp-lime. The second phase involves a targeted investigation of the sustainable construction market to identify a high-strength air lime-based binder that is produced in northern Italy. This binder was intended to be used in the construction of the prototype and has been compared to the formulations identified in the literature review through a parallel sampling campaign

designed to monitor the solidification behaviour of the mixes over an extended period of one year, consistent with the carbonation reaction of air lime. Finally, a physical correlation study was conducted between laboratory-tested samples and the constructed prototype, with the objective of establishing quantitative relationships between carbonation depth, moisture content, temperature, and elastic modulus. The goal of this study was to quantify the averaged compressive strength of the mixture used to build the prototype of the low pointed arch.

For further reading, it seemed interesting to develop a reflection upon statistics. Thus, conclusions have been drawn based on tests on a quantity of samples [30]. Empirical knowledge of a physical phenomenon can be described statistically following a succession of tests.

5.1.2 Tradition and Statistics

The nature of statistical approaches involves a necessary simplification of reality, like a transition from the abstract to the real, because from the infinity of the world, human beings require the construction of a finite order in order to make sense of their context. [53]. The drive to create a finite order is deeply rooted in human cognition. As Georges Perec wrote, "it is so tempting to want to distribute the whole world according to a single code".

Another extremely important aspect of construction is human safety. Society has a duty to protect itself, and the trust of its members becomes the only factor that can guarantee the cohesion of the whole. The opposite is a dictatorship, an order of repression and submission, more akin to the mechanical world of machines than to the human world. Confidence in the social order is established through the group's management of the injustice experienced by the individual, or more broadly, through preventive measures taken before an incident occurs, eliminating the damaging event to take place. The designer, along with the builder and other technical professionals, is protected by society in the exercise of professional duties. However, this protection is conditional upon adherence to established codes, at least those recognised by a defined group acting as a guarantor. Accepted practices represent the earliest form of contractual agreement, allowing professionals to demonstrate good faith and respect toward society, which, in return, grants permission to proceed. Historically, the regulations governing the industry were transmitted in an informal manner, or without adherence to contemporary legal principles The phenomenon under consideration was characterised by empirically validated repetition, and over time, it was subject to a process of increasing consolidation. Assessments were not measurements, but rather a binary and practical validation of the technique used.

However, the role of statistics in this context merits further consideration. The notion of statistics has existed since the earliest civilisations, with the counting of items such as

livestock and the role of data collection. Despite the early mathematical work of Fermat and Pascal in the 17th century, the predictive use attributed to statistics today dates more likely from the 18th century, when Antoine Depracieux wrote about the probability of human lifespan. This concept soon came to be used by life insurance companies.

Drawing on Yannick Macé's thoughts on the use of statistics in medicine [53], the use of nomenclatures ensures the transition from specific analysis to categorical analysis. Thus, standards protect professionals from error by aligning practice with the logic of statistical reasoning, thus reinforcing reliability and consistency in outcomes. In addition, the concepts of classification and categorisation have facilitated a means of communication among professionals and the transmission of proven expertise.

In conclusion, consenting to prefer relevant information about a population of samples, a mechanical strength phenomenon or fracture kinetics entails renouncing reality and its infinity. This question is approached here through discrete and continuous statistical analyses on a population of samples of various hemp-lime mixtures subjected to a compression fracture test.

5.1.3 Load-bearing purpose

Recent developments in the construction market have seen the emergence of load-bearing hemp-lime blocks, marking a significant advancement in the field. Despite its natural Roman cement binder, the product’s load-bearing capacity is derived from the numerous steel rebars cast in place. Indeed, certain blocks are equipped with a provision hole that enables them to function as moulds for the casting of reinforced concrete. Similarly, the lintels are reinforced concrete beams. Therefore, even if the construction times are significantly reduced, the carbon and energy footprints remain considerable. It would appear that the key issue is not solely the composition of the hemp-lime blocks; it is crucial to take a step back and examine whether the geometry can be a determining factor for this technology.

In case evidence that the material can withstand compression and shear forces induced by the structure’s geometry, as well as accidental and variable actions in use, then architectural shapes can be generated to contain the forces in the hemp-lime material.

Consequently, the implementation of a pointed vault represents a precise structural solution to managing the transition from vertical supports to horizontal spans. This approach enables for the exploration of the concept that a single material can be employed to construct the entire structure of a building. It is evident that this would necessitate

adherence to the architectural expression inherent in the fundamental properties of this innovative composite mixture of lime and hemp.

5.2 Experiment setup

5.2.1 Introduction

As the term "correlation" is used to quantify the strength of an association between two variables, it was preferable to use the term "relationship" in this context. Here the affinity between several quantities have been studied in order to assess the soundness of the experiments. Eco-construction technology seems to be closer to biological behaviour than to an equation whose solutions are known or solvable in advance. For this reason, it maked sense to observe the behaviour of materials from a practical point of view. It might be conceivable to attempt to approximate a reaction by a repeated observation. Based on this observation, numerical parameters were extracted, and an attempt has been done to correlate the statistical values with a regression whose equation is known.

The utilisation of sample results to determine the strength and Young's modulus of a material is an input parameter in numerical modelling. This has been considered further as the first method. The results were then compared to the actual results recorded through the Digital Image Correlation technique [54]. In order to complete this statement, it is necessary to detail the strategy adopted here. The endeavour was to highlight a certain relationship between carbonation and the strength of the material. Carbonation was measured using a phenolphthalein solution as pH indicator in the mixture, as the basicity of the fresh mix decreases in proportion to the carbonation. Recalling the chemical reaction in question, calcium hydroxide absorbs carbon dioxide from the air to generate calcite once again. The further the carbonation reaction progresses, the more the material regains the solidity of the original limestone from which it is derived. The correlation between the mechanical compressive strength, and the distance between the outer edge of the subject and the outline of the purple reaction spot, have been established through compression tests on a series of samples. This will be achieved by bringing the phenolphthalein and the $Ca(OH)_2$ base into contact, as previously described. Some studies have previously been conducted on the correlation between carbonation and compression resistance [55].

5.2.2 Full-scale prototype

The real dimensions of a full-scale prototype necessitated a specific expertise in the design, organisation of construction phases and, finally, construction itself. On several occasions during the design stage, technical solutions turned out to be unfeasible due to the

emergence of constructability issues. It is crucial to emphasise that the materials used are not conventional. However, the human scale enables immediate feedback regarding the decisions made during the design phase and the actual construction, enabling the conceptual development to take on an irrefutable tangible form.

A critical attribute of the prototype is its enhanced capacity to align with the contextual constraints. This is particularly the case when the research involves observing the behaviour of the artefact and the relationship with the climatic context. It is therefore necessary to distinguish between two considerations. The first one implies that high dimensions are an added value because the boundary conditions are relatively weaker than for a scaled prototype. The second, on the other hand, enables the assessment of dependence on external parameters by probing multiple depths in the mass.

The prototype thus provided an opportunity to construct a significant electronic circuit for the purpose of conducting surveys, as illustrated in the Figure 19.

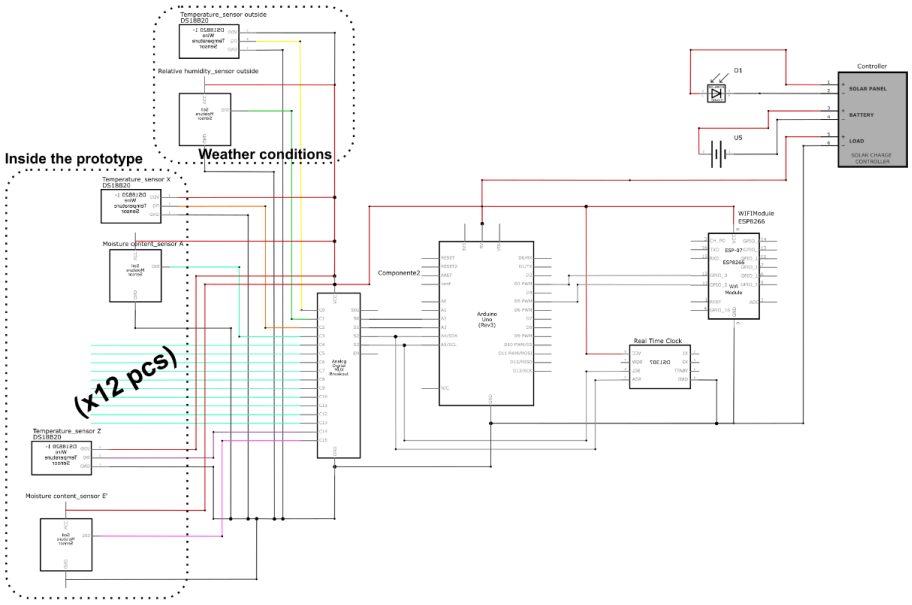

Figure 19: Circuit diagram of hand-made datalogger

The circuit consisted of an Arduino Uno board, which the analogue acquisition sensors were connected to with a 16-channel multiplexer. This component allowed the number of connected sensors to be multiplied fourfold, as the Arduino Uno board only supports four analogue inputs by default. Three types of sensors were used: the first combined the temperature and relative humidity of the air, the second type probed the temperature in the mixture, and the third probed the water content of a relatively homogeneous medium such as soil. The whole system was linked to a battery-powered clock, so it was possible to

record the precise moment of acquisition of each data item. Data were acquired via a continuous internet connection and a NodeMCU platform, which enabled the data to be transferred in real time, based on IoT (Internet of Things) technology. To power the entire circuit, an off-grid photovoltaic power supply set up with a 50-Watt panel and a 17 Ah battery was installed. The scheme of the entire system is shown in Figure 19.

Computer scripting and design are developed concurrently with the technological implementation and the configuration of electronic components. It seemed useful to illustrate here one of the most crucial phases for the accuracy of the analogue data perceived and then transmitted by the probes.

In order to avoid errors during the construction phase, it was essential to test multiple times, especially with each circuit update. All the moisture content probes are powered up to ensure that the connections and soldering have been carried out flawlessly. This will greatly facilitate the task during installation inside the arch prototype.

5.2.3 Samples

The laboratory samples represent a significant part of the research summarised here because they bring to understand how certain additives may improve the mechanical properties of lime-hemp mixtures. In addition, two options were considered beyond the selection of the additive, with the consideration of the presence of hemp fibres measuring an average of 2.5 cm. Thus, the research demonstrates the relationship between lime-hemp mortars and their most common additives found in the market and construction sector : quicklime, gypsum and pozzolan.

The sample quantity population was an important factor in the robustness of the results. Therefore, each result presented in the tables and graphs is calculated based on the average of three values, derived from three identical samples in terms of construction, proportion, and compaction. Each sample must be prepared continuously, without interruption or change in procedure, throughout the entire experimental campaign.

The storage of the materials was conducted in a dry environment, protected from climatic conditions. However, for practical reasons, the research was unable to conduct quantitative monitoring of the temperature and hygrometric conditions. It isimportant to note that the storage area was an opened barn. The samples were therefore able to withstand external conditions without being exposed to the risk of rain.

5.2.4 Correlation between measured values and trends

Subsequent to this, a correlation has been established between the two experiments. The objective of this research study on hemp-lime was to integrate the results from the samples with those from the prototype at a scale (indicated in red). The representation of relationships in the form of dotted arrows was developed and results are presented in the chapters 7.1.9, 7.2.6 e 7.3. The entire methodological process has been implemented using several logical connections represented by letters on Figure 20.

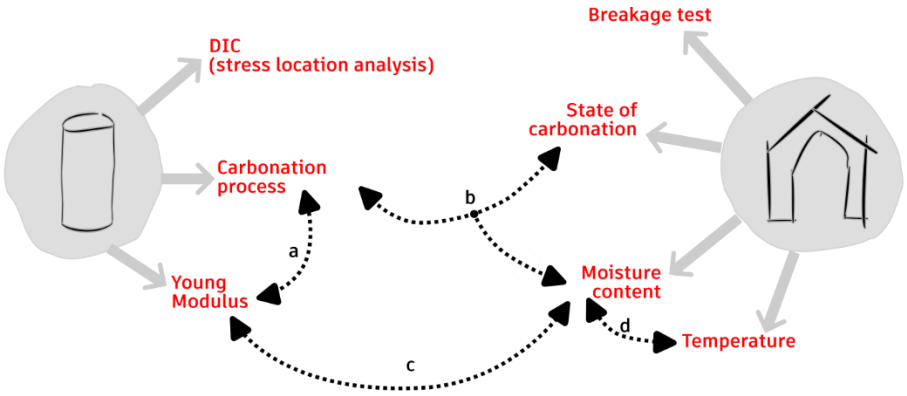

Figure 20: Scheme for hemp-lime study showing the diverse correlations

These are detailed below:

a: After breaking up the samples, the carbonation strain was measured using a phenolphthalein solution. This depth of carbonation was then related with the value of the Young's modulus measured during compression fracture: $Carbonation_{samples}$ **vs** $E_{samples.}$ See 7.2.6.4: Strength over Carbonation for results.

b: Once the prototype has been broken, carbonation was measured at the points where the probes were used to measure water content, and the results were compared with the carbonation levels in the samples: $Carbonation_{prototype}$ **vs** $MC_{prototype.}$ See results in 7.3.2: Moisture content over carbonation.

c: The level of carbonation was then plotted on the graph drawn up in phase "a" to determine the strength of the mixture. A correlation was then established between the water content at the time of breakage of the prototype and its mechanical strength, using Young's modulus: σ(Carbonation) **vs** MC. See 7.3.4: Moisture content over compressive strength.

d: This stage proposed to observe the interactions between water content and temperatures as a function of the thermo-hygrometric outdoor conditions. Results are shown in [21] and in 7.1.9.1: Temperature.

5.3 Physical equipment for data acquisition

5.3.1 Full-scale prototype examination equipment

In order to collect data continuously and without destructive testing, sensors needed to be inserted during the construction phase. Below is illustrated the range of instruments that enabled continuous monitoring of the internal state of the prototype.

Results are indicated in 7.1.9 : Results, according to the positions of the sensors illustrated in Figure 21. The name is composed of a letter (representing the position inside the prototype), a number (1 or 2 depending on the depth inside the section cut of each position), and MC (Moisture Content) or T (Temperature).

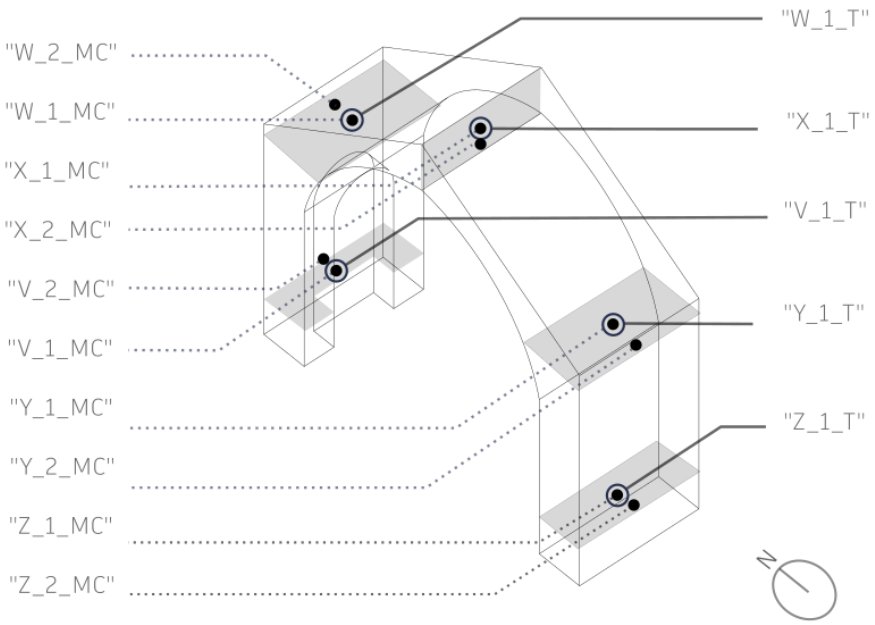

Figure 21 : Sensor positioning inside the prototype

5.3.1.1 Arduino Uno Board

Arduino is an electronic component company that was born of a revolutionary idea to design an electronic board capable of processing input information and outputting other

information. It is widely used in mechatronics because it supports numerous combinations of components thanks to its pins and can be programmed using its programming language. In research, it is a major, cost-effective asset because it can be used to collect information from probes of all kinds and process it in real time, as well as storing or sending it depending on the experimental strategy chosen.

For the purposes of this research, the Arduino Uno board was used to concentrate integrated probes in the material being studied, and to send the results at defined intervals, together with the date and time to which each set of values corresponds. Thanks to a Wi-Fi component, the entire thread at each interval could be published on a shared document in the cloud.

5.3.1.2 Moisture content sensor

The "Hygrometer Modul V1.2" sensor (manufacturer: Sing Fat, Honk Kong) was supplied with 5 V DC (Figure 22). About the type of sensor, a capacitive approach was considered, as opposed to a resistive one. It is connected to the Arduino circuit via a phase cable, a ground cable and a data acquisition cable. Arduino Uno supports 10-bit ADC, which means the resolution of the output was $2^{10} = 1024$. Therefore, in order to convert the analogue-received resistivity value R into relative water content, the following equation (Equation 6) was applied:

$$mc_{rel} = 100 - (\frac{R}{1023}) \times 100$$

Equation 6 : Calculation of relative moisture content

This involved converting the analogue value of the signal into digital value. It was impossible to express the value of the volumetric water content because density of the dry mixture was unknown beforehand, which is why a scale of relative values was opted. Furthermore, in order to calibrate the values from each sensor, measurements were taken beforehand in a dry environment and in an environment saturated with water, making it possible to calculate the relative position of the raw values from each probe.

Figure 22 : Moisture content sensor

5.3.1.3 Temperature sensor

The DS18B20 sensor (manufacturer: Hilitchi, Shenzhen, China) directly read the temperature value in °C (Figure 23). It was therefore not necessary to correct the input received. The accuracy was ±0.5 °C, and the acquisition range was from −55 to 125 °C. The DS18B20 is a 1-Wire bus device, that requires only one data line for communication with a central microprocessor. The acquisition voltage was 5 V DC.

Figure 23 : DS18B20 (Temperature sensor)

5.3.1.4 Temperature and relative humidity sensor

DHT11-digital temperature and humidity sensor is a calibrated digital-output sensor that combines temperature and humidity measurements. It has three connections, including a phase, a ground connection and a digital output.

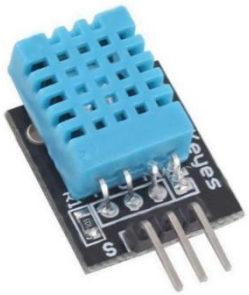

Figure 24 : DHT11 (Temperature and Humidity sensor)

5.3.1.5 Internet of Things

The devices and applications can serialise the data into JSON format before transmitting it over to the internet. The receiving device or application at the other end of

the internet “de-serialises” the JSON data and extracts the required information (Figure 25).

JSON is a common data-interchange format across the internet. IoT devices powered by Arduino can receive data in JSON format only. As microcontrollers like Arduino boards can easily encode data into JSON, it is the standard for embedded devices and applications to serialise data (like sensor data) for transmission over the internet. JSON enables IoT devices and IoT platforms and services to exchange data in a minimal footprint.

Arduino needed to be connected to the internet through Ethernet or Wi-Fi to exchange data over the internet as an IoT device. A module ESP8266 allowed to connect to the internet. On the programming side, apart from Ethernet or Wi-Fi libraries, Arduino and its compatible boards needed ArduinoJSON library to encode or decode JSON for effective communication. Attached in Annex 2 : the script document of the Arduino program.

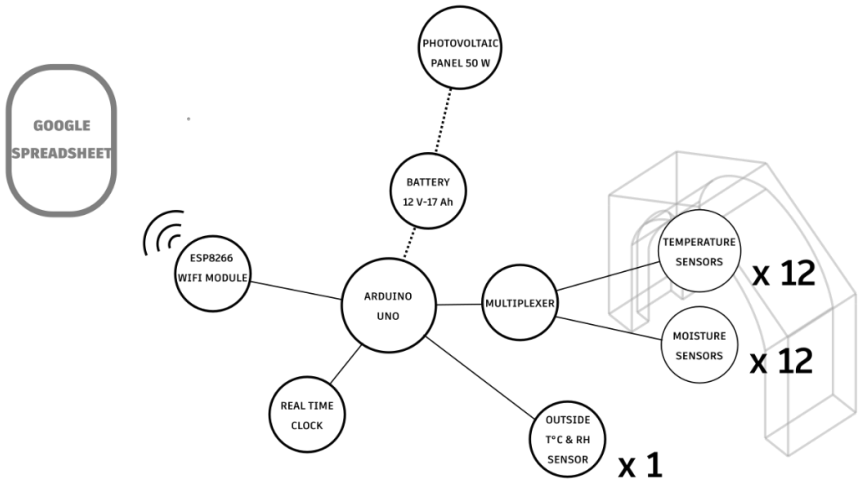

Figure 25 : Conceptual system of datalogging

5.3.2 Design and realisation of the press

5.3.2.1 The Frame

The press was made of square tubular steel with a cross-section of 40x40mm and a thickness of 2.5mm. The objective was to facilitate its transportation; consequently, the concept of dismantling it was devised. To do this, each part was screwed together so that the whole press could fit into the boot of a car, for example. The screws were fitted with a

butterfly, allowing them to be handled by hand without the need for tools, and the 6mm thread was also cut in negative in the steel of the elements, both the one on the outside of the assembly and the intermediate one. This double connection was a way of ensuring that all the parts work together when the system were loaded. The final weight was approximately 10kg.

The base was also welded to two legs by which the press could be fixed to the floor with screws (Figure 26). On the other hand, the base on which the sample under study rests was a set of welded parts that fit into the base. The press was therefore a closed system that could withstand forces in its plane that were far greater than those that could have been applied to the hemp-lime samples.

Figure 26 : Self construction of the press

A pantograph cylinder was then attached to the press frame and turned in the opposite direction so that its extension pushed down and could compress the sample simply placed on a plate welded to the frame. The cylinder was then coupled to a load sensor which transmitted in real time the pressure experienced. Its reading on a computer rendered results in continuous values and not discrete values.

The elongation of the jack was not uniform because it was derived from the square root of the sum of the squares of the sides of the triangle that modulated the jack (Figure 27). The curve represents an elongated half parabola, and its appearance was not far from a straight line (Figure 28). However, it was advisable to use only the second part of the curve if possible. That is to say that after having made a test and having made sure that the rupture was contained within the 10cm of collision, one has been able to use the displacement going from a length B of the screw of 10cm*2=20cm to 0cm (theoretical value).

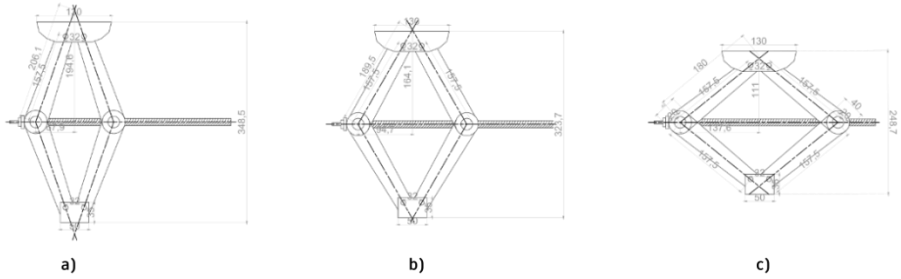

Figure 27 : Different angulations of the scissor jack element; a) 30° angulation; b) 60° angulation; c) 80° angulation

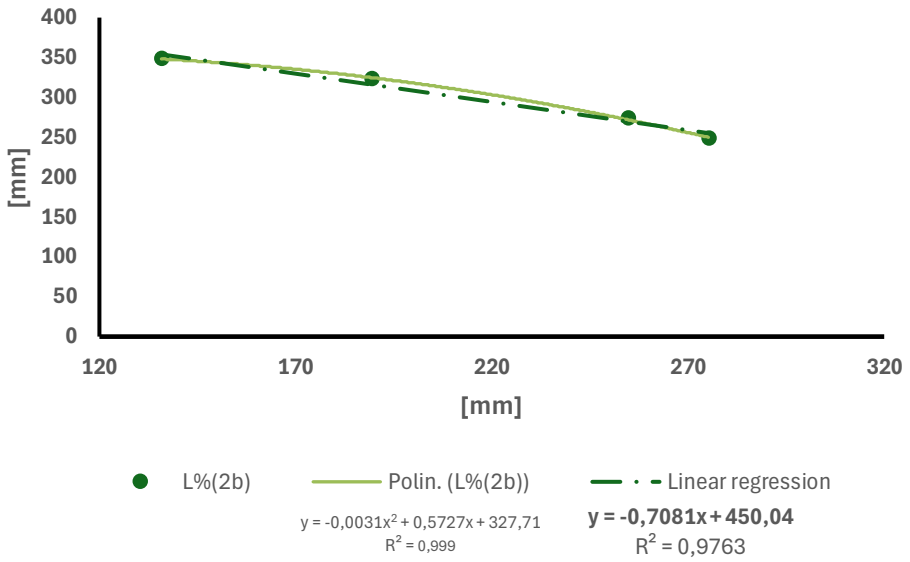

Figure 28 : Polynomial Regression of the most appropriate formula

The compressor element was a pantograph jack whose primary role was to lift a car by an axle in order to change the tyre on a wheel. The idea came up to use this instead of a hydraulic jack for the reason of having a continuous compression movement. The result iwa quite compelling; however, it iwa imperative to consider the velocity of the vertical movement. In fact, as an infinite screw in the horizontal position whose role is to bring the two articulated arms of the press closer together, the latter modified the sides of a double right-angled triangle at each instant, which had the effect of changing the hypotenuse, the final length for measuring the effect of the press on the sample.

As a mechanical test, it was necessary to take into account the speed of the solicitation. This was not automatic for these tests. It would have been more precise to fix a motor with high torque and to program using a potentiometer connected to an Arduino the inverse curve of the vertical displacement of the jack. The graph on Figure 28 shows the elongation values of the jack as a function of screwing. The linear regression indicated that it was possible to consider the parabolic curve as a straight line. This maked it much easier to assess the deformation values, which could then be read using infrared distance probes.

Figure 29 : Picture of the press during construction

The press underwent modifications during the course of the research due to the forces to which it was subjected, which rendered it unreliable. It was necessary to affix the press to the ground using buttress arms. The two axes perpendicular to the ground were consequently anchored (Figure 30).

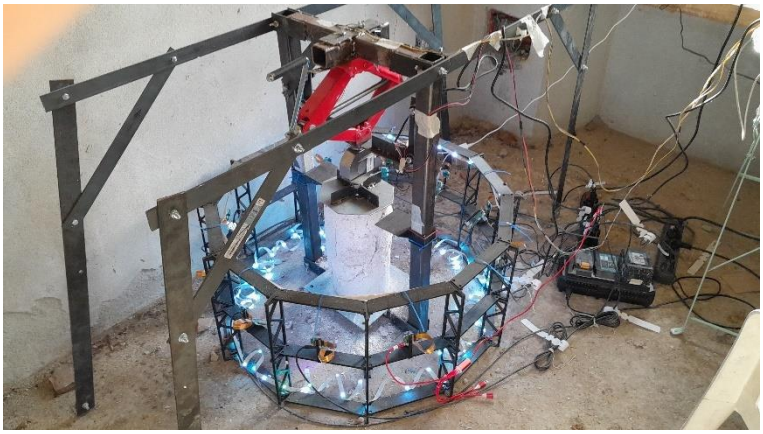

Figure 30 : Picture of the press during use

5.3.2.2 Load cell : Arduino component

The electronic components that made up the data processing and reading part are now presented in turn. Welded to the jack, the load cell measured the received weight. The load cell could withstand up to 5 tons (Figure 31).

Figure 31 : Load cell

5.3.2.3 Infrared sensors : Arduino component

Distance probes can be categorised based on the measurement method employed: ultrasonic or infrared. In this instance, infrared probes were utilised (Figure 32). In comparison to ultrasonic probes, infrared probes have been demonstrated a superior degree of accuracy, which is in the order of a tenth of a millimetre. It was important to choose a type of probe that was sufficiently accurate to recognise the first moments of compression of the samples. It therefore became necessary to choose a probe with a resolution of 0.1mm.

Figure 32 : GP2Y0A51SK0F (IR sensor)

It was important to distinguish between resolution and distance accuracy. Resolution accuracy is the capability of the measurement to discern a disparity of 10 µm between the probe and the moving object. Distance accuracy is the precision of the probe in estimating the distance value. While the initial parameter is attributed to the quality of the hardware, the second can be modified through the calibration of the probe.

The next paragraph explains the empirical method of correlating distance and the voltage value recognised by the probe. Subsequently, the mathematical translation employed a regression curve to interpret the voltage reading and establish a correlation with a precise distance.

A correlation needed to be made between the voltage received and the distance measured, as follows. Firstly, an initial programme was written to read the voltage values for a series of fixed distances from 2cm to 12cm.

The program below provided a continuous display of the voltage reading and used to acquire voltage value for each measurement 5mm apart. Successively, it was possible to interpolate the points and build a regression curve.

```
    void setup()
    {
    Serial.begin(9600);
    }

void loop()
    {
    int sensorValue = analogRead(A1);
    float voltage = sensorValue * (5.0 / 1023.0);
    Serial.println(voltage);
    }
```

Figure 33 : Script for reading voltage

Below is the corrected reading program for the 4th-order polynomial regression equation. The two infrared sensors had different equations coefficients due to physics of elements.

```
/*
Link qui correspond à la corrélation de cette sonde :
https://docs.google.com/spreadsheets/d/1m3OEWfMMs7f1mGY4LEw86iYhGoFlWV-
HNxhUsEWPXpQ/edit#gid=933372104
*/


const int sensorPin[] = {A1};
float distance[1];
const int AVERAGE_OF =10;
const float MCU_VOLTAGE = 5.0;

void setup()
{
  Serial.begin(9600);
}

void loop(){
  readDistance(0);
  Serial.print("__");
  Serial.print("d1 =");
  Serial.print(distance[0]);
  Serial.println("cm");
  delay(1000);
}

void readDistance(int sensor)
{
  //Robojax.com code for sharp IR sensor
      float voltage_temp_average=0;

      for(int i=0; i < AVERAGE_OF; i++)
    {
      int sensorValue = analogRead(sensorPin[sensor] );
      delay(1);
      voltage_temp_average +=sensorValue * (MCU_VOLTAGE /
1023.0);
    }
    voltage_temp_average /= AVERAGE_OF;

Serial.print(voltage_temp_average);
  // equation of the fitting curve
  //26,6 + -50,6x + 45,3x^2 + -19,7x^3 + 3,31x^4
  distance[sensor] = 26.6 - 50.6*(voltage_temp_average)+
45.3*pow(voltage_temp_average,2)-19.7*pow(voltage_temp_average,3)+
3.31*pow(voltage_temp_average,4);
    }
```

Figure 34 : Script for calibration curve

Each probe had its own correlation graph because the signal received was analogic. It was therefore necessary to experimentally correlate the voltage values transmitted by the probe with distance values measured on a set model.

A non-linear regression was then performed [56], and a 4th-order polynomial regression curve was found to be the most suitable choice for calibrating the infrared distance sensor according to a specific calibration curve.

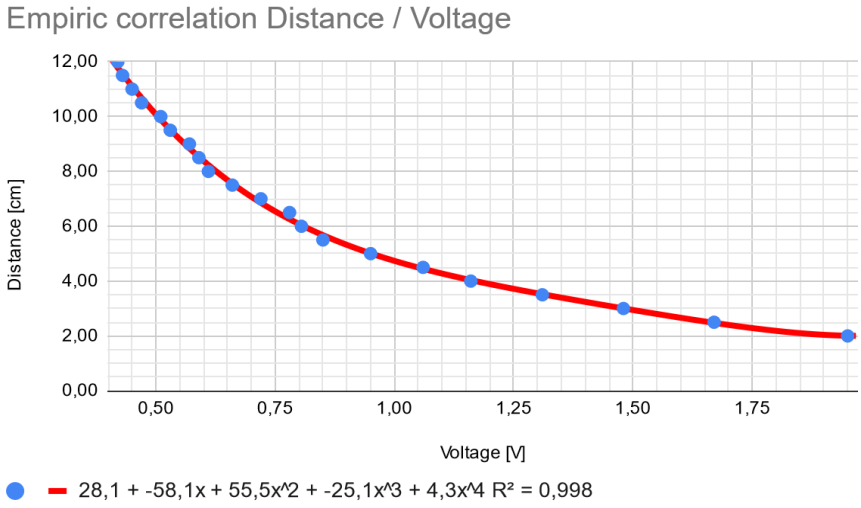

Figure 35 : Graph between voltage and distances

After calibrating the probes, the next step was to securely install the probes to the load cell. This was done by means of a thick steel bar welded to the jack and then to the screw thread that held the load cell. The attachment (in blue in the Figure 36) was a custom-made 3D model, which was then printed using a 3D printer. The probe was then clipped onto it.

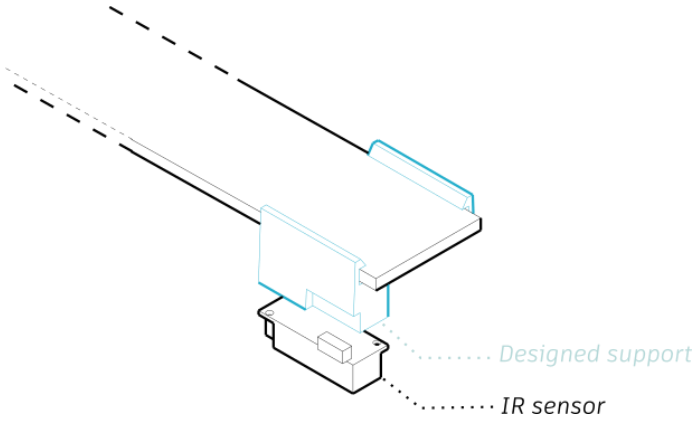

Figure 36 : fixation of the IR sensor to the support

5.3.3 Digital Image Correlation

5.3.3.1 Raspberry Pi Zero Board

Raspberry was useful for this experiment because it is a microprocessor (Figure 37). Therefore, it has the ability to manage image files. In addition, the Wi-Fi component enabled it to communicate with another informatical device. The huge advantage was that

it could display the raspberry interface on the base PC screen. However, it was not possible to preview what the camera was observing. To do this, it was necessary to connect a screen via the mini-Hdmi port.

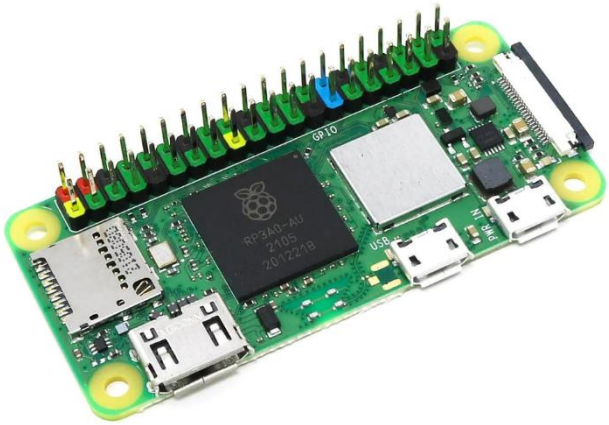

Figure 37 : Raspberry pi Zero W

5.3.3.2 Raspberry PiCamera

This small camera (30mm x 30mm) allowed to accurately record the contrasts required between black and white to build up the deformations when the model was compressed.

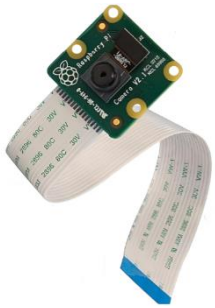

Figure 38 : Rpi camera v.2

5.3.3.3 DIC Scanner

Digital Image Correlation is a methodological framework that uses photogrammetry to digitise reality. The camera observes an object through a succession of images over time and converts point-by-point displacements into relative displacements.

The plan was to develop the Digital Image Correlation method using a series of cameras covering the revolution of an object located at the centre of the cameras. It is

based on Dana Solav's research in Biomechanical Engineering. Her biomechanics research team has developed a scanner for 3D point cloud mapping [57]. The aim of Solav's research was to observe the contraction of a muscle, in particular the calf muscle. The entirety of the points was interconnected by a total of 12 cameras, which were positioned along the entire circumference of the object.

For non-planar objects, it is interesting to place more cameras that create a 3D shape of the sample. An opensource software of imaging for medical purpose has been chosen to investigate on this feature [57]. The process of acquiring correlated images is predicated on two fundamental principles. The first one is the system calibration, used for stereo triangulation (Figure 40), and the second is the data merging.

Each point on the object has coordinates in the global reference system. And the cameras that detect this point transform it according to a combination of two matrices, the rotation matrix and the translation matrix (Figure 39).

$$\begin{bmatrix} X_C \\ Y_C \\ Z_C \end{bmatrix} = \begin{bmatrix} R_{11} & R_{12} & R_{13} \\ R_{21} & R_{22} & R_{23} \\ R_{31} & R_{32} & R_{33} \end{bmatrix} \begin{bmatrix} X \\ Y \\ Z \end{bmatrix} + \begin{bmatrix} T_X \\ T_Y \\ T_Z \end{bmatrix}$$

Figure 39 : Changing coordinates of a point to the camera reference

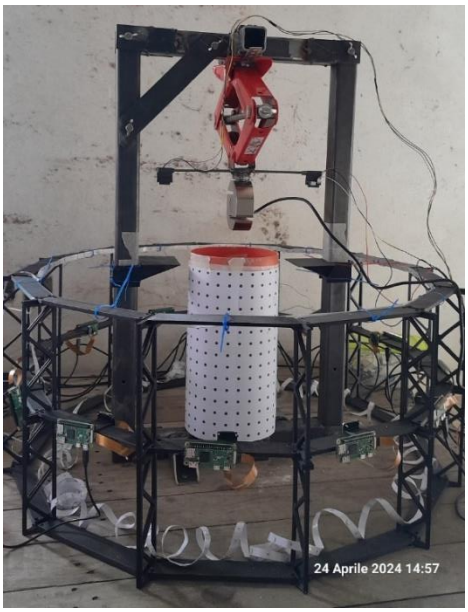

Figure 40 : Calibrating the DIC system

5.3.3.4 Scripting

The Annexes Annex 2 : and Annex 3 : contains the two scripts used to communicate from the ‘base’ PC to the 12 Raspberry Zero microcomputers. The MQTT technology (MQTT stands for Message Queuing Telemetry Transport) was used here to launch the simultaneous start-up of all the components. This technology is a lightweight, publish/subscribe messaging protocol. MQTT is widely used in Internet of Things (IoT) applications because of its simplicity and efficiency in transmitting small amounts of data between devices or systems. Consequently, I was able to organise a set of precise data as a function of time. Two scripts therefore had to be created in order to create publisher and subscriber behaviour. The first is the ‘base’ PC from which the order is sent to start and finish running the code written in each Raspberry. Secondly, each Raspberry launches the code in which it is asked to create a time-lapse and store it in a certain location in its own local memory. Annex 2 :“Publisher” python script for MQTT Connection is the script launched on the 'base' PC to start communication, launch image acquisition and stop it. Secondly, Annex 3 :“Subscriber” python script for MQTT Connection is the script that each Raspberry Zero had integrated and whose run was launched as soon as the device was powered up. This meant that no synchronisation had to be done, and acquisition could be started directly from a unique command on the ‘base’ PC.

Following the acquisition of the images, they had to be processed through Matlab scripts developed by [57]. During the processing, it became evident that some sequences of images no longer aligned after several iterations. The synchronisation was gradually challenged by the electric tensions of each device and the processing power of the microprocessor. This was why manual correction of the phenomenon was required, even if naming logic of this data enabled direct translation into input files for digital image correlation. To address this, some images were deleted. However, this resulted in the loss of the numerical sequence. At this point, a new micro-script, as outlined in Figure 41, had to be executed.

```
import os
folderPath = r'E:\CALCECANAPA\C14M1\RPI_2'
fileNumber = 1

for filename in os.listdir(folderPath):
    os.rename(folderPath + '\\' + filename, folderPath + '\\' + '2_'
+ str(fileNumber).zfill(3) + '.jpg')
    fileNumber += 1
```

Figure 41 : Renaming files python script

Thus, when using Ncorr, the images corresponded precisely to the desired sequence.

5.4 Measurement on samples

5.4.1 Descriptive parameters

The two elements under examination here, namely the full-scale prototype and the sample population, possess descriptive variables that can be compared, such as density, compaction rate, and the water-to-mix ratio. However, it should be noted that certain variables, such as compressive strength, may not be observed in the full-scale prototype due to the nature of the sample rupture tests. This text therefore sought to establish a correlation between certain parameters in order to understand their impact on the compressive mechanical strength of a construction.

5.4.1.1 Compaction ratio

The compaction ratio is defined as the ratio between the volume of the fresh mix, in its original state and immediately after being discharged from the mixer, and the volume when subsequently compacted. This ratio is of particular importance in showing the extent to which the volume decreases, despite the increase in volume of the hemp due to water absorption. Consequently, this ratio can be utilised to estimate the voids index of the fresh mix, which is estimated to be zero after compaction.

5.4.1.2 Water ratio

The water ratio can be analysed in terms of several parameters. There are water ratios by mass and by volume, calculating the quantity of water divided by that of the total of the elements, but also the ratio with only the binding part of the elements. The latter, however, can be biased by the water absorption of the hurds, resulting in a reduction of available free water for the chemical reaction with the binder. One hypothesis is that this phenomenon is positive because it releases water progressively following the initial chemical setting of the lime thereby facilitating the development of its mechanical strength more rapidly.

5.4.2 Post experiment resulting parameters

5.4.2.1 Compressive strength

The samples are stored for a pre-selected period. Once the required maturation has been reached, the monoaxial compression test shows us the evolution of the load as a function of the vertical deformation of the sample. This well-known curve allows us to determine the compressive strength of the sample. The shape of the curve also indicates the brittleness or ductility of the mix. Before the element is brought to failure, the elasticity threshold of each mix should be observed by means of load/unload phases.

5.4.2.2 Young's Modulus

As a result of the curve produced previously, it will then be possible to graphically evaluate the approximated value of the modulus of elasticity (this research proposes to establish a relationship between the water content during the setting phase of the mixture and its mechanical strength, through the value of the modulus of elasticity).

A simplified relationship, similar to that for concrete, of the following type will be implemented:

$$E = \alpha \cdot \sqrt{f_{ck}}$$

Equation 7 : Generic correlation between Young modulus and Compressive strength

with :

- E : Young's modulus of the mix
- α : parameter depending on the nature of the aggregate.
- f_{ck} : characteristic compressive strength of the mix

5.4.2.3 Carbonation depth by phenolphthalein staining

The chemical reaction when calcium hydroxide is setting produces water by absorbing carbon dioxide from the air. This reaction restores the pH of the medium to a near-neutral pH of around 9. Calcium hydroxide is a strong base with a pH of around 13. By measuring the presence of calcium hydroxide using a 1% alcoholic solution of dissolved phenolphthalein, it is possible to determine the level of carbonation in the mixture. Subsequent to the application of compressive forces, the pH of each sample will be determined. Subsequently, the sample if not totally crushed, is cut to obtain a smooth surface section, upon which the phenolphthalein solution is applied. The reaction is immediate, and the purple stain indicates the high basicity of the medium. Consequently, it is straightforward to quantify the level of carbonation by measuring the distance between the edge of the stain and the edge of the cylinder. The method of measurement applied to each sample is indicated in Figure 42 and results are collected in 7.2.6.2:Carbonation over time.

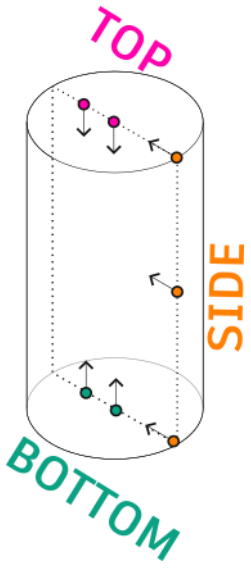

Figure 42 : Carbonation depth measurement method

5.5 Measurements on the protoype

5.5.1 Continuous measurement parameters

Here are discussed the two parameters that provided insight into the hydrothermal state of the internal mass of the prototype. The parameters in question are the water content and the temperature within the mixture over the course of the entire observation period, which extended over a period of one year. This allowed to consider the breathing behaviour, evaporation, and thermal inertia of the arch. Furthermore, the study involved comparing these patterns with continuous measurement curves of external temperature and relative humidity. In order to be able to interpret more easily some trends, daily average solar radiation values and local rainfall data are collected for the entire period from the Meteorological Observatory of the University of Turin, Department of Physics (https://www.meteo.dfg.unito.it/anno-2024) [58]. Correlating these parameters facilitated a more confident explanation of certain behaviours that are visible in the graphs. Indeed, if solar radiation is high during a given dry period, it was of interest to understand how temperatures evolve depending on the orientation of the prototype, as well as the water content when considering either the base of the pillar or the keystone of the arch.

5.5.2 Discrete measurements

Unlike the parameters discussed in the previous paragraph, some data were only revealed after the destruction of the prototype. These data primarily consisted of carbonation values, which were measured through a chemical reaction with a phenolphthalein alcoholic solution. These measurements were performed manually and on-site, immediately after the arch's failure. Thus, it was possible to handle the collapsed fragments in order to measure all faces exposed to the air.

5.6 Correlations

This chapter refers to Chapter 5.2.4, where the methodological sequence of the various correlations made between the two experiments is highlighted, with the purpose of drawing well-founded conclusions between different parameters that were previously difficult to relate.

5.6.1 Elastic modulus as a function of Carbonation?

Following the fracture of the samples, the carbonation task was measured using a phenolphthalein solution. This distance was then associated with the value of the Young's modulus measured during compression fracture.

The relationship between modulus of elasticity and carbonation is well established for concrete [59]. However, there is a risk of corrosion of the reinforcement in reinforced concrete due to the reduction in basicity of the medium caused by carbonation, even at a pH of around 9-10. In the research on hemp-lime, the objective of carbonation was to enhance the strength of the mixture.

5.6.2 Compilation of carbonation measurements

By carrying out the carbonation test with an alcoholic solution of phenolphthalein, it was possible to calculate the state of progress of the carbonation and to position the average value of the depth distances on the graph previously produced using the samples. This established a tangible link between the two experiments.

5.6.3 Relationship between moisture content and elastic modulus

A correlation has been identified between the water content at the time of breakage of the prototype and its mechanical strength, as indicated by the Young's modulus. The water content indicates the extent of free water present in the mixture at a given point in time. This approach has two advantages. The first benefit was to gain insight into the affinity of the arch with the hygrometric context in which it hardened. It was therefore essential to observe whether there was a growth in water content in the material, given the importance of the water molecules generated by the carbonation reaction. If this was indeed the case, it would indicate that the reaction was occurring in the area next to the probe. At the very least, the water could be migrating from the carbonation reaction boundary towards the centre of the mixture.

5.6.4 Relationship between temperature and elastic modulus

In contrast, there appeared to be no direct correlation between temperature and carbonation. In opposition to the exothermic chemical reaction that occured during the hydration of quicklime, which resulted in the emission of heat, carbonation did not involve the temperature variable. Nevertheless, the prototype's mass could potentially alter its thermal inertia value indirectly. In such a scenario, the shape of the graph might suggest a probable correlation between the absorption and release of calories. In other words, effusivity and diffusivity could be associated with the carbonation of the mixture, and consequently with its mechanical strength. There are no further discussion of this topic in this thesis.

6 Optimising Numerical Models through comparison with real prototype of confined recycled aggregates

The second study focused on a system of dry gabions like filled with materials of reuse. This system was modelled numerically using the DEM and FEM methods and tested in a real-world loading scenario. The objective of this study was to compare the mechanical behaviours observed (settlements, displacements, and chains of force) with the results obtained from the simulation. This would allow for the adjustment of the model to real-world conditions.

6.1 Presentation

The second technique, the confined recycled aggregates (CRA) is a dry technique. This indicates that the addition of water is not required for the implementation and solidification of the parts. This technique is frequently observed in various woodworking methods. Mineral blocks are placed one on top of the other and blocked in space with a metal mesh or fence. This technique is analogous to the gabion and has been developed for the last twenty years mainly for humanitarian projects by the French association "Architecture & Développement" [60].

6.2 Load-bearing purpose

The load-bearing capacity of gabions is a crucial element in determining the durability and intrinsic quality of the work. The present study was constrained in its scope to the evaluation of the technique's deterioration over a period of three months, commencing on the date of the structure's completion. Considering the accumulation of solid matter within the enclosure, it was obvious that the intensity of the pressures during the construction process would result in the disruption of the descent loads due to the occurrence of small

displacements within the CRA. This could potentially result in the random breakage of elements. This phenomenon would thus produce a second equilibrium to be reached, potentially recreating a new local rupture. Consequently, the triviality of the element becomes more complex than initially anticipated, and the implementation of preventive and quantitative measurement is not straightforward.

The objective of this research was to empirically measure the settlement caused by a woody structure on a CRA foundation and to compare the results with a numerical model designed to explore the local load conditions between the elements that comprise the CRA. If it can be assumed that the load produces the same action on the prototype as in the numerical model, then, it is conceivable to extrapolate the results by manipulating the configuration of the structure through a series of simulations where the input can be changed.

6.3 Full scale prototype

6.3.1 Introduction

Confined recycled aggregates (CRA) has been used as a foundation for the light-earth pavilion. This foundation stemmed from the ground level, with no excavation. This support technique distributed vertical loads through a wide and thick footprint. The role was to prevent deformation similar to that described by the Winkler beam model in the case of continuous footings, or localised ground settlement when the support is discrete. The physical detachment from the ground is an architectural gesture that is both interesting from the point of view of architectural expression because it is clear and irrevocable, and beneficial to the structural and environmental integrity of the building.

The measurement of settlement was then compared with a numerical model of such CRA exposed to the same pressure quantity. The limitation of this research was the complexity of defining a numerical model that integrates the displacement of its elements in a transient state. Nonetheless, the present study restricted its scope to the application of an equivalent load to a segment of the numerically modelled CRA, with subsequent observation of the stress states of each aggregate in the initial phase of loading.

6.3.2 Connection interfaces for structural purposes

6.3.2.1 Simply supported aggregates

It can be observed that the aggregates within the gabion are not bonded. The wire mesh serves to hold the components together. The construction of a compressed mix serves

to contain displacement between the inert material. It should be noted that movement is inevitable, particularly if the load fluctuates in intensity or position. The support system, in its simplicity, is not easily analysed due to the numerous unknown variables present (Figure 43). If the support is not uniform and horizontal, it is not reasonable to assume that the vertical component is zero. Instead, equilibrium is achieved between multiple local elements, which results in a zero vertical resultant.

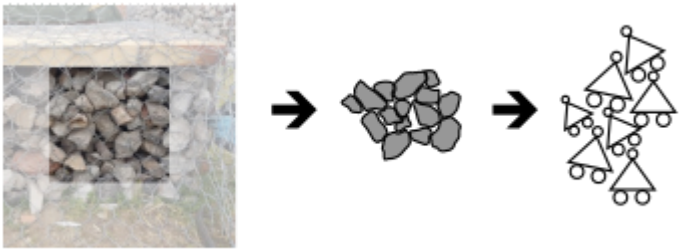

Figure 43 : Simply supported aggregates diagram

6.3.2.2 Fixed connection between aggregates and wooden curb

The wooden beam rests directly on the aggregates and is trapped by the wire mesh. As it is not simply supported but compressed by the metallic cage in tension, its behaviour may be unique with the whole gabion system (Figure 44). The theoretical fixed connection is challenged by the gradual nature of the tightening process.

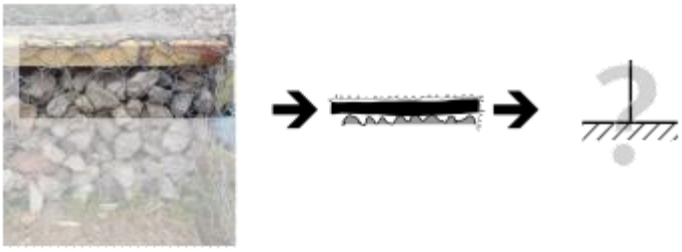

Figure 44 : Fixed connection of the wooden curb diagram

6.4 Computational Fluid Dynamics

In order to understand how a numerical model can be developed, it is imperative to first understand the response of the structural model of CRA to external loads. In essence, the system under consideration involves a set of substantial objects, characterised by their considerable mechanical strength. These objects are constrained in space by a metal mesh, which is regarded as an infinitely rigid and static element within the system. This assumption restricts observations to the phenomena of charge transmission between particles. For this reason, two software packages using two different physical models has been considered. Subsequently, an evaluation of the merits and drawbacks of each option has been conducted.

The first calculation mode was FVM (Finite Volume Mesh), a variant of Finite Element calculations. The principle is to numerically solve the conservation laws for the required parameters by integrating them into each unitary volume. The transfer is made incrementally through the faces of the volumes by applying the conservation of mass and energy flows. The transmission of charge by energy transfer for each sub-volume of each aggregate can be visualised. The limit of this solution was the huge quantity of computations involved. The research has therefore not produced the expected result, but it has enabled us to visualise locally how some solids locally transmit a certain load to each other.

The second calculation mode was discrete, where each solid was considered as an undividable particle in the calculation. The computational weight was therefore massively reduced, and the interactions between these particles were easier to calculate. These interactions were translated into forces (collision, friction, contact, etc.) and the results were then translated into dissipation or elastic deformation. The advantage of this solution was the simplicity of calculation, and in the case of the gabion construction technology, it appeared more realistic to operate with this type of numerical calculation afterwards.

6.4.1 OpenFOAM

OpenFOAM (Open Field Operation And Manipulation) is a C++ toolbox for the development of customised numerical solvers, and pre-/post-processing utilities for the solution of continuum mechanics problems, most prominently including computational fluid dynamics (CFD).

6.4.2 Solvers for stress analysis

OpenFOAM also has two solvers for calculating local stress analyses in solids. These are *solidDisplacementFoam* and *solidEquilibriumDisplacementFoam*.

solidDisplacmentFoam is a solver that calculates the equation in a transient state, that is at each time step, the solver takes the previous situation and feeds it back into the calculation. At each writing step, the calculation produces a file containing the values of the variables calculated for each point of the geometry.

solidEquilibriumDisplacementFoam is the solver that solves the energy conservation equation by iterations. This is referred to as a steady state. The outcome is not a result of kinetics; rather, it is a scenario in which the number of iterations enhances the precision and accuracy of the solution. The official description reports: "Transient segregated finite-volume solver of linear-elastic, small-strain deformation of a solid body, with optional thermal diffusion and thermal stresses."[2]

It therefore involved the equation of a transient state, the calculation time steps of which were progressively fed back into the next step, in order to arrive at a state of stress. The two solvers were tested to understand how the CRA reacts as a function of various vertical and compound loads. Evaluation of goodness about the transient results, as a function of the stationary result using the second solver was also carried out.

[2] *(https://www.openfoam.com/documentation/guides/latest/api/solidDisplacementFoam_8C_source.html*

6.4.3 Case setup

OpenFOAM computer simulations are configured by several plain text input files located across the following three directories: “system”; “constant”; “0”.

1st level directories	2nd level directories	Files	Notes
0			
		D, T, U	Initial conditions
constant			
	polymesh		Geometry translated
	triSurface		Initial geometries
system			
		controlDict	Solver use
		fvScheme	Sets the numerical schemes for terms of the equation
		fvSolution	Tolerance solver values

Table 2 : OpenFOAM Case Nomenclature

6.4.4 Model setup

It was imperative to consider the fundamental limitations of numerical models in order to ensure their validity and reliability. Firstly, it was imperative to recognise that a numerical model must possess a certain geometric limit. Restrictions were to be done about the analysis, considering the importance of the phenomenon under study and the volume of data processed by the computer. This entails the delineation of the discretisation of the geometry under examination, the external parameters that are to be accounted for when solving the equations, and the intrinsic properties of the material(s) to be studied.

In order to facilitate the calculation process, it was recommended that the aggregates be represented as a virtual material. This could be achieved by weighting the average mechanical strength and density values in accordance with the proportion of each type of debris. This approach allowed for the injection of a single variable into the differential equation, thereby significantly reducing the complexity of the resolution.

In addition, in the case of the *solidEquilibriumDisplacementFoam* solver, it was also useful to consider the solid aggregates as immutable, by setting the displacements to 0 in all directions. This enabled the simulation of the metal cage under the assumption of infinite rigidity and static behaviour. However, this is a strong simplification hypothesis that could not be verified in this study, but as part of more in-depth research into the numerical part.

6.5 Discrete Elements Method

6.5.1 Description of LIGGGHTS

DEM (Discrete Element Method) simulates the behaviour of individual particles and their interactions (e.g., collision, friction, and cohesion). LIGGGHTS is a powerful open-source tool that allows to model granular materials, such as sand, gravel, or stones, which is ideal for simulating gabion-like systems.

In LIGGGHTS, particles are treated as discrete objects with properties like mass, size, and velocity. Forces are calculated between interacting particles based on laws of contact mechanics.

6.5.2 Particle Properties definition

6.5.2.1 Size and Shape

The aggregates inside the metallic cage were modelled as spherical particles. The geometry exhibited by real aggregates was unique to each element. The process of compaction was instrumental in achieving stability. The utilisation of spherical particles of varying dimensions presented a disadvantage, as it gave rise to fragility issues that vary in intensity among the elements. Indeed, support from one element to another was only punctual in the real model as in the proposed numerical model. It was therefore more a question of dissonance in terms of the quantity of objects inside the metallic cage, and it was not relevant to dwell on this divergence. More significant was the loss of point resistance that a solid may have experienced when its geometry contains local weaknesses. Thus, the spherical shape was a reasonable assumption. To mitigate the potential discrepancy between the model and reality, two particles sizes were selected, thereby proposing distinct resistances to charge transfer.

6.5.2.2 Density

Despite the heterogeneity of the constituent elements, the density of the agglomerates remained relatively uniform. Therefore, the decision has been made to calculate a mean density that adequately represented the entire population of elements despite their varied natures.

6.5.2.3 Friction

In this model, friction was a crucial parameter. Indeed, the coefficient of friction was specific to the adhesion that could occur between two or more elements during movement. It is defined as the resistance to relative movement between two surfaces in contact.

6.5.2.4 Elasticity

The stones' elastic properties (Young's Modulus, Poisson's ratio) are important for understanding how they deform under external forces. As was the case with density, the elastic and plastic properties, as well as the Poisson's ratio, were relatively similar for each constituent of the mixture. Consequently, there was no necessity to create distinct materials; rather, it was sufficient to create a single virtual material that was the mean of all the elements. In order to proceed, it was necessary to quantify a fictitious module of elasticity and a Poisson's ratio that illustrates the average behaviour of all elements.

6.5.3 Modelling the metallic cage

LIGGGHTS doesn't natively simulate wire mesh. But using boundary conditions or contact models, the presence of the mesh that contains the stones could be simulated by setting up fixed or moving boundaries that constrained the motion of the particles (stones). Gabions underwent deformation under load, so it was important to simulate how the individual stones interacted to form a stable structure under pressure.

Ultimately, the metal cage was not physically modelled. Following the 3D modelling process using Blender software, the model was exported in ".stl" format, designated as rigid container for the particles. Given that the force applied exerted no effect on the cage itself, but rather on the particles within it, it was possible to propose this strategy, which required fewer computer iterations, with the objective of visualising solely the reaction of the particles with each other.

In alternative of the loading pressure generated from the wooden tables on the top of the CRA, two pressure surfaces have been created from Blender in ".stl" format and then imported into the LIGGGHT case. They exhibited a surface area smaller than the upper part of the metal cage, which was left open to receive the flow of particles generated during the run simulation.

6.5.4 Setting up the simulation environment

6.5.4.1 Boundary Conditions

The boundary conditions represented a critical parameter that had to be satisfied because the simulation was limited to the parameters defined by these boundaries. In this

scenario, the virtual prototype was isolated and subjected exclusively to a vertical load. Conversely, attention had to be given to particles extending beyond the simulation limits. In such instances, the most straightforward approach entailed their elimination. The purpose was to fill the gabion with particles, while disregarding those that could rebound or exceed the capacity of the metal cage container.

6.5.4.2 Gravity

It is imperative to delineate the gravitational force within the script in order to ensure the provision of accurate inputs to the simulation model. Therefore, it was necessary to generate an acceleration due to gravity of 9.81 m/s^2.

6.5.4.3 Interaction Forces

The interaction forces were managed by loading a contact model. In this case, the "Hooke tangential" model was chosen because it allowed realistic simulation of interactions between solid particles, taking into account both normal and tangential forces. The model is commonly used in granular fluid simulations, where it is important to capture contact interactions between solid particles. It can be used to model situations where the particles slide, jam or move irregularly, which was exactly the situation in the gabion where the organisation of the particles plays a key role in the overall strength.

6.5.4.4 Young's Modulus

Young's modulus (E) measures the stiffness of a material, that is how much it resists elastic deformation when a force is applied. In LIGGGHTS, the Young's modulus is used in contact models to calculate how particles deform when they collide or interact. Specifically, it governs how particles compress under normal forces.

6.5.4.5 Poisson's ratio

Poisson's ratio (ν) is defined as the ratio of the lateral contraction to the longitudinal elongation of a material under the action of traction. In LIGGGHTS, Poisson's ratio influences the shape of the deformation when particles interact. In granular material simulations, this helps to replicate realistic material behaviour.

6.5.4.6 Coefficient of restitution

In LIGGHTS, the coefficient of restitution (COR) represents the amount of energy that is conserved during an elastic collision between two particles. This parameter is crucial for simulating the behaviour of particles in terms of bouncing and energy dissipation. The value of COR varies between 0 (for a perfectly inelastic collision, without rebound) and 1 (for a perfectly elastic collision, without energy loss).

6.5.4.7 Sliding friction coefficient

Sliding friction is the force opposing the relative movement between two contacting surfaces. It is caused by microscopic interactions between surfaces and can depend on various factors, such as the roughness of the surfaces, the adhesion force between the materials or even the sliding speed.

The sliding friction coefficient (μ) is defined as the ratio of the friction force acting on the surface to the normal force (i.e., the force pressing the two surfaces against each other):

$$\mu = \frac{F_{friction}}{F_{normal}}$$

Equation 8 : Sliding friction coefficient equation

where:

- $F_{friction}$ is the force opposing the relative movement between the surfaces
- F_{normal} is the force acting perpendicular to the contact surface

It is imperative that each interaction is characterised by its own friction coefficients. Thus, both the friction coefficients between the stones and the wire mesh, and the one between the stones had to be known.

6.5.4.8 Rolling friction coefficient

The rolling friction coefficient(μ_{roll}) quantifies rolling resistance. It is generally much lower than the coefficient of sliding friction.

The general formula to describe rolling friction is as follows:

$$\mu_{roll} = \frac{F_{roll}}{F_{normal}}$$

Equation 9 : Rolling friction equation

Where:

- F_{roll} is the rolling resistance force.
- μ_{roll} is the coefficient of rolling friction.
- F_{normal} is the normal force (the weight of the rolling object or the force pressing the object against the surface).

6.5.4.9 Time Step and Duration

The duration of the analysis and the time measurement interval are two parameters that can be modified according to the case under study. In this case, movements of mesoscopic elements were visible to the naked eye. As a result, the analysis took a few seconds. The method required in LIGGGHTS had to start by defining the time interval. This, multiplied by a number of iterations, gave the duration of the study.

6.5.5 Running the Simulation

The script first set up the particles in the cage by defining initial conditions and launching a simulation with particles inserted through a virtual surface created in Blender, marked in LIGGGHTS as the "surface of insertion" (Annex 25 :LIGGGHTS Input Script). Since aggregate quantity was limited, insertion stopped once a threshold was reached, requiring script adjustments to control insertion time and particle count. After insertion, the script handled particle packing, with settling being the longest phase—about 10^5 iterations (5 seconds). Multiple test runs were needed to fine-tune the final configuration.

6.5.6 Post-Processing and Analysis

Following the execution of the simulation, the data were subjected to post-processing. Actually, in this research, different results filters were used to present the reaction occurring inside the gabions. Here the list of the different post-processed results.

6.5.6.1 Particle Displacement

The transient displacement of the particles was not a consistent result. However, their relative positions at the end of the simulation were interesting to comment. The purpose was to visualise the settlement of the whole, so a graph plot should be created with the heights of the particles on the ordinates and the time on the abscissae. This rendered measurable the difference in heights before and after loading.

6.5.6.2 Stress and Strain

Investigating the stresses within the stones and the system to assess stability, stress and strain visualisation was particularly interesting in showing how stress was accumulating for a given pressure.

6.5.6.3 Force Chains

Visualising force chains in the system helped to understand how forces were transmitted through the gabion. It was also worthwhile to conceptualise the distribution of forces on the surface during the transfer of load.

PART III / CASE STUDIES

7 Hemp-limes

7.1 Full-scale application: the prototype

7.1.1 Genesis of the experiment

The reaction of a heterogeneous material like hemp-lime is not immediate to forecast. At the microscopic level, the interface between the binder and the plant material was the critical topic for matrix cohesion.

This research focused on the construction and monitoring of a pointed arch, based on a previous workshop entitled *Hemplime Studio* held at the Welsh School of Architecture in Cardiff in 2009 (Figure 45), as part of the *Vertical Studio* educational programme and under the direction of the late architect David Lea [61].

The students were divided into two groups, self-selected by year, with a mixture of both years. These groups operated in a series of shifts, engaging in construction, research, and design activities. The project's management approach was similar to that of a miniature construction site. The students received instruction on the proper use of materials and equipment, as well as on timekeeping and the maintenance of the building area. Furthermore, they were obligated to maintain meticulous records of their daily progress and to maintain individual learning journals. This approach offered students at the early stages of their education an understanding of architecture as a process. The "hands-on" approach of the project deviated from conventional textbook learning, thereby introducing a more integrated and authentic mode of operation, aligning more closely with practical applications.

David Lea was the founding partner of the Centre of Alternative Technology in Powys, Wales, together with Pat Borer. The conception of this project has led to an increased interest in the subject of hemp-lime. In essence, the external walls were constructed through the application by projection of a mixture of lime and hemp,

encapsulated within a wooden framework, resulting in a thickness of 50 centimetres and a heat transfer coefficient of 0.14 W/m^2K. The research continued with a holistic approach to the material, as it was hypothesised that the hemp-lime could function as a structural element, independent of additional support, thereby providing a cost-effective and environmentally responsible solution. This approach would enable the integration of multiple functions, including the provision of the enclosure, the structure, the insulation, and the air tightness.

Figure 45 : Vault made in hemp-lime at Cardiff University (2009)

The design of Lea's hemp-lime Pavilion draws inspiration from the vaulted mud-brick structures developed by Hassan Fathy [29]. These structures, in turn, represent a reinterpretation of traditional Nubian vaulting techniques. The pavilion's catenary curvature closely resembles the structural logic of early Gothic arches found in medieval Europe, such as those at Le Thoronet Abbey mentioned by Fernand Pouillon in his book “Les Pierres Sauvages” [62]. As explained before, David Lea had the intuition that hemp-lime could be structurally self-sufficient in vault architecture. The application of arches and vaults is the most common architectural shape because it facilitates the transfer of loads to the underlying soil, thereby reducing the exposure of the material to tensile and flexural stresses by converting horizontal forces into vertical loads to the basement. In collaboration with engineers Prof. Abid Abu-Tair and Dr. John Kinuthia of the University of Glamorgan’s Civil Engineering Research Unit, Lea developed the profile of a pointed arch. The slenderness of the last third of the arch suggests a high level of technological refinement.

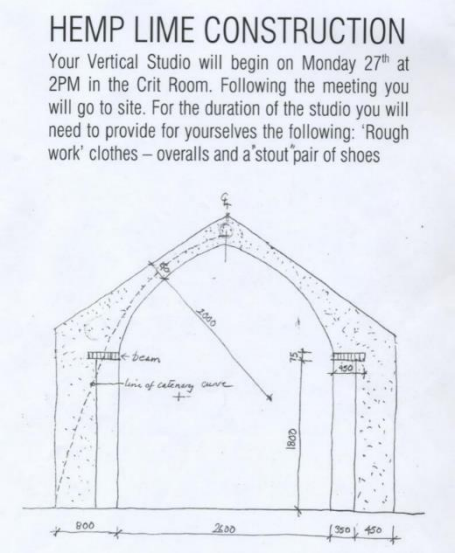

Figure 46 : Flyer of the workshop

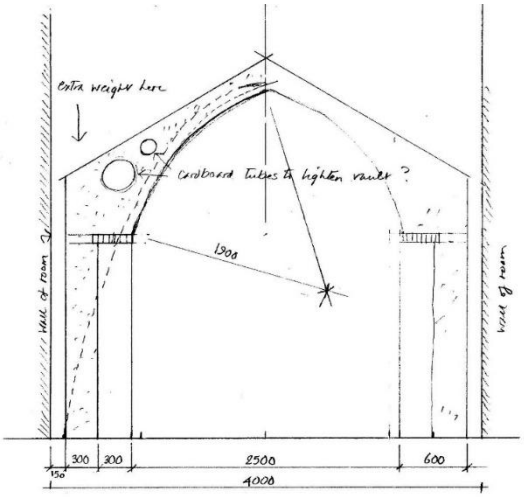

Figure 47 : Quoted section of the arch

The flyer in Figure 46 does not show the dimensions of the final arch, which evolved over time during the workshop design process. However, final dimensions are shown on Figure 47.

7.1.2 Algorithmic design

It should be remembered that the ogive vault reacts better to a point load at the ridge of the roof, and that a barrel vault exhibits a superior response to a distributed load. The architectural decision is strongly associated with the Cardiff test, ensuring that the results can be compared without the influence of unforeseen factors.

The generation of the final vault's geometry was based on Mery's method [63], in order to incorporate a graphical method within the Grasshopper parametric design software inegrated into Rhino3D. The generation of the arc profile enabled an empirical approach to the design process while concurrently generating the pressure curve. The employment of a parametric approach constitutes a significant advantage, as it facilitates the conception process by rendering it highly dynamic and accessible through graphical representation.

The Grasshopper script (Annex 4 :Grasshopper Script for Mery's Method) is articulated in 6 macro phases. Below are listed the steps that revealed the pressure curve of the geometry.

1. Input of the mid-arc geometry by the position of 8 points
2. Division of the arc into blocks

3. Input of loads and dead loads
4. Creation of load vectors
   4.1. Revealing the centroids of each block
   4.2. Norms of the charge vectors
5. Polygon of forces
6. Pressure curve

Following the discretisation of the arc into a series of blocks, each characterised by an identical width, the subsequent step entails the calculation of the weights engraved on these blocks. This calculation enables the subsequent generation of a series of force vectors.

Posted
Computed

Width of each block	*[m]*	*0,15*
Thickness of the prototype	*[m]*	*1,20*
Density	*[kN/m3]*	*12,00*

Area of each block	Volume of each block	Weight of each block	Linear Weight of each block
[m2]	*[m3]*	*[kN]*	*[kN/m]*
0,07	0,08	1,01	6,72
0,07	0,08	1,01	6,72
0,07	0,08	1,01	6,72
0,07	0,08	1,01	6,72
0,06	0,07	0,86	5,76
0,06	0,07	0,86	5,76
0,06	0,07	0,86	5,76
0,07	0,08	1,01	6,72
0,07	0,08	1,01	6,72
0,07	0,08	1,01	6,72
0,08	0,10	1,15	7,68
0,10	0,12	1,44	9,60

Table 3 : Dead load analysis of the arch

The Table 3 was completed before measuring the final density of the mixture. The initial assumption of a density greater than that of water was thus confirmed. In the end, the density of the mixture after one year of setting was almost reduced by half, reaching 780kg/m^3 (7.8 kN/m^3). The actual value was incorporated into the script afterwards, but the overall response of the pressure curve remained largely unaltered. Consequently, the initial conceptualisation and design of the model aligned with the actual conditions to a

considerable extent. After inputting the revised value, the curve exhibited negligible displacement, thereby diminishing the horizontal peak thrust by 1.5 kN.

The following figures show the status at the time of conception. The diagrams are arranged sequentially and follow the methodology outlined in the Grasshopper script for generating the pressure curve.

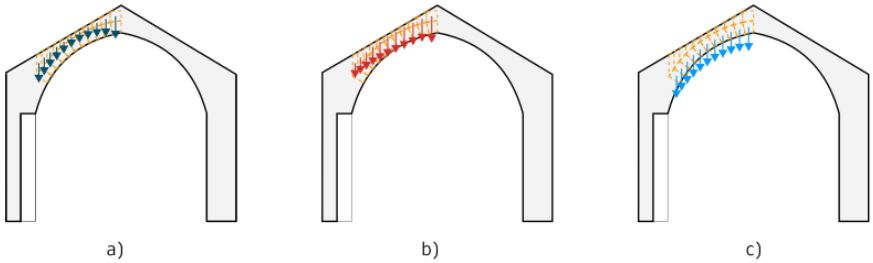

Figure 48 : a) dead load of the upper part - b) live loads - c) dead loads of the blocks

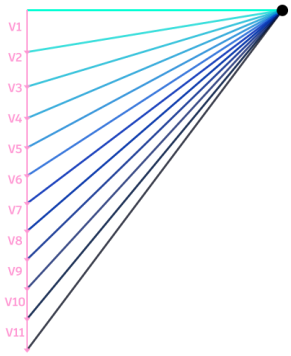

Figure 49 : Convergence in an arbitrary point

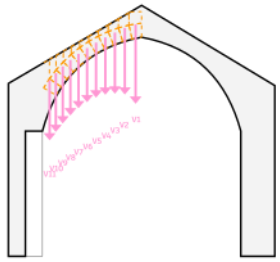

Figure 50 : Total loads vector display

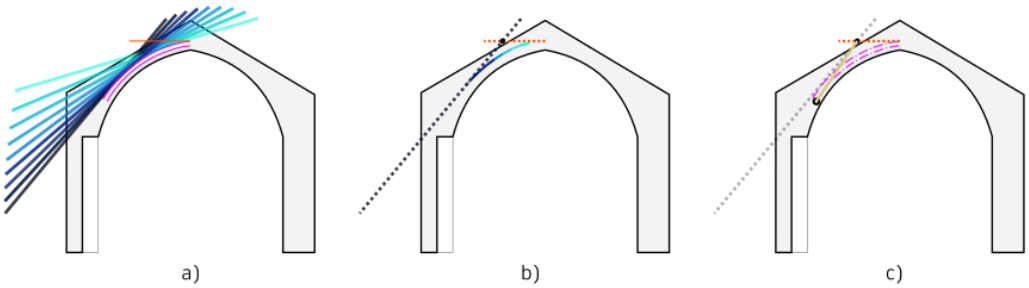

Figure 51 : a) Generation curve - b) Intersection as centroid of the entire loads - c) direction of the capacity vector S

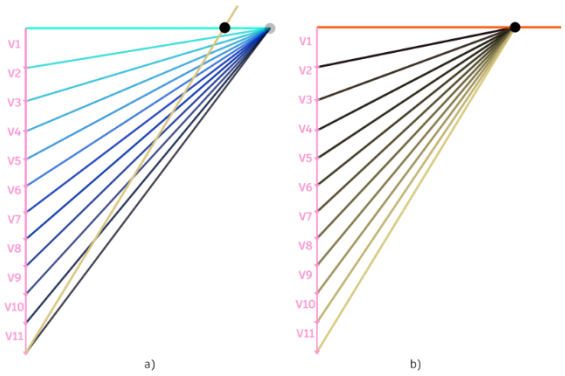

Figure 52 : a) applying direction of S on the convergency diagram - b) New convergency to find the pressure curve

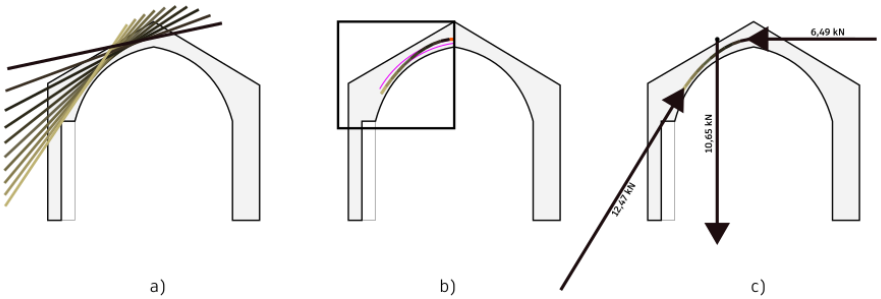

Figure 53 : a) Generation of the curve of pressure - b) rimmed pressure curve - c) vector of loads for static state

The graphical representation is shown in Figure 54 and allowed to proceed with the construction of such geometry. However, despite this result, the construction exhibited fractures at the points of tangency between the curve and the edges of the central nucleus. The experiment was unsuccessful in validating the Mery technique for the self-supporting, hemp-lime pointed arch.

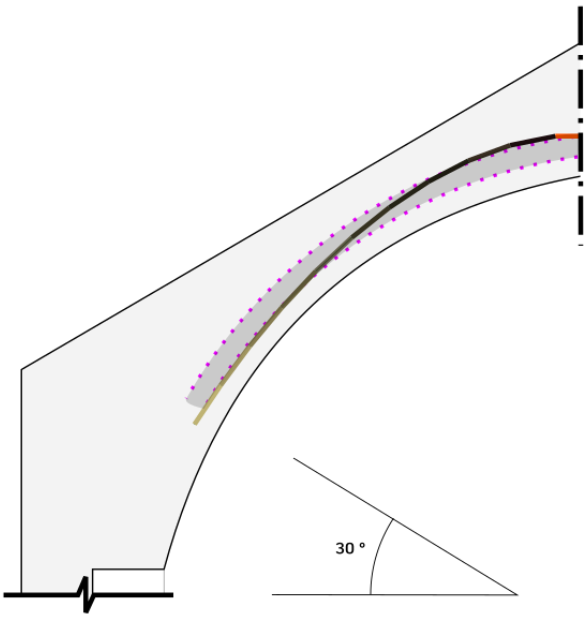

Figure 54 : Pressure curve _ 1:20

7.1.3 Formworks

The arch formwork was a wooden construction with larch frames and stainless steel grids. The challenge was to find a way of pouring the mixture gradually, while leaving enough space to compact it from above. The various formworks were a repetition of 5 modules whose dimensions are fixed and can generate other shapes for possible future uses. Each corner was defined by a vertical element approximately 2 metres long, onto which the mesh panels are screwed. The relatively small dimensions of the panels led to a certain amount of deformation during the compaction stage. This had to be counteracted. To achieve this, wooden tables were fixed at certain elevation points, in a horizontal position, but in such a way that the thrust of the horizontal pressures was held back by the large size of the tables, so as to make the most of their static inertia.

The arch was cast on a curved plank of numerous larch battens covered with a plastic film designed to prevent sticking. Supporting this floor were three arch centrings built beforehand, resting on 5 beams propped to the ground (Figure 55).

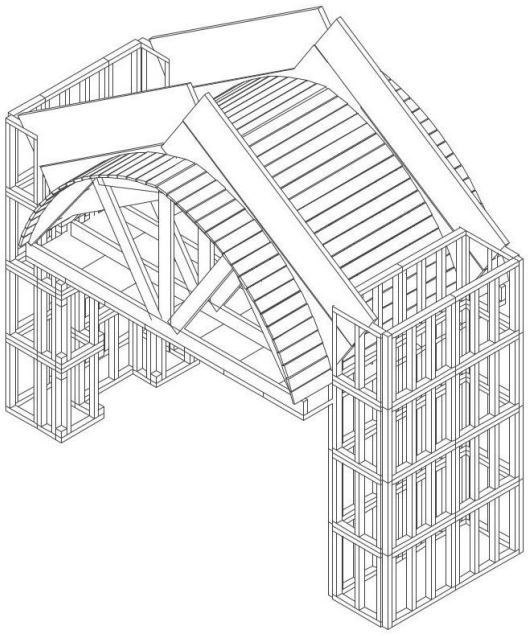

Figure 55 : Formwork axonometry

Figure 56 represents the assembly phase of the formwork of the barrel vault at the top of the north pier. Metallic grid was not used for the curved surface for practicality, but a succession of boards was, as for the pointed arch vault.

Figure 56 : Formwork of the transversal little arch

The formwork was designed in modules with the objective of facilitating its reuse, and was made upstream, using local larch wood with a cross-section of 5 cm x 7 cm, screwed together with Torx 35 screws with a length of 120 mm (Figure 57). A double stainless mesh system was stapled on top from the inside with the help of a pneumatic stapler set at approximately 4 bars. The thicker net measured 3cm in pitch and was strong enough to guarantee a maximum pitch of 30cm between two wooden uprights, while the second net had a 5mm opening to hold the mixture.

Each formwork was identified according to its laying plan, its direction with an upward arrow, its orientation and its position in the plan by writing 'angle' or 'flat' on its outer posts.

Figure 57 : Building frames of the formworks

7.1.4 Centrings

The arch centrings were made from local spruce. Each centring is 7cm thick, making it sufficiently rigid in its own plane. As a result, handling and levelling did not affect its mechanical performance. They all were composed of a king-post and two struts fixed to the tie beam. Each connection was made with T35 torx screws, minimum length 120mm, inserted into the diagonal of the wood fibres. The centrings were made with the help of Lorenzo Torre, a professional carpenter, guaranteeing the quality of the work.

Figure 58 : Junction of wooden parts

Figure 59 : Centring

The preliminary assembly (Figure 60) made it possible to assess the continuity of the internal planes, and to precisely understand the spatialisation of the volumes above the excavations. To delimit the footprint on the ground, a rope shifted 7cm on each side was used in order to respect the thickness of the formwork. The mixture was then directly cast in contact with the expanded clay, which was intended to prevent capillary rise.

Figure 60 : Preliminary assembly

7.1.5 Mix process

The 350L concrete mixer made it possible to finish the two piers up to a height of approximately 2.5m in three days with a team of 10 students. The mixture was initially tested in a formwork built next to the building. It was also used during dismantling to check the suitability of the mixture and ensure that the setting time had been respected.

Compaction was performed by pestles similar to the ones used for ramming earth, but with a smaller contact surface, allowing each blow to be effective. It was enough to lift it and drop them vertically to achieve the desired tamping.

The proportions of the mixture were slightly different from the mixture of the footings as an attempt was made to save binder. This meant a reduction from 5 sacks of 10kg each to 4.5 sacks for the same amount of hurd. The result was still very similar.

The process was methodically the same:

1) Clean the concrete mixer with clean water from the hose (about 5L)
2) Pour in 43L of clear water
3) Pour 45kg of "Pantheon" lime from Calchèra San Giorgio
4) Wait 10 minutes for the mixture to set

5) Gently pour in 10kg of fine dry hemp hurd (0-6mm)
6) Gently pour in 25L (2 full buckets) of uncompacted coarse dry hemp hurd (0-25mm).
7) Wait about 10 minutes before taking the mixture.

A 350L concrete mixer (Figure 61) produced a total volume equivalent to one wheelbarrow, two mortar pans and one bucket of mix. The consistency was very grainy, with balls of about 4 cm in diameter, and malleable. This was due to the fact that the mixture had to be compacted, without it being too wet. It was assumed that all the water has reacted with the lime, and that the hurd has not deprived the chemical reaction between the binder and the water itself. Subsequently, results demonstrated a lack of lime curing.

Figure 61 : Hemp-lime mixer

7.1.6 Testings

The first test enabled us to get to grips with the panels in practice and to learn how to fix them securely. It also enabled to understand whether the subtraction of material due to the metal rods used as tie rods was significant, or whether it could be neglected when assessing the results. The experiment showed that the void created by the tie rods was not significant compared with other parameters such as the perturbation of fixing and dismantling of the formworks. In fact, when the mesh is removed, it should not cause friction with the mixture. If it does, it brings with it a great amount of material, which could lead to general breakage. As can be seen in the Figure 62, the panels were built in a "U"

shape and were dismantled in two pieces, leaving the half-faces in contact with the untrimmed faces orthogonally to the hemp-lime cube.

Figure 62 : Tested formwork waiting to be filled

The panels used for the test were two U-shaped elements from the North pillar. Given their geometry, already designed to fill a space, it seemed intuitive to use two identical panels.

The picture in Figure 63 shows the original fixing system. When the panels were designed, the main consideration was the horizontal thrust of the mix once it had reached a certain height. This is why the tie rods are positioned in the centre of the elements. However, the importance of the junctions between the different edges of the panels was not highlighted. Despite their forced constipation due to the tie rods, this was not sufficient to counteract sliding or rotational movements between the layers of the panels.

Figure 63 : Detail of fixing the rods on the frames

After a month of curing, in outdoor weather conditions, and with only a tarp sheet as a roof, the experiment was unmoulded. The panel was only half-filled, as the completing the volume was not the intention, although the compaction calculation was made and will be explained later. The idea here was to understand whether the tie rods could make dismantling difficult, and whether it was easy to do so. Unscrewing the tie rods was not difficult. However, dismantling the two U-shaped elements changed a number of things. The short parts that formed an entire face had to be extracted in their plane, which caused stress tangent to the surface of the mixture (Figure 64).

Figure 64 : Opening the formworks

The friction created got the better of the material, which was still a little fresh and far from having hardened significantly. The friction created got the better of the material, which was still far from having hardened significantly. The crack was quite clean. The fracture plane did not show any hemp shives positioned orthogonally to the plane. When the formwork was removed, a lot of material remained attached to it because of the friction of the mortar, as explained above. It was found that the North face was strangely spared from this phenomenon, while the West face was the most affected. A comparison of the two observations reveals that the faces that had been subjected to friction in the plane exhibited a comparatively lower level of damage. the one exposed to the East had relatively saved the sample, whereas of the faces that had been extracted by pure detachment, the South face had damaged the block to a greater extent (Figure 65).

Figure 65 : Unwashed formworks

These were rather coarse elements and numerous air bubbles trapped in the mixture were also clearly visible. After this experiment, the bubbles inside indicating an excess of water were recognised to be avoided and resulting in the mixture hard to tamp (Figure 66).

Figure 66 : Observation of the patterns

In addition, the excess water washed out the mixture by gravity, creating a liquid mortar that clung to the mesh (Figure 67).

Figure 67 : Behaviour of the mortar in function of its hydration. from left to right : very liquid ; muesli ; paste

The block thus dismantled represented a fracture positioned at the junction of the two walling elements, and a series of spurs of material no more than 2cm thick (Figure 68). It would be prudent to assert that these weaken the structural integrity of the sample, but this has not been fully proven.

Figure 68 : Result of the first test

7.1.7 Construction phases

A light excavation was carried out under each pier. The depth is a minimum of 5cm up to 20cm in order to level the ground. Four screws were placed in each excavation to measure the desired final depth. This was done with the help of a laser level tool. Expanded clay was used (Figure 69), relying on its ability to act as a barrier to capillary rise in the

hemp-lime material. In order to compact the expanded clay, a wooden pestle with a base of approximately 30cm side and relatively low weight was used to reproduce a vibration that would settle the grains.

Figure 69 : Expanded clay compaction

Figure 70 : First floor of formworks fixed with the wooden corners

The modularity of the formwork offered the possibility of reusing it. The preliminary assembly made it possible to assess the continuity of the internal planes, and to perfectly understand the spatialisation of the volumes above the excavations. To delimit the footprint on the ground, a rope shifted 7cm on each side was used to respect the thickness of the formwork. The mixture was then directly cast in contact with the expanded clay.

Figure 71 : Pouring in the piers formworks

The panels were placed in position, then screwed together to check that they were precise, and also that the drills needed for their fixings matched up. Each element had its own position, and each one must be moved and then stored. This helped to keep them organised so that they were not messed up when it was time to mount them.

Figure 72 : The northern pier, containing an alcove

Once the position of the two empty uprights had been verified, a temporary bracing was realised with 2.5 cm thick site boards, connecting them to the hinges (Figure 73). Due

to limitations to the length of wooden planks the bracing system was divided into two shorter elements.

Figure 73 : Bracing between the piers

The corners were risen with 5 cm x 7 cm rigid wooden uprights temporarily tightened with clamps and then connected with rod and butterfly bolt systems. The entire formwork structure was connected with the same system, which is easy to dismantle, and perfectly stable during the construction phase. The 350L concrete mixer made it possible to finish the two piers up to a height of approximately 2.5m in three days.

Figure 74 : Filling the formwork with hemp-lime

Temperature and water content probes were inserted at heights of 40 cm above the ground, at 2.5m, and into the prototype's top. The mixture was compacted all around the sensors to avoid air bubbles that would have compromised both the stability of the structure and the collection of data (Figure 75).

Figure 75 : Positionning the sensors

Figure 76 : Manual tamper

To prevent the formwork from opening, a belt system had to be added at certain weak points. Despite the system of tie rods aided by the system of joints on the edges of each formwork, the entire structure showed some deformations due to the continuous

compaction of the mixture (Figure 76). This is the reason why several boards and rods were bolted together to counteract this effect (Figure 77).

Figure 77 : Local reinforcements

Hemp-lime placement was a repetitive activity, but care had to be taken to compress the entire area uniformly and to respect a certain flatness in order to simplify the physical activity, but also to avoid any heterogeneous reaction in the material once it had been compressed by the vault.

The shoring system was carried out two days later, to avoid temporal interference during the compaction of the footings. 20 props were erected and loaded 6 'H' beams (Figure 78). The props were fixed at 230cm, holding 15 kN each according to manufacturer's specifications.

Figure 78 : Shoring

Figure 79 : Preparing the system for the centrings

Centrings were screwed from the tie beam onto the 6 beams and braced between them. The centering was lifted using a hoist attached to an axle positioned on two scaffolding units. The weight of each rib did not exceed 40 kilograms; however, their height precluded manual lifting (Figure 80).

Figure 80 : Fixing centrings by cross bracings

The process of lifting the centring beams was a meticulous operation. Once the centring reached the height of the shoring beams by pulling a rope, it was moved upon them.

The planking was nailed in very few places to facilitate future disassembly of the vault. Nailing also made it possible to stabilise the structure and secure the entire site (Figure 81).

Figure 81 : Tables of the lower level

Once the whole formwork had been executed, the pouring process of the arch could begin (Figure 81). At the sides, construction boards were moulded to fit perfectly into the curves of the planking. The slope of the arch was created with a movable plank, which was fixed every time the height was increased. In this way, the casting remained constant and could be continued with the jackhammer technique (Figure 82).

Figure 82 : Roof scaffolding

Unfortunately, the mixture had no contact with the air in this part (Figure 83). However, this was not relevant as the zenith part was totally open and formwork free.

Figure 83 : Mix during compaction

The compaction also kept the non-stick cloth in place. For every 10 cm or so of compacted mixture, the top plank was moved, allowing a certain homogeneous compaction to be maintained throughout the vault section. The balls being rammed seemed to be a sign of proper compaction.

A pneumatic hammer (Figure 84) made it possible to compact also in the normal direction. To do this, a plate welded onto an SDS insert capable of withstanding vibration was prepared. Five different plates were used for the entire vault because the steel showed signs of fatigue and would break into pieces after approximately two days of heavy use.

Figure 84 : Pneumatic handcrafted tamper

The side boards were fixed to the planking from the outside with wooden angle brackets, and from the inside with bolted rods, so that here too they could be dismantled, and each formwork element could be reused.

The polypropylene sheet was torn with a box cutter in contact with the planking to allow a little air exchange, and to allow the mixture to cure.

An Arduino microcontroller was installed to connect the 14 probes (Figure 85). The system was designed to operate autonomously during both day and night. To this end, a 50 W photovoltaic panel system, a 27 Ah battery, and a charging controller were integrated (Figure 86). Data is sent via a router that is also connected to the off-grid power supply.

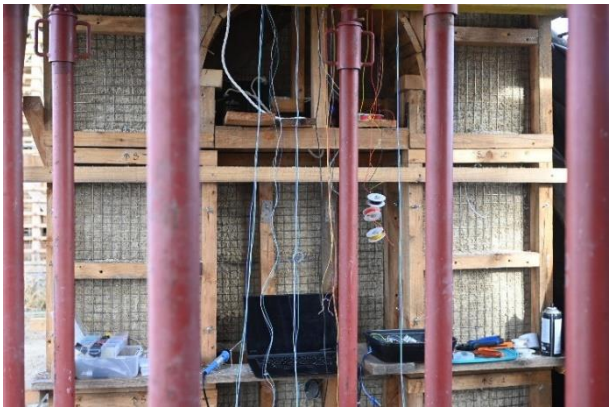

Figure 85 : Arduino datalogger

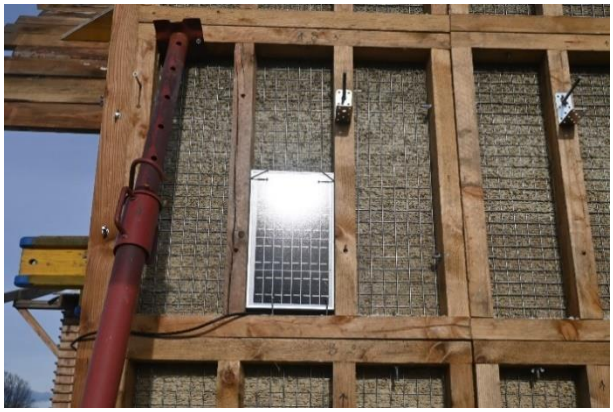

Figure 86 : Photovoltaic supply

7.1.8 Critical observations

7.1.8.1 Formwork handcraft

The main component in terms of working time was inevitably the creation of custom-made panels. While it is true that they were designed for reuse, it remains imperative that they undergo repair after each use. This was particularly evident in the fine metallic mesh, which, due to its exposure to the high pH medium, has undergone corrosion and is no longer suitable for reuse. The original intention was to build a pavilion over 8 metres long. For this reason, it was decided to build formwork for 1.2 metre sections of the pavilion. However, during construction, the idea of building an entire pavilion became more and more remote, given the human resources available and the time required for installation and hardening.

However, the choice of metal mesh was a major change from the original project to let the mix breath. Its role was to maintain constant contact between the mixture and the air. As mentioned above, the binder used was mainly air lime, only part of which reacts with the micronised pozzolan to form a hydraulic set. This led to the need to decide how to imply the gas/solid exchange between the carbon dioxide in the air and the calcium hydroxide in the wet mix. Initially, the idea of the mesh was borrowed from a project on the generation of a structural earth mixture [64]. The mesh selected was a gauge 11' grid 30mm wire spacing, which allowed the fine hurd particles to pass through. It was therefore judicious to add a second stainless steel mesh, which was much finer (gauge 23' and 6.35mm of wire spacing) and therefore suitable only as an addition to the previous one. It was therefore only by placing the two meshes together that it was possible to contain the compressed mixture.

7.1.8.2 Congruence of preparation and installation times

Construction time was closely linked to the hydration of a wet mix containing chemically reactive binders. It was imperative to consider the operational dynamics of concrete mixer trucks, which were constrained by temporal limitations in their ability to deliver mixes that have undergone hydration processes from the facility to the construction site. While it is true that hydration of air lime is much slower than that of concrete or a hydraulic setting lime such as NHL 5, it was nonetheless important to ensure that it set in its final form from the outset. However, given the impracticality of setting due to various constraints, including the excess of workers and the restricted availability of hand tools for construction, it became imperative to employ a preparation method that was compatible with these limitations. It was therefore decided to use a 350L concrete mixer. Synchronisation was almost optimal, as during the 30-40 minutes the mix required to be prepared, there was enough time to place and compact the previous mix.

7.1.8.3 Hydration level vs compaction

The fresh mixture clearly did not resemble traditional poured hemp-lime. The paste had to be sufficiently viscous and liquid to ensure it can be cast and fill all the geometric features of the shuttering. The it had to be vibrated to evacuate the air trapped due to intrinsic viscosity. Here, the situation was different. Firstly, because of the aerial setting and the mesh of the formwork, such liquidity was not possible, as illustrated in Figure 67. Secondly, it was essential to compress the hemp-lime mixture to evacuate the air trapped within it. Although it was not possible to vibrate hemp-lime because of its materiality, mechanical compression enabled the air to be expelled through the top, and also thanks to the "sieve" formwork, which only retained the solids.

7.1.9 Results

As mentioned in 1.7.1 Hemp-lime research contribution, this section has largely been published in the scientific journal "Sustainability", vol. 16 (2024), issue 20 [21]. The article was published in October 2024 and covers nearly the entire temperature and moisture content monitoring measured by the probes incorporated into the hemp-lime prototype. The purpose here was to present the complete data and methodology and to update the dataset with the subsequent months. The results are referenced in the schema Figure 21 delineated in Chapter 1.7.1.

7.1.9.1 Temperature

Work started at the beginning of November 2023. The major risk at that time was frost, but temperatures did not fall below 0°C. Frost is detrimental to the carbonation of lime. Observation lasted from December 22, 2023 to May 13, 2024. Evaluating the effect of boundary conditions on the temperature inside the mass for each critical part of the arch such as piers, vault hinge and top was crucial for discussing the importance of hemp-lime thickness in temperature. The “Z-1-T” probe seemed to have failed, probably due to the damp constructive process. The plot shows regression curves calculated according to a moving average over a period of 145 values, easing the readability. The sampling for each value represents 24 hours which is still reasonable for such a long-term observation.

The sensor inside the north pier (probe “V-1-T”) recorded higher values than the others, with a mean value along the whole observation period of 1,171°C higher than the mean of probes W, X and Y. In fact, despite its northerly aspect, it received sunlight all day long, except for the short hours when it was shaded by the south pier – a duration insignificant to influence probe “V-1-T” due to the low thermal effusivity. (Thermal effusivity indicates the rate at which the surface temperature of a material rises.) Assuming the following equation:

$$\beta = \sqrt{\rho . c_p . \lambda} \quad [\mathrm{W}.\sqrt{\mathrm{h}}/\mathrm{m}^2.\mathrm{K}]$$

Equation 10 : Thermal effusivity formula

where: ρ = density [kg/m3]; cp = specific heat [W.h/kg.K]; λ = thermal conductivity [W/m.K]

it can be observed, according to Oliva et al. [65], that hemp-lime effusivity is lower than standard infill materials (Table 4).

	Hemp-lime	perforated bricks	solid bricks	stone (gen.)	wood (gen.)	concrete (gen.)
thermal effusivity $[W.\sqrt{h}/m^2.K]$	4.8	9.3	26.1	45	9.5	33.9
specific heat $[W.h/kg.K]$	0.42	0.29	0.28	0.28	0.44	0.28

Table 4 : Thermal effusivity of infill construction materials

Furthermore, the north pier thickness is 30cm, while sensors “W-1-T”, “Y-1-T” and “Z-1-T” were placed in 60cm thick elements. During the periods when the temperature increased (4 weather periods can be recognised, as represented on Figure 87) it was observed that the heat of hemp-lime heated up faster as the solar radiation increased. In addition, during period (2) referred to Figure 87 : Thermal curves for the curing period, when there were 9 days of stable daily radiation of 15MJ/m^2, probe V recorded temperatures 3°C higher on average than probes “W-1-T”, “X-1-T” and “Y-1-T”. Similarly, the other sensors took 5 days instead of 9 to reach the peak temperatures.

Furthermore, the “X-1-T” probe at the top of the prototype recorded a faster increase in temperature from March onwards, when the sun reached it. The temperature probes all suffered malfunctions in mid-May – they transmitted little data, which rendered difficult to observe particularities. These failures could be explained by a lack of waterproofing of the sensors.

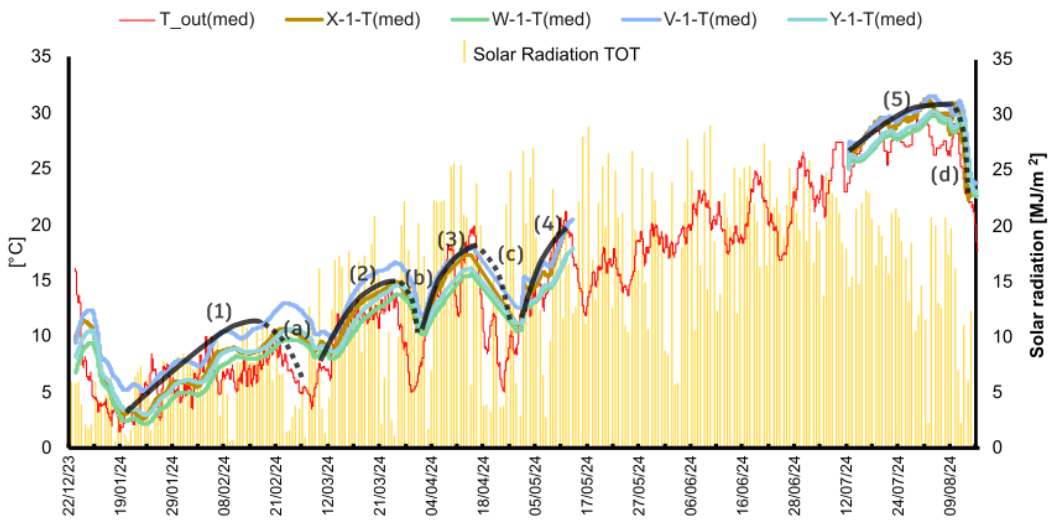

Figure 87 : Thermal curves for the curing period

Following several attempts at repair, it was found that in July, the system resumed measuring and transmitting data. Furthermore, only the probes incorporated into the mixture encountered issues, while the external probes for temperature and moisture content did not experience any technical problems.

7.1.9.2 Moisture content

The research was based on the possibility of monitoring scientific data using low-cost probes extending the studied areas and the quantity of measurements [66].

Moisture content was measured from December 22, 2023 to July 11, 2024. The method applied for data acquisition reveals the trend of moisture content, since the equipment doesn't record the absolute amount of water but an electrical resistivity value, changing relative to the amount of moisture inside the mixture. Compared to the relative humidity measured inside a hemp-lime prototype like the HemPod built in June 2010 at the University of Bath [67], the moisture content showed a trend more responsive to the weather conditions. The indoor air is a result of a thermo-hygrometric balance between outside and inside, which was not the case here, where no pressure gradient from face to face existed.

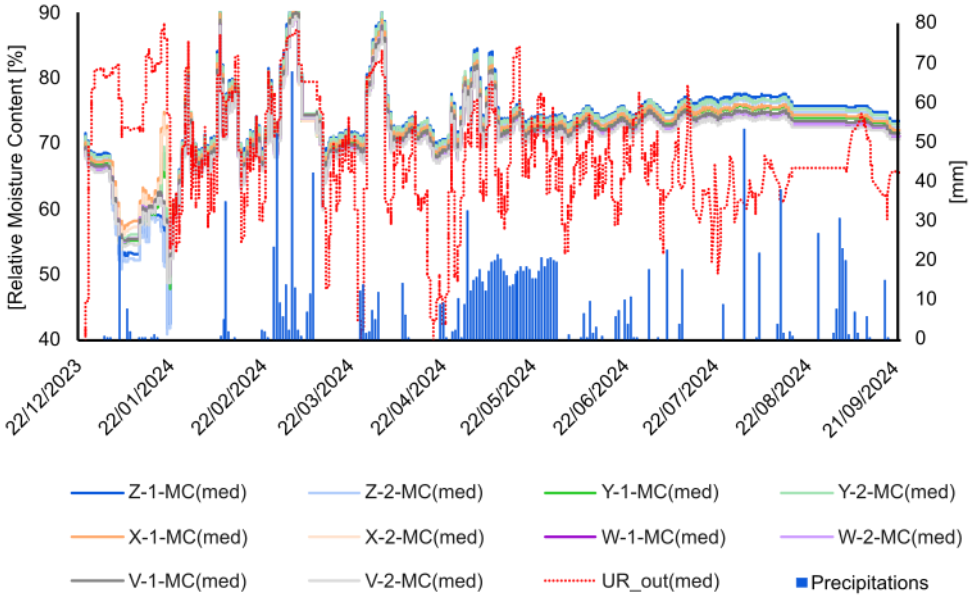

Figure 88 : Moisture content and rainfall plots

When there was a lot of rainfall, the moisture content rose. There were three events of this kind: the last week of February, the last week of March and one month from the end of April to the end of May.

The linear regressions represented in the Figure 89 indicated the trends of the mean moisture inside the mixture and the relative humidity of the air. It is interesting to notice the opposite sign of the two coefficients. If the coefficient of outdoor air is negative (-0.0132), i.e. air has been drying from winter to summer, the coefficient of the hemp-lime mixture is positive and four times higher (0.0489). This means that the mixture contained an increasing amount of water.

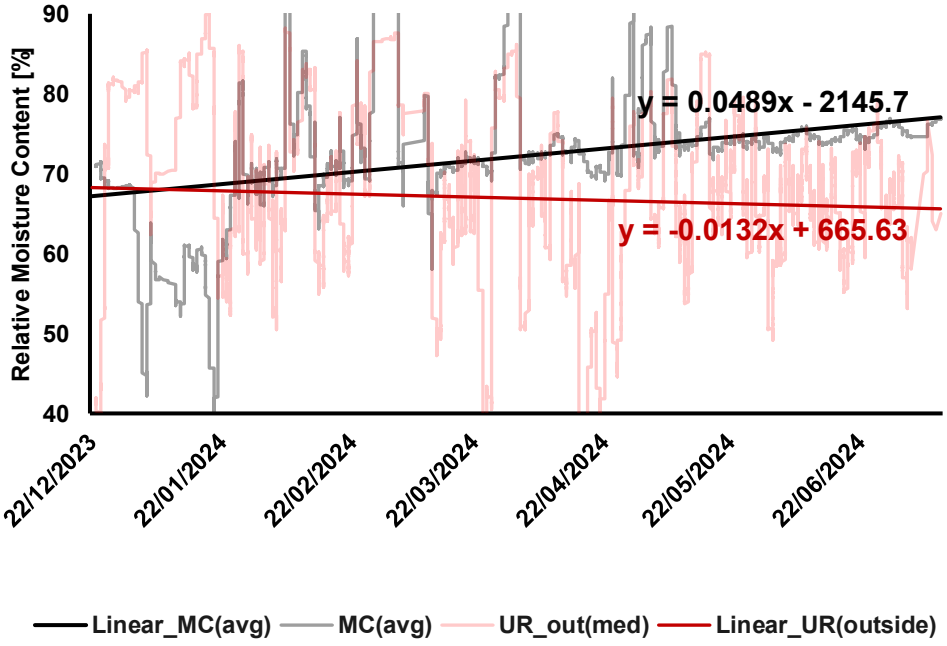

Figure 89 : Moisture content linear regression

This is explained by the chemical setting lime reaction (Equation 1) induced inside the mixture. Carbonation released water and evaporation was not enough to counteract the increase in moisture content in the material.

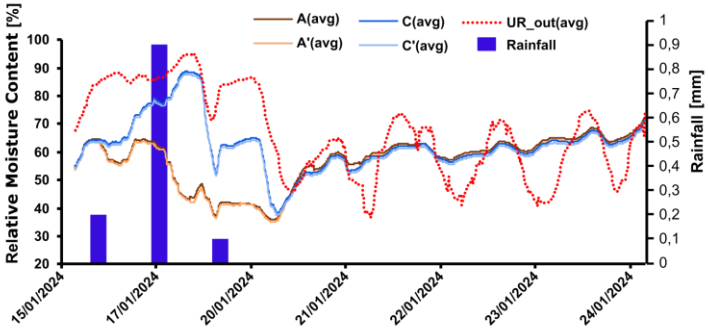

Figure 90 : Relative moisture content and rainfall at the beginning of the setting

Over the period from January 16 to January 20, the “Z-1/2-MC” and “X-1/2-MC” probes were in opposition to each other. That is, for probes “Z-” , the relative moisture content fell by 22 points, while for probes “X-”, it rose by 30 points. Rainfall exceeded 1.3

mm in these days, which led external relative humidity to rise by 25 points, and moistened the top of the arch, while the pier probes A and A' remained unaffected.

7.1.9.3 Sorption/Desorption

Hemp shiv is very porous [68] and is therefore subject to rapid weathering. Figure 91 shows how reactive the mixture is according to the hygrometric conditions. The smoother curve is due to the mass involved in the hygrometric balance ratio, while the saw tooth curve shows the outdoor humidity. This period was shortly after the construction, so the mixture may not have still set yet, which could explain the closeness of the curves.

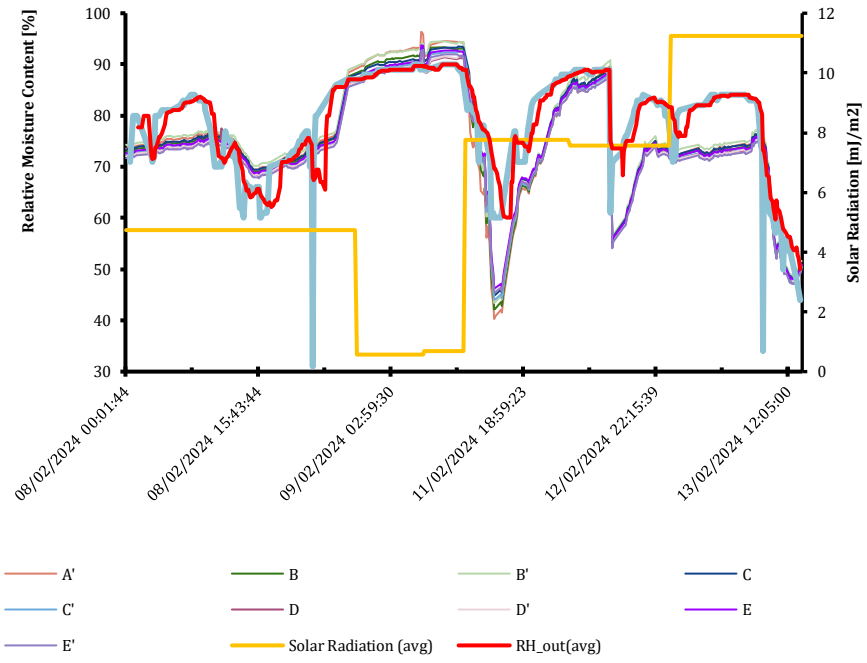

Figure 91 : Mixture sorption behaviour

While this porous material seems to quickly absorb water (Figure 91), desorption is relatively slower (Figure 93). Once the mix has taken up water in the form of gas, there are periods when it seems very difficult to release it. As can be seen in Figure 14, the external relative humidity dropped in one day, but the mixture only underwent a 7-point drop over the following five days. The absence of sun shining, or significant wind may be responsible for this. Indeed, referred to Figure 91, wind was three times greater than the seasonal average (14m/s on average from 16/04/2024 to 18/04/2024 compared with an average of 1.9m/s over the whole month of April) [23].

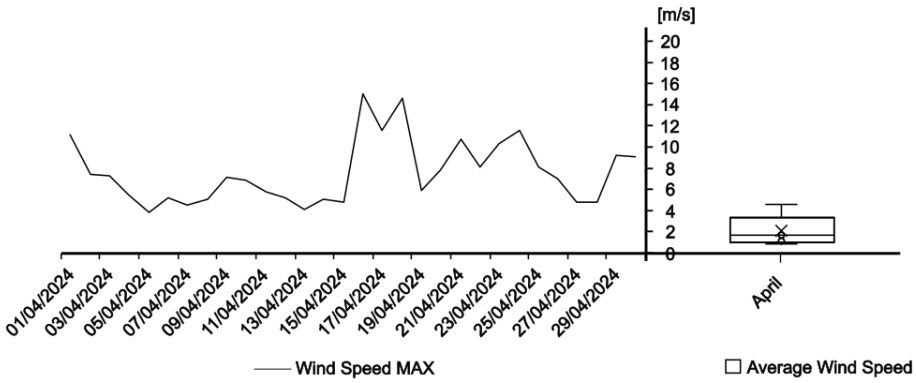

Figure 92 : Measurement of wind in April 2024

Moreover, as this period was 4 months after the construction, the mixture may have set enough to be less dependent on weather conditions. Indeed, looking back to Figure 90, the mixture began to react gently from that moment on.

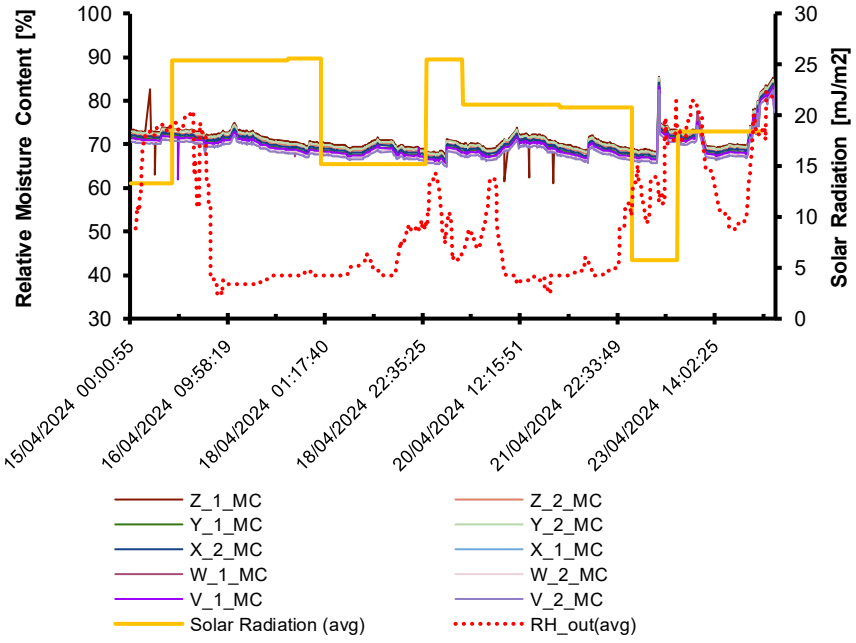

Figure 93 :Moisture desorption behaviour

7.1.9.4 Carbonation measurements

Once the prototype had been excavated, carbonation was measured where the probes had been located. This will enable us to understand whether there is a link between the water content and the progression of carbonation in the mixture. Figure 94 shows the five cross-sections that were analysed.

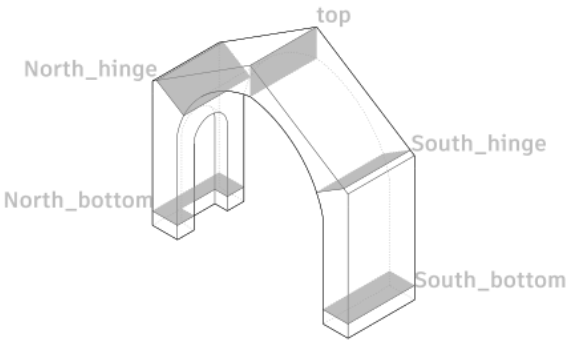

Figure 94 : Axonometric view showing the measurements locations

The results of the measurements can be found in Annex 8 :Carbonation measurements. The scale of representation of each section may vary in order to obtain optimum visibility of the measured values. They are therefore not to the scale of the drawing, but allow certain trends to be identified. For example, at first glance it can be seen that orientation seems to play a fairly important role in carbonation.

Measurements of the outer surfaces generally yield lower values compared to the more internal faces. It is possible that exposure to air movement could be an aggravating factor in carbonation. Indeed, forced evaporation due to air wind may have slowed down the chemical reaction.

The northern zone, at the hinge, was very carbonated. This seemed to be due to the mixture being washed away by excess rainwater that came down here. It could be that the plastic cover had deteriorated during the windy months, and as a result the water had run off without having evaporated quickly. In fact, the picture in Figure 95 shows that the mixture has taken on a grey-black colour, typical of early rotting of the hemp. Another explanation for the excessive carbonation would be the accumulation of carbon dioxide from the organic decomposition of the hemp in this area.

Figure 95 : Rotten hemp-lime on northern top

In addition to the risk of rotting, the faces of the arch more exposed to the air, meaning the faces facing upwards, had a carbonation index between 3 and 10 times greater than the faces facing downwards.

It is also important to acknowledge the physical and geometric phenomenon that is evident in the assessment of plane measurements in comparison to those of the corners. Double exposure to the air is very effective in providing the carbon dioxide needed for the carbonation process. On the other hand, the negative angle measurements taken on the north pillar do not give any better chemical reaction results.

7.1.9.5 DIC on the prototype failure (failed)

The following experiment was unsuccessful because the vault collapsed before the test set could be put in place. The next few lines will therefore present attempts of understanding what happened (and particularly why the collapse was so rapid) and identify the limits of such method and nature of mixing.

The DIC supposed to be operated here was outdoor, generating optical issues for photogrammetry. Digital Image correlation is a method of acquiring a real phenomenon by moving points from one situation to the next [69]. It is an optical and non-invasive method. The scale of the measurements can vary, and this is what makes DIC very powerful and versatile in the assessment of alterations in samples.

The experiment aspired to observe the breaking mechanism that is created at the hinge points of the vault. Unfortunately, the arch did not hold up for more than a few days after dismantling. Cracks appeared at the hinges of the arch, suggesting that the mixture was not strong enough to support the load of the arch in places where tensile forces might have appeared. However, it is disturbing to observe this failure mechanism, since the pressure curve measured with Mery's method proved that the central core of the vault was in perfect compression. No account was taken of the catenoidal curve, which contains only elements in compression, as this was not the desired architectural form. However, in retrospect, it

would have been desirable to understand where this curve, theorised by Hooke, was positioned within the vault. Consequently, here is the comparison made after the vault broke.

Figure 96 : West elevation of the arch

The east and west elevations give a very clear explanation for the unexpected collapse of the arch. Indeed, deep cracks appeared from the surface of the structure. These are located exactly at the arch's kinematic hinges. On the east façade (Figure 97), the crack in the interior, marked by the hooping at the top of the arch, is due to local tensile stress. The other cracks are circled on the Figure 96.

Figure 97 : east elevation of the arch

7.1.10 Conclusions

The prototype enabled to observe that hemp-lime is a material that reacts to its climatic context, even after many weeks following its production. Testing it under natural conditions allows to obtain an appreciation of its thermal and hygrometric reactivity.

The temperature of the mixture was clearly influenced by the outside temperature. Thermal lags showed that the mixture takes 1 to 4 days to lose heat. Thanks to its low effusivity (4,8 (W.√h)/(m^2.K)= 288 J/(K.m^2.√s)) and high specific heat ((0,42 W.h)/(kg.K)=1.512 J/(kg.K)) [65], hemp-lime absorbed an important amount of solar radiation energy and releases such heat even after a week. If thickness increases from 30 to 60cm, the duration of heat absorption doubles, and conversely, the thicker the wall was, the slower the temperature decreased. It was also observed that the temperature peaks inside the mass were higher than the peaks at its edge. This stands to indicate that the studied mixture absorbed solar energy radiation in an effective way thanks to its peculiar combination between high specific heat and low thermal effusivity.

During the first month after construction, the water content of the mixture showed no relationship with the outdoor relative humidity. It then balanced out quite steadily. Finally, it absorbed and released water vapour more quickly in a windless environment. Wind is therefore an important parameter in the drying process of the mixture.

The water content of the mixture has relatively followed the fluctuations in outdoor relative humidity. However, there has been a slight and steady increase since May 20, despite the very pronounced fluctuations in outdoor relative humidity. In fact, since the mixture was formed, it has steadily gained around 10 points, apart from singular events of weather change.

The monitoring of the setting state allowed the formwork to be removed in time when the material reaches an acceptable mechanical strength. Nevertheless, it seems interesting to notice that during the curing phase, the mixture began to behave more independently from relative humidity and rainfalls. Such response may have been the signal of a deep carbonation. A chemical approach using a pH indicator like phenolphthalein to quantify such carbonation was an interesting complement to our investigation. The purpose stood to observe whether the moisture content and the internal temperature would provide any hints on when the state of a self-supporting structure is reached. Such would imply a correspondence between the curing time of the hemp-lime and its moisture content.

7.2 Experimental analysis : the samples

The second part of the research into the mechanical properties of hemp-lime was based on a campaign of compression samples.

Figure 98 : Collection of hemp-lime samples

This photo shows some curing samples. They are not all present in Figure 98, as it was impossible to produce the entire experimental campaign at the same time. A timetable was therefore drawn up specifying when to build and when to test each sample to compression in order to optimise the time spent in the laboratory.

7.2.1 Binders investigated

7.2.1.1 Putty lime

The lime paste used for the series of samples comes from Fornace Conta in the province of Torino, to the north of the Canavese pores. It is a CL90 - SPL lime, which indicates that it is calcitic and not dolomitic. CL 90 calcium lime must contain at least 90% (by mass) of calcium and magnesium oxides and must also contain more than 80% (also by mass) of free lime, i.e. quicklime or calcium hydroxide. The term S PL means that the lime is in paste form, i.e. slaked and even saturated with water [70].

Figure 99 : Putty lime

7.2.1.2 Hydraulic lime NHL 5

The hydraulic lime selected for the experiment is NHL 5 di Saint-Astier, extracted and fired in the Dordogne, south-east of Bordeaux.

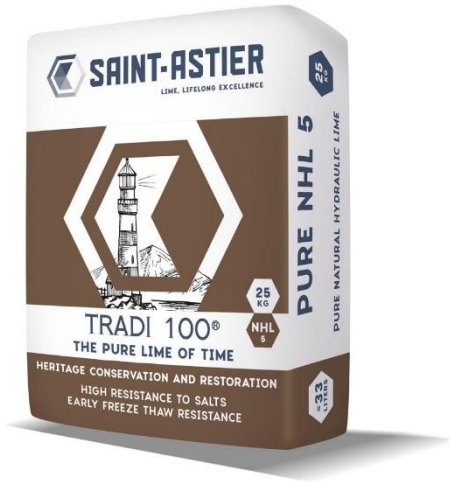

Figure 100 : Natural hydraulic lime

7.2.1.3 « Pantheon » lime

Pantheon lime is what is known as a geopolymer, because it is a mineralogical mixture of two main elements: air lime and pulverised pozzolan. The dry combination of the two materials gives a balanced ratio between the elements during overhydration.

Figure 101 : Pantheon Pozzolanic lime _ Calchèra SanGiorgio

This is an air lime micronised by pozzolan to get a hydraulic reaction even if the lime is an air lime.

CARATTERISTICHE TECNICHE

Forma	**Polvere**
Colore	**Ambrato**
Finezza	**40-80 µm**
Massa volumica apparente della polvere	**≈ 0,5 g/cm^3**
Resistenza a flessione a 28 gg UNI EN 459-2	**> 3 N/mm^2**
Resistenza a compressione a 7 gg UNI EN 459-2	**> 8 N/mm^2**
Resistenza a compressione a 28 gg UNI EN 459-2	**> 12 N/mm^2**
Resistenza alla diffusione del vapore UNI EN 1015-19	**µ < 8**
Calce libera [Ca(OH)$_2$] a 28 gg UNI EN 459-2	**Assente**
pH	**13**
Reazione al fuoco	**Classe A1**
Definizione	**FL 5.0 conforme alla norma EN 459-1**

Figure 102 : Data sheet of the Pantheon lime _ Calchèra San Giorgio

It can be seen that the compressive strength is almost higher than with NHL5 hydraulic lime. Furthermore, tests have described the strength curves as a function of the setting time [71]. NHL5 hydraulic lime only reached a strength of 12MPa after 6 months.

Laboratory tests precedently done studied mixes with compressive strengths rarely exceeding 1MPa. The addition of natural cement raised the curve initially to 0.3MPa. It remains to be seen whether 'Pantheon' lime is even more effective with a plant aggregate.

7.2.1.4 Binders densities

Figure 103 illustrates the process of developing measurements during the sampling phase. These values are the result of empirical measurements and, as such, are considered factual. The putty lime exhibits a higher density, attributable to its significant water content. In contrast, the "Pantheon" lime demonstrates a reduced density, resulting in its lighter composition, attributable to the lower density of the pozzolana.

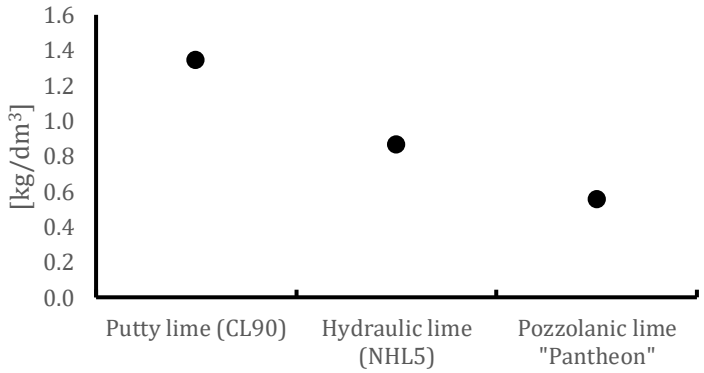

Figure 103 : Binders densities

7.2.2 Additives investigated

7.2.2.1 Quicklime

Quicklime (Figure 104) is the direct result of firing limestone at a temperature of around 900°C. Quicklime is the result of the reduction of chalk stone $CaCO_3$ to CaO, releasing a molecule of carbon dioxide. This simple molecule is very basic. It is not hydrophilic, but when it comes into contact with water, it reacts very strongly and exothermically (up to 150°C). Recent research [39] has taken up the work of learned engineers of the past, such as Loriot [38], and demonstrated the value of quicklime in a mixture based on air lime to increase its mechanical strength.

Figure 104 : Quicklime from Calce Piasco furnace

7.2.2.2 Gypsum plaster

Plaster comes from the firing of gypsum, a rock containing a base of calcium sulphate $CaSO_4$. It is easy to confuse plaster and chalk in Italian and French, as the Latin origin of the two terms is very similar. So care must be taken when using either of these names. Plaster is a powder made from dehydrated calcium sulphate, which is mixed with water to form a paste that hardens by air setting. This hydration simply consists of forming gypsum.

Figure 105 : Plaster of Paris from gypsum Gyproc kiln

7.2.2.3 Pozzolan

Due to concerns regarding the provision, two pozzolans were utilised. As illustrated in Figure 106, the distribution of particulate matter is found to be relatively uniform in terms of both mass and volume.

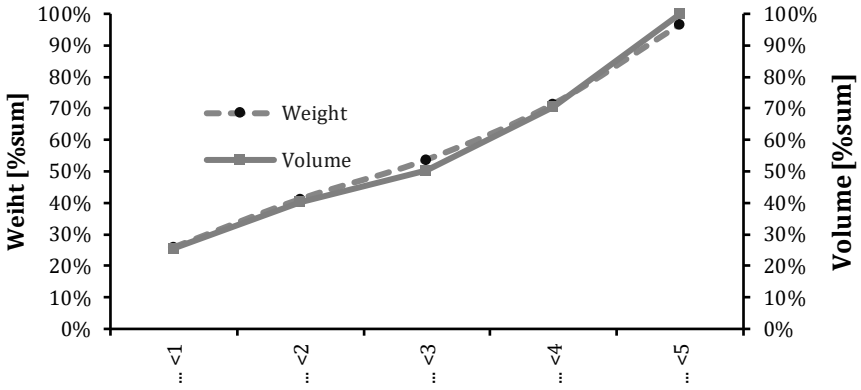

Figure 106 : Particle size distribution of pozzolan

However, Figure 107 indicates that there was a slight variation in the densities of the two products according to particle size. Specifically, the densities of grains between 2 and 4 differ by 25% to 100%, a discrepancy that may be attributable to various factors, including the hydraulic setting of the mixture.

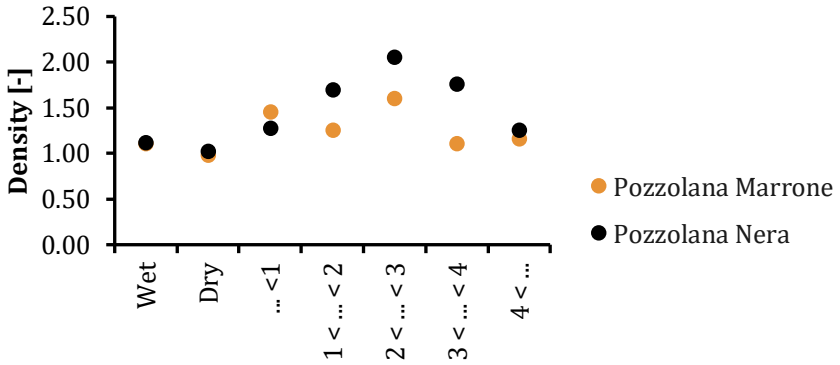

Figure 107 : Densities of pozzolan

As a summary, here (Figure 108) is a box-and-whisker graph showing the distribution of the various measurements made during the samples. It shows that the densities are close to 1.15kg/dm^3.

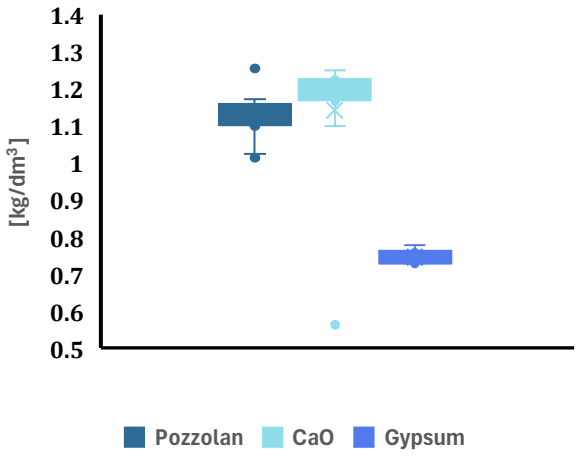

Figure 108 : Box plots of additive densities

7.2.3 Hemp aggregates selected

The hemp hurd used in the experimental campaign was sourced from a single supplier. Conversely, the fibre was sourced from another producer. It is important to note that the fibre was derived from a by-product of a transformation process to become an end-product. After a rigorous selection process intended at identifying materials suitable for this study, only fibres with optical homogeneity were retained, which were then cut to smaller lengths and stored under conditions that prevented compression (hemp fibres had to be cut mostly due to workability issues). The measurements were obtained successively. Consequently, the mean density recorded was found to be relatively low (Figure 109).

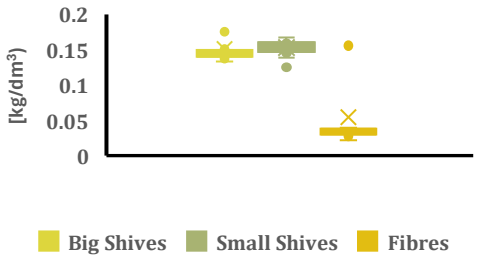

Figure 109 : Box plots of aggregates densities

The initial trials involving the incorporation of long-fibre components proved unsuccessful, as these fibres failed to mix with the other constituent materials (Figure 110). The decision was made to trim the fibres by approximately 2.5 centimetres to facilitate adequate cohesion and thereby enhance the mechanical performance.

Figure 110 : Hemp-lime mix with long fibres

Hemp fibre was very difficult to blend with long fibres. Hemp fibres have been shown to possess hygroscopic properties, rapidly absorbing water from the reaction mixture of calcium oxide, thereby expediting the chemical reaction. Furthermore, a notable distinction in the molecular composition of hemp fibres and hurd has been identified, attributed to the varying levels of pectine. The aforementioned phase encompasses calcium atoms, thereby precluding its capacity to react with the water present in the mixture and subsequently with the CO_2 in the ambient air during the carbonation phase . Nevertheless, the lignine of the hurd is more akin to the concept of an inert material, such as sand. This attribute contributes to the anticipated strength of the mixture, which is achieved through the physical interlocking of the binder and aggregates during the encasement process. However, an exception exists, exemplified by the kerterres [72], whose fibres serve as the primary binding agents, uniting structural elements with aggregates and lime. In this instance, the "nuisance" of the fibres did not appear to have a deleterious effect on the mixture.

7.2.4 Recipe selection

The compositions of the samples shared a common base. The hemp hurd, despite slight variations in proportion intended to maintain consistencies suitable for casting into formwork, serves as the primary inert component to be evaluated for its mechanical role in the hemp-lime composite. Additionally, each formulation includes a variant containing hemp fibres. These fibres are cut into 2.5 cm lengths to ensure homogeneous distribution during mixing.

The Table 5 indicates that, for each composition, the version without fibres is marked with an apostrophe. The first two compositions use putty lime (that is hydrated air lime) as the binder, with pozzolan as a common additive. These two compositions (samples A vs B) are to determine which additive, between quicklime (samples A and A') and gypsum (samples B and B'), offer better mechanical performance.

Composition C is defined by a commercial binder made of air lime mixed with micronised pozzolan. It is therefore relevant to compare the results of compositions A and B with those of C. Could the commercial solution offer higher strength than a traditional mixture that relies on similar chemical processes during mixing?

Compositions D and D' were conceived as an improved version of the hemp-lime composite, as they were based on a hydraulic binder. This formulation is essential for comparing a pozzolanic air lime mixture that develops hydraulic bonds, with a natural hydraulic lime binder.

		Sample Mixes							
		A	A'	B	B'	C	C'	D	D'
Binders	Calcium hydroxyde - "CL90"	30%	30%	30%	30%				
	Hydraulic lime - "NHL 5"							30%	30%
	Pozzolanic lime - "Pantheon"					34%	34%		
Additives	Pozzolan	6%	6%	6%	6%				
	Quick lime	12%	12%						
	Gypsum			12%	12%				
Hemp	Rough hurd	15%	23%	15%	23%	9%	10%	15%	21%
	Fine hurd	15%	23%	15%	23%	28%	34%	15%	21%
	Bast fibers	15%		15%		7%		15%	
Water		8%	8%	8%	8%	22%	21%	24%	28%

Table 5 : Samples mixes compositions

7.2.5 Properties measurements

The following contents have been presented in the following research paper [73] presented at the ICBBM2025 conference and included in the Bio-Based Building Materials Proceedings [74]. Below are the detailed results of testing the samples. The results of this research are very similar to those found in literature [75]. Further elucidation on this subject are provided in the section dedicated to compressive strength. It is clear that numerous studies conclude that lime needs an additive to express its full resistance over time.

7.2.5.1 Density

Density seems to be a parameter with some responsibility for the mechanical strength of hemp lime (Figure 111).

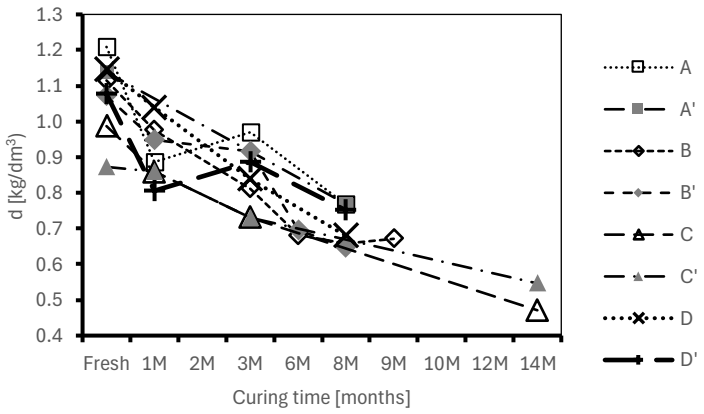

Figure 111 : Mixes densities over time

Here, the mixes have an average density of 1kg/dm^3 at the time of mixing, then this decline to 0.5 kg/dm^3.

7.2.5.2 Compaction rates

The compaction rate is an important factor in understanding how the fresh mix reacts to formwork and placement. From the table in Figure 112, compaction values are quite varied, but can be grouped into two categories, namely low compaction (mixes B/B', D/D'), and medium compaction (mixes A/A' and C/C').

	A	A'	B	B'	C	C'	D	D'
Compaction Rates (compacted/loose) [-]	0.77	0.67	0.97	0.88	0.66	0.64	0.91	0.92

Figure 112 : Compaction rates of the fresh samples

7.2.5.3 Consistency

Consistency is an important factor, as it allows the builder-mason to assess hemp-lime performance during mixing. In the concrete mixer, for example, you can see the difference between a liquid, pasty or lumpy mixture. Additionally, the rebalancing of the mixture at the conclusion of the process requires attention to respect proportions, as this may lead to overcompensation across all dimensions, consequently distorting the original composition.

As can be seen from the diagram below (Figure 113), the mixes with and without hemp aggregates are consistent, with the exception of mixes C and C'. In fact, several preliminary experiments led to the conclusion that the 'Pantheon' binder had to undergo considerable hydration, giving it a liquid consistency, before the hemp could be added to the mix. Despite the liquid consistency of the binder, the proportions of hemp added later gave the mixture the driest consistency of the campaign.

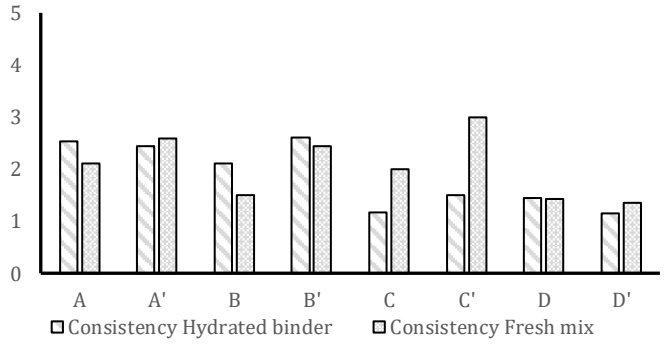

Figure 113 : Fresh samples consistencies plot _ (0:very liquid – 5: dry)

7.2.5.4 Water ratios

In Figure 114, the water/binder ratio consists of the sum of all binders, reacting with water. However, densities of the binders are very diverse (Figure 103) generating a questionable meaning of the water-binder ratio. The water/hemp ratio supports this hypothesis, as it is three times lower in the air lime mixes than in C and D mixes. Consequently, the goal of obtaining relatively homogeneous hemp-lime mixtures required that more water was added to the hydraulic setting mixture. The water thus available would

more easily bind with the hemp hurds before fully reacting with the hydraulic or pozzolanic binder.

	Water / Hemp [kg/kg]	Water / Binder [kg/kg]
A	1.352	0.121
A'	1.209	0.128
B	1.488	0.142
B'	1.186	0.137
C	4.255	1.194
C'	3.511	1.199
D	4.850	0.897
D'	4.701	1.132

Figure 114 : Samples water ratios in fresh mix

7.2.5.5 Hemp-Binder Ratios

The proportions have been designed to make the mix as usable as possible on site (Figure 115). This criterion is therefore the basis for the proportion between binder and water. In a similar way, for the addition of hemp, the study was based on an empirical approach. Several trials were carried out in order to understand what proportion of hemp could be stable in the different mixes.

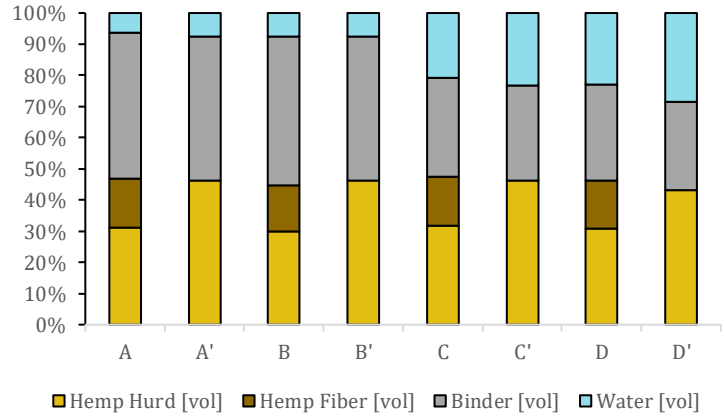

Figure 115 : Hemp-Binder-Water proportions

Figure 115 gives a direct graphical representation of the components of the mixtures, but it is worth taking another look at Table 6, which offers a numerical approximation of the ratios. For samples A/A' and B/B', the volumes of hemp and binder are equivalent, whereas for mixes with pozzolanic or hydraulically setting limes, the ratios are 3:2 in favour of hemp.

As far as the water content is concerned, similarly, combinations based on hydrated lime saturated with water have a very low water content, given that the mixture is already saturated with water. For other combinations, the volume of water added varies between 0.4 and 0.66 times the volume of hemp.

	Hurd:Fiber:Binder:Water By Volume	**Hemp:Binder:Water By Volume**
A	1 : 0.5 : 1.5 : 0.2	1 : 1 : 0.13
A'	1 : 0 : 1 : 0.16	1 : 1 : 0.16
B	1 : 0.5 : 1.6 : 0.25	1 : 1.07 : 0.17
B'	1 : 0 : 1 : 0.16	1 : 1 : 0.16
C	1 : 0.5 : 1 : 0.66	1 : 0.67 : 0.44
C'	1 : 0 : 0.66 : 0.5	1 : 0.66 : 0.5
D	1 : 0.5 : 1 : 0.75	1 : 0.67 : 0.5
D'	1 : 0 : 0.66 : 0.66	1 : 0.66 : 0.66

7.2.6 Results

7.2.6.1 Failure modes

The following is a synopsis of the compression tests. The Digital Image Correlation technique appeared to be a valuable tool in this particular case study, as it provided insights into the kinematic behaviour of the material's rupture. The ensuing presentation highlights the findings derived from samples that have undergone a period of maturation spanning between six and eight months. This decision stems from the recognition that conducting this analysis on samples in their fresh state, or those that exhibit excessive malleability, might not have yielded optimal results. The fresh samples, due to their inherent deformability, would have rendered the assessment of material resistance based on its deformation behaviour somewhat challenging. The results of this study facilitated the characterisation of the rupture mechanism, enabling the categorisation of the findings into three primary classifications. The following diagrams illustrate the system of norms applied in Italy, as referenced by the European system in accordance with the UNI EN 12390-3 standard.

Figure 116 : Failure typologies according to UNI EN 12390

However, the various models of rupture of the UNI EN 12390 have been constructed for concrete, which is a material that exhibits a fragile rupture. The objective of this study is to categorise the rupture behaviour of hemp-lime samples in a similar manner, while taking into account the more ductile behaviour resulting from the heterogeneity in their composition. The purpose was to categorise the ruptures of the hemp-lime samples in a similar manner. However, it is imperative to consider the samples' ductile behaviour, which is influenced by their heterogeneous composition.

Mix typology	Name of the sample	Resulting image correlation	Notes
A	A6M3	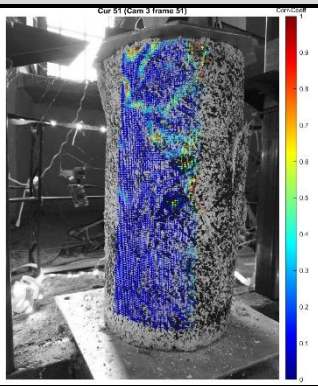	A crack starts at an angle, and some cracks are growing at right angles to it. The fracture happened because of the system's completion. It's a composite break.

A’	A’6M3	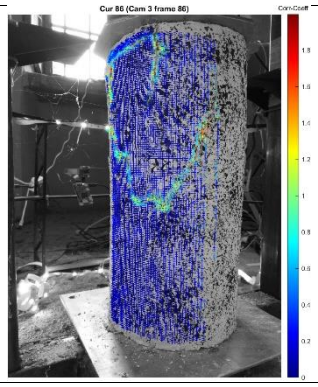	The main crack is from a hole, because the crack goes through the middle of the high part of the cylinder and cut the sample in half.
B	B6M2	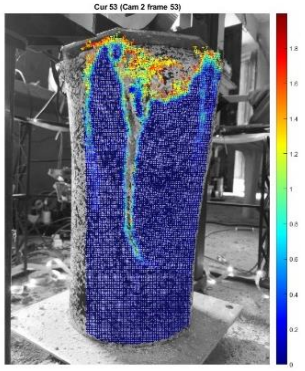	The break in the sample opened it up a lot, but the top part, which was stronger, stayed almost all the way intact. It worked as an escape route during the pressure that was applied vertically. There is a split running the length of the specimen.
B’	B’6M1	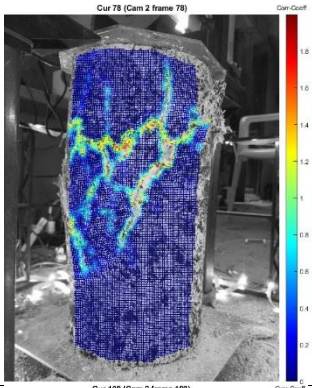	There's a clear dip in the middle of the sample. There isn't a specific plan, but rather a uniform rupture of multiple weak connections within the object being studied. This fracture is a category all its own.
C	C14M1	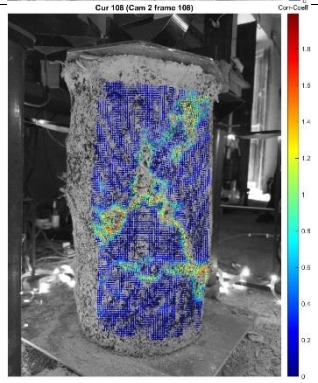	There's a clear dip in the middle of the sample. There isn't a specific plan, but rather a uniform rupture of multiple weak connections within the object being studied. This fracture is a category all its own.

C’	C’14M1	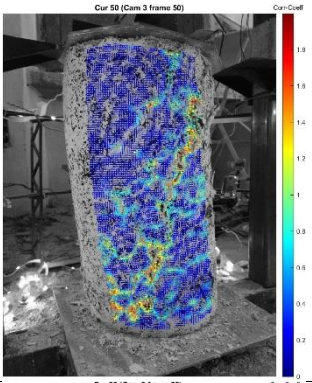	The general configuration of the test is somewhat off-centred. The compression process has undergone a substantial deformation, attributable to a « p-delta »[3] effect. The fracture is singular and aligns with the predominant deformation patterns. Furthermore, the specimen exhibited a multitude of micro-fractures, suggesting that the compressive stress was gradually dissipated throughout the testing process.
D	D8M1	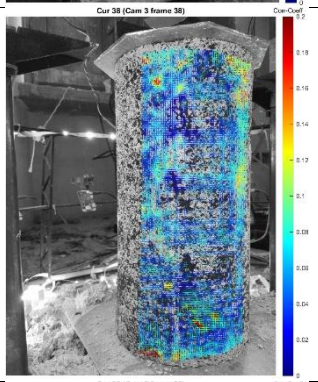	This sample didn't reach the rupture point. However, there is a clear difference in the ends of the sample. Here, it seems like the whole object of study is taking in all the effort. The text is now simpler.
D’	D’8M3	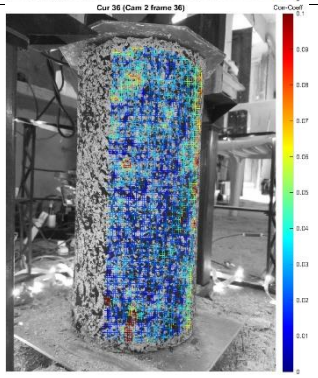	The "D' sample" looks a lot like its copy with fiber, but there's an extra area involved in releasing the pressure, specifically in the middle, in some places. Also, the coefficients of correlation are two times smaller than those for sample D. This suggests that, for the same load, sample D is more solid, while sample D' is more flexible.

Table 7 : DIC Samples Results

As demonstrated in the preceding results (Table 7). The subsequent step involved classifying the various types of rupture in order to formulate an hypothesis regarding the relationship between the measured compressive strength and the observed rupture mode.

[3] The "p-delta" effect is a secondary effect that arises from the lateral deformation of a structure that is subjected to a vertical load.

7.2.6.2 Carbonation over time

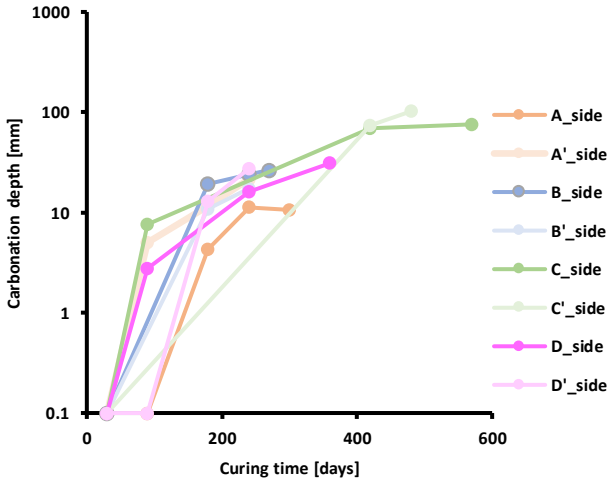

Figure 117 : Carbonation depth_Side

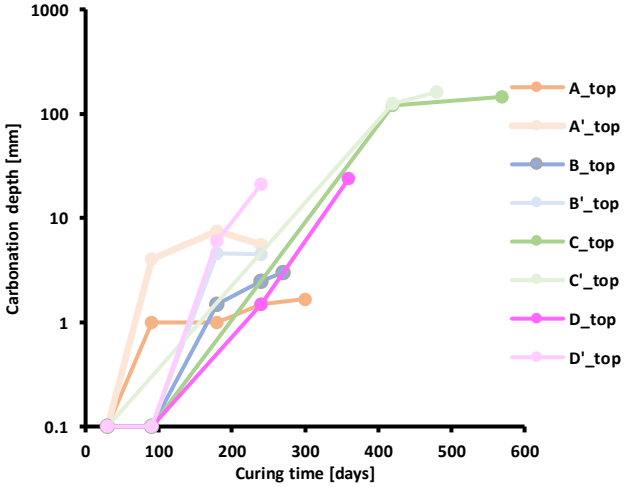

Figure 118 : Carbonation depth_Top

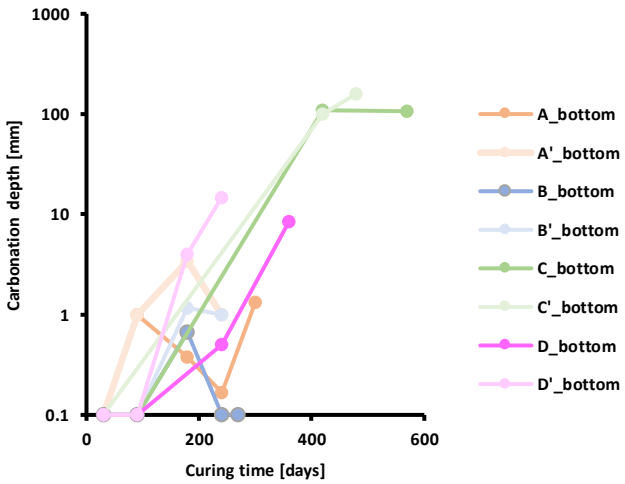

Figure 119 : Carbonation depth_Bottom - detailed

Carbonation behaviour of lime measured empirically here has the same behavioural profile as that of reinforced concrete [76] . Indeed, in the concrete construction sector the relationship between carbonation and strength is calculated as follows:

$$s = K * \sqrt{t}$$

Equation 11 : Carbonation over time concrete typical equation

Where the product of a carbonation coefficient and the square-root time implies a graph in the form of a horizontal parabola. K is a coefficient whose values for conventional concrete can vary between 5 and 10 mm/($t^{0.5}$).

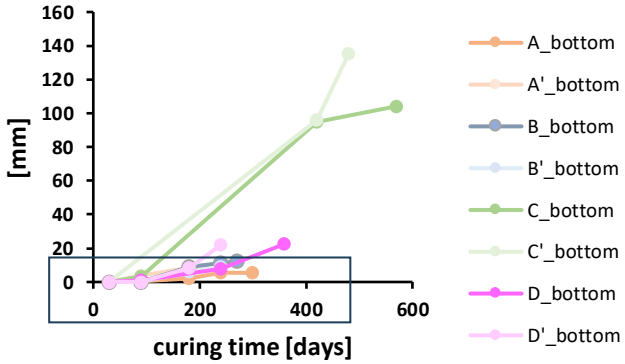

Figure 120 : Carbonation depth _ d(average)

Thus, it is clear that the mixtures containing the "Pantheon" pozzolanic lime exhibited a significantly better carbonation capacity than the other mixtures, which include air lime and hydraulic lime. Long-term measurements of samples C and C' provide an advantage in understanding the long-term carbonation levels but do not offer information on the profile of the carbonation process. Indeed, it is likely that the carbonation process followed an exponential pattern. At this point, each sample could eventually approach the values observed for C and C' over an extended period of time.

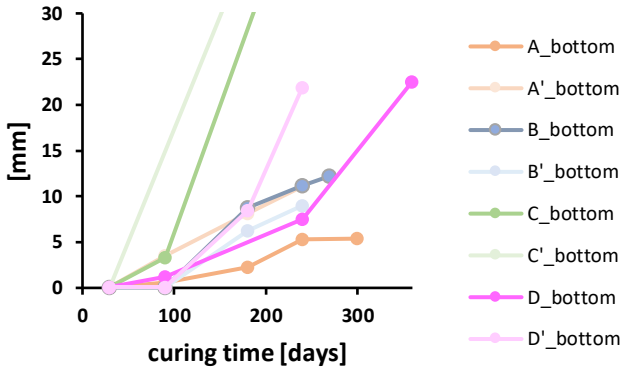

Figure 121 : Carbonation depth _ d(average) – detailed

In the graph above (Figure 121), the analysis considers short- and medium-term measurements in order to compare the samples over periods that are more representative of typical construction project timelines, or at least durations more aligned with our requirements. It is observed that the hydraulic lime samples D and D' show a better carbonation progression compared to the air lime-based mixtures. Furthermore, the carbonation phenomenon appears to be more pronounced in the samples devoid of fibres. Indeed, with the exception of mixtures B and B' (which contain Plaster of Paris), carbonation shows better results in the mixtures without fibres.

It seems that carbonation was significantly activated at the top of the samples, and much less at the sides and base. It could be that the reaction is triggered when the mix is made, rather than a priori. Indeed, the samples were generally kept for at least a day in their forms before being stored. This could well explain why the carbonation at the top is much greater than at the sides. The low carbonation at the base, on the other hand, is explained by the fact that the hydrated mixture was not exposed to air (and therefore to CO_2).

7.2.6.3 Strength over Time

The entire sample population exhibits an elasto-plastic behaviour, as shown in Figure 122 . Each curve, reconstructed from 5th-order polynomial regressions, displays a pseudo-linear phase as the initial step. The coefficient of the slope of the tangent to this phase is considered to represent the elastic modulus of each mixture.

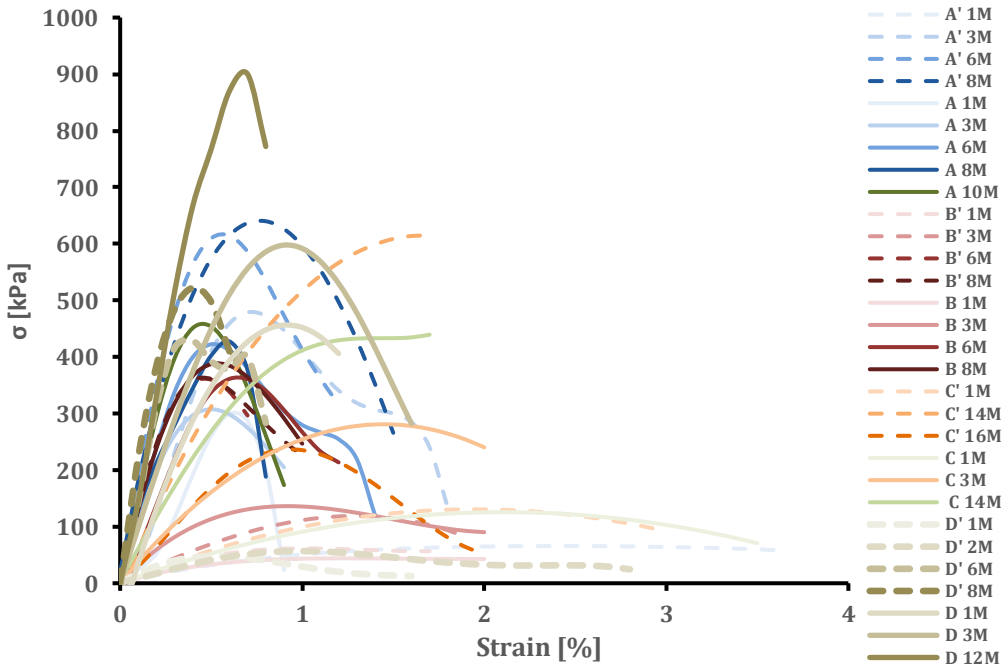

Figure 122 : Stress-strain curves of samples

Two trend zones can be recognised. Samples C and C' exhibit lower elastic modulus values compared to the other types, despite longer curing times (Figure 122 and Figure 123). It is also observed that samples A and A' exceed the elasticity modulus values of samples D and D', while the compressive strength of the latter is slightly higher. This suggests that the combination of quicklime with pozzolana and air lime results in greater hardness than hydraulic lime. Finally, mixes B and B' show very low values, especially during the first months of curing.

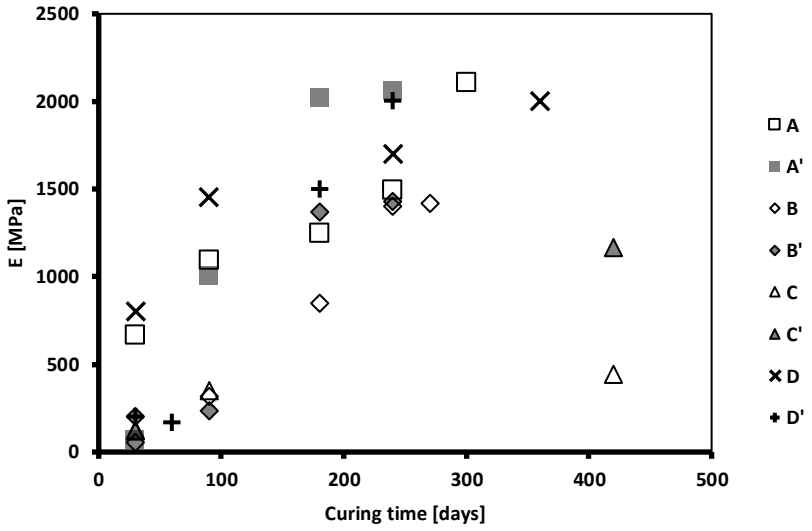

Figure 123 : Young Modulus over Curing time

7.2.6.4 Strength over Carbonation

By correlating the elasticity modulus of the samples with the carbonation depth in Figure 124, it is observed that the air lime mixes show a faster trend toward achieving hardness as a function of carbonation depth, whereas samples C and C' do not seem to exhibit a direct relationship between the two parameters, as the Young's modulus values do not evolve significantly despite the long observation period.

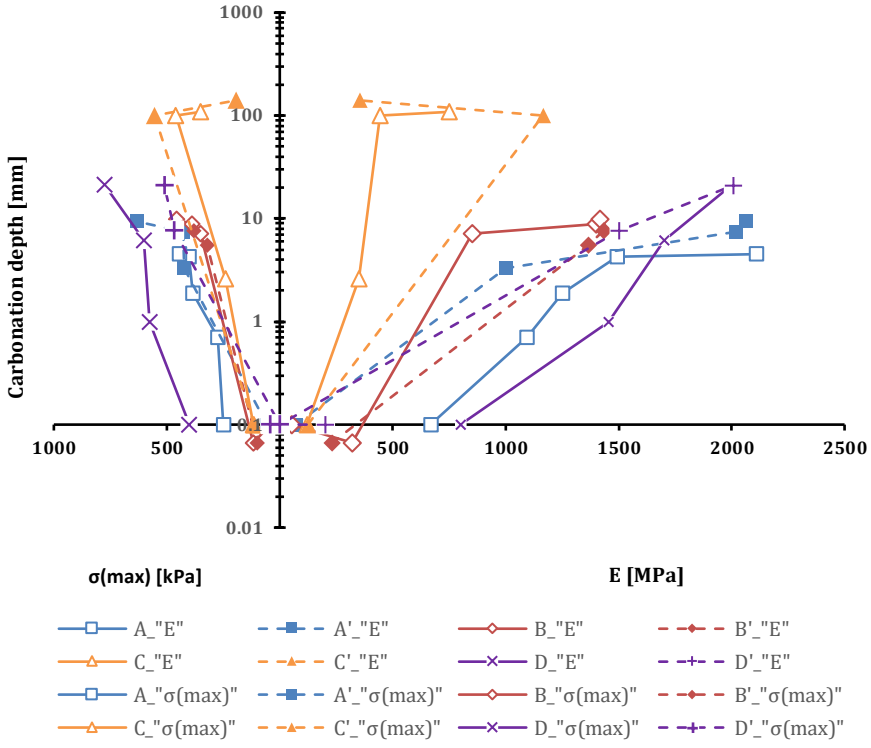

Figure 124 : Compressive strength and Elastic modulus over carbonation depth

A comparison of the compressive strength and elastic modulus reveals that the results demonstrate analogous trends. However, it is noted that the samples with the air lime/quicklime/pozzolana binder mix (A, A') are the strongest, even exceeding the samples based exclusively on hydraulic lime (D, D') (Figure 124).

7.2.6.5 Discussion of compressive strengths reported in the literature

The analysis of compressive strength data serves to evaluate whether the experimental formulations developed in this study have contributed to enhanced mechanical performance in hemp-lime composites. For the comparison of strength values to be meaningful, it was necessary to consider equivalent material densities. Indeed, when examining the relationship between density, curing duration, and compressive strength, it became evident that the specific weight of the mixture was a key parameter that had to be accounted for in the interpretation of results.

A higher compressive strength can be seen in other mixes containing only hurds, with a different binder. For example, lime-based plaster gives better results [77]. The table [77 b)] shows the results of compressive strength around 5 times greater than that of the hemp-lime studied here.

Research by Murphy, Savia and Walker [78] shows convincing results for the Tradical mix containing 10% hemp, as this sample achieved a compressive strength approaching 1 MPa. This is promising as the contrast with other mixes they analysed is obvious: these do not exceed 0.5 MPa. So it is useful to conclude that the proportions and dosage of each element is probably a very important key to the success of hemp-lime.

Another study [79] also focused on a binder known as Tradical, which contains 75% calcium hydroxide, 15% calcium chloride, and 10% pozzolan. In addition, this research analysed four studies ([80–83]); mixes with a water/binder ratio of 1:2 have a mechanical strength that is twice or even three times higher than mixes where the same ratio was reversed.

According to a literature review carried out by Asghari and Memari in 2024 [75], a number of mechanical tests have been carried out on different hemp-lime mixtures since 2005. Strengths values located at an average density of 0.7kg/dm^3 at 28 days (Figure 125), are contained between 0.2 and 3 MPa.

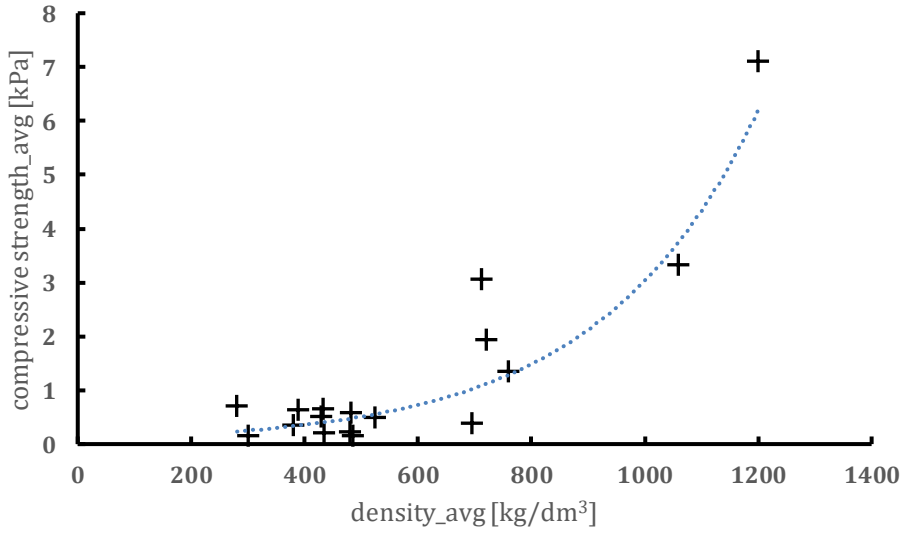

Figure 125 : State of he art of hemp-lime compressive strengths - source : Asghari et al. (2024)

The comparison of compressive strength values reported in the literature has allowed us to contextualise the results obtained in this study. When comparing densities with the measured strength values, the tested formulations did not appear to show significant improvement. However, when considering curing time, it became evident that the values reported in the literature generally correspond to materials subjected to shorter curing periods (typically 28 days), whereas the specimens tested in this research underwent longer maturation times, ranging from 28 days to 18 months.

7.3 Results of comparisons between the prototype and the samples

7.3.1 Carbonation

By integrating the measurements taken on the prototype after stripping the formwork into the carbonation progression curves for the samples, it was possible to notice the possible degree of carbonation. The principle was to input this new data to the correlated curing time and compare it with the curves for the same mixture, as well as those for other recipes, in order to make assumptions about similarities.

As shown in Figure 126, the measured depths of carbonation appear to be consistent with those obtained from the samples.

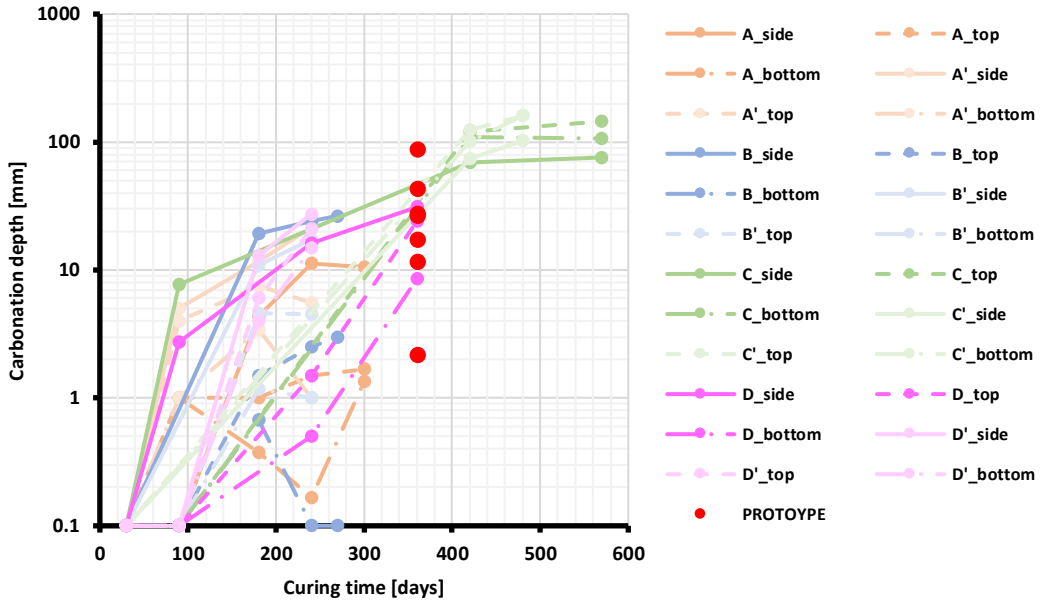

Figure 126 : Carbonation measures of samples and prototype

7.3.2 Moisture content over carbonation

In order to clarify the relationship between the water content and the carbonation of the mixture of hemp-lime used for the prototype, it is necessary to revisit the results previously presented (7.1.9.2).

The object of this analysis was not a population but rather composed of few individual values. Rather than continuous values that might offer insights into overall behaviour, the focus is on specific, instantaneous measurements. The measurement of the carbonation was conducted for each position of the probes during the removal process, since this is a destructive experiment that cannot be repeated at the same location. The determination of the content of water in the sample was made just prior to the demoulding. To that end, a value averaged over the last ten measurements was calculated in order to obtain a more reliable and representative figure.

It appeared challenging to draw a consistent conclusion between the moisture content and the position of the sensors (Figure 127). One potential explanation for this discrepancy could be the absence of an intermediate variable, such as solar exposure.

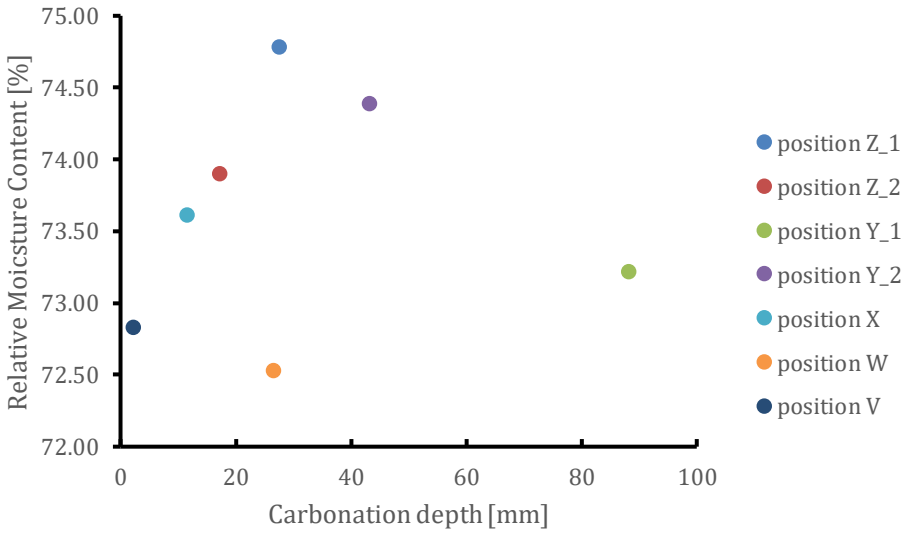

Figure 127 : Relative moisture content over Carbonation depth

7.3.3 Carbonation over compressive strength

It is essential to point out that the method outlined here was a preliminary attempt to establish a correlation, and thus differs from any established methodoloagy. From Figure 122, it was possible to isolate the curve of the mixture C' in Figure 128, that is, the mixture utilised in the fabrication of the prototype. The constant curves represent the measured values of carbonation of the prototype according to their positions. By intersecting the constant values on the curve characterising the behaviour of mixture C', the x-axis is defined by the compressive strengths corresponding to the different states of carbonation.

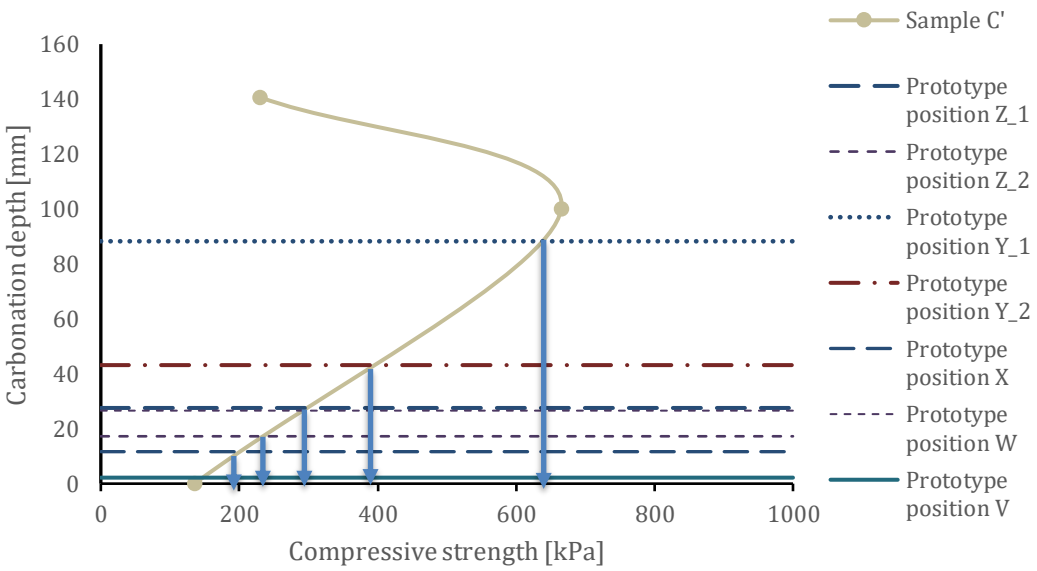

Figure 128 : Carbonation of prototype over compressive strength of C' samples

7.3.4 Moisture content over compressive strength

It seemed that the compressive strength was related to the moisture content measured from the probes right before formwork stripping. Figure 129 Figure 129 suggests a potential relationship between water content values measured by embedded continuous monitoring sensors and mechanical strength. It should be noted that this is a momentary snapshot, and it has not been verified through additional experiments. Consequently, the result must be considered with a certain degree of caution.

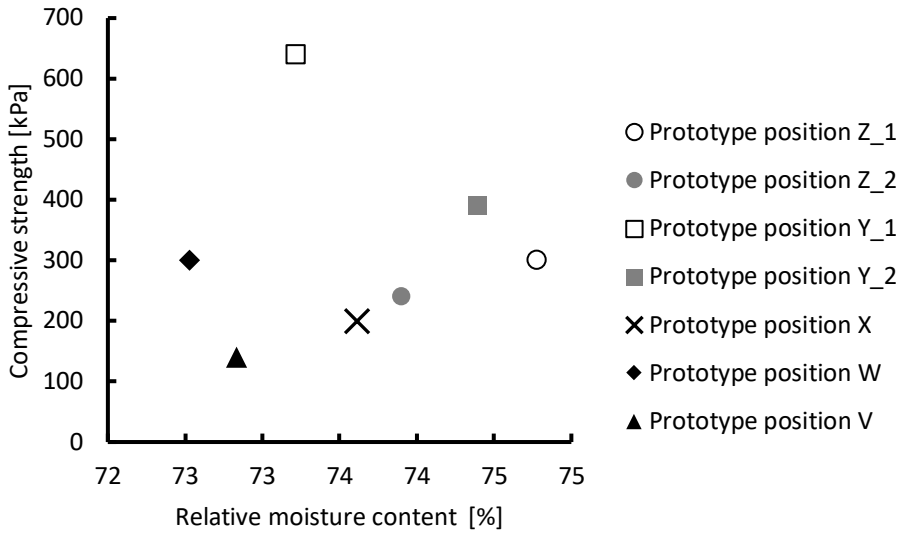

Figure 129 : Compressive strength over relative moisture content on all points

Sensors placed at the same height were clustered to see if there was a logical pattern that could be explained by the amount of sunlight depending on the direction.

Figure 130 shows the relationships based on height and direction. It appeared that, for a given height, the northern orientation (sensors D and E) exhibits a reduced level of resistance and contains a slightly lower amount of water compared to the southern sensors at equivalent heights.

It appeared that, as mentioned in 7.1.9.2, a higher moisture content, might be associated with enhanced strength, at least over the first 12 months for a thickness of 60 centimetres.

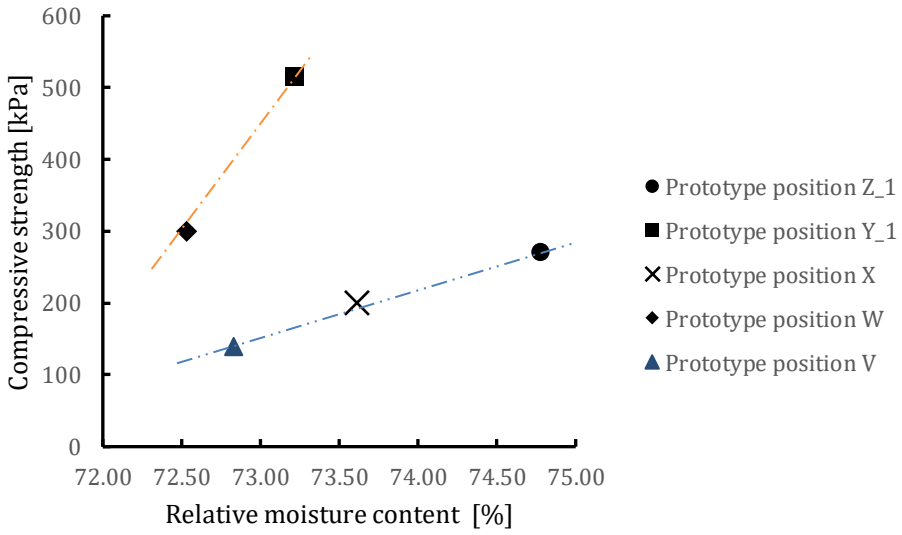

Figure 130 : Averaged compressive strength over relative moisture content

8 Confined recycled aggregates

The experiment conducted on the CRA was derived from a model pavilion constructed by a team of students under the direction of my colleague, Redina Mazelli, and myself (Figure 131). The structure under consideration is a pavilion measuring 4 by 8 meters. Its wooden framework, composed of larch from Piedmont, is affixed to a foundation of CRA, which itself was laid directly on the ground. The walls were composed of a mixture of earth and straw, with varying densities depending on the orientation of the walls, to ensure optimal thermal comfort. The following text is intended to provide a comprehensive overview of the subject matter. At the time of writing this thesis, the construction had not yet been completed. Specifically, the exterior and interior walls had not yet been covered with earthen plaster, and the roof had not been completed. A further interdisciplinary purpose of this investigation entailed conducting a Life Cycle Assessment of the aforementioned pavilion and subsequently comparing it to an alternative pavilion constructed with load-bearing straw bale, which foundation composed of substantial stone slabs [84]. According to the data presented in the Annex 18 : Light-earth pavilion _ Structural floor plan _ 1:50, the CRA system has a total length of 32 meters.

Figure 131 : Lightearth pavilion sketch (drawing created by the author)

8.1 Testing

The construction of the entire project was carried out by a team of students enrolled in the Master of Architecture program. The team was under the direction of my Ph.D. colleague, Redina Mazelli, and myself. Henceforth, the pronoun "we" will be used to denote the entire team. A preliminary test was administered during the delivery of aggregates to facilitate understanding and the development of competence. The procedure involved the construction of a box, achieved through a meticulous cutting and assembly process. A formwork was not created; rather, the cage, which had been positioned on a platform, was filled in a loose manner. At the midpoint of the cube, a metal tie rod was briefly affixed, and the filling process was continued. The closure of the grid was accomplished through the implementation of simple twisted iron wires on two sides of the block. The closure of the grid was facilitated by the implementation of simple twisted iron wires on two sides of the block.

Figure 132 : First attempt of CRA

The result seemed convincing in terms of stability, shape and workability (Figure 132). The height used for the test was the same as that of the pavilion foundations. We, the working team composed of 3 students for this stage, Redina Mazelli and I, have decided that the formwork will not be used for a larger height.

8.2 Construction phases

8.2.1 Preparing the cage

When preparing the first strip footing, we did not prepare any formwork. The linearity seemed to hold despite its 8-metre length. But we realised too late (during the filling of aggregates) that it was necessary to pre-stress the cage with diaphragms, and to form the whole thing before creating the lateral thrust due to the amount of rubble. It was necessary to remove the excess elements, re-tension the cage, constrain it with internal diaphragms and refill the assembly. This misjudgement required a total of 7 days work with an average of 3 people per day. The remaining of the confined recycled aggregates was much more efficient, because we did the necessary work beforehand. The formwork and pre-stressing of the diaphragms is the most time-consuming activity. For the next 8 metres, the time spent was 2.5 days with 3 people. Almost 1.5 days were needed to organise the cage and 1 day for filling and closing.

To create the galvanised steel cage, we started from the braided metallic sheet, which we measured (Figure 133). We used a grinder to cut the wires, and pliers to make the twists. For the twisting of the cover, in order to effectively tighten the grid we used the crowbar, which allowed us to have a much higher torque.

Figure 133 : Fixing the fence by hand

Pre-tensioning of the mesh has to be done frequently, as the whole is completely flexible. Therefore, we fixed one sheet every meter. The diaphragm is folded at both edges so that one or two cells can be twisted together. The static assembly is practically conditioned by the strength of the diaphragms. It is important to take into account the orientation of the cells because the diaphragm resists horizontal tension. Therefore, the rhombus of the cell must be elongated, so that the twists are also horizontal and resist the tension by friction (Figure 134).

Figure 134 : Fixing the bracing meshes

When the cage is prepared, even before the formwork is fixed, we had to position it in its exact location. The side of the mesh that is in contact with the other CRA element must be fixed. Therefore, before proceeding with the next step, we had to twist the two sides in contact at several points (Figure 135). We made about ten twists on the surface of 0.75m *

0.5m = 0.375m^2. The complexity of this action lies in the lack of space to twist the two faces. While in general, having both sides free made the work easier, twisting with only one side available seemed an awkward and very slow job. We also used the back of the pliers to make all the connections (Figure 135).

Figure 135 : Attaching gabions together

Once the positioning and fixings were done, the action was to organise in the same way as the dry-stone walls (Figure 136). The intention is to build a wall that can take all the vertical loads by close contact with the rubble. Here, the rubble is mostly made of concrete, bitumen, stone and screed debris. We placed the larger pieces against the grid so that they could be contained by the cage with no movement, and so that they themselves contained the smaller pieces inside. Every piece of debris is necessary for locking the system. It is therefore important to avoid using chalk or plaster rejects as was sometimes the case. We therefore decided to organise a rough sorting before placing the rubble in the cage. When we encountered mica-bearing stone, we kept it aside so that we could grind it into the raw earth plaster on the walls of the pavilion.

Figure 136 : Positioning the first stones by hand

8.2.2 Filling

The formwork was made using conventional 30 cm wide formwork boards (Figure 137). The cages were 40 cm high with rubble and 5 cm thick with the larch table. We therefore decided to place them 5 cm from the ground, so that they could hold the whole thing together as evenly as possible. The boards were blocked with larch strips cut on site at a height of 50cm, and drilled at the foot and head to accommodate tie rods made of 6mm diameter threaded rods. As a washer for these tie rods, we used the metal angles of the future posts. In order to maintain the required width, i.e. 75cm wide, we measured all the thicknesses and subtracted them from the threaded rods. 4 cm on either side of the rod gave us the precise width on the inside. To block the system, we used butterfly dices for ergonomic reasons.

Figure 137 : Preparing the grid in the formwork

The verticality of the system was guaranteed by brackets derived from the formwork boards cut on the diagonal and coupled at 90° to optimise its resistance to tipping (Figure 138). These makeshift angle brackets were then screwed to the ground in plumb with the horizontal formwork, and then with the help of pieces of wood, we took over the verticals during the filling and closing of the cages.

Figure 138 : Fixing the formworks

After a few buckets of aggregates inside the cage, and a minimum of manual ramming, we fixed tensile cables always in galvanised steel between each compartment made by the diaphragms, at a height of 10cm and 30cm (Figure 139). This means that the cage was stressed by linear tension and by point tension every meter in a phase-shifted manner. This compromise avoids a significant amount of steel wire. The twisting was still done by means of pliers. However, the risk of cutting the wire led us to file the cutting part of a plier in order to pinch without cutting the wires during twisting.

Figure 139 : Tie rods

This phase is very physical as it involves moving large volumes of debris from the storage area to the foundation site. The dust generated was a hazard to be considered. For this reason, regular rehydration breaks were strongly recommended and adhered to by all staff. As the cage filled up (Figure 140), we had to be careful to arrange the stones in a certain geometry along the cage, to avoid the escape of smaller stones.

Figure 140 : Filling the gabions

The placement of stones is a limiting process because of the small dimensions of the aggregates. The average grain size of the rubble was around 5cm to 12cm, but it was common to find gravel below the 6/8cm threshold of the cells. These had to be compacted

to fill the voids created by the angularity of the larger stones. The method chosen was manual ramming, as we could not vibrate manually. It was therefore decided that after two passes of placing the gravel we should use the sledgehammer (Figure 141) to create this stability. We were instinctively aware of compaction was taking place by walking on the pile.

Figure 141 : Smashing the rubble for compaction

8.2.3 Bearing plate setup

Once the cage was almost completely filled and after a final constipation, we put the tables on the pile. With the help of a laser placed at the beginning of the construction at a height of 37.5cm higher than the high limit of the table, we measured the altimetric positioning and the horizontality of the boards. Once levelled, we withdrew it for a moment to definitively fill in the smallest hollows and increase the support areas to distribute the future loads evenly. We tried to use the spirit level but its effectiveness was very limited because almost all the larch boards were spilled. The reason for this may have been geometrical, as the larch section was thin at 5cm thick and 24cm long.

Figure 142 : Positioning the beams

The two larch planks also had to be stabilised within the cage and prevented from moving during the closing and tensioning of the system. To do this we placed 5cm larch

spacers on each side and screwed them in place to take up the 75cm width of the cage (Figure 143). We placed them every 50cm and then filled and compacted the rest with aggregates before closing the confined stone wall.

Figure 143 : Spacing of the beams

The closure was made with sheets of wire mesh placed in such a way that we could "twist the twists" of the two sheets together (Figure 144). We started with one edge by giving a few turns. Then the other side was made after tensioning with the crowbar. The knot was first described by Louis Geiswiller, an experienced French architect-craftsman who was contacted for training purposes.

Figure 144 : Closing the gabion edge

8.3 Observed criticisms experienced on the site

The initial foundation has undergone numerous modifications due to its status as the first attempt for the entire team. The removal of significant amounts of aggregates, which occurred several times, may have created imbalances in certain areas. In addition, insufficient consideration was given respect to the other foundations when placing the fill material.

Another critical point was the connections between the different faces of the cage. The first base plate is entirely connected by independent wires of the mesh, but of a larger diameter. This could create voids in some areas, giving the mineral matrix more space.

Manufacturing errors will not be considered hereafter. Rather, the construction will be assessed in accordance with the modus operandi advised by the artisan architects who have been practising it since 2003 [85]. The measures applied to achieve a Confined Recycled Aggregates foundation are listed below:

- The formwork should be set up in such a way that the cage is crushed against the walls. This results in a relatively smooth surface.
- The mesh diaphragms are to be fixed every metre, coupled with tie rods 50cm out of phase.
- The connections are made by twisting the cells of the two meshes together for at least three whole turns.
- The connections are made every 3 cells to ensure a perfect joint.
- The formwork is only removed once the covering face has been fixed at almost all points.
- The arrangement of the stones must always be thought out in order to lock them together.

Despite all the good practices, there is always a risk of erroneous installation, especially when placing the stones. It is possible that the strength of the different materials is not homogeneous, and that a bitumen breaks when it meets a granite point. This breakage naturally causes a gravitational rearrangement of the aggregates. It is therefore interesting to know the reaction to the meeting of the different materials that constitute it.

8.4 Results on site

The main experimental results of this experiment consisted in measuring the local displacements, or in other words the settlement, that the gabions underwent as a result of the load of the successively placed wood structure.

In accordance with Annex 23 :, we measured the load emitted on the gabion at this level of construction. Since only the timber structure is involved, we were able to extract the G1 value from the table. At this stage of construction, the total weight is 54.15 kN. Distributed over the total surface area of the gabions (21.54m^2), this gives a surface load of 2.51 kN/m^2

In order to maintain a certain level of accuracy, the measurements were taken using a laser placed at a height distant from the structure (Figure 145).

Figure 145 : Laser measurements of settlement

The measurement is then repeated three months after the structure has been installed on the gabions. The measurements at the four corners are shown below (Figure 146).

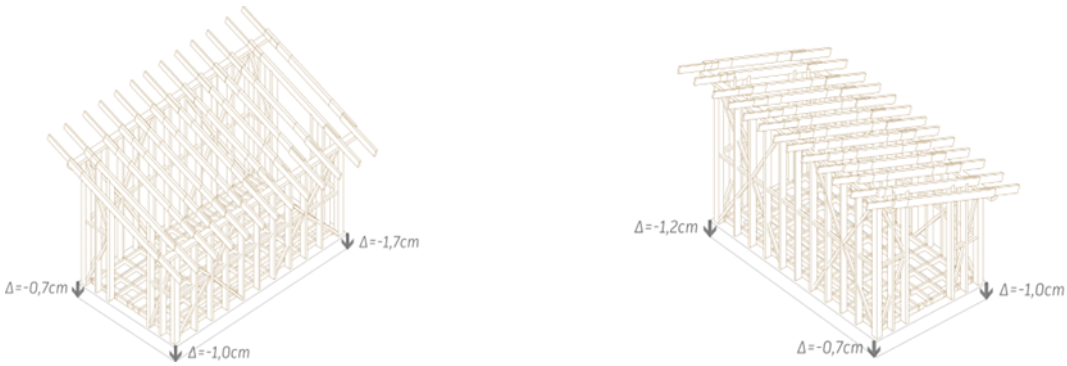

Figure 146 : Synthesis of local settlements

8.5 Aggregates

8.5.1 Analyse of the recycled aggregates

With reference to the Italian standard UNI 933-11:2009, it is important to define of the components of the aggregate (Figure 147).

prospetto 2 **Costituenti non galleggianti di aggregati grossi riciclati**

Costituente	Descrizione
Rc	Calcestruzzo, prodotti di calcestruzzo, malta Elementi per muratura di calcestruzzo
Ru	Aggregato non legato, pietra naturale Aggregato legato con leganti idraulici
Rb	Elementi per muratura di laterizio (per esempio mattoni e piastrelle) Elementi per muratura di silicato di calcio Calcestruzzo aerato non flottante
Ra	Materiali bituminosi
Rg	Vetro
X	Altro: Coesivi (ossia argilla e terreno) Varie: metalli (ferrosi e nonferrosi), legno non flottante, plastica e gomma Gesso rinforzato

Figure 147 : UNI 933-11:2009 _ Table 2

The real granulometric composition has been documented by the furnisher. According to UNI 933-11:2009, the furnisher declares the mass distribution of the different components (Figure 148). 20% is recycled concrete, 20% stone, 50% bricks, lightweight screeds and calcium silicate, 2% bitumen (there seems to be more in the mix, but this is due to its relative lightness in this context), 2% glass and traces of earth and floating materials.

Informazione sul Prodotto	Unità di misura	UNI EN 13242
2007 DoP e cod. identificativo: 28 Riciclato 40/100		
Dimensioni-Granulometria	Aggregato Grosso riciclato (d/D) mm	40-100 d/D Gc 85-15
Massa volumica delle particelle SSD	Mg/m3	2,02 Mg/m3
PUREZZA		
Contenuto dei fini	categoria	f2
Percentuale di particelle frantumate		C 90/3
COMPOSIZIONE / CONTENUTO		
- Classificazione di aggregati grossi riciclati		Rc20, Rcug 40, Rb 50, Ra 2, Rg
2-, X 1, FL 5-		
- Solfato solubile in acido		0,476%
- Zolfo totale		S 1
- Cloruri idrosolubili metodo di Mohr		0,005% CI
- Costituenti che alterano la velocità di presa e di indurimento delle miscele legate con leganti idraulici		Esente da sostanza organica
Assorbimento di acqua		WA24 3,9%
Rilascio di altre sostanze pericolose		Esito conforme ai limiti test DM
05/04/2006		
Emissione : Ed2 rev. 10 a partire dal 28/02/2023		

Figure 148 : Transport document describing the composition of the material.

8.5.2 Dimensional analysis of the aggregates.

The facility for the treatment of demolition waste contained a variety of materials resulting from this process, including the product under consideration, which consists of aggregate particles ranging in size from 40 to 100 millimeters (Figure 149). The material was exposed to the conditions of the atmosphere, resulting in the formation of these accumulations, each exhibiting a distinct angle of friction derived from the natural inclines of the aggregates. This observation highlights the notion that the technical capabilities of a given material can vary significantly based solely on its geometric statistics.

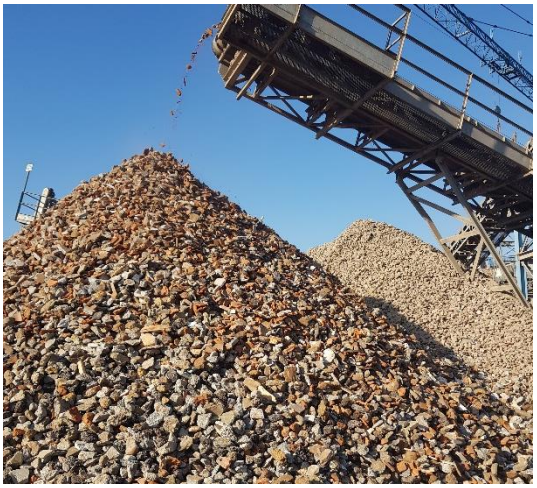

Figure 149 : Landfill of crushing plant _ CAVIT Company (Turin)

There was no risk of the elements passing through the screen as it is industrially sieved to a certain particle size. In fact, as shown in the image in Figure 150, the test was carried out on site using a piece of wire mesh brought in for the purpose.

Figure 150 : Recycled aggregates 40-100mm

8.5.3 Definition of the virtual aggregate properties

A number of studies have sought to formulate a hypothesis regarding a comprehensive physical model that encompasses the constituent elements of a gabion. As indicated in the references, the publications of Brocato et al. are of particular relevance [86]. The research team's efforts have culminated in the development of a model for elements extruded along six distinct orientations, meticulously aligned along the axes X, Y, and Z. The defining characteristics of these elements are attributed to the surfaces of friction that exist between them. Thus, each element is defined by its contact surface. In order to modulate this contact surface, a gradual parameter was defined, allowing to increase or decrease the value for each orientation of the cube. Consequently, this model significantly reduces the computational time required by the finite element method.

Secondly, following the establishment of the problem of geometry and the physical approach undertaken by the preceding research team, it is imperative to address the materiality of the elements, particularly given the heterogeneity of the components in this study. Therefore, by developing research into the mechanical characteristics of the various recycled aggregates, enabled justifying the hypothesis that it is possible to use a single standard material to develop numerical simulation. This is a measured simplification, since the mechanical strengths of fired brick, concrete and other recycled materials are approximately the same, at least when the population is large and homogeneously distributed.

	Young Modulus	Density	Part
Type of aggregate	**(MPa)**	**(kg/m^3)**	**(%)**
Concrete	$20 - 50 \cdot 10^3$	2400	20
Natural stone	$25 - 60 \cdot 10^3$	2600	20
Bricks	$15 \cdot 10^3$	1700	25
Calcium silicate	$10 - 20 \cdot 10^3$	800-1300	25

Sources : Wikipedia ; https://www.researchgate.net/figure/Evolution-du-module-dYoung-du-platre-en-fonction-de-la-porosite-ajustement-avec-la_fig7_281015332; https://materiautheque-laplace.second-degre.ac-normandie.fr/spip.php?article26

The theoretical material values are calculated as follows:

$$E_d = \frac{(20 \times 35 \cdot 10^3) + (20 \times 42{,}5 \cdot 10^3) + (25 \times 15 \cdot 10^3) + (25 \times 15 \cdot 10\text{^}3)}{100} = 2.3 \cdot 10^4\ MPa$$

Equation 12 : Weighted average of the virtual Young Modulus material

$$\rho_d = \frac{(20 \times 2400) + (20 \times 2600) + (20 \times 1700) + (25 \times 1550)}{100} = 1{,}728\ kg/m^3$$

Equation 13 : Weighted average of the virtual Density material

Understanding the shapes of each type of aggregate allowed to model meshes that are consistent with reality. The contact between them will be random, by creating a gravity drop on the Blender software. The mechanical strength of each of the materials broken down into recycled inert materials needs to be analysed.

8.6 Computational simulations

8.6.1 First attempt : OpenFOAM

8.6.1.1 Expectations

The utilisation of open-source software known as OpenFOAM was desired for the given undertaking [87]. Firstly, the software was previously utilised in a bioclimatic project that was the subject of the author's master's thesis in engineering. The objective of this thesis was to attempt to simulate the climatic effects of conceptual decisions of the "passive solar" type on the designed space. To this end, the simulations were conducted in a fluid dynamic framework, with the ambient air and its heating by solar radiation stored in radiating masses serving as the primary focus.

It was hypothesised that the software would be capable of handling mechanical equilibrium equations, as well as working out transient mode solutions to equations such as the Navier-Stokes equation. A segment of the software has been developed for the solution of solid mechanics problems. An attempt was made to test this functionality by modelling a gabion composed of randomly dispersed particles, confined within a fully modelled metal mesh.

The initial challenge encountered pertained to the modelling process itself. While the aggregates did not pose a significant challenge in terms of managing the connections, as they were simply superimposed, the metal mesh emerged as a distinct concern. The challenge lay in articulating the intricate mesh nature and ensuring the integrity of each surface. The advantage gained from prior construction experience was significant;

however, the complexity of the model, as evidenced by the number of links, was a substantial challenge. The simulation calculations proved unsuccessful, and the computer malfunctioned. Consequently, following multiple attempts to simplify the model, it was decided to focus on a specific subset of a few elements that were merely compressed. Consequently, the focal point of this inquiry transitioned from the endeavour to visualise the descent of charge within the material composition of an entire gabion to the transmission of forces between two particles that are intimately linked by simple supports.

Another obstacle was the rearrangement of particles within the gabion during loading and stressing. Despite attempts to simulate a transient condition, visualisation of the relative displacements of the particles with respect to each other remained impossible. However, a detailed description of the research process is justified in order to explain the reasoning behind the decision to change software resources and use an alternative software package (LIGGGHTS) designed for the management of physical particles.

8.6.1.2 3D Modelling

The axes of the mesh wires were drawn in AutoCAD so that these segments could be extruded in steel wire with a quantitative thickness. The objective is to reproduce the weaving geometry with precision; however, the twists have not been created. The resulting structure is more similar to a mesh (Figure 151). The purpose here is not to observe the local friction between two twisted wires, but rather to gain an overall understanding of the stress obtained on the metal mesh. Nevertheless, subsequent analysis will demonstrate that the calculation was unsuccessful.

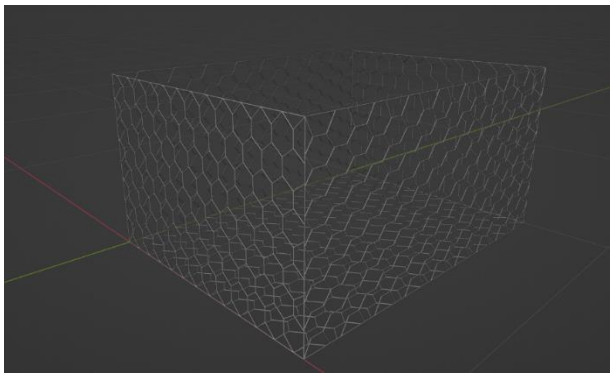

Figure 151 : Metallic cage 3D model

The second phase regards the generation of fillings and the random setup. Thanks to the management of ”modifiers” function within Blender, the creation of the aggregates did not require the elements to be generated one by one (Figure 152). Instead, it was necessary to

create a cube with a volume slightly smaller than the cage, and to divide it in space. This technique allowed us to create very realistic aggregates, as the angles and shapes are constructed completely at random. The dimensions of the elements are not completely managed, but it was possible to roughly assume the dimensions by comparing them with the mesh of the cage.

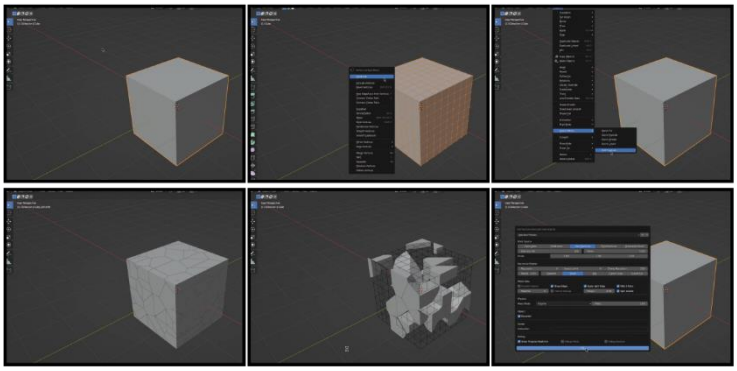

Figure 152 : Cube crushing for aggregates

Blender is a software that allows the user to simulate forces on objects (Figure 153). The risk is that there could be voids inside the cage. To reduce this effect, it was necessary to wait for a number of calculation iterations in order to make the assembly stable.

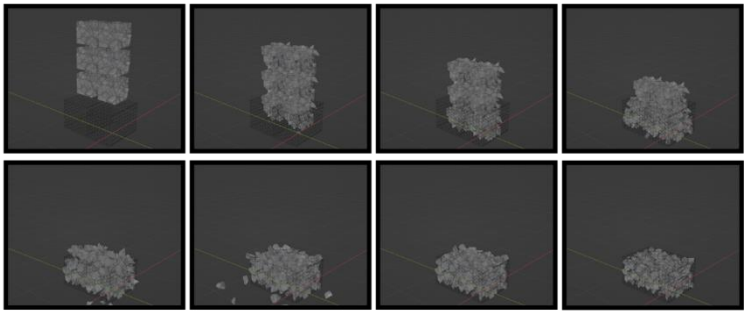

Figure 153 : Step motion of gravity fall _ Blender

Meshes were then created from the 3D model by exporting .stl files from Blender. Each group of geometry corresponding to a study element of the calculation was exported in ASCII version, which means that it is not encoded in binary, but in a readable file, where it is possible to read the coordinates of each point in addition to the name of the geometry. This is the encoding that is readable by the OpenFOAM software. The data was then stored

in a folder called "constant/triSurface". Next, it was necessary to start the "blockMeshDict" and "snappyHexMeshDict" files in the Linux terminal after starting OpenFOAM. The Ubuntu version 18.04 operating system, which has openfoam-v2012 and Paraview 5.6 installed, was utilised in this instance. The ".eMesh" files generated by the two scripts described above were located in the "constant/extendedFeatureEdgeMesh" folder. Also included were the boundary and patch constitution files, which defined the contacts between the elements.

The screenshot below (Figure 154) shows all the meshes generated by the scripts, with the colours showing that each aggregate is a unique element.

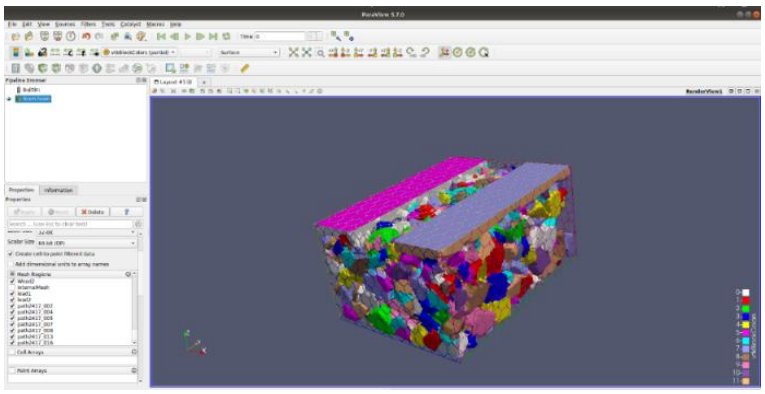

Figure 154 : Coloured meshes by ID

8.6.1.3 Transient state Solving

What is presented here is the compressive force values for each face of the mesh. The results shown in the screenshot in Figure 155 highlight the gradient of the "sigma" normal force propagating from near to near in the gabion. The increase in values can also be seen at the edges of the wooden plank, the surface of which is subjected to a pressure of 5.0 MPa.

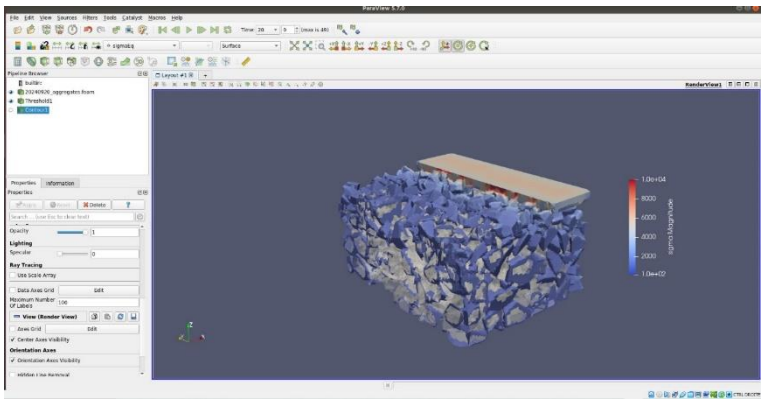

Figure 155 : Screenshot transient state from OpenFOAM

8.6.1.4 Steady state Solving

The steady state numerical analysis is limited in its ability to recalculate the position according to the time of exposure to an increasing load. Consequently, the present study focused on reiterating the calculation to achieve minimal convergence for a given equilibrium state.

The section studied here is a simulation test that illustrates the success of the load transfer calculation. The simulation starts by applying a homogeneous pressure of 150 Pa (=N/m^2) to one of the elements (Figure 156). The normal forces are then transferred to the surrounding elements. Upon modifying the range of values in the legend, it becomes evident that diffusion is significantly restricted despite the stiffness of the material. The result was a success, but the calculation time was too long to consider loading the entire gabion into the calculation.

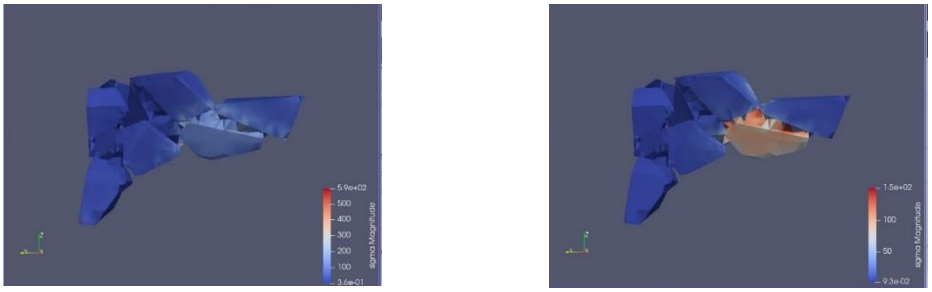

Figure 156 : Transient state local simulation in OpenFOAM : high range legend (left) - small range legend (right)

8.6.2 LIGGGHTS simulations

In light of the failure of the numerical calculation-based finite element method (FEM) to effectively monitor the general population of confined agglomerates, a complete rethinking of the information technology infrastructure was considered necessary. Rather than conceptualising the aggregate as a population of distinct entities, it was determined that a more fruitful approach would be to adopt the concept of a group of particles, with interactions serving as the primary parameters requiring calculation, as opposed to the internal forces of individual elements.

The notion of calculating a group of particles in a simplified manner has been previously explored in a 2024 study, which elucidated the deformations of a gabion [88]. In this research, the software used is PCF3D, a proprietary software developed since the 1970s and used in both academic and professional settings. In this study, an alternative open-source software, LIGGGHTS (LAMMPS Improved for General Granular and Granular Heat Transfer Simulations), was utilised. This software is well-regarded within academic circles for its capacity to customise analyses [89].

Indeed, LIGGGHTS is a software that functions through an array of text files. Its primary strength lies in its adaptability, particularly in the domains of data insertion and simulation calculation management. In particular, despite the lack of a native graphical interface, the software can be effectively converted into a graphical representation through the use of a complementary opensource software called Paraview. While LIGGGHTS is indeed a highly customisable software, its complexity is proportional to its level of customisation, as it involves encoding within a specialised language.

Therefore, the ".in" files use a unique software scripting language, which is different from conventional programming languages such as Python or C++, but rather a specialised command language analogous to a configuration language or shell script.

8.6.2.1 Definition of particles properties

The simulation involves filling a gabion with a base dimension of 1m by 0.75m and a height of 0.5m with a set of particles. The particles are composed of two types of spheres, with radii of 0.02cm and 0.05cm. The composition is indicated by 40% small particles and 60% large particles. In addition, to make the model more complex and realistic, two densities were assigned, 1,500kg/m^3 and 3,000kg/m^3 respectively.

8.6.2.2 3D Modelling

The modelling is also done on Blender, and the various elements are then exported in ".stl" format in ASCII mode. It is important to produce simple, error-free meshes, so that

the calculations can be carried out without error. So, in order to produce the total model, here is the list (Table 8) of singular elements exported:

Name	Dimension
« FenceFence.stl »	2,13 kB
« FenceFenceCenter.stl »	7,56 kB
« InsertionTotInsertion.stl »	0,423 kB
« Load1.sl »	0,391 kB
« Load2.stl »	0,391 kB
« Load3.stl »	0,391 kB
« Load4.stl »	0,391 kB

Table 8 : List of .stl models for simulation

8.6.2.3 Set Up simulation environment

Annex 25 : shows the various stages in the construction of the case study. Note the two parameters that affect the time analysed are the calculation interval and the number of iterations. The temporal framework for each iteration is defined by the following parameters: In this instance, the temporal span allocated for each iteration is defined as $10^{(-5)}$ seconds. And the different "runs" produce $1,1*10^{(5)}$ seconds. The product gives 5.5 seconds of analysis.

The configuration of the quantity of the particles and the determination of their initial position within the simulation proved to be a particularly onerous aspect of the procedure. They were integrated using two main parameters, the total mass of particles and the mass flow rate per second. In this way, the simulation perfectly understands the method of integration, although it can be noted during the script launch log that the masses are approximate, due to the spherical geometries. At each iteration, the number of particles was the ultimate quantity that ensures that the value given in the script is not exceeded.

Upon completion of the packing run, the script integrates new parameters that comprise the second phase, loading, that are the force (in Newton or more specifically in $kg*m/(s^2)$), the speed of completion (in m/s), and three other parameters specific to the function used immediately afterwards, which is "servo", and which explicitly indicates that a load is being applied (Annex 25 :LIGGGHTS Input Script).

The force applied is calculated from the dimensioning calculation of the timber structure. Since, at the time of the laser measurement on site, the pavilion contained only the timber of the structure (Table 9), the total weight of the structure is extracted. Dividing this weight by the total surface area of the gabions gives the surface load. Finally, this value is multiplied by the surface area in m^2 of the gabion studied in the simulation. The result is :

$$F = \frac{54\ kN}{21.5\ m^2} * 0.75m^2 = 1{,}875\ N$$

Structure under examination	Element	Structural element	Mass density	Density	Volume	Weight					
		[G…]	[kg/m³]	[kN/m³]	[m³]	[kN]					
Foundation CRA							« G1 »	« G2 »	Total weight	G1	G2
	Vertical wood	1	800.00	7.85	3.85	30.21					
	Roof timbers	1	800.00	7.85	1.99	15.62					
	Ceiling timbers	1	800.00	7.85	1.06	8.32					
	Roof cob	2	1,000.00	9.81	8.66	84.95					
	Heavy infill wall	2	1,000.00	9.81	12.67	124.29	[kN]	[kN]	[kN]	[kN/m²]	[kN/m²]
	Light infill wall	2	300.00	2.94	9.65	28.40	**54**	**243.38**	**297.53**	**2.51**	**11.30**

Table 9 : Loading analysis snippet

8.7 Results

Subsequent to the construction of the foundation, the primary empirical outcome of this experiment entailed the measurement of the local displacements, otherwise known as settlement, that the gabions experienced as a consequence of the load imposed by the successively positioned wooden structure.

8.7.1 Force magnitude verification

In order to verify the validity of the simulation, it is prudent to attempt to understand the evolution of the simulation. To that end, two aspects merit consideration. Firstly, one can examine the analysis log file, which displays the sequence of operations that the computer undertakes subsequent to the initiation of the script. This approach facilitated the identification of errors in the machine's interpretation of the file. The second tool was the virtual interface, which allowed for the visualisation of the results. Prior to examining the results that have been identified as being of interest, it was imperative to employ graphical visualisations to illustrate the imposed constraints from the script.

Figure 157 shows that the total force of 1.9 kN was applied in a punctual manner to the larger aggregates. In order to check the values, it was necessary to perform a rapid multiplication. Here, there are 30 large spheres, whose values are approximately 60 N. The result was 1,800 N, aligning with the established parameters of the simulation model.

The smaller spheres also have a different colour to the zero value. In fact, this is the consequence of the forces applied to the spheres touching the loading surfaces first.

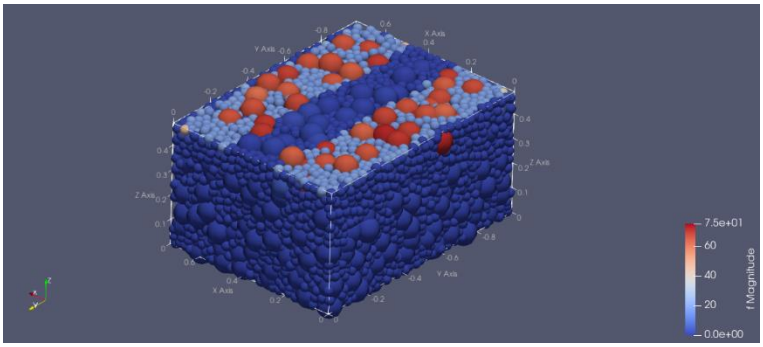

Figure 157 : Simulation of loading forces

8.7.2 Displacements of particles

The graph below (Figure 158) shows the position of the top quartile of the population on the Z axis. This choice is mainly due to the desire to reduce the noise of a few particles that bounced back after charging at time t=4.9s.

Here, during the first 2.5 seconds, the particles filled and then settled. Once global equilibrium is reached, the particles remain in their positions. Then, at the moment when the charge was applied, a slight settlement of 5 mm was perceived. The numerical result is therefore more optimistic than the experimental readings (Figure 146). In fact, the numerical data is two to four times lower than the real value. This may be due to the geometric shape of the particles, which cannot be considered heterogeneous in the simulation. Thus, the settling of spheres does not suggest the possibility of equilibrium breaks or even micro-falls.

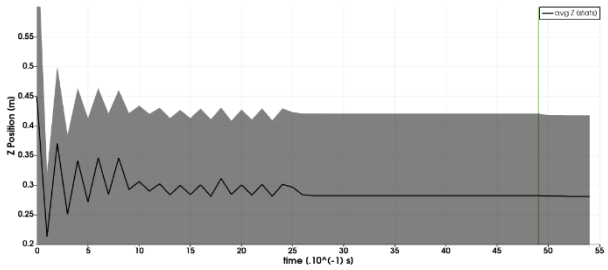

Figure 158 : Plot positions on z axis over time

8.7.3 Force chains results

Simulating the Annex 25 : LIGGGHTS Input Script takes few minutes. In terms of calculation time, the Discrete Element Method required much less time than Computational Fluid Dynamics, which uses the Finite Element Volume method. During its calculation, the simulation created files as snapshots of the .stl and .vtk models as a function of the specified increment time. Here the increment was $10^{(-4)}$ seconds, but a file of each element was created every 500 d(t), so that each file represented an image of the phenomenon of the order of 0.05 seconds. The first 6 steps from t(0) to t(0.3sec) are shown below.

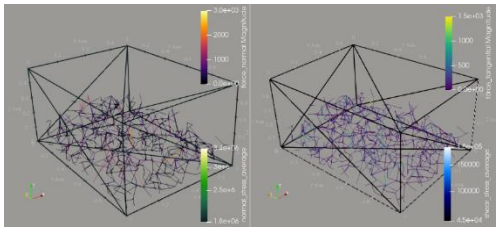

Step 0

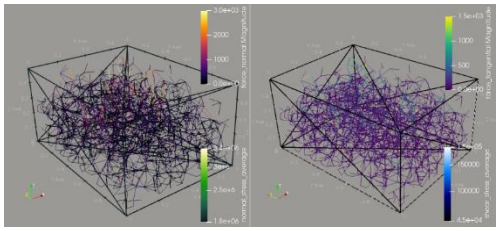

Step 1

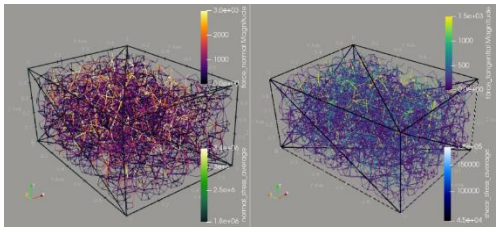

Step 2

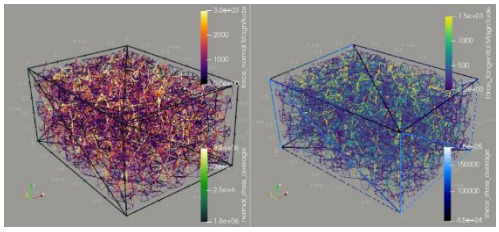

Step 3

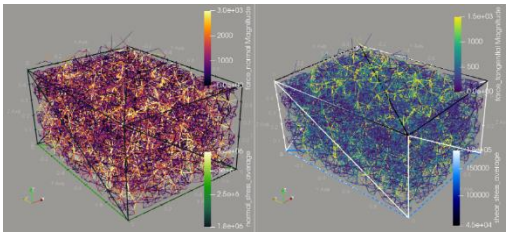

Step 4

Figure 159 : Filling the gabion - steps 0-4

The evolution of the initial filling stages enabled to establish the veracity of the script and to verify the accuracy of the results of interest. This tells us that during filling, the connection between the particles only exists once they have 'fallen' into the cage, and that the normal forces and shear forces increase as the gabion fills, with a slight gradient from top to bottom, due to the gravitational pressure. Each link shown in the images represents a point of contact between two particles. As each of these is spherical in the simulation, it is obvious to assume that the relationship between two particles is less than or equal to 1, and therefore that the chain of force represented is univocal.

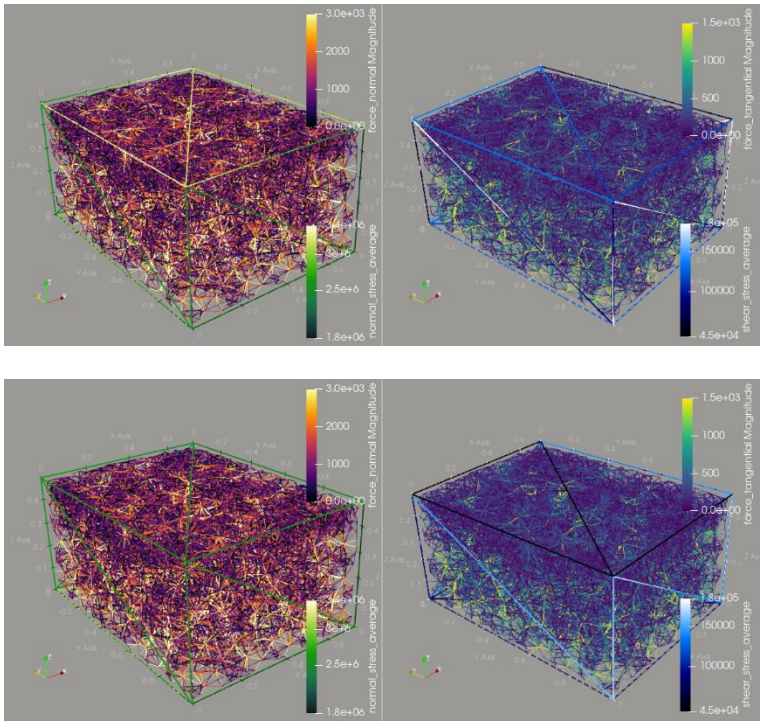

Figure 160 : Comparative force chains between unloaded (up) and loaded (down) phases

When the gabion was loaded, the arrangement of the internal forces did not change significantly as a result of the diffuse load generated by the progressive lowering of the four "load" surfaces. This action was activated by the natural arrangement of the particles

in the cage, which is considered to be infinitely rigid. However, it can be seen that the cage receives forces that can be quantitatively measured by means of colours on the contours of the triangular meshes that make it up. For example, normal forces reach around 3 MPa on the vertical faces, while shear forces reach 150 kPa after loading, compared with barely 100 kPa before.

8.8 Conclusions about numerical methods for gabions

In this session, the focus stands on the advantages and disadvantages of an approach based on design assisted by computer simulations. Uncertainty emerges in design thinking when the inquiries posed do not yield satisfactory answers through traditional tools. By "traditional tools," it is meant the approximate calculation rules that are employed to achieve a result by conceptualising geometries and materials through the use of numbers. While the capacity to manipulate the universe is undoubtedly essential, it is equally crucial for designers to be receptive to new tools if the competencies to utilise them are available.

In light of these considerations, the employment of computer simulations can assume a substantial role in the formulation of conceptual solutions during the early stages of a project. Moreover, the utilisation of Rhino software and the Grasshopper plug-in served as indisputable evidence that design has evolved into a domain for experimentation, given that the parameterisation of data is dependent on its manageability. Design is no longer static and defined in a linear and temporal manner; rather, it is now a multi-dimensional matrix, whose temporal and practical comings and goings are, in reality, no more than singular decisions that can be likened to the topology of the labyrinth. While the labyrinth offers a single solution that can be reached through a multitude of possibilities, computer-aided design can seem like a labyrinth in which the final decision is just one of the many exits generated by so many paths.

Therefore, it is by perceiving design as an end, rather than merely as a means to an end, that the challenge posed by computer simulations, such as understanding the local settlement of a gabion, is fully realised. The visualisation of the chains of forces involved (8.6.2). The design is predicated on a novel transversal dimension, which is characterised by its non-linearity and the resultant logical consequences.

9 Annexes

Annex 1 : Technical drawings of the press (in mm)

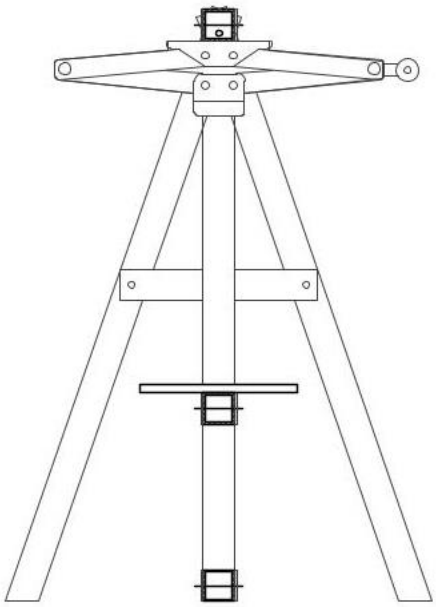

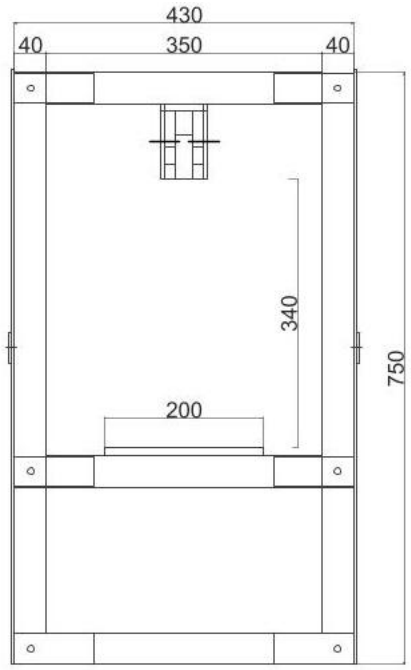

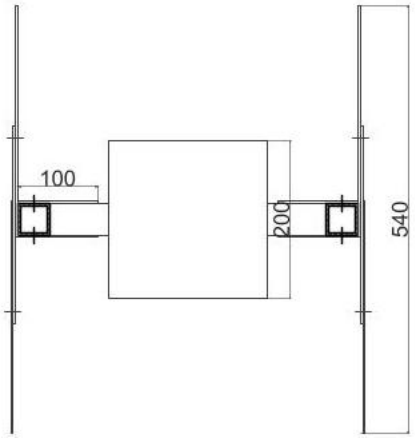

Annex 2 : “Publisher” python script for MQTT Connection

```
import time
import curses
import paho.mqtt.client as mqtt

#setup capture keyboard

screen = curses.initscr()
curses.noecho()
curses.cbreak()
screen.keypad(True)

#broker IP address : IP de windows car le borker est sur le windows

Broker = "192.168.1.100" #'www.dic-hemplime.duckdns.org' #
Port = 1883

#topic

pub_topic = "DIC/keyboard";
sub_topic = "DIC/scanning";

#on connect : imprime la bonne connexion au broker
def on_connect(mqttc, obj, flags, reason_code):
    print("Client windows opérationnel avec rc : " + str(reason_code))
    mqttc.subscribe(sub_topic)

#on message : imprime la foncion de réaction des RPI
def on_message(mqttc, obj, msg):
    message = str(msg.payload)
    print("tu viens d'envoyer le message suivant :" + message + "sur le topic : " +
msg.topic )

#on publish
def on_publish(mqttc, obj, mid):
    print("message id de l'ordre envoyé" + str(mid))

# connect MQTT Client

mqttc = mqtt.Client()
mqttc.on_connect = on_connect
mqttc.on_message = on_message
mqttc.on_publish = on_publish
mqttc.connect(Broker, Port, 60)
mqttc.loop_start()

#commandes
try:
    while True:
        char = screen.getch()
        #quitter le scanning
        if char == ord('g'):
            print('Quit')
            mqttc.publish(pub_topic, "Quit")
        #commencer le scanning
        elif char == ord('s'):
            print('StartScanning')
            mqttc.publish(pub_topic, "StartScanning")
finally:
    curses.nocbreak()
    screen.keypad(0)
    curses.echo()
    curses.endwin()
```

Annex 3 : “Subscriber” python script for MQTT Connection

```
import time
import paho.mqtt.client as mqtt

from time import sleep
from datetime import datetime, timedelta
from picamera import PiCamera

import os

import queue
from queue import Queue,Empty

import threading

import subprocess
import pathlib

#pour avoir le hostname
import socket

camera = PiCamera()

x = 1

# Broker IP address. Donc celle de windows.
Broker = "192.168.1.100"
Port = 1883

# topics
pub_topic = "DIC/scanning"
sub_topic = "DIC/keyboard"



# on connect
def on_connect(mqttc, obj, flags, reason_code):
    print(f"Client che riceve commandi attivato con docide rc :" + str(reason_code))
    mqttc.subscribe(sub_topic)


# on message
def on_message(mqttc, obj, msg):
    print(str(msg.topic) + " " +  str(msg.qos) + " " + str(msg.payload))
    message = msg.payload.decode()
    global q
    if message == "StartScanning":
        q = queue.Queue()
        q.put("StartScanning")
        threading.Thread(target=timelapse, args=(q,)).start()
    if message == "Quit":
        q.put("Quit")

#fonction scanning avec timelapse
def timelapse(q):
    while True:
        try:
            message = q.get_nowait()
            if message != "StartScanning":
                break
            print(message)
        except:
            global x
```

```
            y = str(x)
            hostName = socket.gethostname()
            pathlib.Path('/home/pi/Desktop/DIC_RPI_' +
hostName).mkdir(parents=True,exist_ok=True)
            fileName= hostName + "_" + y.zfill(3) + ".jpg"
            #fileName= hostName+"_"+datetime.now().strftime("%Y%m%d_%H-%M-%S-
%f")+img{counter:03d}+".jpg"
            camera.resolution = (1640, 1232) #picture resolution
            camera.capture('/home/pi/Desktop/DIC_RPI_' + hostName + '/' + fileName)
            x += 1
            sleep(2)

#on subscribe
def on_subscribe(mqttc, obj, mid, reason_code_list):
    print("Subscribed: " + str(mid) + " " + str(reason_code_list))


#on log
def on_log(mqttc, obj, level, string):
    print(string)

# on publish
def on_publish(mqttc, obj, mid):
    print(f"risposta inviata con message  id:" + str(mid))

# connect MQTT client
mqttc = mqtt.Client() #(mqtt.CallbackAPIVersion.VERSION1)

mqttc.on_subscribe = on_subscribe
mqttc.on_connect = on_connect
mqttc.on_message = on_message
mqttc.on_publish = on_publish

mqttc.connect(Broker, Port, 60)
mqttc.loop_forever()
```

Annex 4 : Grasshopper Script for Mery's Method

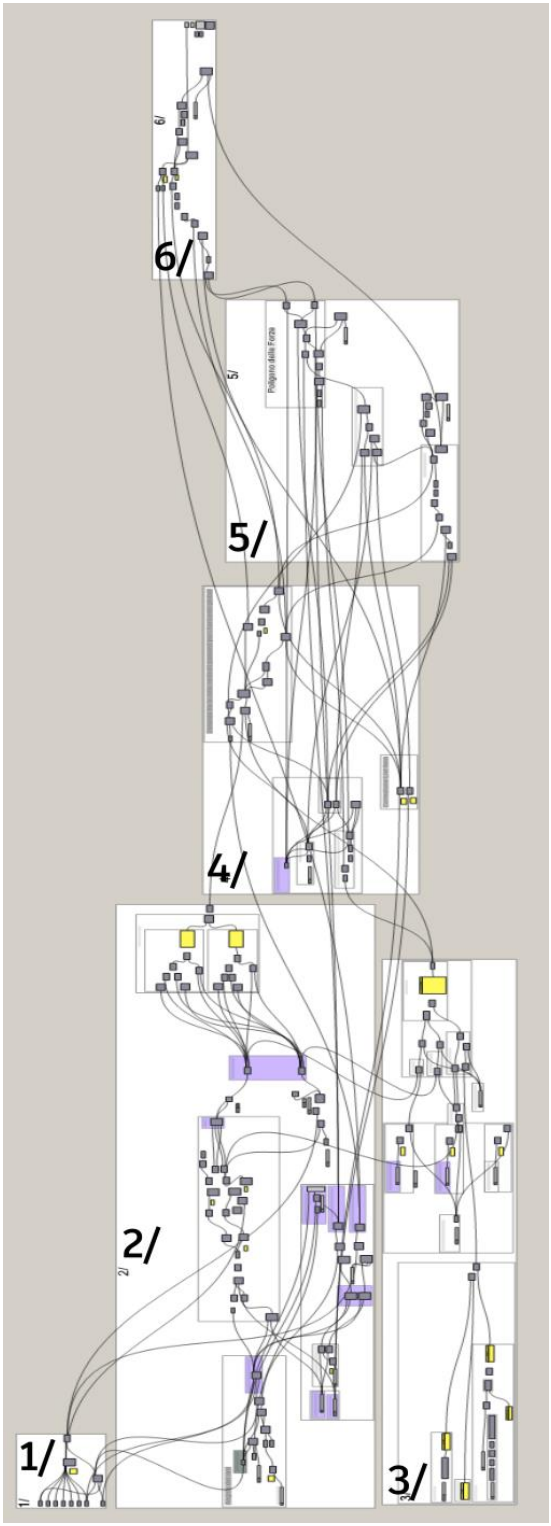

Annex 5 : Arduino program for prototype probes

```
//Watchdog timer
#include <avr/wdt.h>

//DHT11 Lib
#include <DFRobot_DHT11.h>

//Arduino to NodeMCU Lib
#include <SoftwareSerial.h>
#include <ArduinoJson.h>

//=============Libraries for SDCard
#include <SPI.h>
#include <SD.h>

//\\\\\\\\\\\\\ Libraries fo Real Clock Time
#include <Wire.h>
#include <DS3231.h>

// / / / / / / DS18B20 Temperature inside
#include <OneWire.h>
#include <DallasTemperature.h>

//\\\\\\\\\\\\\ Clock
RTClib myRTC;

//=============For SDCard
const int chipSelect = 10;

//===========For SD Card : File creation
File dataFile;

//_ _ _ _ _ _ _Multiplexer control pins
int s0 = 4;
int s1 = 5;
int s2 = 6;
int s3 = 7;

//_ _ _ _ _ _ _Multiplexer in "SIG" pin
int SIG_pin = 0;

//Initialise Arduino to NodeMCU
SoftwareSerial nodemcu(8, 9);

//Initialisation of DHT11 Sensor
DFRobot_DHT11 DHT;
#define DHT11_PIN 2

// / / / / / / DS18B20 Temperature inside
OneWire oneWire(A2);
DallasTemperature temp(&oneWire);

//_____________________________________________________________________________
void setup() {

  //_ _ _ _ _ _ Multiplexer : We reset the control pins
  pinMode(s0, OUTPUT);
  pinMode(s1, OUTPUT);
  pinMode(s2, OUTPUT);
  pinMode(s3, OUTPUT);
```

```
      digitalWrite(s0, LOW);
      digitalWrite(s1, LOW);
      digitalWrite(s2, LOW);
      digitalWrite(s3, LOW);

      Serial.begin(115200);

      ///\/\/\/\ Watchdog Timer : Disable here to avoid perpetual reset
      wdt_disable();
      Serial.println("Setup depuis le watchdog");
      wdt_enable(WDTO_8S);  // if no activity for 8 seconds, the watchdog reset the
program


      //dht.begin();
      nodemcu.begin(115200);
      delay(1000);

      Serial.println("Program started");

      //\\\\\\\\\\\\Clock
      //clock inistialisation
      Serial.println("Initialize Horloge");
      Wire.begin();

      delay(500);
      Serial.println("Horloge OK");


      //===========For SDCard
      Serial.print("Initializing SD Card...");
      //===========For SD Card : default chip is set to output
      pinMode(SS, OUTPUT);
      //==============see if the card is present and can be initialised:
      if (!SD.begin(chipSelect)) {
        Serial.println("Card failed, or not present");
        while (1)
          ;
      }

      Serial.println("SD Card Initialized");

      // Open up the file to log data
      dataFile = SD.open("datalog.txt", FILE_WRITE);
      if (!dataFile) {
        Serial.println("error opening datalog.txt");
      } else {
        Serial.println("File datalog.txt opened");
      }
      // Wait forever since we can write data

      // / / / / / / DS18B20 Temperature inside
      temp.begin();
    }

    //_____________________________________________________________________________
_____
    void loop() {
      //\/\/\/\/ Watchdog Timer
      wdt_reset();

      while (true) {
        data_sd();
        data_wifi();
      }
```

```
}


float readMux(int channel) {
  //_ _ _ _ _ _ _ _ MUX :
  int controlPin[] = { s0, s1, s2, s3 };
  //_ _ _ _ _ _ _ _ MUX :
  int muxChannel[16][4] = {
    { 0, 0, 0, 0 },  //channel 0
    { 1, 0, 0, 0 },  //channel 1
    { 0, 1, 0, 0 },  //channel 2
    { 1, 1, 0, 0 },  //channel 3
    { 0, 0, 1, 0 },  //channel 4
    { 1, 0, 1, 0 },  //channel 5
    { 0, 1, 1, 0 },  //channel 6
    { 1, 1, 1, 0 },  //channel 7
    { 0, 0, 0, 1 },  //channel 8
    { 1, 0, 0, 1 },  //channel 9
    { 0, 1, 0, 1 },  //channel 10
    { 1, 1, 0, 1 },  //channel 11
    { 0, 0, 1, 1 },  //channel 12
    { 1, 0, 1, 1 },  //channel 13
    { 0, 1, 1, 1 },  //channel 14
    { 1, 1, 1, 1 }   //channel 15
  };
  //_ _ _ _ _ _ _ _ MUX : loop through the 4 sig
  for (int i = 0; i < 4; i++) {
    digitalWrite(controlPin[i], muxChannel[channel][i]);
  }

  //_ _ _ _ _ _ _ _ MUX : read the value at the SIG pin
  int val = analogRead(SIG_pin);

  //_ _ _ _ _ _ _ _ _MUX : reurn the value
  float valeurs = (val);
  return valeurs;
}

void data_sd() {
  //==============For SD Card : make a string for assembling the data to log:
  String tString;
  String dataString = "";

  //\\\\\\\\\\\\\\  Clock
  delay(1000);
  DateTime now = myRTC.now();

  //\/\/\/\/ Watchdog Timer
  wdt_reset();


  Serial.print(now.year(), DEC);
  Serial.print('/');
  Serial.print(now.month(), DEC);
  Serial.print('/');
  Serial.println(now.day(), DEC);
  //Serial.print(' ');
  Serial.print(now.hour(), DEC);
  Serial.print(':');
  Serial.print(now.minute(), DEC);
  Serial.print(':');
  Serial.print(now.second(), DEC);
  Serial.println();

  //\/\/\/\/ Watchdog Timer
  wdt_reset();
```

```
//==========For SD Card : Ecrit la date sur le file dans la SD
dataFile.print(now.year(), DEC);
dataFile.print('/');
dataFile.print(now.month(), DEC);
dataFile.print('/');
dataFile.print(now.day(), DEC);
dataFile.print(',');
dataFile.print(now.hour(), DEC);
dataFile.print(':');
dataFile.print(now.minute(), DEC);
dataFile.print(':');
dataFile.print(now.second(), DEC);
dataFile.print(',');

//\/\/\/\/ Watchdog Timer
wdt_reset();

//Obtain Temp and Hum data
dht11_func();

//\/\/\/\/ Watchdog Timer
wdt_reset();

//===========For SD Card : Ecrit temp et hum depuis DHT11
dataFile.print(DHT.temperature);
dataFile.print(',');
dataFile.print(DHT.humidity);
dataFile.print(',');

//\/\/\/\/ Watchdog Timer
wdt_reset();

//=============For SD Card
for (int i = 0; i < 16; i++) {
  int sensor = readMux(i);
  dataString += String(sensor);
  if (i < 15) {
    dataString += ",";
    delay(500);
  }
}

//==========For SD Card : Ecrit sur le file dans la SD
dataFile.print(dataString);
dataFile.print(',');

//\/\/\/\/ Watchdog Timer
wdt_reset();

// / / / / / / DS18B20 Temperature inside
temp.requestTemperatures();
for (int i = 0; i < 5; i++) {

  int t = temp.getTempCByIndex(i);
  tString += String(t);
  if (i < 5) {
    dataString += ",";
    delay(500);
  }
}

dataFile.println(tString);

//\/\/\/\/ Watchdog Timer
wdt_reset();
```

```
      dataFile.flush();
    }

    void data_wifi() {

      //\/\/\/\/ Watchdog Timer
      wdt_reset();

      //Nodemcu
      StaticJsonDocument<1000> dax;


      //RELEVER LES DATA DES SONDES ET LE ASSIGNER DANS LE JSON
      dax["humidity"] = DHT.humidity;
      dax["temperature"] = DHT.temperature;

      //_ _ _ _ _ _ MUX : Loop through and read all 16 values
      dax["A"] = (readMux(0));
      dax["Aprim"] = (readMux(1));
      dax["Z"] = temp.getTempCByIndex(5);  //(readMux(2));
      dax["B"] = (readMux(3));
      dax["Bprim"] = (readMux(4));
      dax["Y"] = temp.getTempCByIndex(4);  //(readMux(5));
      dax["C"] = (readMux(6));
      dax["Cprim"] = (readMux(7));
      dax["X"] = temp.getTempCByIndex(3);  //(readMux(8));
      dax["D"] = (readMux(9));
      dax["Dprim"] = (readMux(10));
      dax["W"] = temp.getTempCByIndex(2);  //(readMux(11));
      dax["E"] = (readMux(12));
      dax["Eprim"] = (readMux(13));
      dax["V"] = temp.getTempCByIndex(1);  //(readMux(14));


      //\/\/\/\/ Watchdog Timer : Disable car trop long
      wdt_disable();

      //\/\/\/\/ Passage du code vers NodeMCU (pas protégé par le watchdog car le
delay entre chaque prise de donnée est trop long)
      //Send data to NodeMCU
      serializeJson(dax, nodemcu);
      delay(10UL * 60UL * 1000UL);  // Toutes les 10 min = 10 * 60 * 1000 ms
      Serial.println("restart loop");
      delay(1000);
      //\/\/\/\/ Fin du passage du code qui n'est pas protégé par le watchdog

      //\/\/\/\/ Watchdog Timer : Enable pour le prochain loop
      wdt_enable(WDTO_8S);
    }

    void dht11_func() {
      DHT.read(DHT11_PIN);
      delay(1000);
    }
```

Annex 6 : Google script for receiving data over time

```
    function doGet(e) {
      Logger.log( JSON.stringify(e) );
      var result = 'Ok';
      if (e.parameter == 'undefined') {
        result = 'No Parameters';
      }
      else {
        var sheet_id = '1BxjSm39s7EOexZEP_VB51aBo8T0jjczUN3xb99vey-w'; //
Spreadsheet ID
        var sheet = SpreadsheetApp.openById(sheet_id).getActiveSheet();
        var newRow = sheet.getLastRow() + 1;
        var rowData = [];
        var Curr_Date = new Date();
        rowData[0] = Curr_Date; // Date in column A
        var Curr_Time = Utilities.formatDate(Curr_Date, "Europa/Parigi",
'HH:mm:ss'); // https://developers.google.com/google-ads/api/data/codes-
formats?hl=it#timezone-ids
        rowData[1] = Curr_Time; // Time in column B
        for (var param in e.parameter) {
          Logger.log('In for loop, param=' + param);
          var value = stripQuotes(e.parameter[param]);
          Logger.log(param + ':' + e.parameter[param]);
          switch (param) {
            case 'temperature':
            rowData[2] = value; // Temperature in column C
            result = 'Temperature Written on column C';
            break;
            case 'humidity':
            rowData[3] = value; // Humidity in column D
            result += 'Humidity Written on column D';
            break;
            case 'A':
            rowData[4] = value; // Moisture content in column E
            result += '--';
            break;
            case 'Aprim':
            rowData[5] = value; // Moisture content in column F
            result += 'Humidity Written on column F';
            break;
            case 'Z':
            rowData[6] = value; // Temperature in column G
            result += 'Humidity Written on column G';
            break;
            case 'B':
            rowData[7] = value; // Humidity in column H
            result += 'Humidity Written on column H';
            break;
            case 'Bprim':
            rowData[8] = value; // Humidity in column I
            result += 'Humidity Written on column I';
            break;
            case 'Y':
            rowData[9] = value; // Humidity in column J
            result += 'Humidity Written on column J';
            break;
            case 'C':
            rowData[10] = value; // Humidity in column K
            result += 'Humidity Written on column K';
            break;
```

```
            case 'Cprim':
            rowData[11] = value; // Humidity in column L
            result += 'Humidity Written on column L';
            break;
            case 'X':
            rowData[12] = value; // Humidity in column M
            result += 'Humidity Written on column M';
            break;
            case 'D':
            rowData[13] = value; // Humidity in column N
            result += 'Humidity Written on column N';
            break;
            case 'Dprim':
            rowData[14] = value; // Humidity in column O
            result += 'Humidity Written on column O';
            break;
            case 'W':
            rowData[15] = value; // Humidity in column P
            result += 'Humidity Written on column P';
            break;
            case 'E':
            rowData[16] = value; // Humidity in column Q
            result += 'Humidity Written on column Q';
            break;
            case 'Eprim':
            rowData[17] = value; // Humidity in column R
            result += 'Humidity Written on column R';
            break;
            case 'V':
            rowData[18] = value; // Humidity in column S
            result += 'Humidity Written on column S';
            break;
            default:
            result = "unsupported parameter";
          }
        }
        Logger.log(JSON.stringify(rowData));
        var newRange = sheet.getRange(newRow, 1, 1, rowData.length);
        newRange.setValues([rowData]);
      }
      return ContentService.createTextOutput(result);
    }
    function stripQuotes( value ) {
      return value.replace(/^["']|['"]$/g, "");
    }
```

Annex 7 : Formwork quoted technical drawing

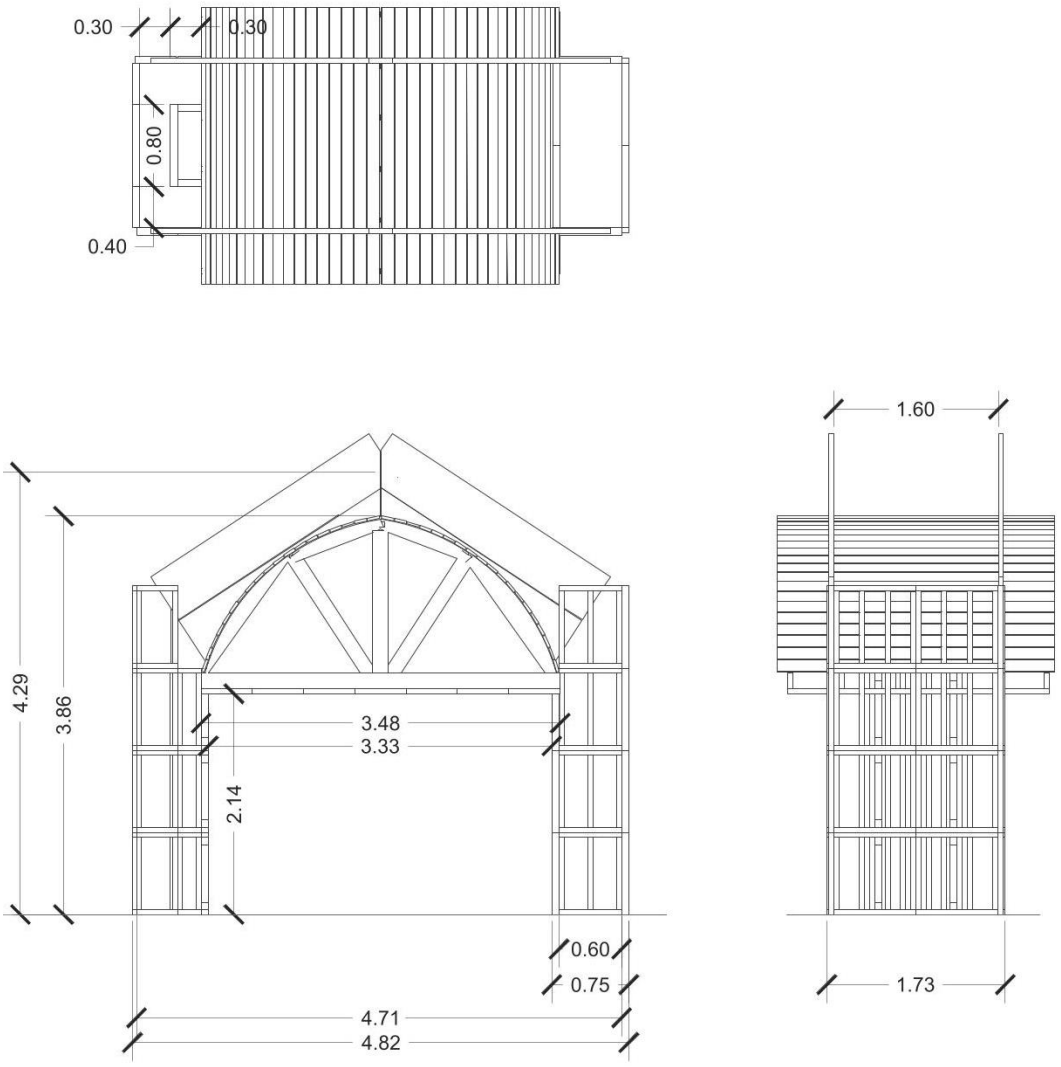

Annex 8 : Carbonation measurements

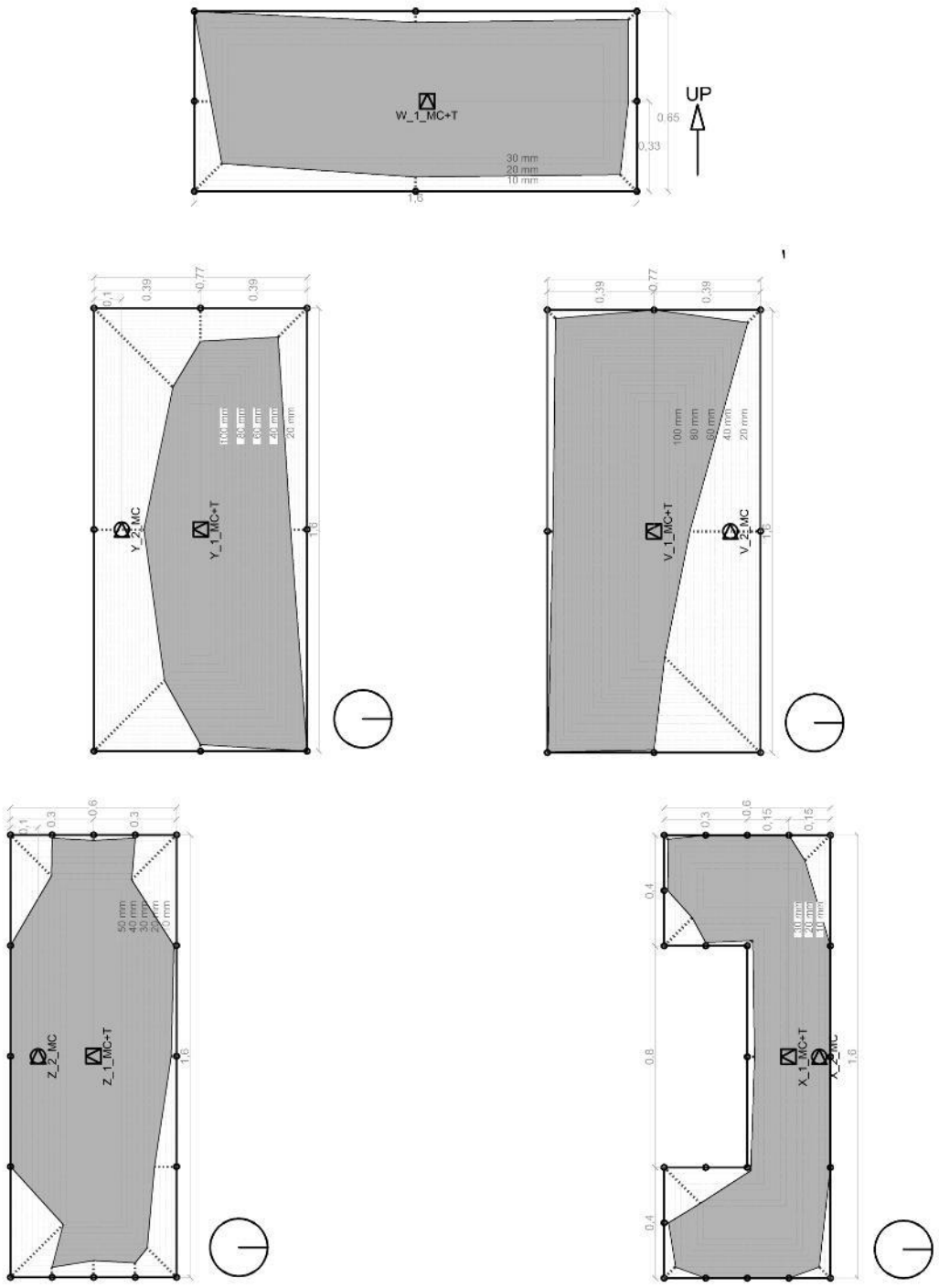

Annex 9 : Compression results database _ Samples 'A'

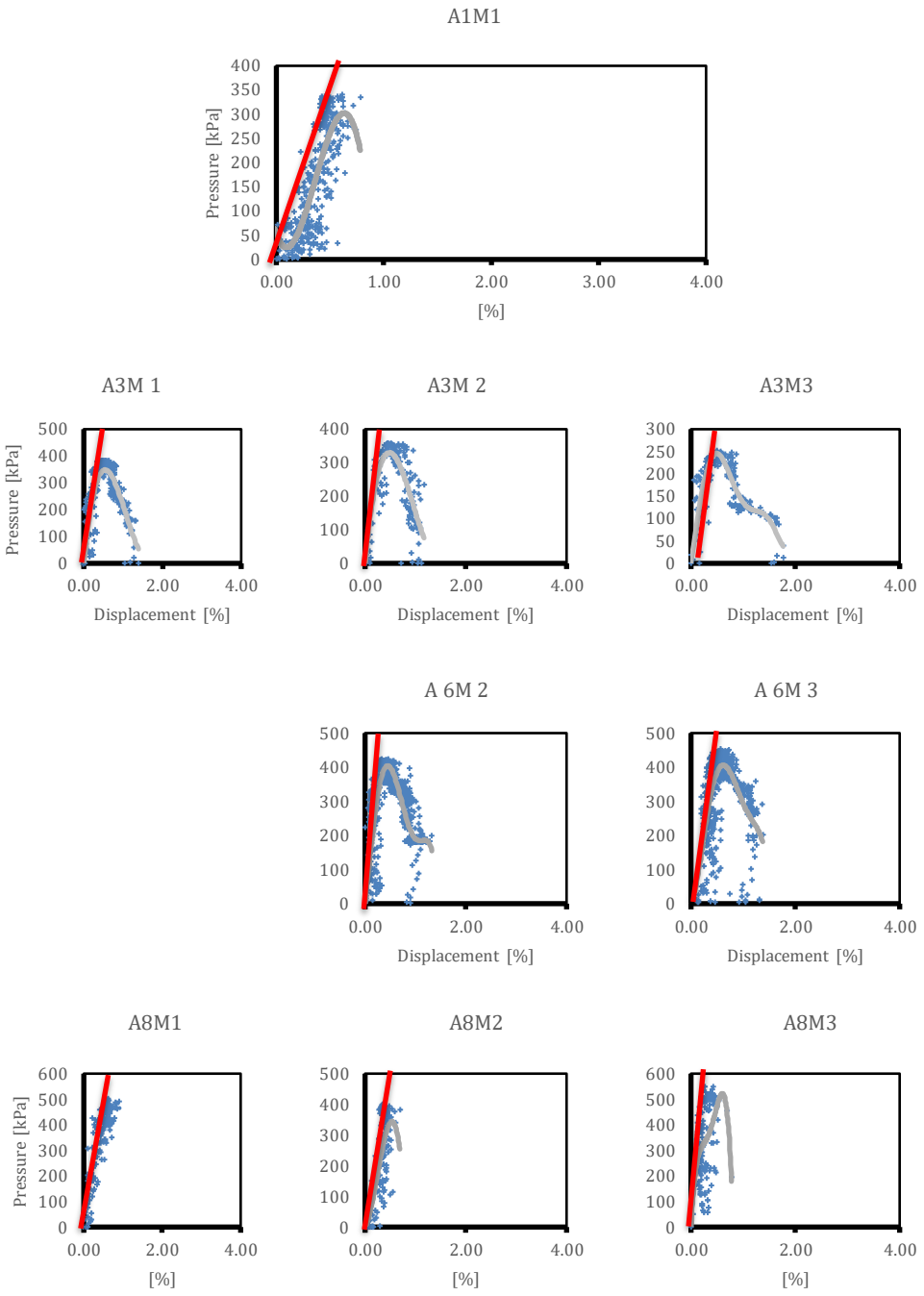

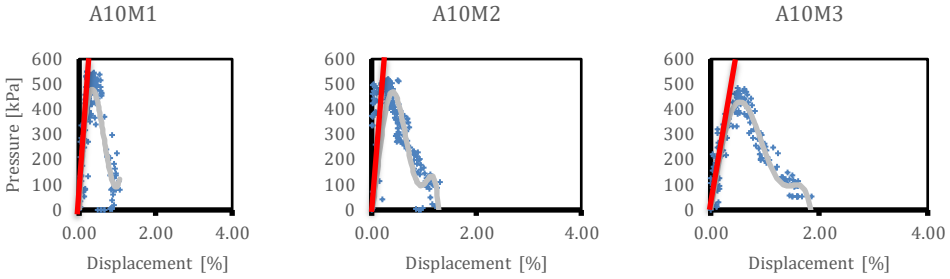
A10M1
A10M2
A10M3
Pressure [kPa]
600
500
400
300
200
100
0
0.00
2.00
4.00
Displacement [%]

Annex 10 : Compression results database _ Samples ” A’ ”

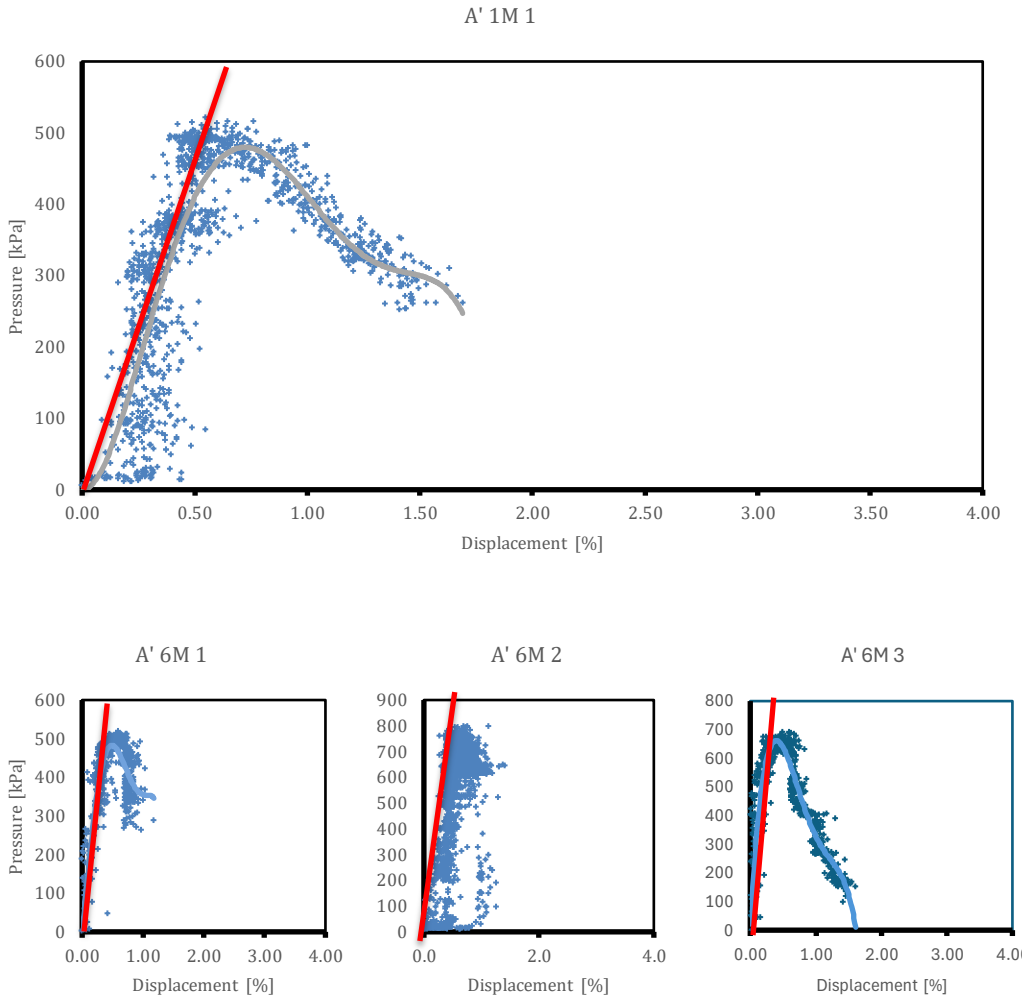

Annex 11 : Compression results database _ Samples “ B ”

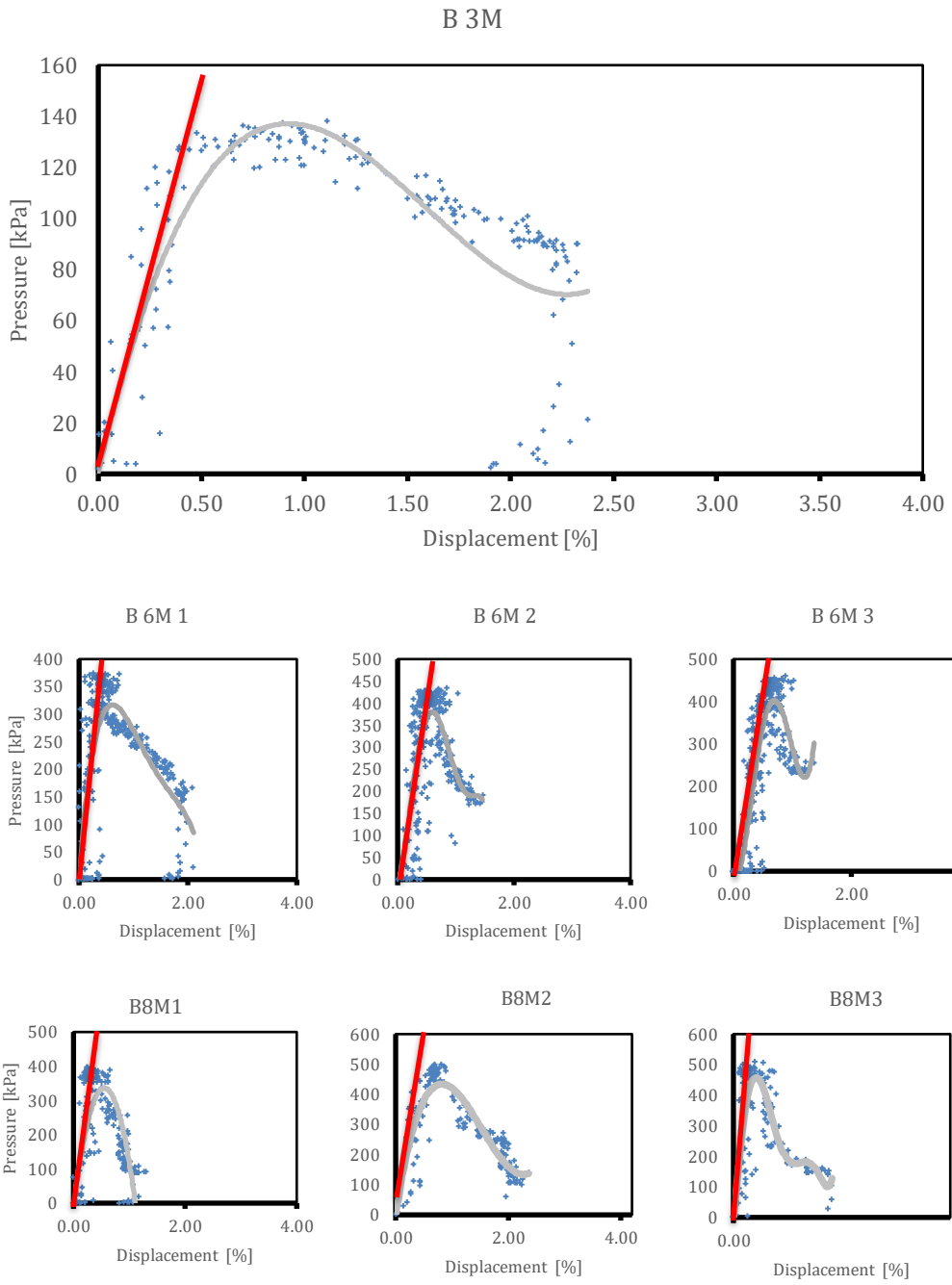

Annex 12 : Compression results database _ Samples “ B’ ”

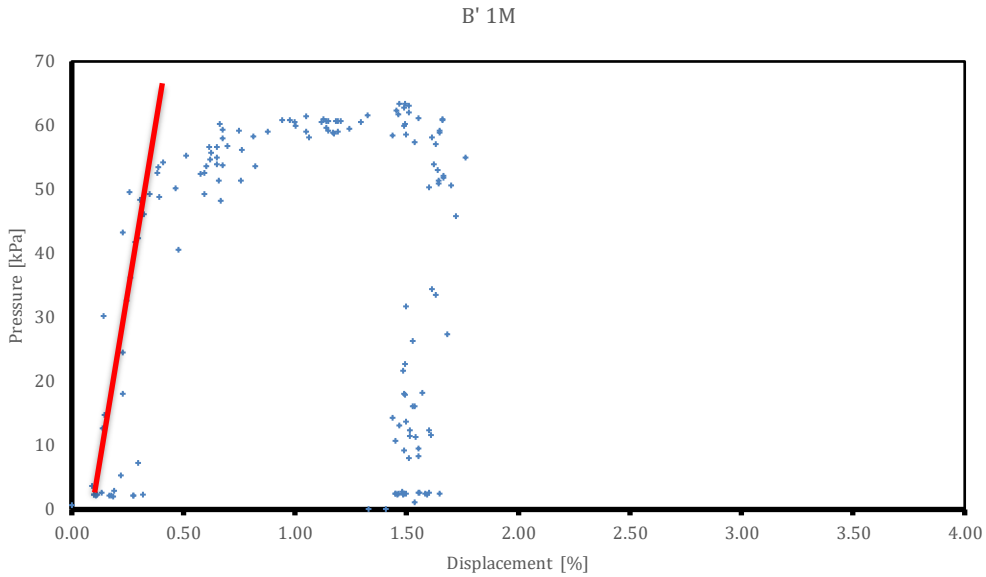

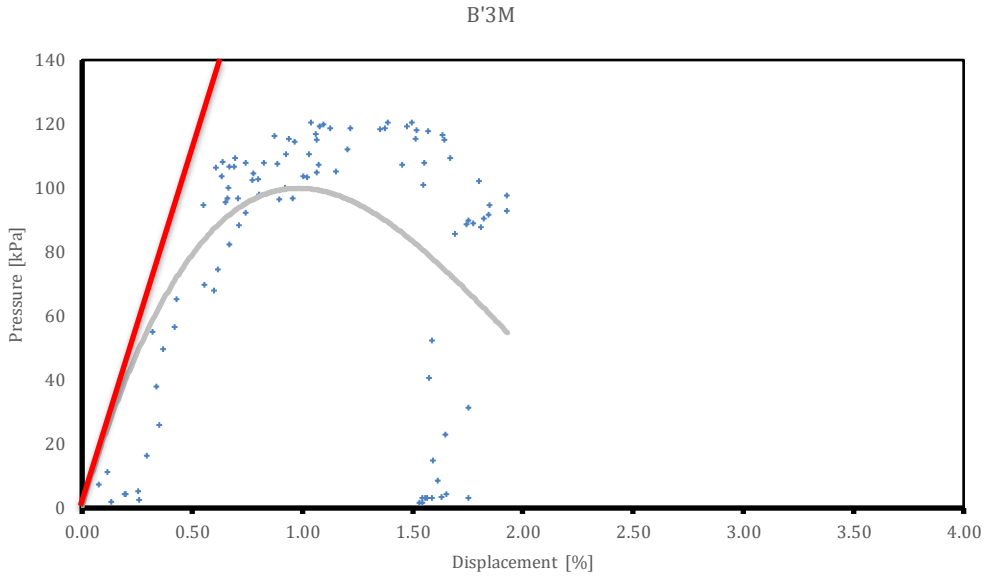

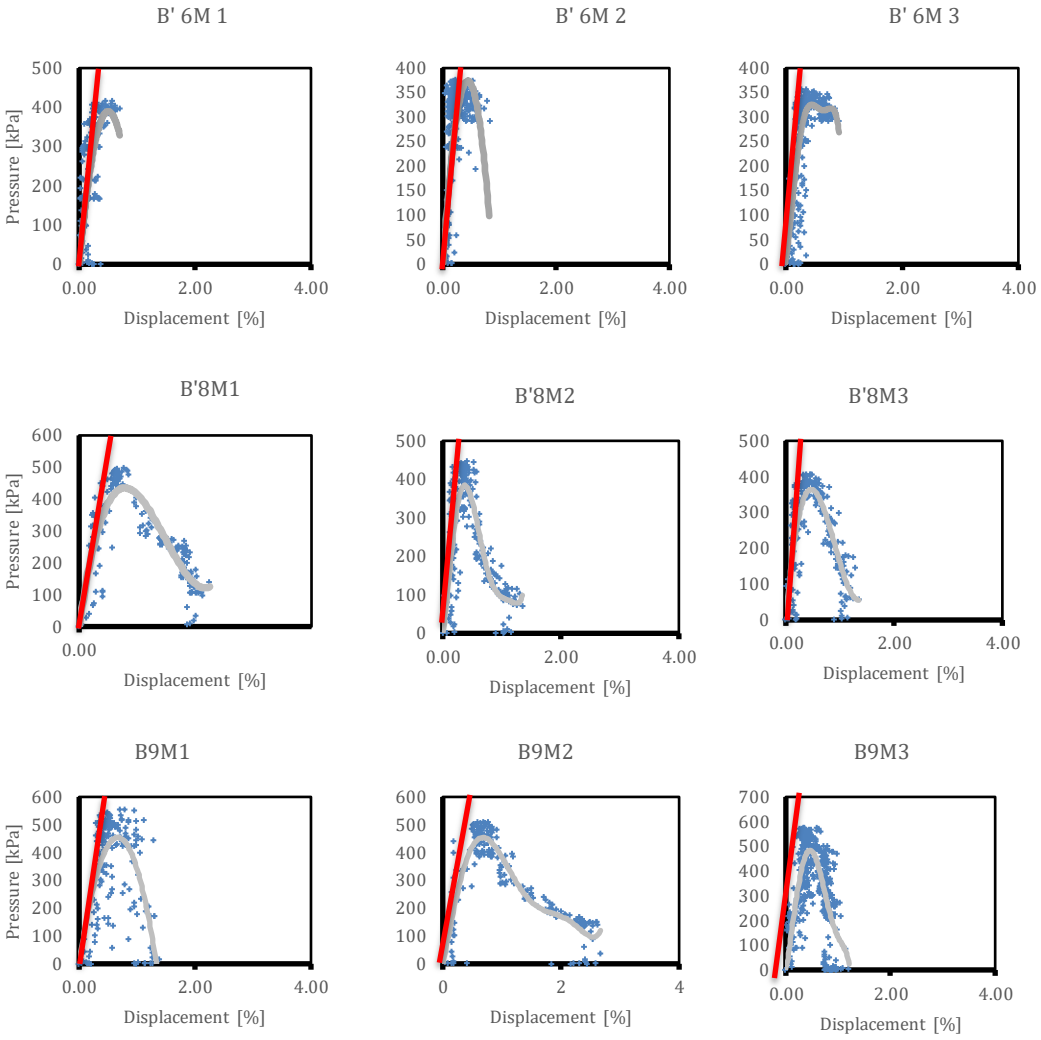
B' 6M 1
B' 6M 2
B' 6M 3
B'8M1
B'8M2
B'8M3
B9M1
B9M2
B9M3
Pressure [kPa]
Displacement [%]

Annex 13 : Compression results database _ Samples “ C ”

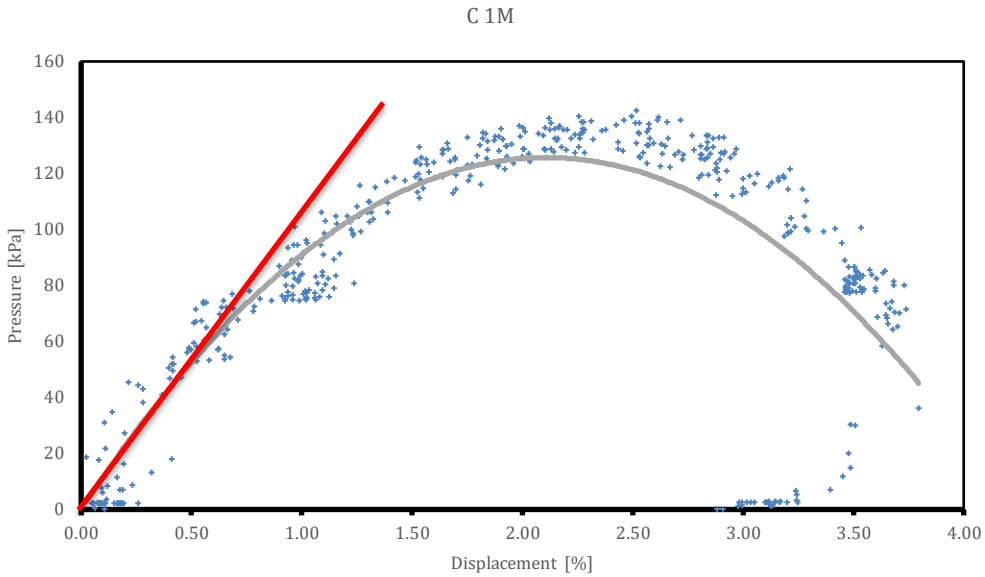

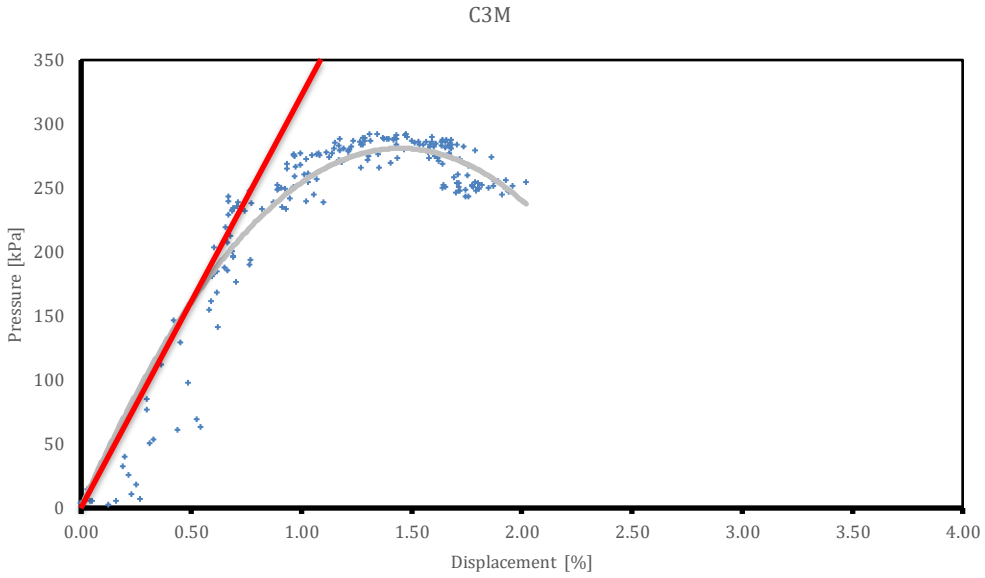

Annex 14 : Compression results database _ Samples “ C’ ”

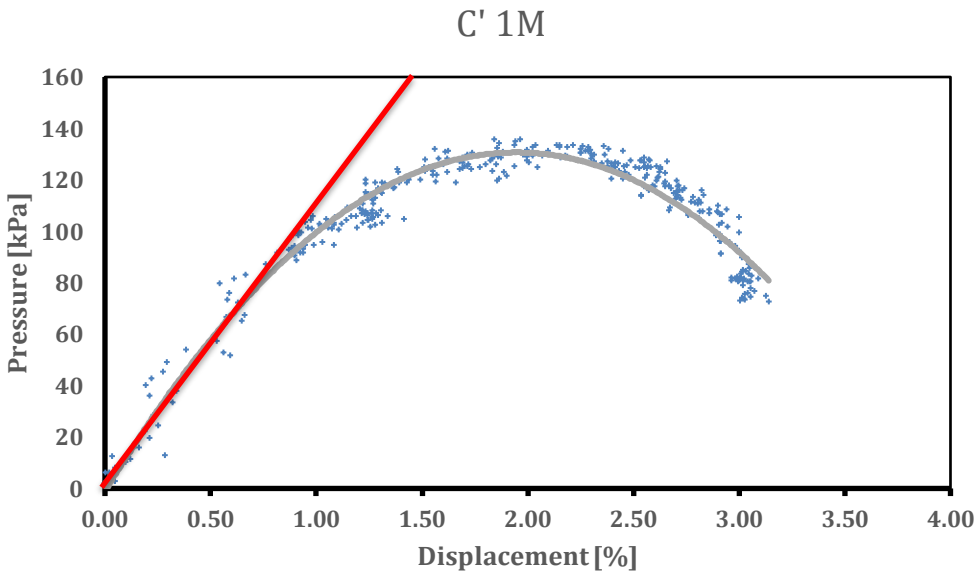

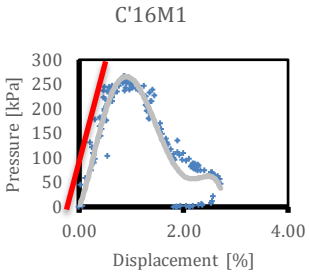

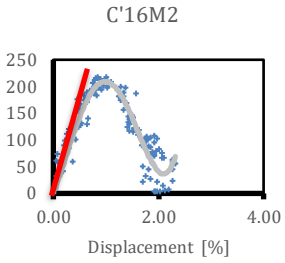

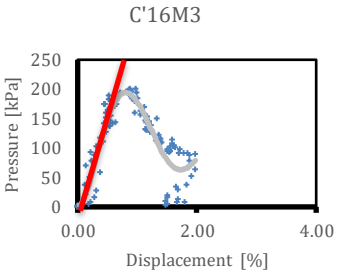

Annex 15 : Compression results database _ Samples “ D ”

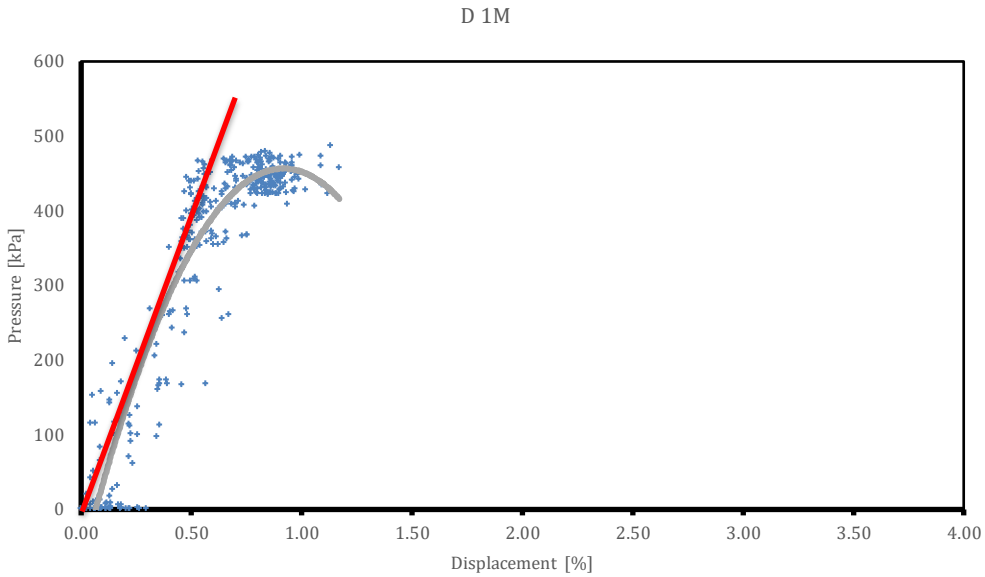

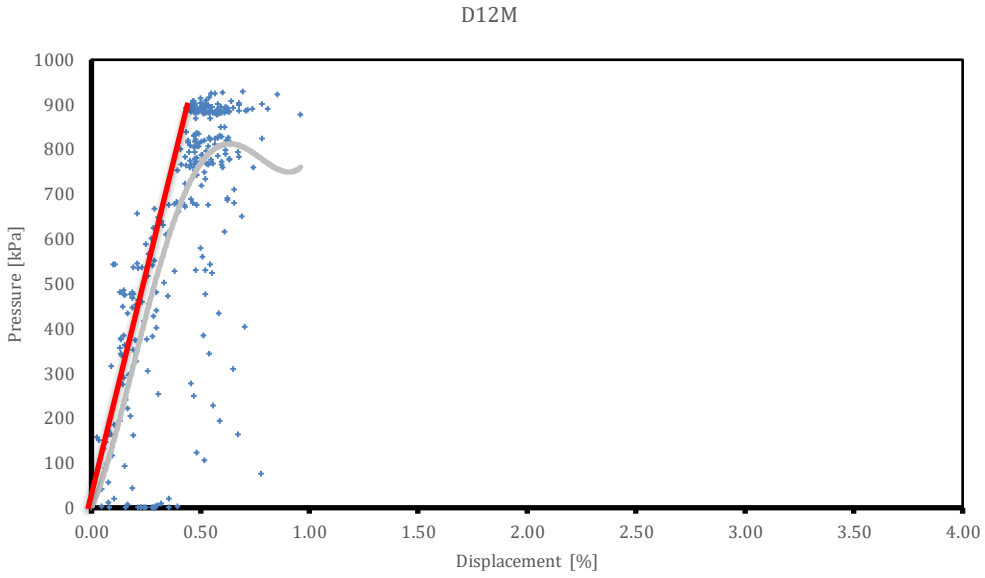

Annex 16 : Compression results database _ Samples “ D’ ”

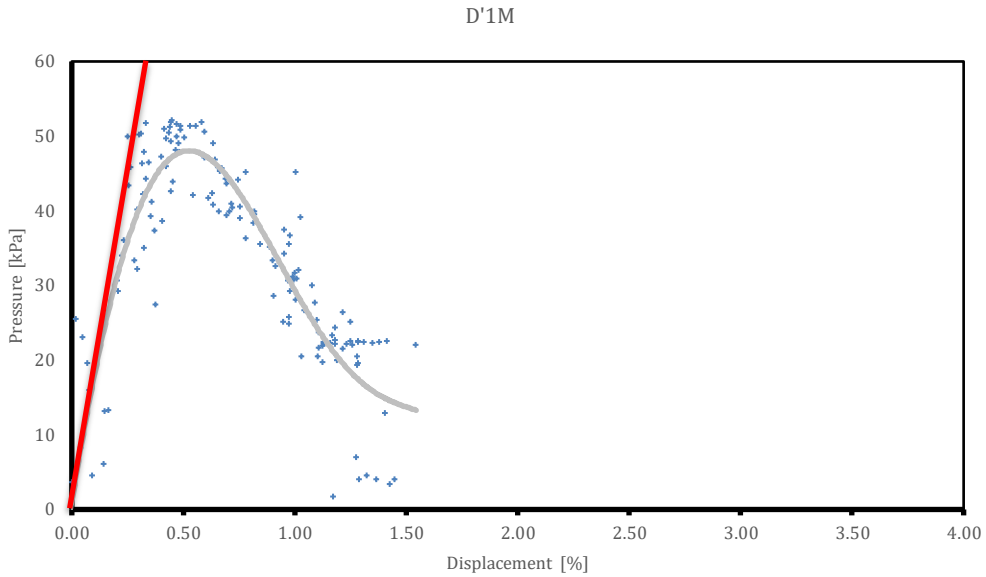

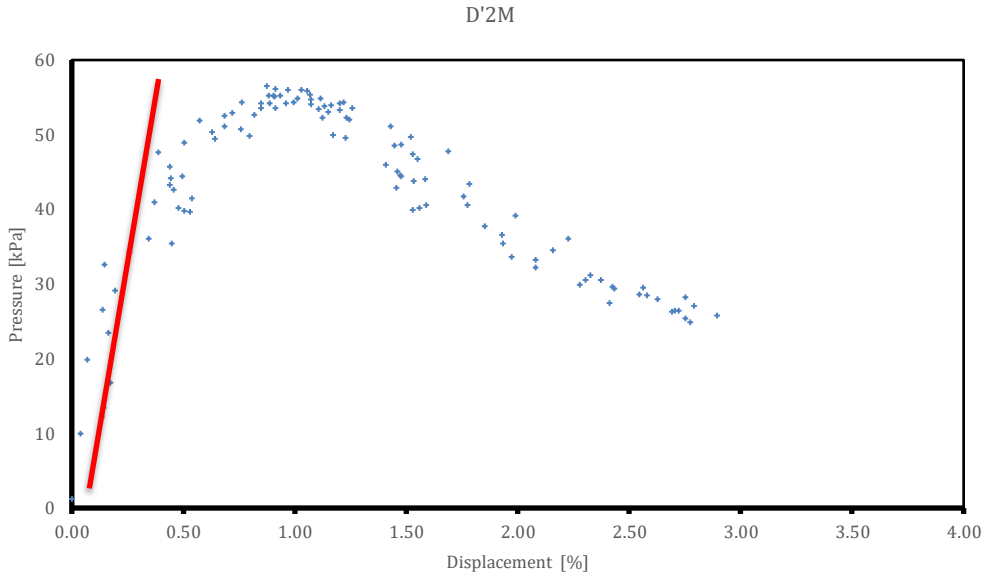

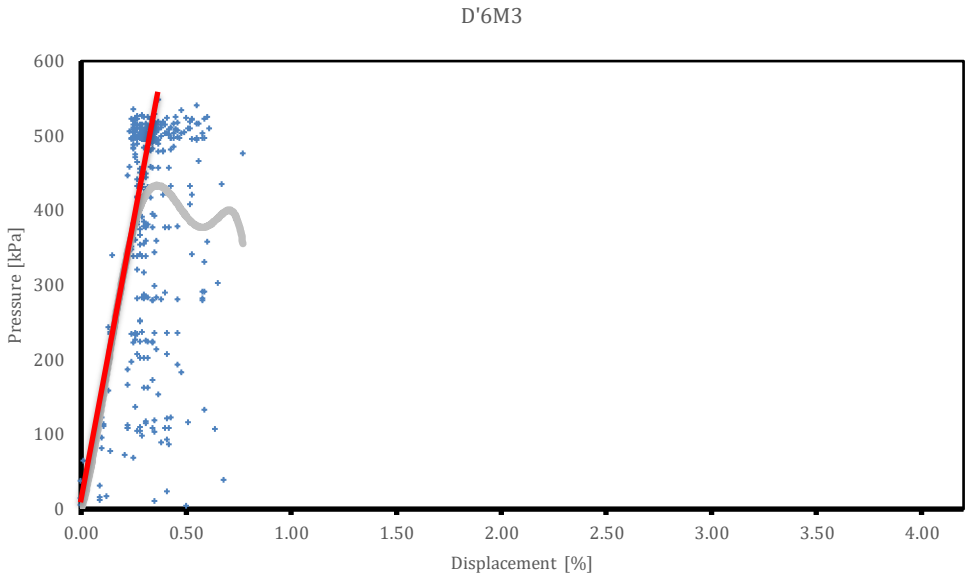
D'6M3
600
500
400
300
200
100
0
Pressure [kPa]
0.00
0.50
1.00
1.50
2.00
2.50
3.00
3.50
4.00
Displacement [%]

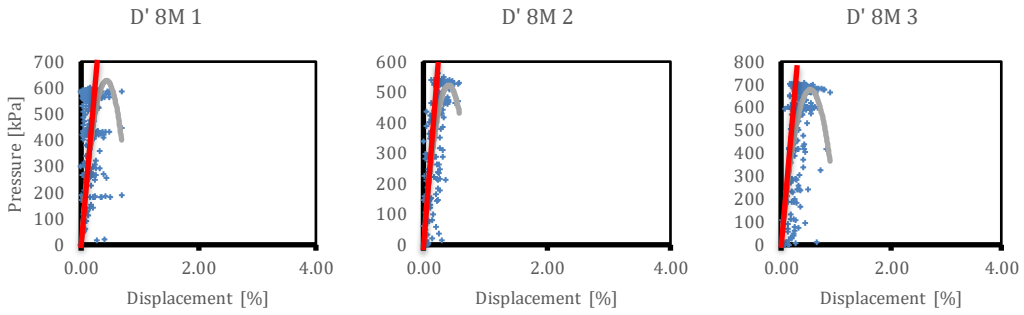
D' 8M 1
D' 8M 2
D' 8M 3
Pressure [kPa]
Displacement [%]
Displacement [%]
Displacement [%]

Annex 17 : Light-earth pavilion _ Plan _ 1:50

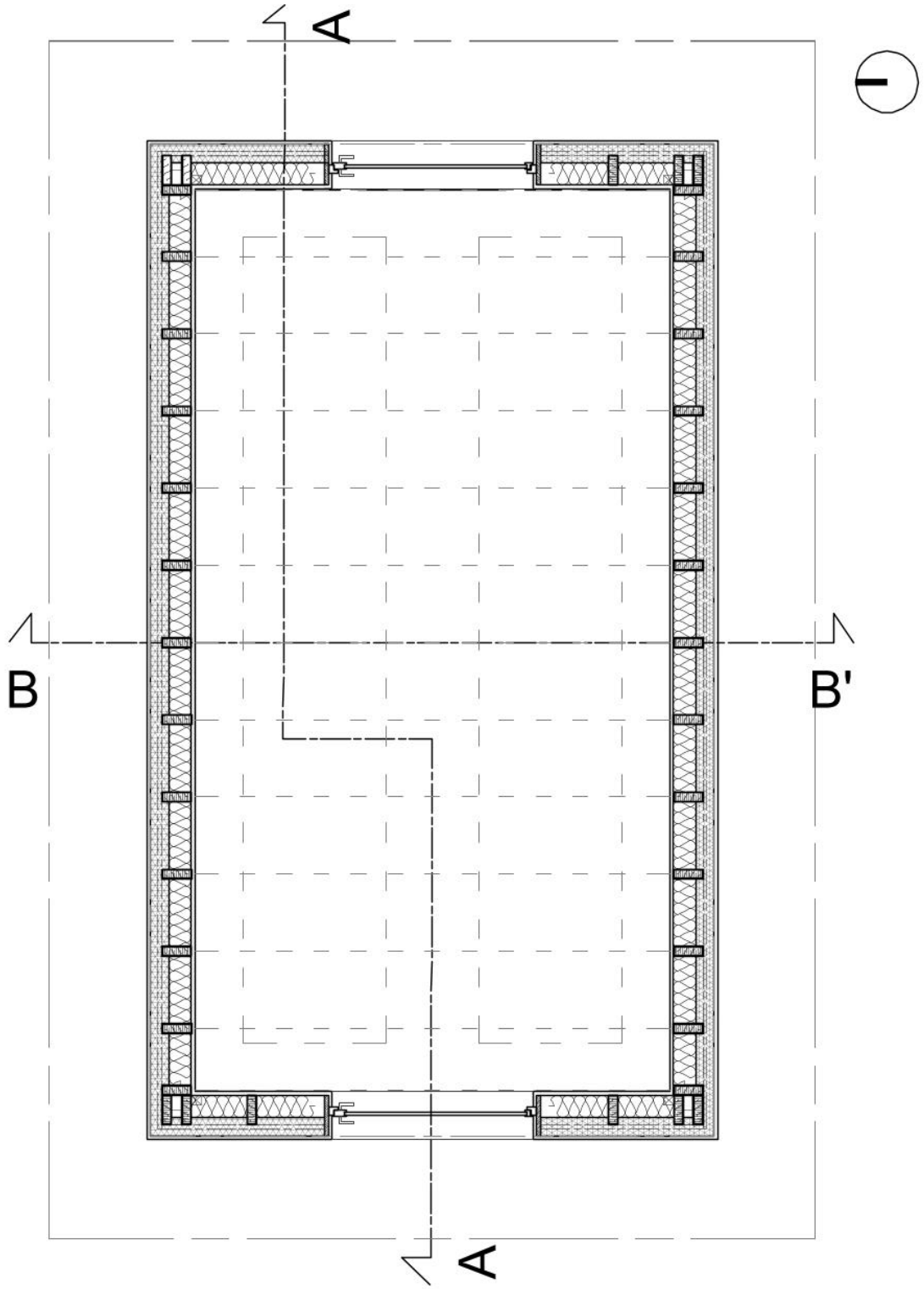

Annex 18 : Light-earth pavilion _ Structural floor plan _ 1:50

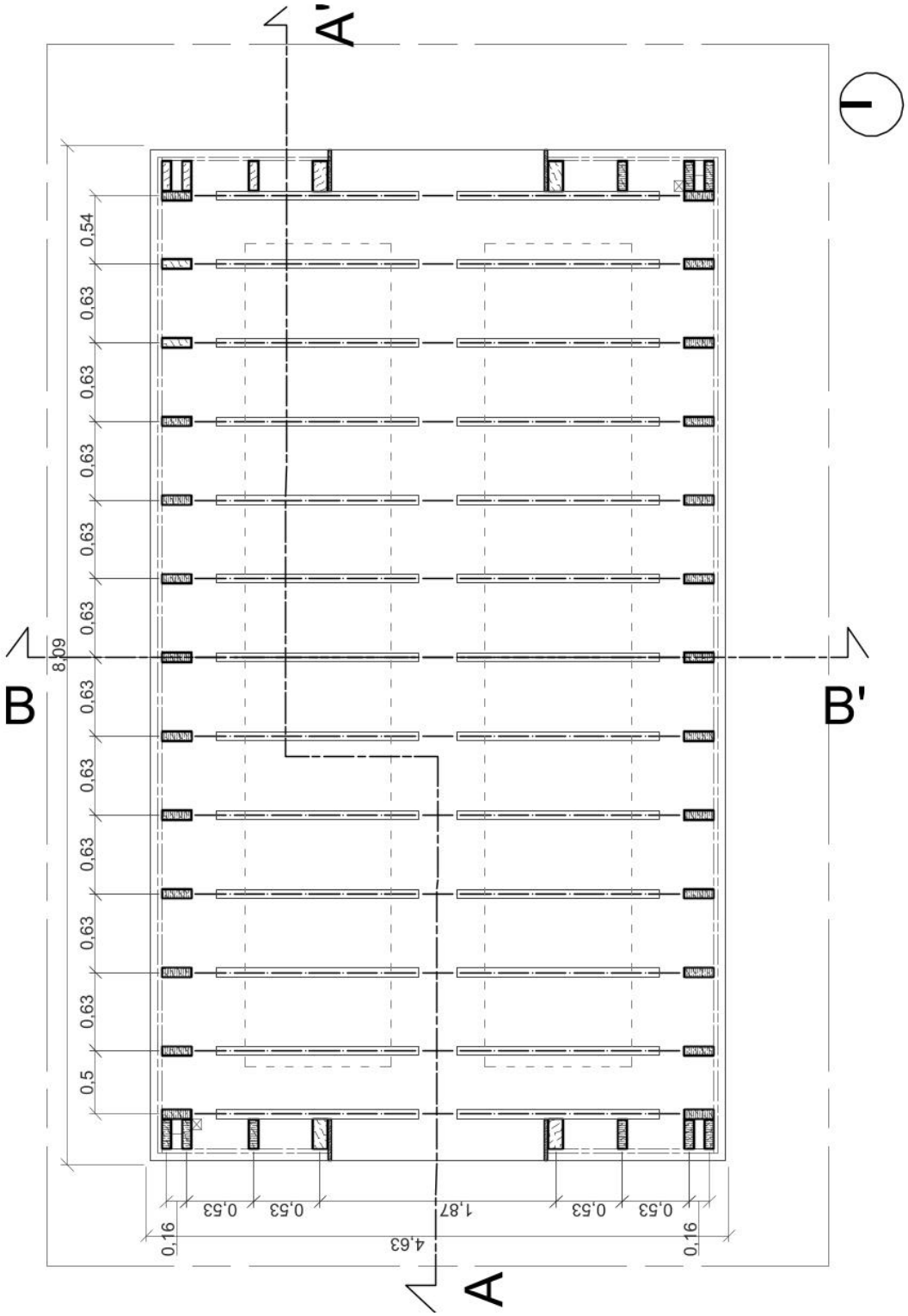

Annex 19 : Light-earth pavilion _ Structural section AA' _ 1:50

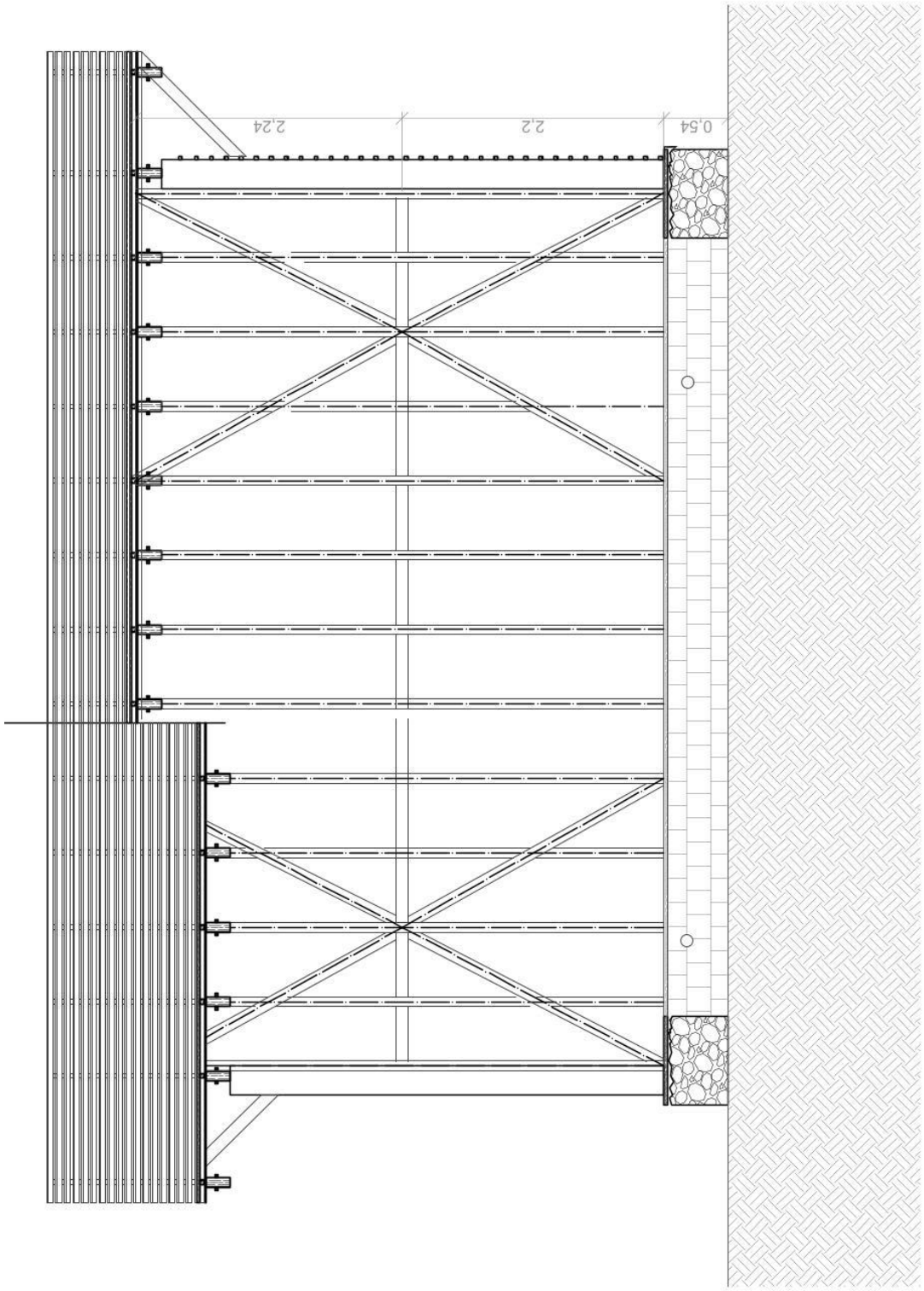

Annex 20 : Light-earth pavilion _ Structural section BB' _ 1:50

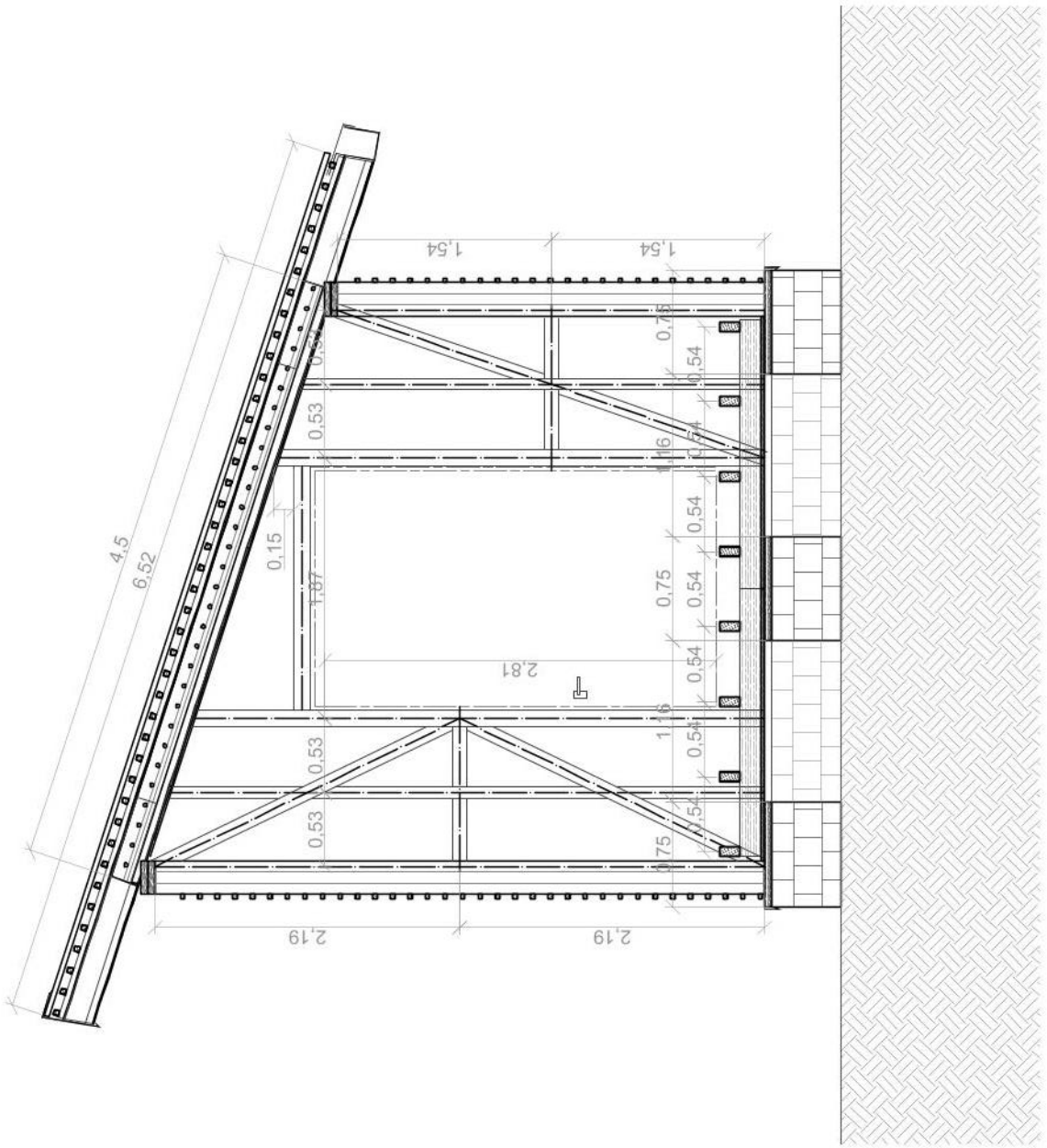

Annex 21 : Light-earth pavilion _ Section AA' _ 1:50

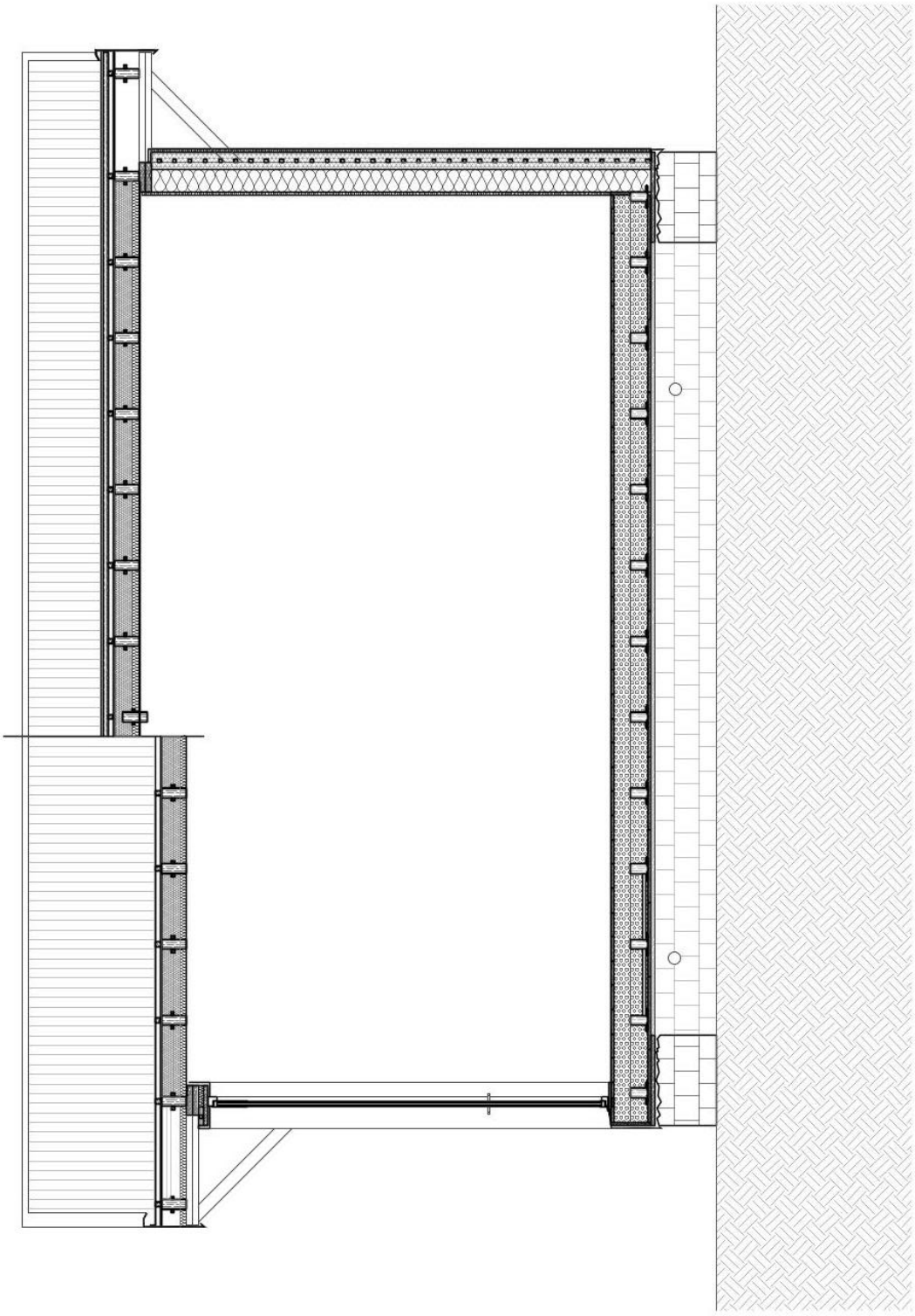

Annex 22 : Light-earth pavilion _ Section BB' _ 1:50

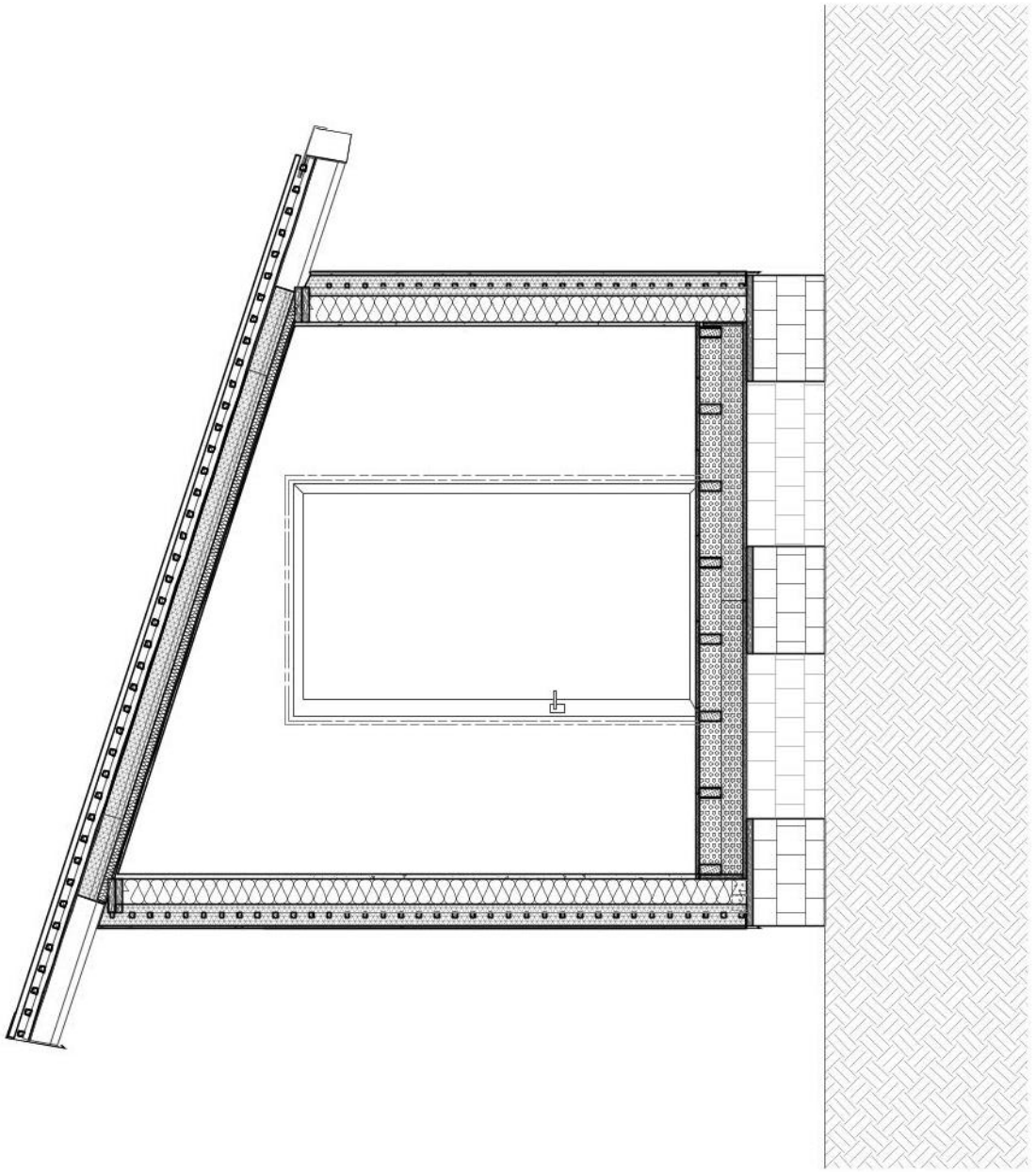

Annex 23 : Light-earth pavilion _ Detail _ 1:20

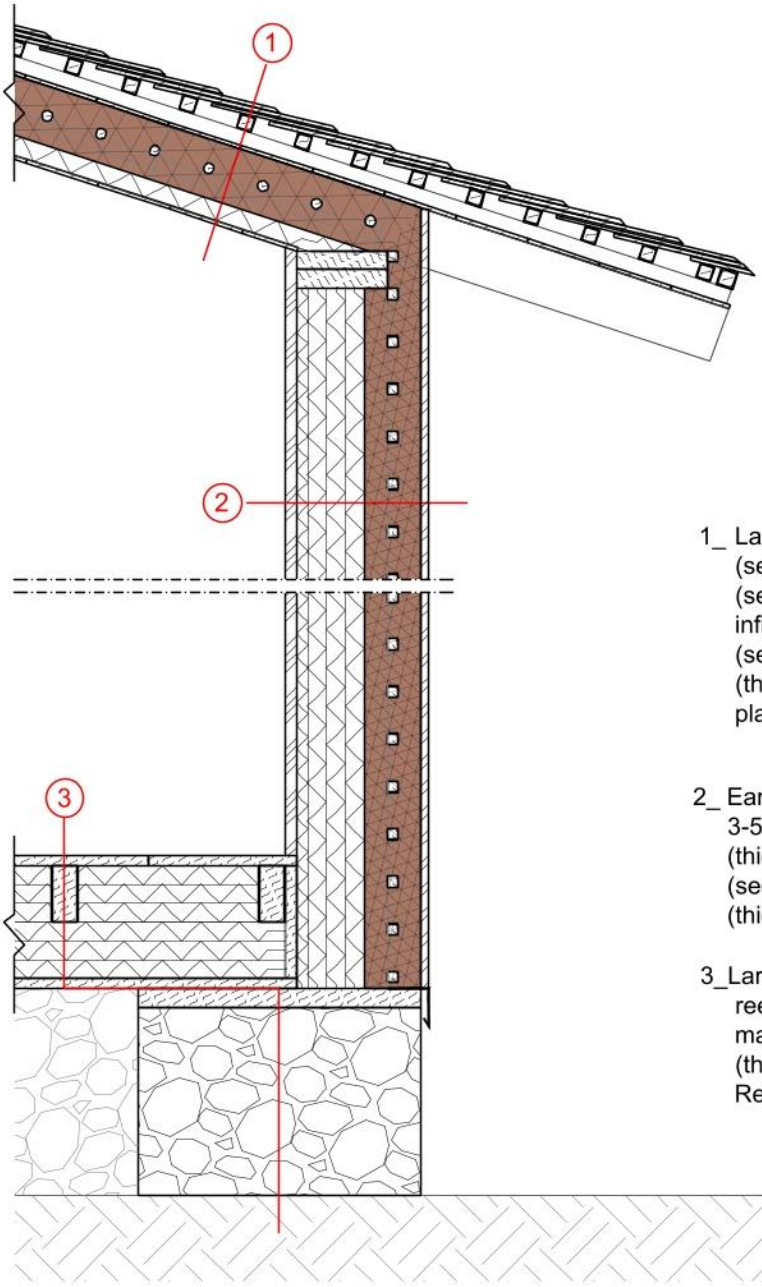

1_ Larch shingles (thickness:1cm);Larch transversal battens (section:4x4cm);Larch longitudinal battens (section:4x4cm);Larch planking (thickness:1cm);Larch beams infilled with 1.1:larch sticks fixed on longitudinal larch laths (section:3x3cm) and enrolled with Lightearth mixture (thickness:15cm), 1.2:Reed mats(thickness:5cm);Larch planking (thickness:1.5cm)

2_ Earthen plaster (thickness:3.7cm); Reed mats (thickness: 3-5+5+5cm);Larch stud (section:cm8x24) infilled with lightearth (thickness:15cm) framed by horizontal larch laths (section:cm3x3); Earth/*cocciopesto*/putty/Sand lime render (thickness:3.7cm)

3_Larch planking (thickness:2.5cm);Larch bearers infilled with reed mats (thickness:cm5x15);Larch joists infilled wih reed mats (thickness:cm5x15);Larch planking (thickness:2.5cm);Larch anchor planking (thickness:5cm); Recycled aggregate gabions (height:50cm)

Annex 24 : OpenFOAM inputs scripts

"0/D"

```
/*--------------------------------*- C++ -*----------------------------------*\
| =========                 |                                                 |
| \\      /  F ield         | OpenFOAM: The Open Source CFD Toolbox           |
|  \\    /   O peration     | Version:  v2012                                 |
|   \\  /    A nd           | Website:  www.openfoam.com                      |
|    \\/     M anipulation  |                                                 |
\*---------------------------------------------------------------------------*/
FoamFile
{
    version     2.0;
    format      ascii;
    class       volVectorField;
    object      D;
}

dimensions      [0 1 0 0 0 0 0];

internalField   uniform (0 0 0);

boundaryField
{
Cube_002_cell_004 {type slip;}
Cube_002_cell_003 {type slip;}
Cube_002_cell {type slip;}
Cube_002_cell_001 {type slip;}
Cube_002_cell_002 {type slip;}
load_002_cell_434{type tractionDisplacement; traction uniform (0 0 0); pressure
uniform 100; value uniform (0 0 0);}
path2417_002 {type slip;}
Cube_002_cell_005 {type slip;}
load_002_cell_435{type tractionDisplacement; traction uniform (0 0 0); pressure
uniform 100; value uniform (0 0 0);}
}
```

"0/T"

```
/*--------------------------------*- C++ -*----------------------------------*\
| =========                 |                                                 |
| \\      /  F ield         | OpenFOAM: The Open Source CFD Toolbox           |
|  \\    /   O peration     | Version:  v2012                                 |
|   \\  /    A nd           | Website:  www.openfoam.com                      |
|    \\/     M anipulation  |                                                 |
\*---------------------------------------------------------------------------*/
FoamFile
{
    version     2.0;
    format      ascii;
    class       volScalarField;
    object      T;
}
// * * * * * * * * * * * * * * * * * * * * * * * * * * * * * * * * * * * * //

dimensions      [0 0 0 1 0 0 0];

internalField   uniform 300;

boundaryField
```

```
{
    left
    {
        type            symmetryPlane;
    }
    right
    {
        type            zeroGradient;
    }
    down
    {
        type            symmetryPlane;
    }
    up
    {
        type            zeroGradient;
    }
    hole
    {
        type            zeroGradient;
    }
    frontAndBack
    {
        type            empty;
    }
}
```

“constant/mechanicalProperties”

```
/*--------------------------------*- C++ -*----------------------------------*\
| =========                 |                                                 |
| \\      /  F ield         | OpenFOAM: The Open Source CFD Toolbox           |
|  \\    /   O peration     | Version:  v2012                                 |
|   \\  /    A nd           | Website:  www.openfoam.com                      |
|    \\/     M anipulation  |                                                 |
\*---------------------------------------------------------------------------*/
FoamFile
{
    version     2.0;
    format      ascii;
    class       dictionary;
    location    "constant";
    object      mechanicalProperties;
}
// * * * * * * * * * * * * * * * * * * * * * * * * * * * * * * * * * * * * * //
rho
{
    type        uniform;
    value       1700; //aggregates - 7854; //galvanised
 }

nu
{
    type        uniform;
    value       0.3;
}

E
{
    type        uniform;
    value       9330e+6; //aggregates - 2e+11; //galvanised
}


planeStress     no; //yes;
```

“constant/g”

```
/*--------------------------------*- C++ -*----------------------------------*\
| solids4foam: solid mechanics and fluid-solid interaction simulations        |
| Version:     v2.0                                                           |
| Web:         https://solids4foam.github.io                                  |
| Disclaimer:  This offering is not approved or endorsed by OpenCFD Limited,  |
|              producer and distributor of the OpenFOAM software via          |
|              www.openfoam.com, and owner of the OPENFOAM® and OpenCFD®      |
|              trade marks.                                                   |
\*---------------------------------------------------------------------------*/
FoamFile
{
    version     2.0;
    format      ascii;
    class       uniformDimensionedVectorField;
    location    "constant";
    object      g;
}
// * * * * * * * * * * * * * * * * * * * * * * * * * * * * * * * * * * * * * //

dimensions      [0 1 -2 0 0 0 0];
value           ( 0 0 -9.81 );

// ************************************************************************* //
```

“constant/thermalProperties”

```
/*--------------------------------*- C++ -*----------------------------------*\
| =========                 |                                                 |
| \\      /  F ield         | OpenFOAM: The Open Source CFD Toolbox           |
|  \\    /   O peration     | Version:  v2012                                 |
|   \\  /    A nd           | Website:  www.openfoam.com                      |
|    \\/     M anipulation  |                                                 |
\*---------------------------------------------------------------------------*/
FoamFile
{
    version     2.0;
    format      ascii;
    class       dictionary;
    location    "constant";
    object      thermalProperties;
}
C
{
    type        uniform;
    value       434;
}
k
{
    type        uniform;
    value       60.5;
}
alpha
{
    type        uniform;
    value       1.1e-05;
}
thermalStress   no;
```

“system/fvSchemes”

```
/*--------------------------------*- C++ -*----------------------------------*\
| =========                 |                                                 |
| \\      /  F ield         | OpenFOAM: The Open Source CFD Toolbox           |
|  \\    /   O peration     | Version:  v2012                                 |
|   \\  /    A nd           | Website:  www.openfoam.com                      |
|    \\/     M anipulation  |                                                 |
\*---------------------------------------------------------------------------*/
FoamFile
{
    version     2.0;
    format      ascii;
    class       dictionary;
    location    "system";
    object      fvSchemes;
}
// * * * * * * * * * * * * * * * * * * * * * * * * * * * * * * * * * * * * * //

d2dt2Schemes
{
    default         Euler; //steadyState;
}

ddtSchemes
{
    default         Euler;
}

gradSchemes
{
    default         leastSquares;
    grad(D)         leastSquares;
    grad(T)         leastSquares;
}

divSchemes
{
    default         none;
    div(sigmaD)     Gauss linear;
}

laplacianSchemes
{
    default         none;
    laplacian(DD,D) Gauss linear corrected;
    laplacian(DT,T) Gauss linear corrected;
}

interpolationSchemes
{
    default         linear;
}

snGradSchemes
{
    default         none;
}
```

“system/fvSolution”

```
/*--------------------------------*- C++ -*----------------------------------*\
| =========                 |                                                 |
| \\      /  F ield         | OpenFOAM: The Open Source CFD Toolbox           |
|  \\    /   O peration     | Version:  v2012                                 |
|   \\  /    A nd           | Website:  www.openfoam.com                      |
|    \\/     M anipulation  |                                                 |
\*---------------------------------------------------------------------------*/
FoamFile
{
    version     2.0;
    format      ascii;
    class       dictionary;
    location    "system";
    object      fvSolution;
}

solvers
{
    "(D|T)"
    {
        solver          GAMG;
        tolerance       1e-06;
        relTol          0.9;
        smoother        GaussSeidel;
        nCellsInCoarsestLevel 20;
    }
}

stressAnalysis
{
    compactNormalStress yes;
    nCorrectors     1;
    D               1e-06;
}
```

“system/controlDict”

```
/*--------------------------------*- C++ -*----------------------------------*\
| =========                 |                                                 |
| \\      /  F ield         | OpenFOAM: The Open Source CFD Toolbox           |
|  \\    /   O peration     | Version:  v2012                                 |
|   \\  /    A nd           | Website:  www.openfoam.com                      |
|    \\/     M anipulation  |                                                 |
\*---------------------------------------------------------------------------*/
FoamFile
{
    version     2.0;
    format      ascii;
    class       dictionary;
    location    "system";
    object      controlDict;
}
// * * * * * * * * * * * * * * * * * * * * * * * * * * * * * * * * * * * * //

application     solidDisplacementFoam;

startFrom       startTime;

startTime       0;
```

```
stopAt          endTime;

endTime         100;

deltaT          1;

writeControl    timeStep;

writeInterval   20;

purgeWrite      0;

writeFormat     ascii;

writePrecision  6;

writeCompression off;

timeFormat      general;

timePrecision   6;

graphFormat     raw;

runTimeModifiable true;
```

Annex 25 : LIGGGHTS Input Script

```
#####################################
######### CASE STUDY GABIONS #########
#####################################

atom_style     granular
boundary       f f f #m m m
newton         off

communicate    single vel yes
units          si

neighbor       0.05 bin
neigh_modify   delay 0

################ Boundary
variable xmin equal -.1
variable xmax equal 1.
variable ymin equal -1
variable ymax equal 0.1
variable zmin equal -0.1
variable zmax equal 4

#################### Definition BoundingBox
region reg block ${xmin} ${xmax} ${ymin} ${ymax} ${zmin} ${zmax} units box

create_box 3 reg              # Doit matcher avec le nombre de natoms(ici 3)

##### Nombre de matériaux
variable natoms equal 3 #1:Fence #2:Aggregates #3:Wood

##### Variables pour chaque matériaux : Valeurs confirmées

#Young Modulus
variable youngsModulus1       equal   2e8     #N/mm2
variable youngsModulus2       equal   5e7     #N/mm2
variable youngsModulus3       equal   5e7     #N/mm2

#Poisson Ratio
variable poissonsRatio1 equal 0.3
variable poissonsRatio2 equal 0.2
variable poissonsRatio3 equal 0.4

#Coefficient of Restitution
variable CoR11 equal 0.95
variable CoR12 equal 0.6
variable CoR13 equal 0.4
variable CoR21 equal 0.6
variable CoR22 equal 0.5
variable CoR23 equal 0.4
variable CoR31 equal 0.4
variable CoR32 equal 0.4
variable CoR33 equal 0.2

#Sliding friction coefficient
variable sf11 equal 0.4
variable sf12 equal 0.7
variable sf13 equal 0.2
variable sf21 equal 0.7
variable sf22 equal 0.8
variable sf23 equal 0.45
variable sf31 equal 0.2
variable sf32 equal 0.45
```

```
variable sf33 equal 0.5

#Rolling friction coefficient
variable rf11 equal 0.003
variable rf12 equal 0.006
variable rf13 equal 0.007
variable rf21 equal 0.006
variable rf22 equal 0.006
variable rf23 equal 0.008
variable rf31 equal 0.007
variable rf32 equal 0.008
variable rf33 equal 0.012

#K_finnie
variable k11 equal 1
variable k12 equal 1
variable k13 equal 1
variable k21 equal 1
variable k22 equal 1
variable k23 equal 1
variable k31 equal 1
variable k32 equal 1
variable k33 equal 1

###############  Material properties required for new pair styles
fix  m1 all property/global youngsModulus peratomtype ${youngsModulus1}
${youngsModulus2} ${youngsModulus3}
fix  m2 all property/global poissonsRatio peratomtype ${poissonsRatio1}
${poissonsRatio2} ${poissonsRatio3}
fix  m3 all property/global coefficientRestitution peratomtypepair ${natoms}
${CoR11} ${CoR12} ${CoR13} ${CoR21} ${CoR22} ${CoR23} ${CoR31} ${CoR32} ${CoR33}
fix  m4 all property/global coefficientFriction peratomtypepair ${natoms} ${sf11}
${sf12} ${sf13} ${sf21} ${sf22} ${sf23} ${sf31} ${sf32} ${sf33}
fix  m5 all property/global coefficientRollingFriction peratomtypepair ${natoms}
${rf11} ${rf12} ${rf13} ${rf21} ${rf22} ${rf23} ${rf31} ${rf32} ${rf33}
fix  m6 all property/global characteristicVelocity scalar 2
fix  m7 all property/global k_finnie peratomtypepair ${natoms} ${k11} ${k12} ${k13}
${k21} ${k22} ${k23} ${k31} ${k32} ${k33}

################## Particles : Aggregates
variable n_types equal 2

variable size1 equal  .02 #ce sont les rayons et non les diamètres
variable size2 equal .05

variable frac1 equal  .4
variable frac2 equal  .6

variable d1    equal 3000 #macerie tipo CLS
variable d2    equal 1500 #macerie tipo leggere

####### pair style

pair_style  gran model hooke tangential history
pair_coeff     * *

#######
timestep       0.00005

#######
fix            1 all nve/sphere
fix            2 all gravity 9.81 vector 0.0 0.0 -1.0


############### Loading STL Files
```

```
fix     fence1         all mesh/surface/stress       file    meshes/FenceFence.stl
        type 1 wear finnie
fix     fence2         all mesh/surface      file    meshes/FenceFenceCenter.stl
type 1

fix     mesh    all wall/gran model hooke tangential history mesh n_meshes 2 meshes
fence1 fence2

############    Generation & Insertion of Particles

fix     agg1    all particletemplate/sphere   10487   atom_type 3    radius constant
${size1}       density constant ${d1}
fix     agg2    all particletemplate/sphere   11887   atom_type 3    radius constant
${size2}       density constant ${d2}

fix     pdd1    all particledistribution/discrete     32452867       ${n_types}
        agg1 ${frac1}  agg2 ${frac2}

fix             ins_mesh       all     mesh/surface/planar    file
        meshes/InsertionTotInsertion.stl             type 2 scale 1

fix             ins                    all insert/stream seed 123457
distributiontemplate pdd1 mass 6000 massrate 2000 overlapcheck yes all_in yes vel
constant 0 0 -5 insertion_face ins_mesh extrude_length 1


#thermo settings
compute         1 all erotate/sphere
thermo_style    custom step atoms ke c_1 vol
thermo          1000
thermo_modify   lost ignore norm no


############ Dumping of the data
#### Create folder
shell   mkdir post

#### Compute
compute ppc all contact/atom #particle particle contacts
compute allcontactsinsystem all reduce sum c_ppc #sum all contacts over all procs

compute fc all pair/gran/local pos force force_normal force_tangential contactPoint
#compute contact force at all granular contacts

#### Run first step to avoid empty dump
run 1

#### Make a dump of particles and the stl file
dump    dmpparticle    all custom/vtk                2000    post/Sphere_*.vtk id
type x y z vx vy vz fx fy fz radius mass
dump    dmpfencestress all     mesh/gran/VTK  2000    post/fence_*.vtk stress fence1
dump    dmp2                   all local/gran/vtk     2000    post/forcechain*.vtp fc



#run with particle insertion
run             50000 upto
unfix   ins

#run to let particle settle
run             99999 upto
unfix mesh

run             100000 upto

#Compression steps
```

```
variable FORCE_down equal 0.0025
variable VMAX equal 0.2
variable KP equal 10.0
variable KI equal 0.5
variable KD equal 0.5

fix        load1 all mesh/surface/stress/servo file meshes/load1.stl type 2 scale
1.0 com 0 0 0 &
                  ctrlPV force axis 0 0 -1 target_val ${FORCE_down} vel_max ${VMAX}
kp ${KP} ki ${KI} kd ${KD}
fix        load2 all mesh/surface/stress/servo file meshes/load2.stl type 2 scale
1.0 com 0 0 0 &
                  ctrlPV force axis 0 0 -1 target_val ${FORCE_down} vel_max ${VMAX}
kp ${KP} ki ${KI} kd ${KD}
fix        load3 all mesh/surface/stress/servo file meshes/load3.stl type 2 scale
1.0 com 0 0 0 &
                  ctrlPV force axis 0 0 -1 target_val ${FORCE_down} vel_max ${VMAX}
kp ${KP} ki ${KI} kd ${KD}
fix        load4 all mesh/surface/stress/servo file meshes/load4.stl type 2 scale
1.0 com 0 0 0 &
                  ctrlPV force axis 0 0 -1 target_val ${FORCE_down} vel_max ${VMAX}
kp ${KP} ki ${KI} kd ${KD}

fix walls all wall/gran model hooke tangential history mesh n_meshes 6 meshes fence1
fence2 load1 load2 load3 load4

run                   10000
```

Annex 26 : Hemp-lime prototype formwork_ Parallel views _ 1:50

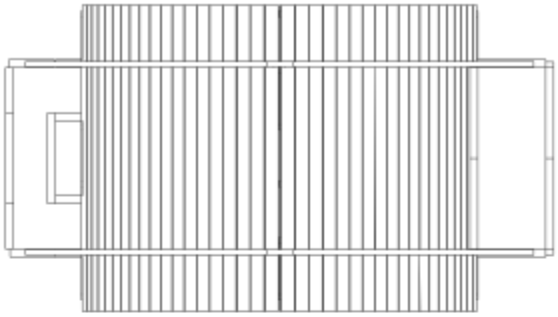

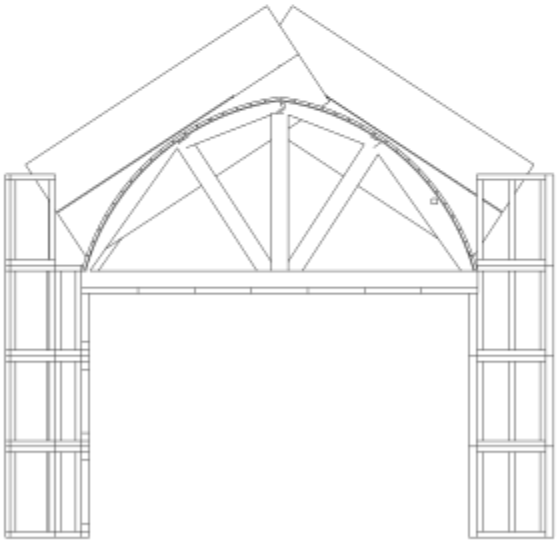

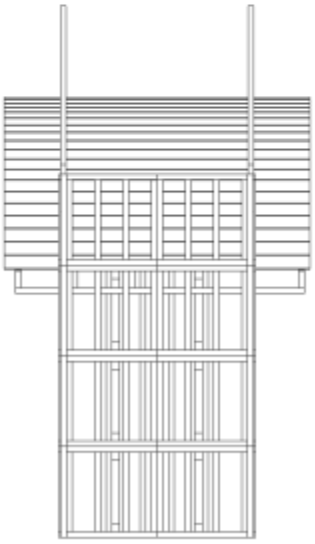

Annex 27 : Hemp-lime prototype formwork_ Isometric view _1:20

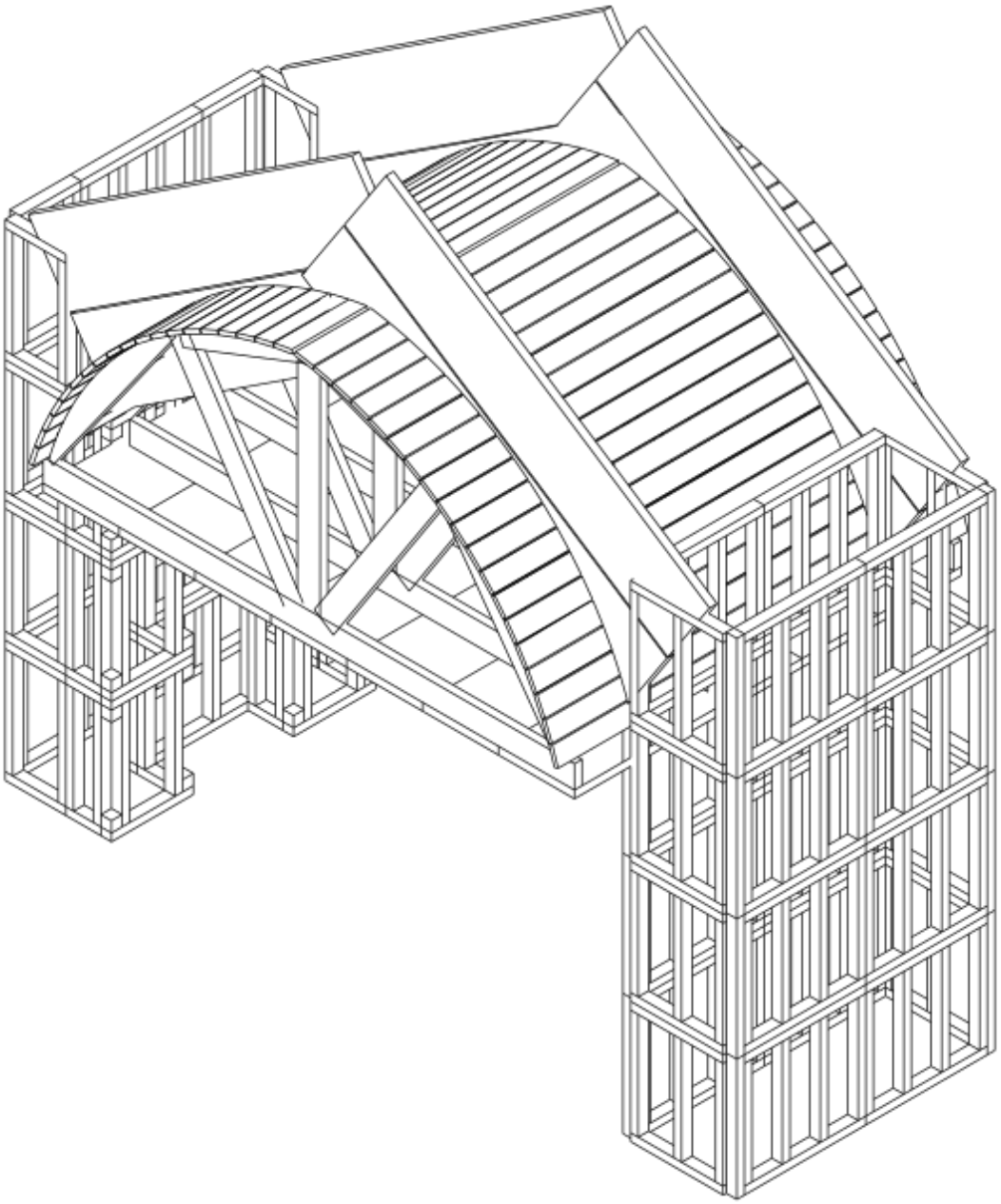

10 List of figures

11 List of tables

12 List of equations

13 References

[1] 'Gueiza 'd la tana'. [Online]. Available: https://www.e-borghi.com/it/sc/2-castelli-chiese-monumenti-musei/torino-angrogna/1319/gueiza-'d-la-tana.html

[2] A. Bocco Guarneri, *Vegetarian architecture: case studies on building and nature*. Berlin: Jovis, 2020.

[3] D. H. Meadows, J. Randers, and D. L. Meadows, 'The Limits to Growth (1972)', in *The Future of Nature: Documents of Global Change*, L. Robin, S. Sörlin, and P. Warde, Eds., New York: Yale University Press, 1972, pp. 101–116.

[4] A. Nebel, A. Kling, R. Willamowski, and T. Schell, 'Recalibration of limits to growth: An update of the World3 model', *J. Ind. Ecol.*, vol. 28, no. 1, pp. 87–99, 2024, doi: https://doi.org/10.1111/jiec.13442.

[5] A. J. Watson and J. E. Lovelock, 'Biological homeostasis of the global environment: the parable of Daisyworld', *Tellus B Chem. Phys. Meteorol.*, vol. 35, no. 4, p. 284, Jan. 1983, doi: https://doi.org/10.3402/tellusb.v35i4.14616.

[6] United Nations Environment Programme, 'Not just another brick in the wall: The solutions exist - Scaling them will build on progress and cut emissions fast. Global Status Report for Buildings and Construction 2024/2025', Mar. 2025, Accessed: Aug. 19, 2025. [Online]. Available: https://wedocs.unep.org/20.500.11822/47214

[7] J. W. Kirchner, 'The Gaia Hypothesis: Fact, Theory, and Wishful Thinking', *Clim. Change*, vol. 52, no. 4, pp. 391–408, Mar. 2002, doi: https://doi.org/10.1023/A:1014237331082.

[8] B. Huang *et al.*, 'A Life Cycle Thinking Framework to Mitigate the Environmental Impact of Building Materials', *One Earth*, vol. 3, Nov. 2020, doi: https://doi.org/10.1016/j.oneear.2020.10.010.

[9] 'CGR Global Report 2020.pdf'. Accessed: Aug. 19, 2025. [Online]. Available: https://cdn.prod.website-

files.com/5e185aa4d27bcf348400ed82/5e26ead616b6d1d157ff4293_20200120%20-%20CGR%20Global%20-%20Report%20web%20single%20page%20-%20210x297mm%20-%20compressed.pdf

[10] 'Glocalizzazione', *Treccani*. [Online]. Available: https://www.treccani.it/enciclopedia/glocalizzazione_(Lessico-del-XXI-Secolo)

[11] 'Technologie appropriée', *Wikipédia*. [Online]. Available: https://fr.wikipedia.org/w/index.php?title=Technologie_interm%C3%A9diaire&oldid=200004816

[12] Ernst Friedrich Schumacher, *Small is beautiful : A Study of Economics As If People Mattered*. Blond & Briggs, 1973.

[13] F. Dejeant, Garnier, Philippe, and Joffroy, Thierry, *Matériaux locaux, matériaux d'avenir ressources locales pour des villes et territoires durables en Afrique*. CRAterre éditions, 2020.

[14] B. Dorsey, 'Building a Foundation of Pragmatic Architectural Theory to Support More Sustainable or Regenerative Straw Bale Building and Code Adoption', *J. Sustain. Res.*, vol. 4, May 2022, doi: https://doi.org/10.20900/jsr20220003.

[15] D. Caputo, G. D'Angelo, M. Fumo, and B. Liguori, 'Materiali leganti: tradizione e innovazione per un'edilizia eco-sostenibile e bioregionale', in *Bioregionalismo ed edilizia sostenibile*, Napoli: Luciano Editore, 2020, pp. 119–135. [Online]. Available: https://hdl.handle.net/11588/832153

[16] United Nations Environment Programme and Global Alliance for Buildings and Construction, 'Global Status Report for Buildings and Construction - Beyond foundations: Mainstreaming sustainable solutions to cut emissions from the buildings sector', Mar. 2024, doi: https://doi.org/10.59117/20.500.11822/45095.

[17] K. Ip and A. Miller, 'Life cycle greenhouse gas emissions of hemp–lime wall constructions in the UK', *Resour. Conserv. Recycl.*, vol. 69, pp. 1–9, Dec. 2012, doi: https://doi.org/10.1016/j.resconrec.2012.09.001.

[18] R. Busbridge and R. Rhydwen, 'An investigation of the thermal properties of hemp and clay monolithic walls', 2010.

[19] Y. Florentin, D. Pearlmutter, B. Givoni, and E. Gal, 'A life-cycle energy and carbon analysis of hemp-lime bio-composite building materials', *Energy Build.*, vol. 156, pp. 293–305, Dec. 2017, doi: https://doi.org/10.1016/j.enbuild.2017.09.097.

[20] Jean-Pierre Oliva - Samuel Courgey, *L'isolation thermique écologique*, 3rd edition. Terre vivante, 2023.

[21] A. Bohn and A. Bocco, 'Thermal and Moisture Content Monitoring of a Full-Scale Load Bearing Hemp Lime Arch Prototype', *Sustainability*, vol. 16, no. 20, Art. no. 20, Jan. 2024, doi: https://doi.org/10.3390/su16208912.

[22] 'Cure'. [Online]. Available: https://www.converge.io/intelligence-platform/cure

[23] K. Bagi, 'Stress and strain in granular assemblies', *Mech. Mater.*, vol. 22, no. 3, pp. 165–177, Mar. 1996, doi: https://doi.org/10.1016/0167-6636(95)00044-5.

[24] M. R. Kuhn and K. Bagi, ‘Specimen Size Effect in Discrete Element Simulations of Granular Assemblies’, *J. Eng. Mech.*, vol. 135, no. 6, pp. 485–492, Jun. 2009, doi: https://doi.org/10.1061/(ASCE)0733-9399(2009)135:6(485).

[25] M. Brocato, ‘A continuum model of close packing granular materials for the study of rock filled gabions’, *International Journal of Solids and Structures*, vol. 187, pp. 38–47, 2020, doi: https://doi.org/10.1016/j.ijsolstr.2018.08.008.

[26] D. Raynaud, *Qu’est-ce que la technologie ?* Editions Matériologiques, 2016. Accessed: Apr. 15, 2025. [Online]. Available: https://doi.org/10.3917/edmat.rayna.2016.01

[27] ‘Tecnologia’, *Treccani*. Accessed: Apr. 26, 2023. [Online]. Available: https://www.treccani.it/vocabolario/tecnologia

[28] K. Marx and J.-P. Lefebvre, *Le capital: critique de l’économie politique*, Nouvelle éd. in Quadrige. Paris: PUF, 2014.

[29] Fathy, Hassan, *Architecture for the Poor: An Experiment in Rural Egypt.*, University of Chicago Press. 1973.

[30] G. Pluvinage and V. Sapunov, *Prévision statistique de la résistance, du fluage et de la résistance durable des matériaux de construction*. Toulouse, France: Cépaduès-Editions, 2006.

[31] ‘Construire en Chanvre : Bonnes pratiques_Tome 1’. Accessed: Jan. 30, 2022. [Online]. Available: https://www.construire-en-chanvre.fr/documents/pdf/formations/CenC_Bonnes_Pratiques_Tome_1.pdf

[32] W. Stanwix and A. Sparrow, *The hempcrete book: designing and building with hemp-lime*. Cambridge: Green Books, 2014.

[33] G. Ferreira Zapponi and E. Tenca, ‘Hempcrete pavilion: a study of a structural natural material building.’, Master Thesis, Politecnico di Torino, 2022. Accessed: Apr. 25, 2023. [Online]. Available: https://webthesis.biblio.polito.it/23268/

[34] *Piano Regionale delle Attività Estrattive (Regione Piemonte, Italia)*. 2016.

[35] ‘Pozzolan’, *Wikipédia*. Feb. 02, 2024. Accessed: Apr. 26, 2024. [Online]. Available: https://fr.wikipedia.org/w/index.php?title=Pouzzolane&oldid=212092157

[36] N. P. Martins *et al.*, ‘The design of a binder for earth stabilisation’, presented at the Nocmat 2022, doi: https://doi.org/10.3929/ethz-b-000573205.

[37] ‘Kaolinite — Wikipédia’, *Wikipédia*. Accessed: Apr. 26, 2024. [Online]. Available: https://fr.wikipedia.org/wiki/Kaolinite

[38] A.-J. Loriot, *Mémoire sur une découverte dans l’art de bâtir faite par le sieur Loriot,... dans lequel on rend publique... la méthode de composer un ciment... propre à une infinité d’ouvrages... / la présente édition est publiée par les soins de M. Ch. Frantz*. 1774. Accessed: Jan. 26, 2024. [Online]. Available: https://gallica.bnf.fr/ark:/12148/bpt6k96851204

[39] L. M. Seymour, J. Maragh, P. Sabatini, M. Di Tommaso, J. C. Weaver, and A. Masic, 'Hot mixing: Mechanistic insights into the durability of ancient Roman concrete', *Sci. Adv.*, vol. 9, no. 1, 2023, doi: https://doi.org/10.1126/sciadv.add1602.

[40] Gilberto Barcella, *Canapa e calce : Tra tradizione e innovazione dalla bioedilizia alla neoedilizia*. Dario Flaccovio Editore, 2021.

[41] T.-T. Nguyen, V. Picandet, S. Amziane, and C. Baley, 'Influence of compactness and hemp hurd characteristics on the mechanical properties of lime and hemp concrete', *Eur. J. Environ. Civ. Eng.*, vol. 13, no. 9, pp. 1039–1050, Oct. 2009, doi: https://doi.org/10.1080/19648189.2009.9693171.

[42] V. Picandet, 'Caractérisation des matériaux cimentaires: propriétés mécaniques et perméabilité', Habilitation à diriger des recherches, Université Européenne de Bretagne, 2015. [Online]. Available: https://hal.science/tel-01242785

[43] 'Top countries for Hemp Harvested Area', NationMaster. Accessed: Apr. 08, 2025. [Online]. Available: https://www.nationmaster.com/nmx/ranking/hemp-harvested-area

[44] J. Summerscales, N. P. J. Dissanayake, A. S. Virk, and W. Hall, 'A review of bast fibres and their composites. Part 1 – Fibres as reinforcements', *Composites Part A: Applied Science and Manufacturing*, vol. 41, no. 10, pp. 1329–1335, Oct. 2010, doi: https://doi.org/10.1016/j.compositesa.2010.06.001.

[45] ISPRA, 'Rapporto Rifiuti Speciali in Italia - Edizione 2023', 389/2023. [Online]. Available: https://www.isprambiente.gov.it/resolveuid/5009aabf94934c12a6b1d226f0cd7ce0

[46] G. J. Cristobal, D. Caro, G. Foster, G. Pristera, F. Gallo, and D. Tonini, 'Techno-economic and environmental assessment of construction and demolition waste management in the European Union', JRC Publications Repository. Accessed: Aug. 13, 2025. [Online]. Available: https://publications.jrc.ec.europa.eu/repository/handle/JRC135470

[47] A. Damgaard *et al.*, 'Background data collection and life cycle assessment for construction and demolition waste (CDW) management', 2022, doi: https://doi.org/10.2760/772724.

[48] R. Industry, 'Rifiuti da costruzione e demolizione, tasso di riciclo all'81%, ma quasi la metà dei prodotti recuperati resta inutilizzato'. Accessed: Aug. 12, 2025. [Online]. Available: https://www.recyclind.it/ita/4101/rifiutidacostruzioneedemolizionetassodiricicloall81maquasilametdeiprodottirecuperatirestainutilizzato/

[49] H.-J. Chen, T. Yen, and K.-H. Chen, 'Use of building rubbles as recycled aggregates', *Cem. Concr. Res.*, vol. 33, no. 1, pp. 125–132, Jan. 2003, doi: https://doi.org/10.1016/S0008-8846(02)00938-9.

[50] G. P. Hammond and C. I. Jones, 'Embodied energy and carbon in construction materials', *Proc. Inst. Civ. Eng. - Energy*, vol. 161, no. 2, pp. 87–98, May 2008, doi: https://doi.org/10.1680/ener.2008.161.2.87.

[51] Agora Industry, ‘Labels for climate friendly basic materials’, 2023. Accessed: Apr. 08, 2025. [Online]. Available: https://www.agora-industry.org/fileadmin/Projects/2023/2023-09_IND_Label_synthesis/A-EW_313_Label_Synthesis_WEB.pdf

[52] J. Salk, ‘Beyond Green Building & Codes: Seeing a Bigger Picture’, 2009. [Online]. Available: https://www.dcat.net/about_dcat/David_Eisenberg_CAZREN_talk_Dec_5_2009.pdf

[53] Y. Macé, ‘L’approche statistique : entre réalité(s) et subjectivité’, *Journal de la société française de statistique*, vol. 147, pp. 85–102, 2006.

[54] P. Lehner and H. Brázdilová, ‘Inverse Analysis of Straw Bale Mechanical Parameters in Load-Bearing Structures Based on a Finite Element Model’, *Buildings*, vol. 12, no. 12, Art. no. 12, Dec. 2022, doi: https://doi.org/10.3390/buildings12122157.

[55] M. Lawrence, ‘A study of carbonatation in non-hydraulic lime mortars’, PhD Thesis, Bath University, 2006. [Online]. Available: https://purehost.bath.ac.uk/ws/portalfiles/portal/187940936/Lawrence_2c2006.pdf

[56] Derek, ‘How To Create a Best Fit Line in Google Sheets Precisely?’, The Fusion Charts Blog. Accessed: Apr. 27, 2024. [Online]. Available: https://www.fusioncharts.com/blog/how-to-add-equation-to-graph-in-google-sheets-accurately/

[57] D. Solav, K. M. Moerman, A. M. Jaeger, K. Genovese, and H. M. Herr, ‘MultiDIC: An Open-Source Toolbox for Multi-View 3D Digital Image Correlation’, *IEEE Access*, vol. 6, pp. 30520–30535, 2018, doi: https://doi.org/10.1109/ACCESS.2018.2843725.

[58] ‘Stazione Meteorologica di Fisica dell’Atmosfera - Torino’. Accessed: Jul. 18, 2024. [Online]. Available: https://www.meteo.dfg.unito.it/anno-2024

[59] S. R. da Silva, F. N. Cimadon, P. M. Borges, J. Z. Schiavon, E. Possan, and J. J. de O. Andrade, ‘Relationship between the mechanical properties and carbonation of concretes with construction and demolition waste’, *Case Stud. Constr. Mater.*, vol. 16, Jun. 2022, doi: https://doi.org/10.1016/j.cscm.2021.e00860.

[60] ‘Architecture et Développement - Un habitat digne et durable pour tous’. Accessed: Apr. 12, 2025. [Online]. Available: https://archidev.org/

[61] C. Spiridonidis and M. Voyatzaki, Eds., ‘An Innovative Educational Approach Studying the convergence between environmental design and architectural form generation’, in *Educating architects towards innovative architecture*, in EAAE transactions on architectural education, no. 50. , ENHSA, European Network of Heads of School of Architecture, 2010. [Online]. Available: https://www.academia.edu/129851661/Educating_Architects_towards_Innovative_Architecture

[62] F. Pouillon, *Les pierres sauvages: roman préface inédite de Laurence Cossé*. in Points. Paris: Éditions Points, 2019.

[63] Conseil général des ponts et chaussées, ‘Mery, Mémoire sur l’équilibre des voûtes en berceaux’, in *Annales des ponts et chaussées. Mémoires et documents relatifs à l’art des constructions et au service de l’ingénieur*, Paris: Carilian-Goeury, 1840. [Online]. Available: https://gallica.bnf.fr/ark:/12148/bpt6k4084533/f53.item

[64] ‘CobBauge’, Ebuki. Accessed: May 02, 2024. [Online]. Available: https://www.ebuki.co/projects-1/cobbauge

[65] S. Courgey and J.-P. Oliva, *La conception bioclimatique: des maisons économes et confortables en neuf et en réhabilitation*. Terre vivante, 2006.

[66] E. A. A. D. Nagahage, I. S. P. Nagahage, and T. Fujino, ‘Calibration and Validation of a Low-Cost Capacitive Moisture Sensor to Integrate the Automated Soil Moisture Monitoring System’, *Agriculture*, vol. 9, no. 7, p. 141, Jul. 2019, doi: https://doi.org/10.3390/agriculture9070141.

[67] M. Lawrence, E. Fodde, K. Paine, and P. Walker, ‘Hygrothermal Performance of an Experimental Hemp-Lime Building’, *Key Eng. Mater.*, vol. 517, pp. 413–421, Jun. 2012, doi: https://doi.org/10.4028/www.scientific.net/KEM.517.413.

[68] S. Elfordy, F. Lucas, F. Tancret, Y. Scudeller, and L. Goudet, ‘Mechanical and thermal properties of lime and hemp concrete (“hempcrete”) manufactured by a projection process’, *Constr. Build. Mater.*, vol. 22, no. 10, pp. 2116–2123, Oct. 2008, doi: https://doi.org/10.1016/j.conbuildmat.2007.07.016.

[69] E. Jones *et al.*, ‘A Good Practices Guide for Digital Image Correlation’, International Digital Image Correlation Society, Oct. 2018. Accessed: Mar. 06, 2023. [Online]. Available: https://doi.org/10.32720/idics/gpg.ed1/print.format

[70] Ente Italiano di Normazione, *UNI EN 459-1:2015*, 2015. Accessed: May 03, 2024. [Online]. Available: https://store.uni.com/uni-en-459-1-2015

[71] A. Costigan and S. Pavía, ‘Influence of the mechanical properties of lime mortar on the strength of brick masonry’, *RILEM Bookseries*, vol. 7, pp. 359–372, Jan. 2013, doi: https://doi.org/10.1007/978-94-007-4635-0_28.

[72] ‘Kerterre - les maisons originales à construire soi-même’. Accessed: Aug. 29, 2025. [Online]. Available: https://kerterre.org/

[73] A. Bohn and A. Bocco, ‘Mechanical Properties and Carbonation Measurement of Various Hemp-Lime Formulations’, in *Bio-Based Building Materials - Proceedings of ICBBM 2025*, S. Amziane, R. D. Toledo Filho, M. Y. R. da Gloria, and J. Page, Eds., in RILEM Bookseries, vol. 61. Springer, 2025, pp. 363–373. doi: https://doi.org/10.1007/978-3-031-92874-1_29.

[74] S. Amziane, I. Merta, and J. Page, Eds., *Bio-Based Building Materials: Proceedings of ICBBM 2023*, vol. 45. in RILEM Bookseries, vol. 45. Springer, 2023. Accessed: Jan. 08, 2025. [Online]. Available: https://doi.org/10.1007/978-3-031-33465-8

[75] N. Asghari and A. Memari, ‘State of the Art Review of Attributes and Mechanical Properties of Hempcrete’, *Biomass*, vol. 4, pp. 65–91, Feb. 2024, doi: https://doi.org/10.3390/biomass4010004.

[76] F. Lollini, ‘Corrosione da carbonatazione: Fenomeno di degrado e prevenzione’, *Concreto*, 2015, [Online]. Available: https://hdl.handle.net/11311/983309

[77] D. Ferrández, M. Álvarez, A. Zaragoza-Benzal, Á. Cobo-González, and P. Santos, ‘Development and Characterization of Innovative Hemp–Gypsum Composites for Application in the Building Industry’, *Appl. Sci.*, vol. 14, no. 6, p. 2229, Mar. 2024, doi: https://doi.org/10.3390/app14062229.

[78] F. Murphy, S. Pavia, and R. Walker, ‘An assessment of the physical properties of lime-hemp concrete’, *Bridge and Concrete Research in Ireland*, 2010, [Online]. Available: http://hdl.handle.net/2262/57402

[79] T. Lecompte, P. Tronet, V. Picandet, and C. Baley, ‘Study of lime and hemp concrete (LHC) – mix design, casting process and mechanical behaviors’, *Acad. J. Civ. Eng.*, vol. 33, no. 2, Jun. 2015, doi: https://doi.org/10.26168/icbbm2015.43.

[80] Véronique Cérézo, ‘Propriétés mécaniques, thermiques et acoustiques d’un matériau à base de particules végétales : approche expérimentale et modélisation théorique’, PhD Thesis, Gustave Eiffel University INSA Lyon, 2005. [Online]. Available: https://theses.insa-lyon.fr/publication/2005ISAL0037/these.pdf

[81] L. Arnaud and E. Gourlay, ‘Experimental study of parameters influencing mechanical properties of hemp concretes’, *Constr. Build. Mater.*, vol. 28, pp. 50–56, Mar. 2012, doi: 10.1016/j.conbuildmat.2011.07.052.

[82] T. T. Nguyen, ‘Contribution à l’étude de la formulation et du procédé de fabrication d’éléments de construction en béton de chanvre’, Université Européenne de Bretagne, 2010. [Online]. Available: https://theses.hal.science/tel-01017510

[83] R. Bevan and T. Woolley, *Hemp lime construction: a guide to building with hemp lime composites*. London: IHS BRE Press, 2008.

[84] R. Mazelli, A. Bohn, E. Zea Escamilla, G. Habert, and A. Bocco, ‘Comparative Life Cycle Assessment of Two “Vegetarian Architecture” Pavilions’, in *Bio-Based Building Materials*, S. Amziane, I. Merta, and J. Page, Eds., in RILEM Bookseries, vol. 45. Springer, 2023, pp. 982–999. doi: https://doi.org/10.1007/978-3-031-33465-8_76.

[85] Architecture et Développement, ‘Plateforme SEKOYA’, Architecture et Développement. Accessed: Apr. 22, 2023. [Online]. Available: https://www.archidev.org/spip.php?article1292

[86] M. Brocato and W. G. Lasciarrea, ‘Analysis of confined granular systems for gabion walls’, *Meccanica*, vol. 54, Oct. 2018, doi: 10.1007/s11012-018-0912-5.

[87] ‘OpenFOAM’. Accessed: Feb. 06, 2025. [Online]. Available: https://www.openfoam.com/

[88] C. Shi, Y. Chen, L. Zhang, X. Zhang, and L. Qiu, ‘Numerical study on mechanical characteristics of gabion mixed media with discrete element method’, *Constr. Build. Mater.*, vol. 438, p. 137108, Aug. 2024, doi: https://doi.org/10.1016/j.conbuildmat.2024.137108.

[89] ‘LIGGGHTS Open Source Discrete Element Method Particle Simulation Code | CFDEM®project’. Accessed: Apr. 13, 2025. [Online]. Available: https://www.cfdem.com/liggghts-open-source-discrete-element-method-particle-simulation-code

End